Novel Partitioned Stator Permanent Magnet Brushless Machines

by

David James Evans

A thesis submitted for the degree of Doctor of Philosophy

Department of Electrical and Electronic Engineering,

University of Sheffield

February 2015

ABSTRACT

This thesis combines two previously separate strands of research in the area of permanent magnet machine design, being magnetic gearing technology and switched flux brushless permanent magnet machines.

Through investigation and understanding of the operation principles of these two strands, it concludes that each has shared commonality in terms of the field harmonics produced through permanent magnet and wound fields and their interactions with salient rotor poles. Hence, applying a magnetic gear structure to a switched flux machine has yielded the opportunity to separate windings and permanent magnets and the partitioned stator switched flux permanent magnet machine is discovered.

This novel machine design is investigated further to validate its benefits, potentials and understand issues that must be addressed in the design of this machine topology. This machine was developed further when the possibility of mechanical flux weakening is observed as a fundamental outcome of the machine geometry. Understanding of this novel machine is presented through analytical, finite element analysis and prototype measured data.

The possibilities opened from this connection between switched flux machines and magnetic gears extend beyond the switched flux machine, as this concept may be applied to multiple variations of switched flux machines and more widely to all machines with stationary permanent magnets and/or stationary field windings.

AKNOWLEDGEMENTS

I firstly thank God for giving me the knowledge to do this research, 'The Lord gives wisdom. From His mouth come knowledge and understanding' (Proverbs 2:6, Bible), without this I would not have been able to perform this research.

I would like to thank Prof Zi-Qiang Zhu for his invaluable support, technical knowledge, direction and encouragement throughout the course of my research. I'm thankful to my colleagues at Sheffield University in the Electrical Machines and Drive Group, particularly Dr Lijian Wu, Dr Wenqiang Chu, and Mr Hanlin Zhan for all their extremely useful advice, help and discussions.

Finally, a special thanks to my wife for her love, patience and support during my research.

CONTENTS

CHAPTER 1 – INTRODUCTION

1.1. General Introduction

Permanent magnet (PM) machines have become a popular choice for electric machine applications due to the advancement in high energy magnetic materials [1] increasing their power density and efficiency. Various PM machine topologies have been developed and many new and novel PM machine topologies are still emerging. The design of PM machines for both low [2] and high [3] speed has been investigated. Fractional slot machines Fig. 1.1 (where the number of slots per pole per phase is not an integer number) have been the subject to much research due to their inherent minimal torque ripples and fault tolerance [4], prediction of the performance of such machines [5] and different slot and pole combinations have been studied [6-7].

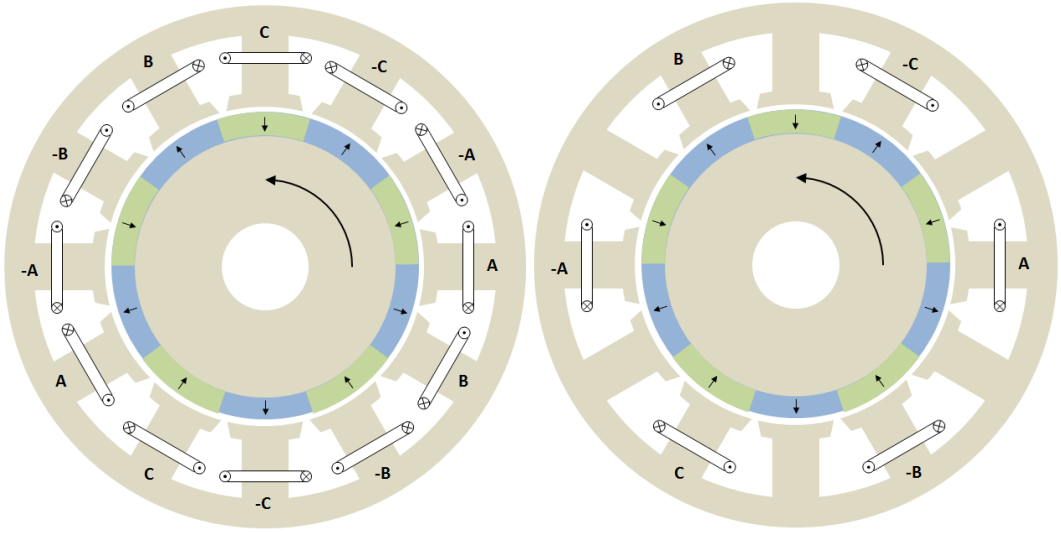

Fig. 1.1. An illustration of a fractional slot machine with 12 stator teeth, 5 PM pole pairs with double (left) and single (right) layer winding configurations.

An area to which PM machines are being applied is to high torque at low speed applications such as electric and hybrid vehicles [8-9] and wind power [10-11] technologies. Direct drive systems which eliminate the need for conventional mechanical gears to achieve high torque density at low speed have been the subject of research [12-13], also magnetic gearing as an alternative to traditional gears has advanced based on high energy magnetic materials and further incorporated into PM machine design.

A particular distinction in different brushless PM machines is the positioning of the magnets in relation to the windings whether stationary or rotating [8]. Leading to two main forms of brushless PM machines Fig. 1.2, the first is with rotating PM and wound stator, and the second is with stationary PM and wound stator with a form of salient rotor. This second arrangement, termed stator PM machines, has been developed and shown to achieve comparable torque density to the more conventional rotor PM machines [14].

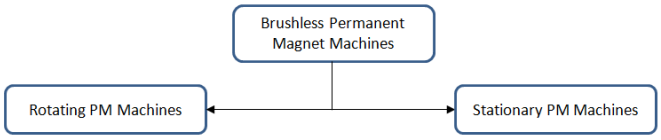

Fig. 1.2. Two main strands of PM machines.

The switched flux PM machine [25] Fig. 1.8 falls into a family of stator PM machines, based on their configuration with stationary PM material. These machines operate on the principle that the back EMF is generated from coupling of flux through coils by virtue of a salient rotor providing time varying permeance along the stator airgap.

An application of high energy permanent magnets has been in magnetic gearing Fig. 1.17 [15] as a substitute to conventional mechanical gears providing advantages over their mechanical counterparts such as mechanical isolation and removing the necessity for lubrication, but with the challenge of providing the required torque transmission magnetically. The opportunities provided considering brushless PM machines and magnetic gears together have been investigated and analysed from many perspectives Fig. 1.3.

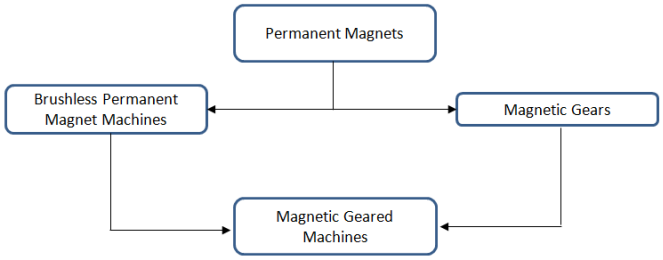

Fig. 1.3. The generation of the magnetic geared machines.

This thesis introduces a novel permanent magnet machine topology Fig. 1.4 that unifies two areas of research being switched flux PM machines and PM gears creating a machine that maintains the principles of a switched flux machine and applies magnetic gearing geometries.

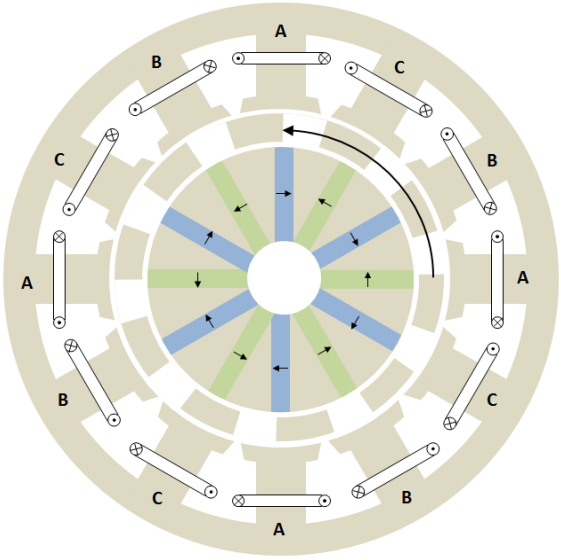

Fig. 1.4. An illustration of a partitioned stator switched flux machine with 12 stator teeth, 6 PM pole pairs and 10 rotating modulating poles.

Fundamentals, characteristics and performance of this novel machine are investigated through use of finite element (FE) simulation, analytical investigation and prototype machine measurements. This novel machine, named the partitioned stator switched flux permanent magnet machine (PS-SFPM), is a PM machine with stationary permanent magnets; it maintains the switching flux principle and draws upon the magnetic gearing method, so may be also considered a magnetic geared machine. Its configuration presents opportunity for mechanical field weakening to enhance the operating speed range, therefore this has been investigated.

1.2. Stator Permanent Magnet Machines

The concept of placing PMs within a machine's stator [16] led to three principle types of stator PM machine, doubly salient [17-20], flux reversal [21-23] and switched flux [24-25] Fig. 1.5.

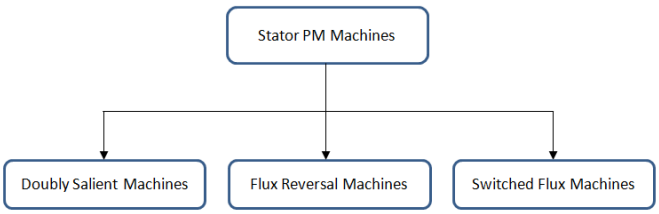

Fig. 1.5. Three main types of stator PM machines.

The distinction between these three stator PM machines is the placement of the PM material; doubly salient machines feature PM embedded within the stator yoke between two teeth, switched flux machines sandwich the PM within the stator tooth and flux reversal machines mount the PM on the tooth surface adjacent to the airgap. Machines of this type do not rely on reluctance torque to generate torque as generally the difference between d and q axis inductance is negligible, the PM excitation of the stator winding through time varying flux dominates the torque production. These forms of machine with stationary PM have been investigated and shown to achieve high torque density with high efficiency [14] with switched flux machines achieving the highest torque density potential as greater amounts of utilised PM material is possible.

1.2.1. Doubly Salient Machines

The doubly salient machine (DSPMM) features a stator with PM embedded within the stator yoke (or back iron) Fig. 1.6. Based on this arrangement it is limited to unipolar flux linkage, yielding a more trapezoidal back EMF most suited to BLDC excitation.

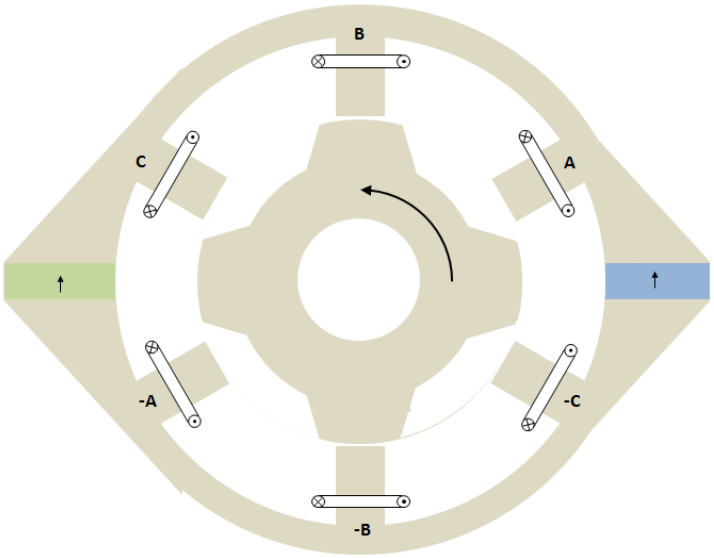

Fig. 1.6. An illustration of a doubly salient PM machine with 6 stator teeth and 4 rotor poles.

This machine design was proposed in [17] and a machine with 6 stator teeth and 4 rotor poles investigated, the potential of simple structure and utilisation of PM material was highlighted and the observation of potential issues with torque ripples identified. These torque ripples were addressed through means of skewing [26] and optimisation of control angles [27]. Alternative numbers of stator teeth and rotor poles, including different possible combinations of PM poles have been investigated [19-20] and identified as providing improved efficiency or minimisation of materials. Non-linear modelling of doubly salient PM machines was developed to analyse the effect of PM and armature field within the stator [18]. While there are benefits of doubly salient PM machines, when compared with alternative stator PM machine such as the flux reversal machine and switched flux machines [28] the ability to harness the magnetic flux to achieve higher torque density is limited by comparison.

1.2.2. Flux Reversal Machines

The flux reversal machine (FRM) was directly derived from the doubly salient PM machine, permitting bi-polar variation of flux linkage [21]. This design was then extended to a three phase arrangement [22] which proposed different stator slot, rotor pole combinations, investigated different arrangements of PM on the tooth surface and skewing to reduce cogging torque Fig. 1.7. For low speed applications arrangements of flux reversal machines with multiple PM poles per stator tooth have been investigated with potential inset magnets to

achieve flux focusing and reduced PM eddy current losses by reducing the armature field variation in the PM [29].

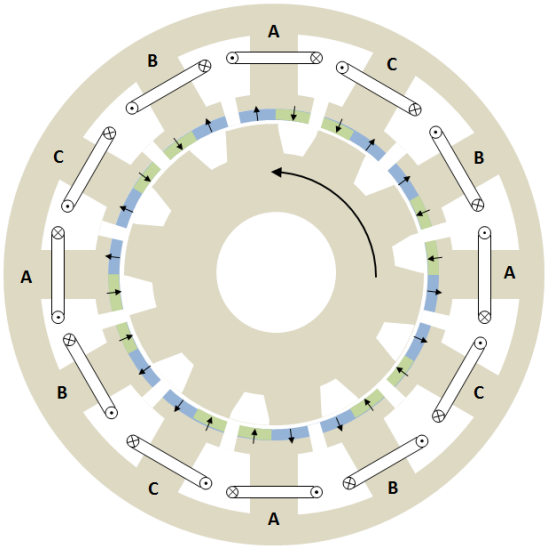

Fig. 1.7. An illustration of a flux reversal machine with 12 stator teeth, 1 PM pole pair per tooth and 10 rotor poles.

The flux reversal machine has been analysed from the perspective of an electrical gear, observing rotating airgap harmonics contributing to back EMF production, the gearing effect between the rotation of the salient rotor and the flux harmonics in the airgap [30]. Significant factors in the flux reversal machine are that the performance is impacted by the magnet thickness, when increased results in a longer effective airgap, also as the stationary PMs on the tooth surface are subjected to time varying armature fields there is potential demagnetisation and eddy current loss implications.

1.2.3. Switched Flux Machines

The switched flux permanent magnet (SFPM) machine Fig. 1.8, also known as the flux switching machine, has been extensively investigated since it was proposed in [24], initially explained from a linear U-core perspective with observation of the switching of the flux linkage alternating as the rotor position is displaced. The switched flux machine has been demonstrated for use at low speeds in hybrid electric vehicles [48] and compared with surface mounted PM generators for high speed applications [33]. The switched flux machine operates on the principle that through one period of rotation of the salient rotor, the coils would

experience a bi-polar flux linkage as was explained diagrammatically considering different rotor positions. The three phase switched flux machine was further analysed through the use of a lumped circuit model to predict airgap flux density, flux linkage, back EMF and ultimately electromagnetic torque [25].

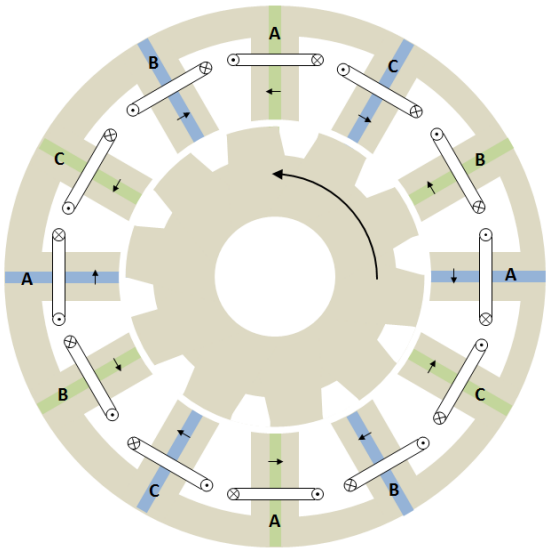

Fig. 1.8. An illustration of a switched flux machine with 12 stator teeth, 6 PM pole pairs and 10 rotor poles.

Conclusions for the optimal split ratio, stator and rotor tooth geometry were obtained and confirmed through finite element (FE) computation and again presented in [31]. The SFPM machine has been modelled with Fourier analysis [32], computing solutions to the magnetic field equations in different parts of the machine, shows good agreement with the linear FE solution, but cannot account for non-linear materials.

Comparison of the SFPM machine with other PM machine topologies has concluded that compared with the double salient PM machine [17] high power density is possible, the similarities and differences between the doubly salient machine and SFPM were compared in [28] in particular that a SFPM machine may have higher airgap flux density through flux focusing. Compared with a surface mounted PM machine [33] the SFPM shows the improvement in torque produced for the same DC copper loss, therefore the SFPM machine requiring lower current excitation to produce the same torque.

Analysis of the back EMF of the SFPM machine reveals the non-sinusoidal nature of the individual coils but the sinusoidal phase back EMF [34], also that the rotor tooth width may be optimised to reduce phase back EMF harmonics. Losses in SFPM machines are quite significant for different reasons, the iron loss is complicated by the introduction of minor loops into the flux loci [35], PM eddy current loss is significant due to the varying working points of the different PM through a rotation of the rotor [36], the PM eddy current loss may be reduced through removal some PM material adjacent to the airgap or through PM segmentation, eddy current losses in the conductors particularly as the stator slot opening is increased and the conductors are exposed to the rotor teeth [37]. Demagnetisation has been considered, as decreasing the thickness of the PM may increase the power density an analytical model to obtain limits for PM design also when considering short circuit currents was given in [38]. Cogging torque in SFPM machines was explored in [39] that the period of the cogging torque could be estimated from the least common multiple of stator poles and rotor teeth, but also the effect of manufacturing on the cogging torque plays a significant role as the modular nature of the stator teeth may lead to misalignment of the modules and intrusion into the airgap.

The combination of stator and rotor teeth and different winding configurations has been the topic of much literature. The initial three phase 12 stator slots and 10 rotor teeth design [24] was adapted from its concentrated wound, double layer winding to single layer windings [40] revealing that for 10 rotor teeth the difference in torque performance was small, but with different numbers of rotor teeth the electromagnetic torque could be increased. A model to predict the largest flux linkage for different rotors was given in [41] based on linear materials and an assumed sinusoid permeance function between the rotor and stator teeth. This model to predict the optimal number of rotor teeth has been extended to many different arrangements of SFPM machines Fig. 1.9.

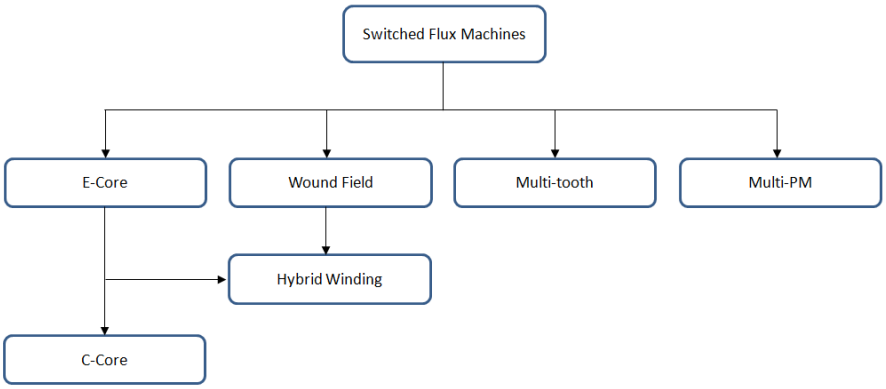

Fig. 1.9. Breakdown of different types of switched flux machines.

Conventional machines with single and double layer concentrated windings [41] have been investigated Fig. 1.8 and Fig. 1.10.

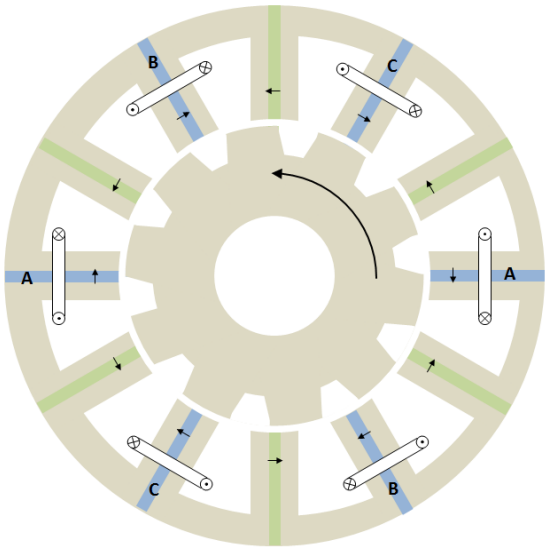

Fig. 1.10. An illustration of a switched flux machine with single layer windings, 12 stator slots, 6 PM pole pairs and 10 rotor poles.

E-core type machines with the removal of tooth PM for every other tooth [42] is shown in Fig. 1.11.

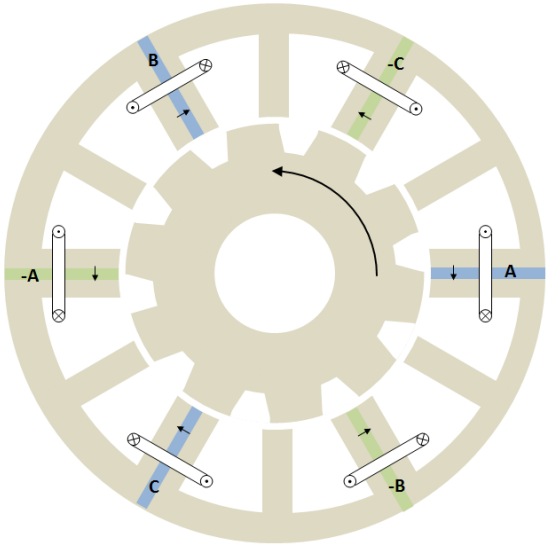

Fig. 1.11. An illustration of an E-core switched flux machine with 12 stator teeth, 3 PM pole pairs and 10 rotor poles.

The C-core with less stator teeth and large slot openings [43] is derived by removal of the E-core teeth that are not wound Fig. 1.12,

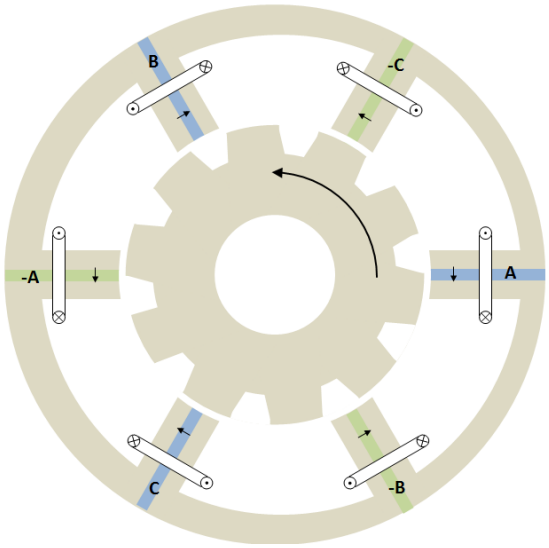

Fig. 1.12. An illustration of a C-core switched flux machine with 6 stator teeth, 3 PM pole pairs and 10 rotor poles.

and the multi-tooth machine with split stator teeth [44-45] is shown in Fig. 1.13.

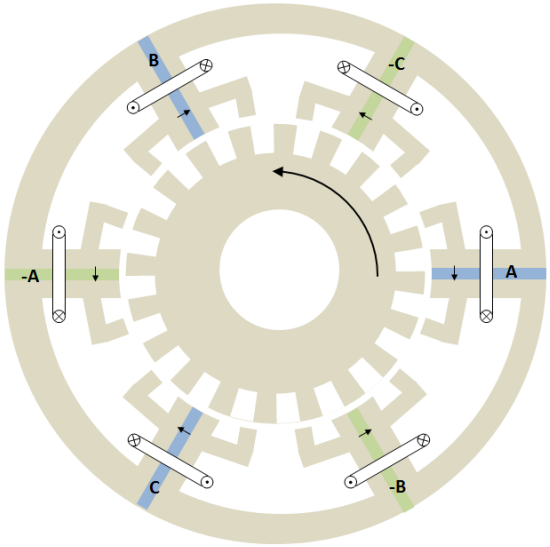

Fig. 1.13. An illustration of a multi-tooth switched flux machine with 6 stator teeth, 3 PM pole pairs, 20 rotor poles and 4 multi-teeth per tooth.

A method for winding machines with different numbers of rotor teeth has been derived for different numbers of phases [41], also that larger electromagnetic torque may be produced when the number of rotor teeth is close to the number of stator teeth, but when odd numbers of rotor teeth are considered there is potential for unbalanced magnetic force (UMF) [40]. A comprehensive study of stator slot opening has been performed both with FE and measured results [43].

Many other variations of the SFPM machine have been considered, with field wound [46] Fig. 1.14, where the PM material is replaced with DC windings to provide the static field linking the three phase winding. As exciting these coils contributes to the system copper loss this must be considered in the design in conjunction with the copper loss from the three phase winding. The inherent advantage of having a wound static field is the ability to adjust the field excitation during operation and hence weaken the field to increase the operational speed range.

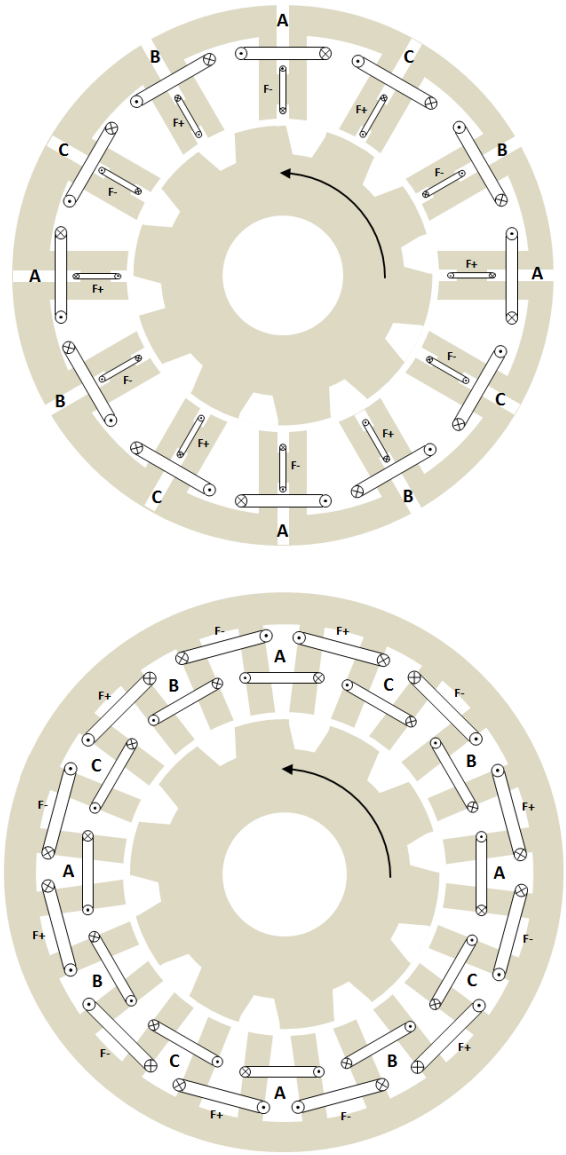

Fig. 1.14. An illustration of a wound field switched flux machine with 12 stator teeth, 12 DC field coils and 10 rotor poles.

Hybrid excitation by means of DC field windings placed on the middle E-core teeth [47] Fig. 1.15 combines the benefits of having a variable static field and permanent magnet field. The DC coils may be adjusted either to enhance or weaken the field and hence the back EMF as required at different speeds to achieve increased performance.

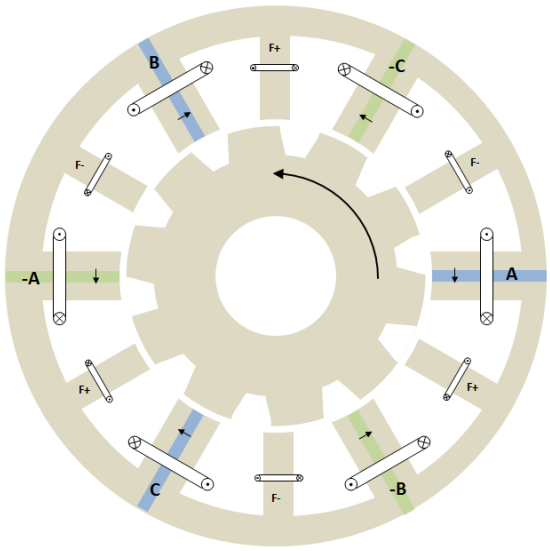

Fig. 1.15. An illustration of a hybrid excitation switched flux machine with 12 stator teeth, 3 PM pole pairs, 6 DC field coils and 10 rotor poles.

Multi-PM with each tooth containing two PM poles [48] is shown in Fig. 1.16, while this arrangement features increased torque density it suffers from significant cogging torque ripples unless skewed.

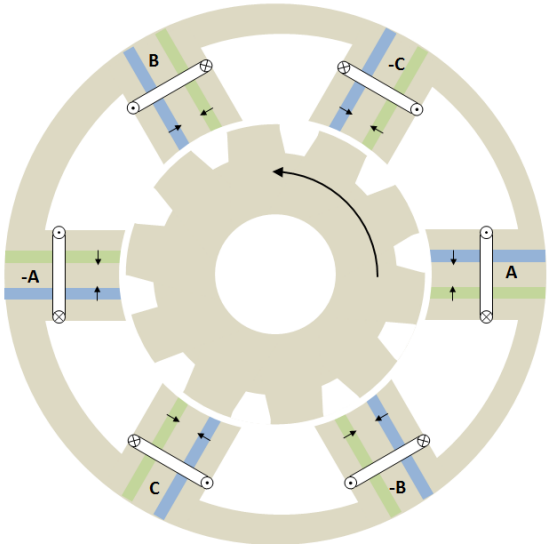

Fig. 1.16. An illustration of a multi-PM switched flux machine with 6 stator teeth, 6 PM pole pairs and 10 rotor poles.

A review of different switched flux PM machines has been given in [49] highlighting features of machines which utilise the switched flux principle.

1.3. Magnetic Gears

Fundamental to design of machines with PMs on the rotor is the magnetic field without coil excitation [5, 50] identifying components of the field that relate to fundamental back EMF [51] and those creating torque ripples and machine losses.

Magnetic gearing is the use of non-fundamental harmonics to produce constant torque which are a result of modulation of the field due to slotting. Such slotting harmonics have been observed in induction machines [52], where the effect of slot permeance introduces harmonics of different orders dependant on the fundamental harmonic and the number of slots. Harmonics that occurred due to slotting were observed through finite element modelling of an induction machine in [53] and further generally expressed for both stator and rotor slots in [54]. The effect of slotting in permanent magnet (PM) machines has been investigated in [55] and [50] and generally considered only for its parasitic effects such as cogging torque.

The gearing effect between two rotating elements through the use of magnetic coupling has been around for many years [56], a gear was then created using electromagnetic poles [57]. Through the use of PM material a magnetic gear with higher torque capacity was introduced in [15] and extended showing the procedure used to create this design in [58] through the modulation of the airgap field Fig. 1.17.

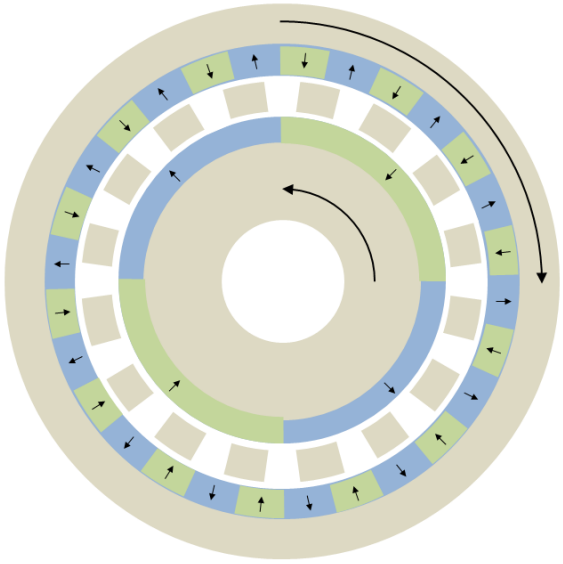

Fig. 1.17. An illustration of a magnet gear with 2 inner PM pole pairs, 16 modulating poles and 14 outer PM pole pairs.

A harmonic magnetic gear was developed in [15] as an alternative to the conventional mechanical gearbox. Its enhanced utilisation of permanent magnet (PM) material featured great improvements on previous magnetic gear topologies [59] that produced very low torque density and efficiency. A recent study compared the magnetic gear to a mechanical planetary gear [60], showing that the magnetic gear can have improved performance with the inherent benefits, such as lubrication is not required and overload protection. From the original design in [15], the relationship between the pole-pair numbers of inner and outer PM rotors was presented [58] Fig. 3.1. It was shown that for the same magnetic gear, it would result in a higher gear ratio with the outer rotor fixed while the inner PM and ferromagnetic rotors rotating Fig. 1.18.

Table I. Different gear ratio options for a harmonic magnetic gear

$\omega_s = 0$	$\omega_l = 0$	$\omega_h = 0$
$G_r = -\frac{p_l}{p_h}$	$G_r = \frac{n_s}{p_h}$	$G_r = \frac{n_s}{p_l}$

n_s = Number of ferromagnetic pieces
p_h = High speed (inner rotor) pole pairs
ω_l = Low speed rotor's angular velocity
p_l = Low speed (outer rotor) pole pairs
ω_s = Ferromagnetic poles angular velocity
ω_h = High speed rotor's angular velocity

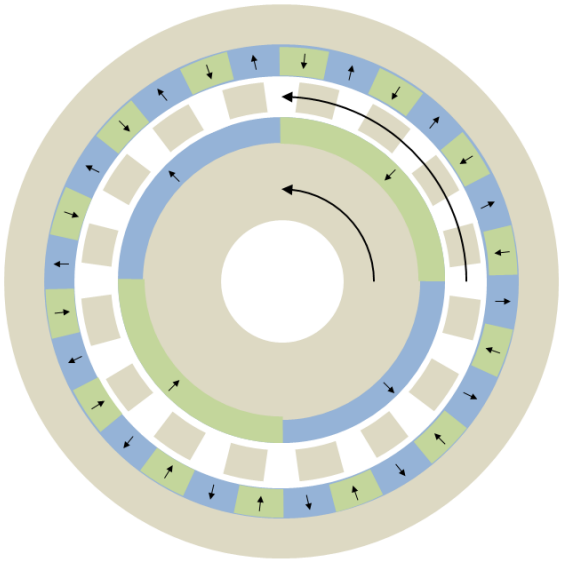

Fig. 1.18. An illustration of a magnet gear with 2 inner PM pole pairs, 16 modulating poles and 14 outer PM pole pairs with rotating modulating poles.

Optimisation of individual parameters to produce maximum torque, for a fixed ferromagnetic rotor, was shown in [61] and investigation of pole and ferromagnetic piece combinations in [62]. Analysis of a gear with an interior PM inner rotor was carried out in [63], providing insight into the static torque capacity of the magnetic gear, where a relative displacement of 90° (considering one cycle as twice the pole pitch) between the two rotating bodies would provide the maximum torque coupling for this type of gear.

The opportunities of this harmonic magnetic gear arrangement are the removal of mechanical transmission of torque between the rotating bodies provides mechanical isolation and protection in a situation where a sudden gear loading would have caused failure. As there is no mechanical coupling of torque between bodies the need for lubrication is removed.

1.4. Magnetic Geared Machines

From the magnetic gearing principle many novel machine designs have been developed based on the inclusion of a magnetic gear within a brushless PM machine. These machine designs have either incorporated a complete magnetic gear with two arrays of PM, such as the pseudo direct drive [64] and the magnetically geared machine with three airgaps [65], or where one of the two arrays of PM in a magnetic gear has been replaced by an armature winding, which have been termed magnetic geared [66] or flux modulated [67]. The vernier PM machine [68] has been noted for its magnetic gearing effect [69] and further connected with the magnetic gearing principle from the geared machine or flux modulated machine [70-72]. Two main strands of PM machines including the magnetic gearing principle have emerged, those with multiple airgaps (Pseudo direct drive, continuously variable transmission and double rotor machines) and with single airgap (magnetic geared and harmonic machines), which have been aligned with vernier PM machines Fig. 1.19.

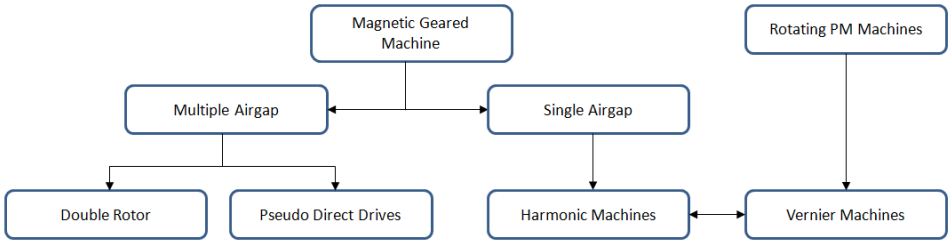

Fig. 1.19. Magnetic geared machine topologies linked with vernier PM machines.

1.5. Multiple Airgap Geared Machines

The first application of the magnetic gear principle was to include a harmonic magnetic gear in its entirety into a brushless PM machine [65]. This arrangement included a wound stator, stationary modulating ring with a PM rotor either side of the modulating ring Fig. 1.20, while this application of the harmonic gear demonstrated its potential to increase torque at low speed, the three airgaps and two rotating components prove complicated mechanically.

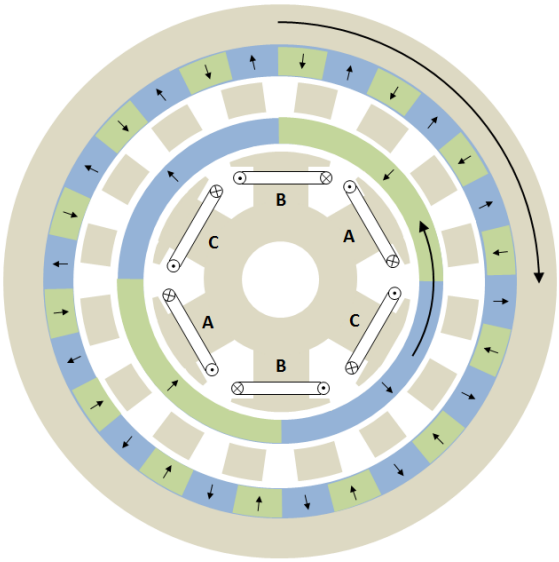

Fig. 1.20. An illustration of a magnet geared machine with 6 stator teeth, 2 inner rotating PM pole pairs, 16 stationary modulating poles and 14 rotating outer PM pole pairs.

A second integration of the magnetic gear within a brushless PM machine is the pseudo direct drive [64, 73], this machine type has two airgaps and utilises the modulating ring as the low speed output Fig. 1.21.

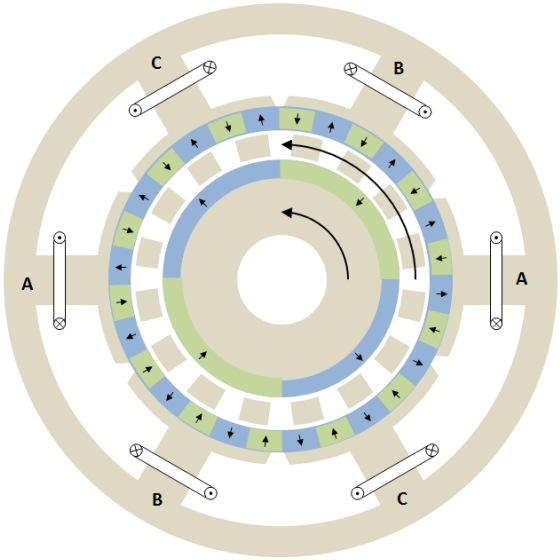

Fig. 1.21. An illustration of a pseudo direct drive machine with 6 stator teeth, 2 rotating inner PM pole pairs, 16 rotating modulating poles and 14 outer PM pole pairs.

The torque is transmitted through in the inner high speed PM rotor between the machine and gearing. The equivalent gear ratio of the inner PM rotor and modulating poles provides a high torque density of the system, for which airgap flux density harmonics have been identified and explained. For this type of machine with a magnetic gear it has been highlighted that an amount of torsional oscillation between the rotors may occur and an observed based feedback control method may significantly reduce this effect [74].

Another application of this multiple airgap magnetic geared machine is to operate as a variable speed transmission, using two of the magnetic gear rotors to transmit torque the third is rotated by a PM machine to adjust the gearing ratio between the other rotors [75] for hybrid electric vehicle and wind power applications.

1.6. Single Airgap Geared Machines

The second type of integration of magnetic gearing within PM machines replaces one of the PM rotors by using a time varying armature winding field to create the required harmonics that would occur due to the PM rotor Fig. 1.22.

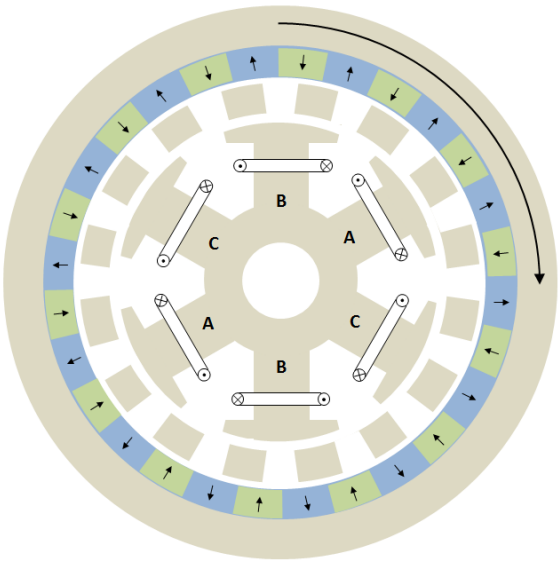

Fig. 1.22. An illustration of a harmonic magnetic geared machine with 6 stator teeth, 16 stationary modulating poles and 14 rotating PM pole pairs.

These machines include a stationary modulating ring which is placed adjacent to the wound stator and a lower number of PM poles on the rotor output interacting with the modulated armature field, this machine type are therefore termed a harmonic machine [76]. This machine geometry was seen to be almost identical to a vernier machine [68-69] Fig. 1.23,

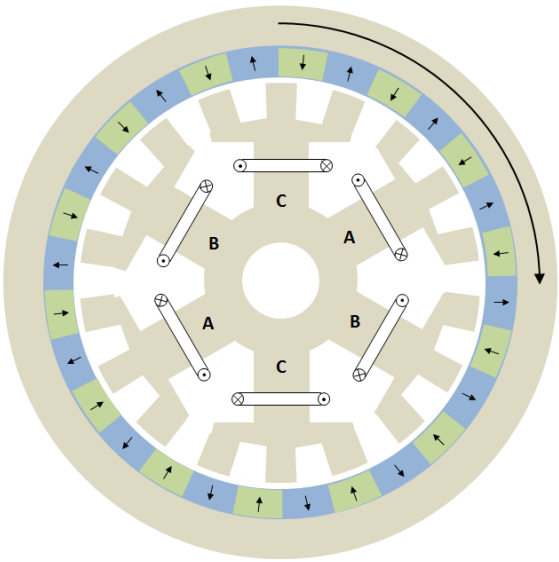

Fig. 1.23. An illustration of a vernier machine with 6 stator teeth, 3 modulating poles per tooth and 14 rotating PM pole pairs.

Hence, these two areas of research were linked [70-72].

1.7. Research Scopes and Contributions

This research identifies a fundamental relationship between switched flux PM machines and magnet gears, permitting the development of a novel machine concept that incorporates a magnetic gear salient rotor structure to switched flux machine design and thus the ability to partition windings and magnets across two stationary bodies Fig. 1.24.

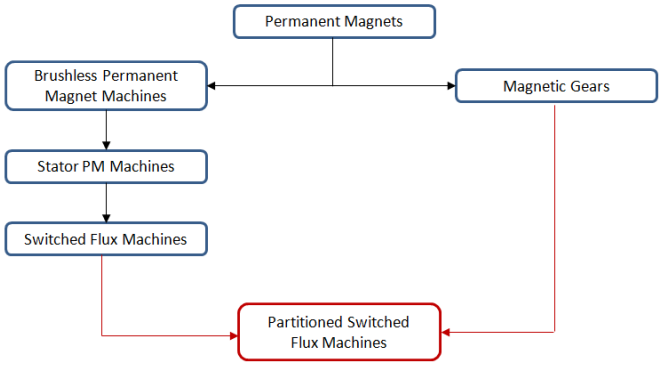

Fig. 1.24. Link between switched flux machines and magnetic gears to create the PS-SFPM machine.

The novel PS-SFPM machine is investigated, analysed and prototyped to validate the concept. With development this machine topology demonstrates the potential of joining two fields of research to produce new concepts providing new opportunities when applying permanent magnet materials to rotating machine applications.

The major contributions of this research are:

- The presentation of a novel brushless permanent magnet machine that combines two previously distinct areas of research being switched flux permanent magnet machines and magnetic gears
- Insight into the opportunities arising from this new machine topology particularly mechanical field weakening
- Investigation into aspects of the novel machines design, considering parasitic effects and design with different slot / pole combinations
- The potential to extend the connection between alternative types of stator permanent magnet machines utilising the magnetic gearing principles

The connections between all the machine and gear types discussed are shown in

Fig. 1.25 to show the relationships between many different topologies. This includes the main focus of this research the PS-SFPM machine, but also include future potential based on the connection between magnetic gears and stator PM machines which was achieved during this research.

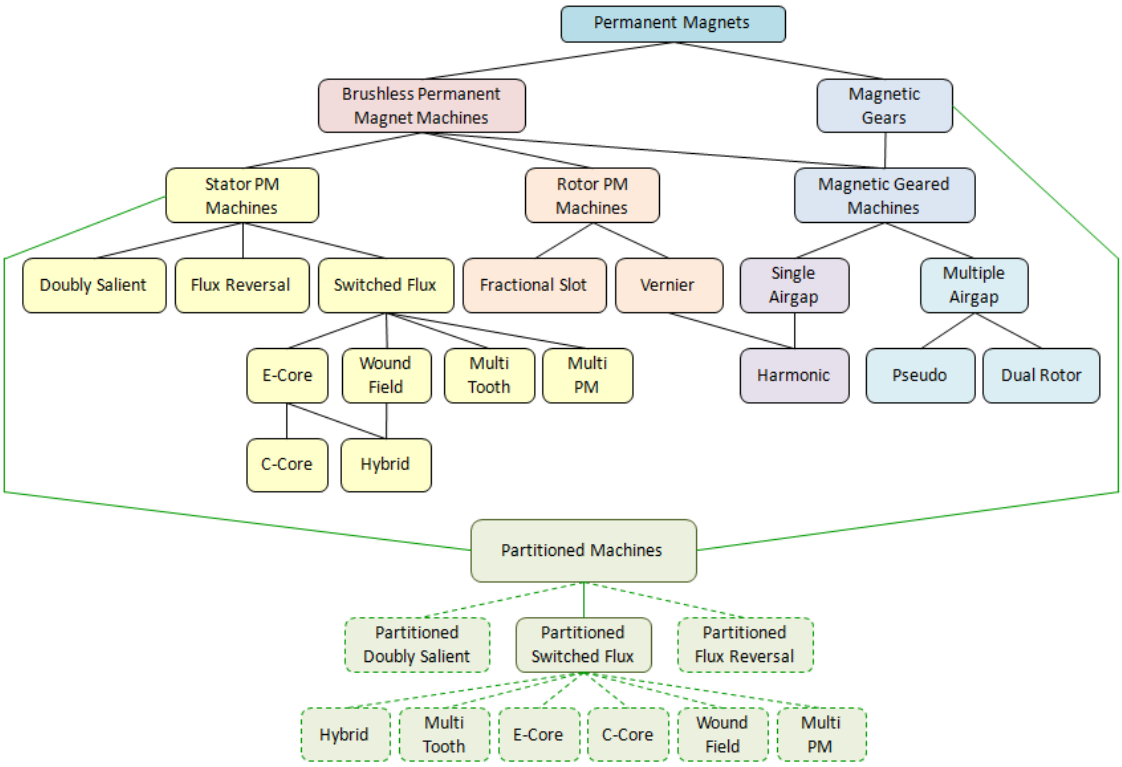

Fig. 1.25. Permanent magnet machines and gears topology map.

1.8. Thesis Outline

Chapter 1: ***Introduction***

Introduction to brushless PM machines and magnetic gears to provide context for research performed.

Chapter 2: ***Partitioned Stator Switched Flux Permanent Magnet Machines***

The concept of a PS-SFPM machine is introduced and optimised. Characteristics such as torque density and cogging torque are investigated; a prototype machine produced and compared with FE predicted data.

Chapter 3: ***Partitioned Stator Switched Flux Permanent Magnet Machines with Alternate Tooth Windings***

Alternative tooth windings are an area of interest in non-overlapping brushless machines and have been considered for switched flux machines, they are applied to the PS-SFPM machine.

Chapter 4: ***Mechanical Flux Weakening of Partitioned Stator Switched Flux Permanent Magnet Machines***

The PS-SFPM machine provides opportunity for mechanical flux weakening by adjustment of the angle between stators to achieve wider speed range.

Chapter 5: ***Parasitic Effects in Partitioned Stator Switched Flux Permanent Magnet Machines***

Losses and unbalanced forces occurring in the PS-SFPM machine are considered for machines with all and alternate tooth winding topologies.

Chapter 6: ***General Conclusions***

Summary of research and findings, with recommendations of continuing research

Appendix I: ***Global Optimisation of Partitioned Stator Switched Flux Machines***

Global optimisation of the PS-SFPM machines using FE

Appendix II: ***Influence of Design Parameters on Magnetic Gears Torque Capability***

Magnetic gear investigation, considering gear ratio and torque capability

Appendix III: ***Optimal Torque Matching of a Magnetic Gear within Brushless PM Machines***

Matching of the torque density of a magnetic gear within a brushless PM machine

Appendix IV: ***Switched Flux Permanent Magnet Machines with Tooth Tapering***

Adjustment to a switched flux PM machine to increase slot area and reduce iron saturation and ultimately increase torque density compared to conventional switched flux machines

CHAPTER 2 - PARTITIONED STATOR SWITCHED FLUX PERMANENT MAGNET MACHINES

2.1. Introduction

A novel permanent magnet (PM) machine topology is presented which combines the synergies of two distinct directions of PM machine design, i.e. magnetically geared machines and switched flux machines.

Magnetic gearing is torque transmission achieved between two rotating bodies through magnetic forces rather than through mechanical interaction, which has been most effectively realised in gears using modulation of airgap flux density. The notion of constructing a gear of magnetic form was suggested in [77] and multiple magnetic gear arrangements presented in [56], further electromagnetic implementation of a magnetic gear device with armature windings providing magnetic poles was developed in [57]. Unity gear ratio couplings were proposed in [59] and [78], but suffered low torque transmission as the interaction between magnetic bodies was restricted to a fraction of the total PM surface.

Recent developments in magnetic gearing feature enhanced utilisation of PM material and benefit from rare-earth magnets, therefore achieving superior torque transmission using salient pole structures in the airgap [15, 58]. This realisation of a higher torque density magnetic gear [15], with mechanical isolation providing inherent overload protection featuring low noise and vibration, inspired further research producing analytical models for harmonic magnetic gears [79], interior PM alternatives, providing flux focusing to achieve higher airgap flux density [63, 80-82], linear [83-84] and axial flux arrangements [85].

Naturally magnetic gears progressed into brushless PM machine topologies with magnetic gear features incorporated within conventional machine structures. These magnetically geared machines fall into two categories, those with complete magnetic gears included, i.e. two arrays of PM, a modulating element and machine stator [64-65, 86] achieving high torque densities but requiring large volume of PM material. The second geared machine type features a PM

array of the magnetic gear substituted by a winding MMF, thus including only a single array of PM while incorporating the magnetic gear effect [66-67, 76, 87]. This geared machine arrangement with a single array of PM has been united with vernier PM machines [70-71] with the stationary modulating element affixed to the stator teeth.

The second synergy, within PM machine design, applied to produce the PS-SFPM machine is the switched flux PM machine Fig. 2.1a. Switched flux machines, also known as flux switching machines, were developed from simple flux-switch alternators, with the PM located within the teeth [16]. The basis of recent investigations of switched flux machines continued from the three phase arrangement of flux-switch alternator presented in [24]. Analysis of the switching flux machine has been performed using lumped magnetic circuit models [25] and finite element analysis to determine the relationship between geometric parameters and torque production [31]. The switched flux machine is beneficial for easier heat dissipation in the PM on the stator [25]. Simple lumped circuit models have been used to predict optimal combinations of stator and rotor teeth [41] and particularly winding connections for multiphase machines with different winding configurations.

Different topologies of switched flux machines have been proposed, such as, E-core [42] and C-core [43] to increase slot area and reduce PM volume while maintaining high torque density, and multi-tooth designs [44] by splitting the stator teeth to increase the number of teeth along the airgap surface, thus reducing the PM volume and increasing the number of rotor poles, but suffering from higher magnetic circuit saturation with current increase. Parasitic effects are investigated including PM eddy current loss reduction through PM segmentation [36], total losses in C-core and E-core machines at rated power are lower than conventional switched flux machines [37], the effect of manufacturing tolerances on cogging torque [39], cogging torque suppression through current injection [88] and PM demagnetization withstand ability under fault conditions [38]. The switched flux machine has been compared with interior [89] and surface [33] mounted brushless PM machines revealing

switched flux machines to have comparable if not increased performance compared with conventional PM topologies.

The proposed PS-SFPM machine Fig. 2.1b may be understood from two perspectives, as a magnetically geared machine with inner stationary PM, rotating iron poles and outer stator's armature field or as a switched flux machine with the PM removed from within the stator teeth, and placed within a secondary stator.

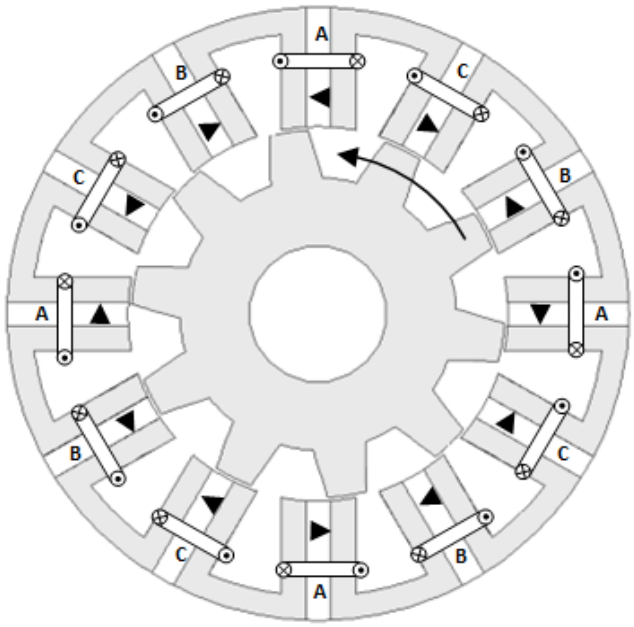

(a)

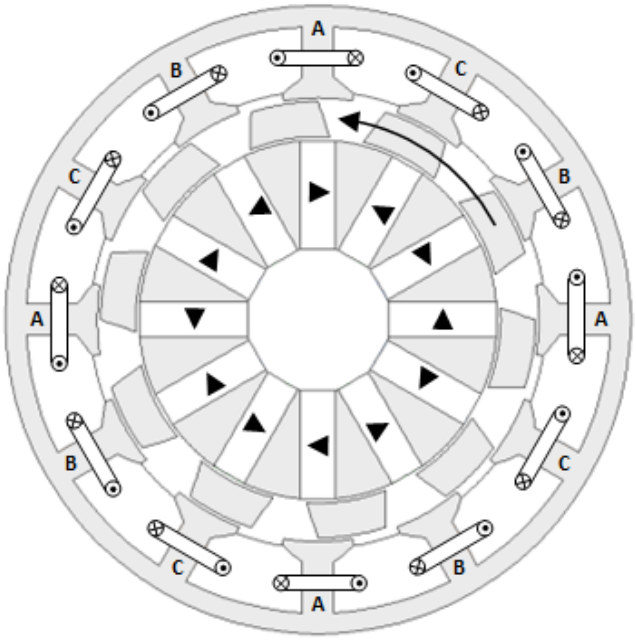

(b)

Fig. 2.1. 12/10 Slot/Pole (a) conventional and (b) PS-SFPM machines

Magnetic geared machines with stationary PM have been briefly investigated [66] as a alternative to rotating the PM rotor, but dismissed as their torque ripple increased compared with rotating PM operation. The PS-SFPM machine differs considerably from previous magnetically geared machines since the number of PM poles is equal to the number of stator teeth, which with PM rotation exhibits extremely large cogging torque, therefore would be generally neglected as feasible combinations of stator teeth and PM poles. By utilising equal number of PM poles and stator teeth and interior mounted PM, the flux focusing effect, which is an advantage in the switched flux machines, is maintained.

The new machine benefits from the removal of trade-off between PM and armature winding space on the stator, allowing for increased copper and PM volume within the same machine volume to increase torque density. While in switched flux machines the temperature rise in the PM may be managed, in this machine the separation of PM and armature windings allows the PM to be cooled on a stationary body removed from the hot copper windings.

In this chapter, the evolution of the PS-SFPM machine and structure is presented. Different numbers of rotor poles and winding configurations are investigated, together with optimisation of geometric machine parameters to achieve maximum torque density. Machine performance with different numbers of rotor poles is compared with conventional switched flux machines including torque, torque ripples, back EMF and inductances.

2.2. Machine Evolution and Structure

The switched flux machine has been shown to achieve torque densities comparable to conventional brushless PM machine topologies [33]. By virtue of this topology constraining the PM and windings to the stator, a trade-off between copper, PM and stator iron materials occurs within the stator volume, rather than the entire machine volume for a machine with PM on the rotor. As observed in [90], many designs presented in literature often compromise on volume of iron to maximise PM and copper volumes achieving higher torque density at the expense of saturating the iron, particularly in the stator teeth and back iron.

The PS-SFPM machine Fig. 2.1b was evolved as a solution to the conflict in switched flux machines between PM, copper and stator iron. By separating the PM and copper, but maintaining the switched flux action, the conflict between PM, copper and iron returns to the situation in conventional brushless PM machines where the airgap diameter determines the ratio of magnetic and electric loading [91].

To achieve the separation of PM and copper, the iron rotor pole structure used in harmonic magnetic gears [15] is applied to switched flux machines. Considering the flux passing through a single coil in a conventional switched flux machine Fig. 2.2a, when the PM is placed within the rotor on a separate stationary body Fig. 2.2b, the flux path is maintained by reversing the magnetisation direction.

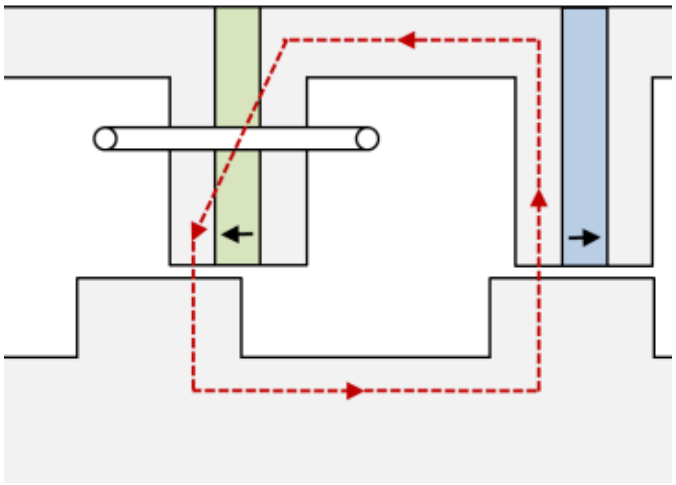

(a)

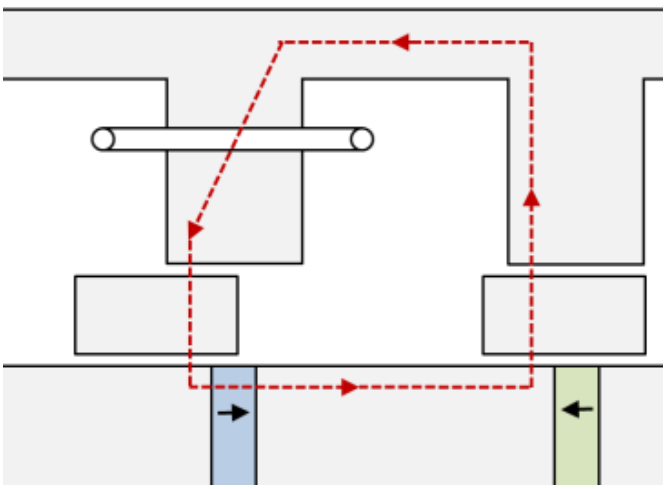

(b)

Fig. 2.2. Flux path and PM magnetisation direction. (a) Conventional and (b) PS-SFPM machines.

For the PM to be placed as shown in Fig. 2.2b a second airgap must be introduced between the salient rotor poles and secondary PM stator. The structure of the rotor, which in conventional switched flux machines is very similar to that of a switched reluctance rotor is now analogous to a magnetic gear's modulating rotor. In order to maintain the direction of flux as in a conventional switched flux machine, the magnetisation direction of the PM associated with an individual tooth is circumferentially reversed as the PM is placed so as to produce the same direction of flux within the magnetic circuit.

The switched flux action of the PS-SFPM machine is demonstrated by considering the open-circuit flux linking an individual coil in a 10 rotor pole machine. The distribution of flux through a single coil is presented in Fig. 2.3, with position A having maximum positive flux linking the coil, B and D having no flux through the single coil and C having maximum negative through the single coil. As the rotor passes the north and south poles of the PM the connection is made positive and negative to the same single stator tooth thus producing bi-polar flux linkage shown in Fig. 2.4.

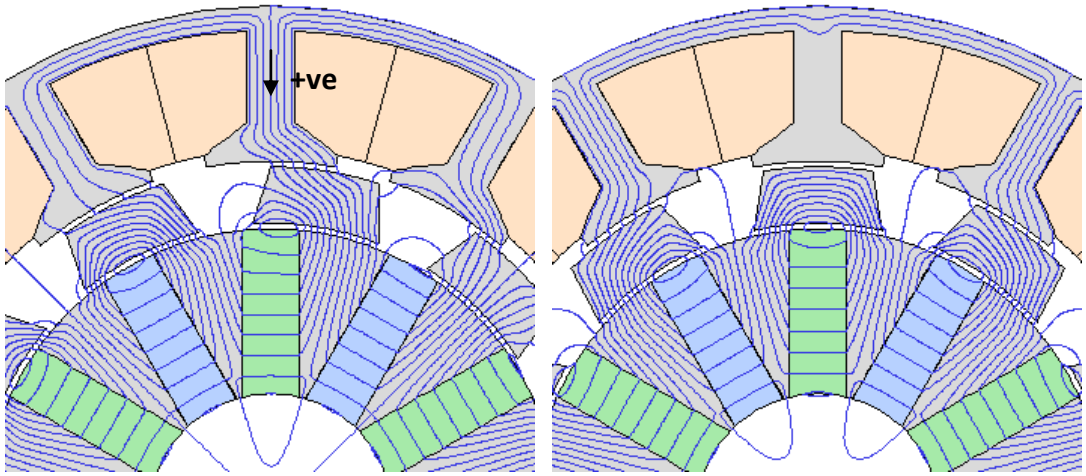

(a) (b)

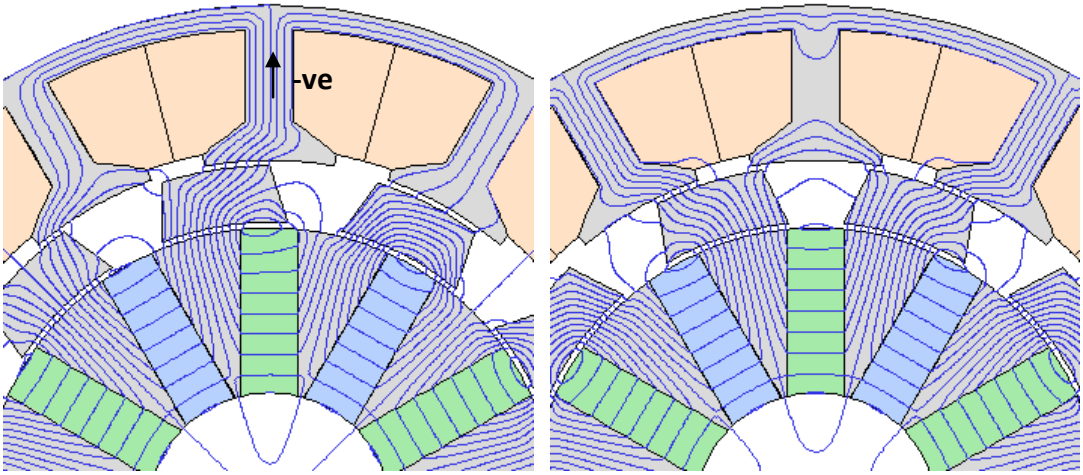

(c) (d)

Fig. 2.3. Open-circuit flux plots for PS-SFPM machine with 10 rotor poles at different rotor positions.

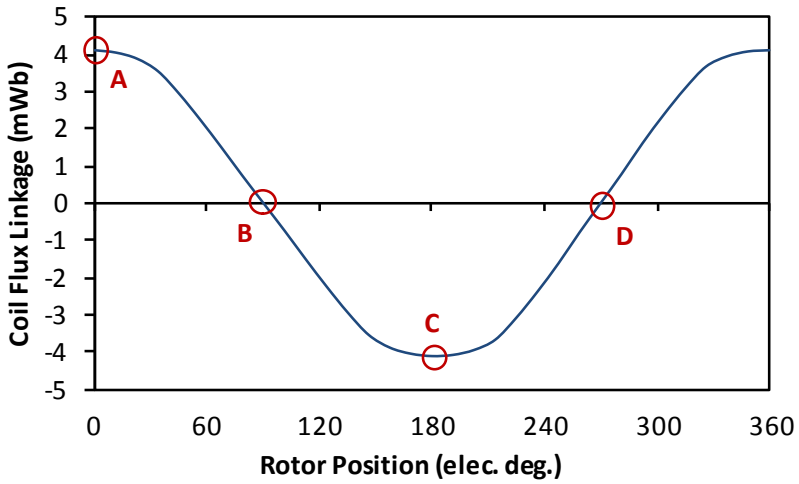

Fig. 2.4. Variation of flux linkage in a single coil of a PS-SFPM machine.

The concept of d and q axes is generally applied to rotating PM machines as a reference frame for the rotor position. As the PMs are not rotating in the PS-SFPM machine, the direct analogy of PM pole flux defining the d-axis no longer applies. Therefore the d-axis is defined, as for switched flux machines [47], where the maximum flux linkage occurs (Point A, Fig. 2.4) and the q-axis leading by 90 electrical degrees (Point D, Fig. 2.4). This is the definition used for d and q axes throughout this thesis.

2.3. Optimal Number of Rotor Poles and Windings Arrangements

Theoretically any number of rotor poles would produce alternating flux linkage in each stator tooth as high and low reluctance paths are experienced between the north and south

PM surface and a single stator tooth. The effective flux linkage is dependent on the number of rotor poles [41]. The stator slot opening and rotor pole arc are important as they determine the variation of reluctance between the PM and stator teeth [43].

To obtain the ability of different numbers of rotor teeth to achieve back EMF and ultimately torque production, the magnitude of the fundamental order of back EMF in a single coil is predicted using finite element methods (FE) with linear materials, for different numbers of rotor poles and 12 stator teeth. The fundamental coil back EMF variation with rotor pole number and different stator slot opening ratios (ratio of slot opening to tooth pitch) is shown in Fig. 2.5. The back EMFs obtained are normalised based on the maximum EMF with 12 rotor poles, to provide comparison independent of speed and number of winding turns for different numbers of rotor poles.

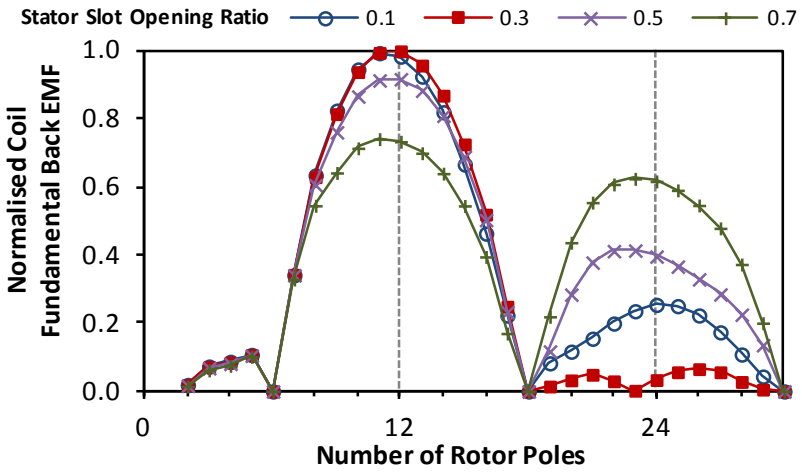

Fig. 2.5. Influence of rotor poles on optimal fundamental back EMF production.

From this simulation data the optimal number of rotor poles for maximum fundamental back EMF in a single coil is when the number of rotor poles is equal to the number of stator teeth, which is also concluded for fractional slot PM machines [92]. It is observed that sub-optimal coil back EMF is also achieved close to multiples of the number of stator teeth, with large slot openings. Therefore, it is seen that optimal back EMF is obtained when the number of rotor poles N_r is a multiple k of the number of stator teeth N_s (1):

$$N_r = kN_s \tag{1}$$

The back EMF is minimal when the number of rotor poles lies between two multiples of stator teeth, as these numbers of rotor poles short circuit the PM at maximum and minimum flux linkage positions, (2):

$$N_r = kN_s + \frac{N_s}{2} \tag{2}$$

The slot opening ratio is investigated for machines with rotor poles numbers with multiples of stator teeth, Fig. 2.6, lower multiples of stator teeth i.e $N_r = N_s$ achieve higher overall back EMF. Higher numbers of rotor poles favour larger stator slot openings as the stator tooth arc is closer to the rotor pole arc reducing flux leakage in adjacent rotor poles. The optimal stator tooth arc is close to 1.5 times the rotor pole arc, for example with 12 rotor teeth the rotor arc is 0.5 times the stator tooth pitch and the optimal stator tooth arch is 0.75 the stator tooth pitch.

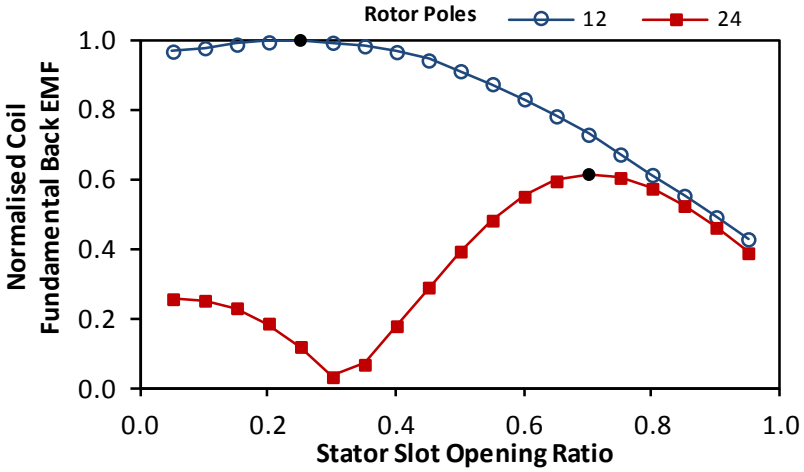

Fig. 2.6. Influence of slot opening on optimal fundamental back EMF production.

While 12 and 24 rotor poles produce the optimal and sub-optimal back EMF production respectively, the back EMF in every coil is in phase and therefore only suitable for a single phase machine design. Single phase machines inherently suffer from large torque ripples as the number of salient rotor poles compared to the number of PM poles is a multiple. Single phase machines also require particular design for starting and therefore numbers of rotor poles which enable a three phase design are pursued further in this thesis.

Based on the FE simulation results (Fig. 2.5) three phase PS-SFPM machines with $N_r = kN_s \pm 1$ achieve higher fundamental back EMF than those with $N_r = kN_s \pm 2$, as the number of rotor teeth approaches a multiple of stator teeth. This data shows that the PS-SFPM differs from the conventional switched flux machine as $N_r = kN_s - 1$ achieves higher back EMF than $N_r = kN_s + 1$.

In PM machines double and single layer windings also known as all and alternate tooth windings are now employed in PS-SFPM machines with different numbers of rotor poles.

As the PS-SFPM machine combines both magnetically geared and switched flux machine principles, the electrical angle between coil vectors are obtained from both perspectives. From the magnetic gearing principle the number of effective pole pairs p' occurring in the outer airgap adjacent to the stator is obtained by the number of PM pole pairs p and the number of modulating poles N_r [58]. Therefore the relationship between mechanical α_m and electrical α_e angle is (3):

$$\alpha_e = |p - N_r|\alpha_m \tag{3}$$

According to switched flux machine design, the electrical angle is (4), where N_r is the number of rotor poles [41].

$$\alpha_e = N_r\alpha_m \tag{4}$$

In switched flux machines with three phases, opposite vectors are reversed to determine the final winding configuration, thus the concluded winding connection is identical from both perspectives. For example, PS-SFPM machines with 10 and 11 rotor poles are shown in Fig. 2.7 and coil EMF vectors in Fig. 2.8, machines with 14 rotor poles share the same winding connection as that of a machine with 10 rotor poles with reversed phase sequence, i.e. phase B and C are reversed, and 13 rotor poles shares with 11 rotor poles respectively.

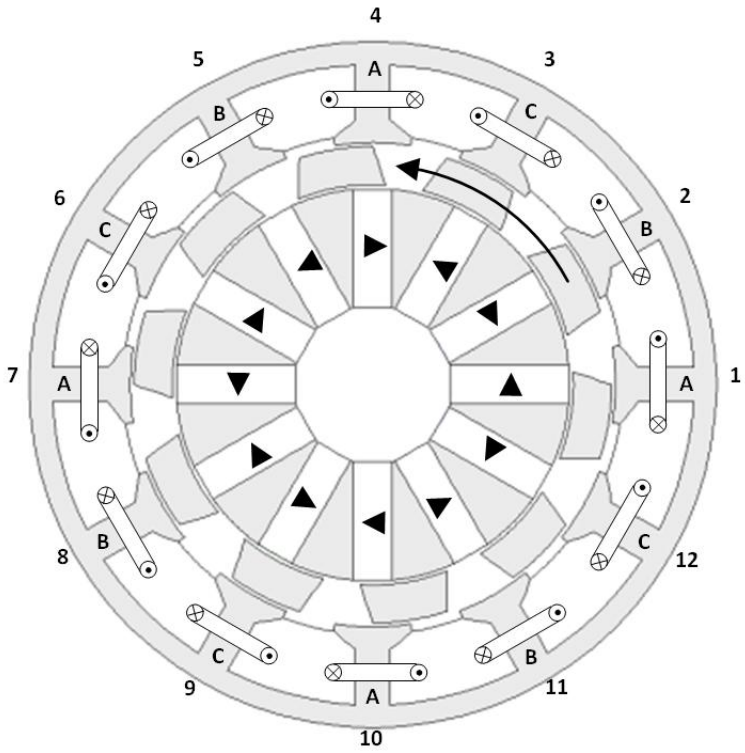

(10 rotor poles)

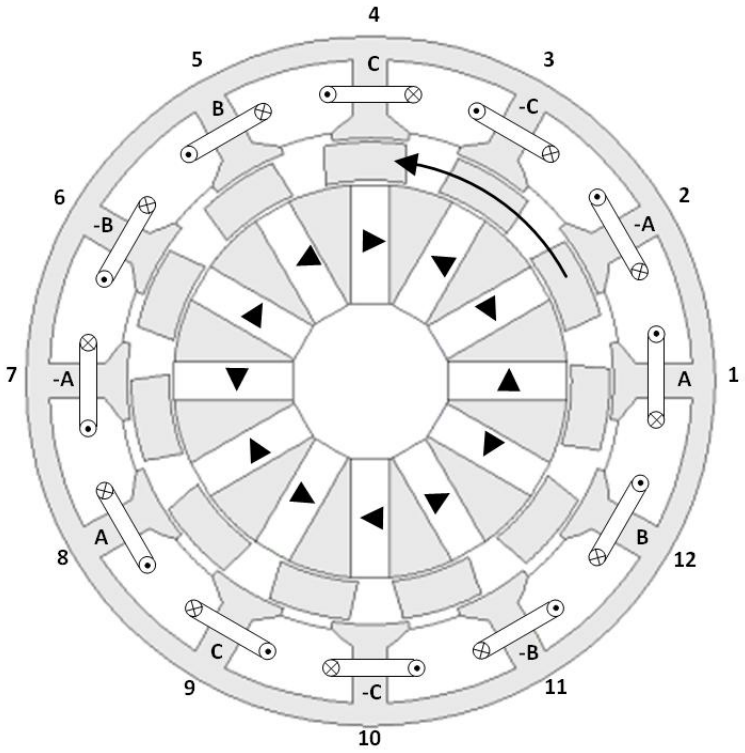

(11 rotor poles)

Fig. 2.7. Machine winding connections with 10 and 11 rotor poles.

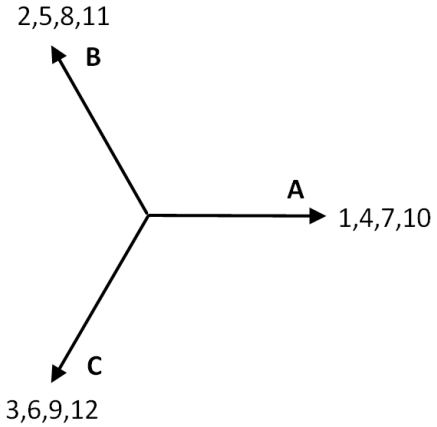

(10 rotor poles)

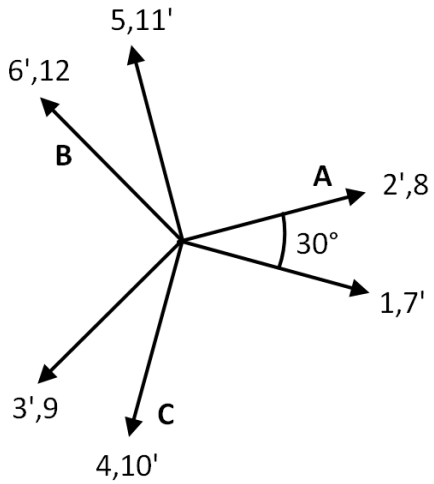

(11 rotor poles)

Fig. 2.8. Coil EMF phasors for with 10 and 11 rotor poles.

In Fig. 2.7 the machine with 11 rotor poles has an angular shift between coils of the same phase thus resulting in a distribution factor less than one. In general, the distribution factor may be expressed as (5) where *Q* is the number of EMF phasor per phase, *v* is the EMF harmonic order and *α* is the angle between two EMF phasors.

$$k_d = \frac{\sin\left(Qv\alpha/2\right)}{\mathrm{Q}\,\sin\left(v\alpha/2\right)} \tag{5}$$

2.4. Optimisation of Design Parameters

Four PS-SFPM machines for three phase operation are optimised for maximum torque density considering the influence of geometric parameters on the machine performance. This

optimisation uses non-linear material FE, as do all subsequent FE simulations in this thesis, the iron laminations are transil300 with a knee point of 1.6T and the PM material is a rare earth magnet NdFeB with a remanance of 1.2T . Three phase machines with 10, 11, 13 and 14 rotor poles are investigated as have been shown to have the highest fundamental coil back EMF for different stator slot openings and suitable for three phase connection.

A schematic of the geometry for the PS-SFPM machine is shown in Fig. 2.9 and parameters defined in Table II.

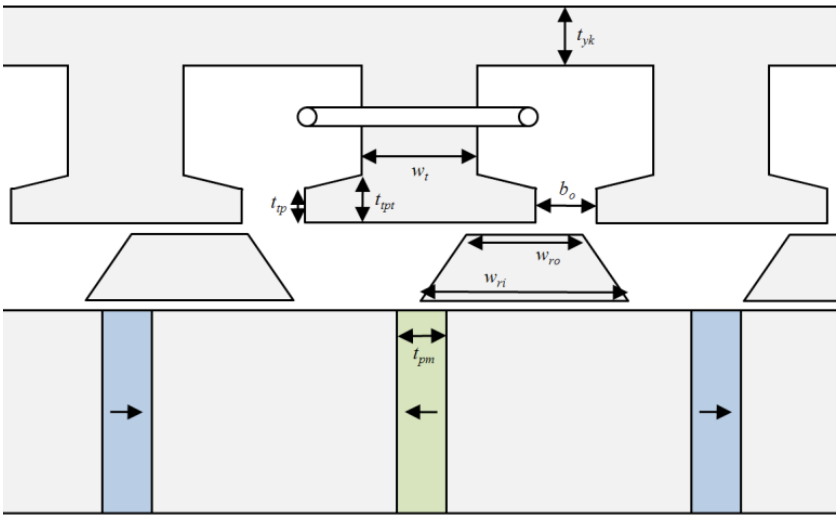

Fig. 2.9. Linear illustration of PS-SFPM machine and major geometric parameters.

Table II. PS-SFPM parameters.

Parameter	**Symbol**
Stator yoke thickness	t_{yk}
Stator tooth width	w_t
Stator slot opening	b_o
Stator tooth tip thickness	t_{tp}
Stator maximum tooth tip thickness	t_{tpt}
Rotor outer width	w_{ro}
Rotor inner width	w_{ri}
PM stator PM thickness	t_{pm}

As a basis for the optimisation the predicted copper loss is constrained and maximum torque obtained, as at low speed the copper loss may be considered as the main contribution of loss. In order to maintain the copper loss for different machine geometry, particularly as the

split ratio changes and therefore the slot area, the phase resistance R_{ph} must be constrained (6):

$$R_{ph} = \frac{4\rho(l_a + l_{ew})mN_{ph}{}^2}{A_s k_p N_s} \tag{6}$$

where, l_a is the active lamination length, l_{ew} end winding length, N_s number of stator teeth, N_{ph} number of turns per phase, A_s single slot area, k_p copper packing factor, m number of phases and ρ copper conductivity (1.68×10^{-8} Ωm). Hence, the number of phase turns N_{ph} is increased proportionally to the slot area A_s to fix the copper loss at the same rated current (7).

$$N_{ph} \propto \sqrt{A_s} \tag{7}$$

For the PS-SFPM machine the split ratio is defined as ratio of the stator bore radius that is the outer airgap R_{gi} to the outer machine radius R_o (8).

$$S_r = \frac{R_{go}}{R_o} \tag{8}$$

As the split ratio is varied with fixed copper loss and varying tooth width to maintain unsaturated stator teeth, the rated torque is compared in Fig. 2.10 for different rotor poles. More rotor poles favour higher split ratio with 11 achieving the highest rated torque.

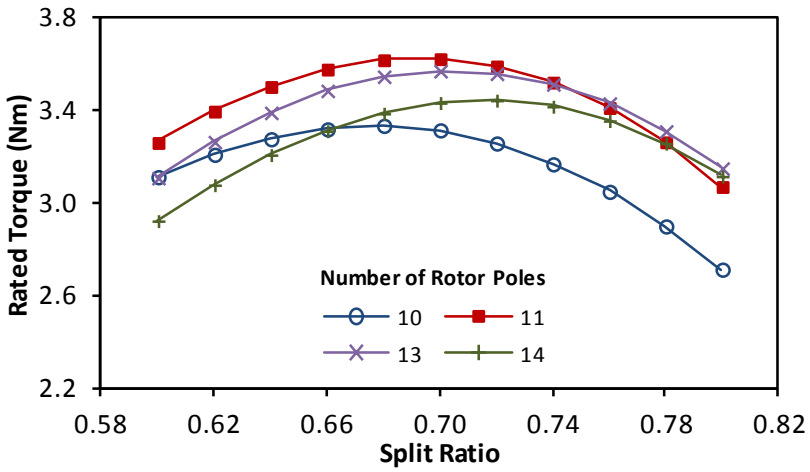

Fig. 2.10. Variation of torque with split ratio for 12 stator teeth with different numbers of rotor poles.

Slot opening ratio has been investigated in the previous section for a machine with 12 rotor poles, now for different three phase machines it is considered. Again as with split ratio, higher numbers of rotor poles favour wider slot openings Fig. 2.11.

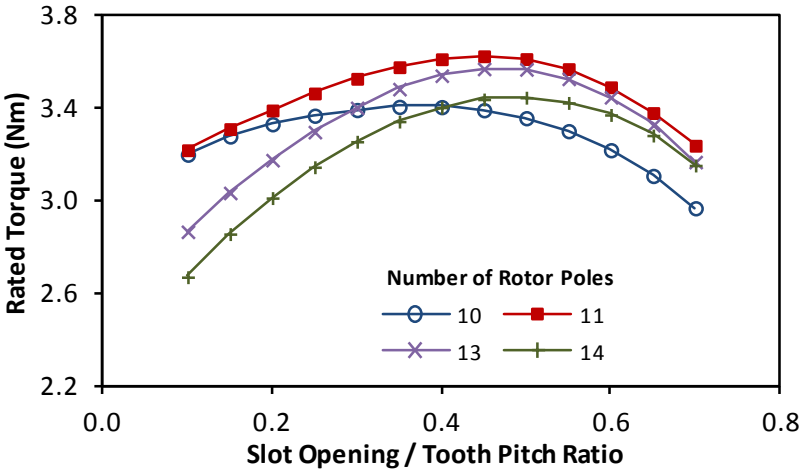

Fig. 2.11. Variation of torque with slot opening ratio for 12 stator teeth with different numbers of rotor poles.

The inner and outer surface arches of the rotor are explored as ratios of the rotor pitch Fig. 2.12, two ratios for the outer surface γ_{ro} (9) and inner surface γ_{ri} (10) are defined. As the width / pitch ratios are changed, for a fixed radial rotor thickness the PM volume remains constant, but the copper volume is required to change to constrain the stator tooth flux density below saturation.

$$\gamma_{ro} = \frac{\alpha_{ro}}{\tau_{rp}} \tag{9}$$

$$\gamma_{ri} = \frac{\alpha_{ri}}{\tau_{rp}} \tag{10}$$

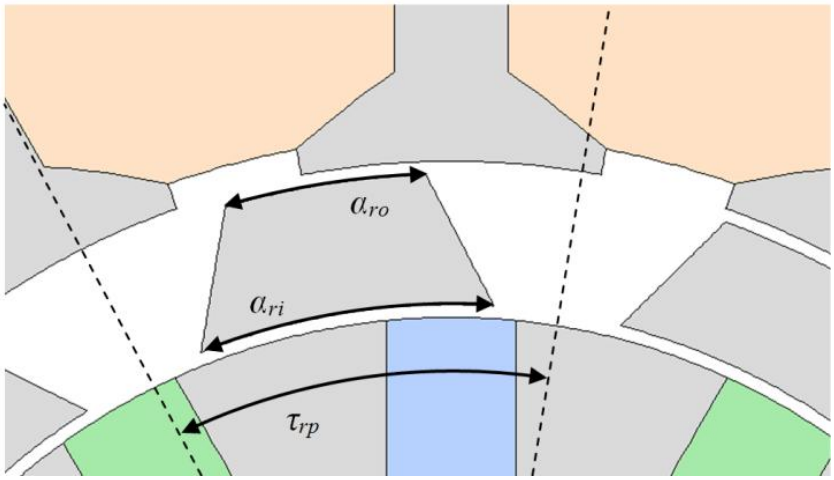

Fig. 2.12. Rotor pole geometry illustration of parameters.

Optimal outer rotor width ratio is higher for numbers of rotor poles 11 and 13 Fig. 2.13, while optimal inner rotor width ratio decreases with increased number of rotor poles Fig. 2.14.

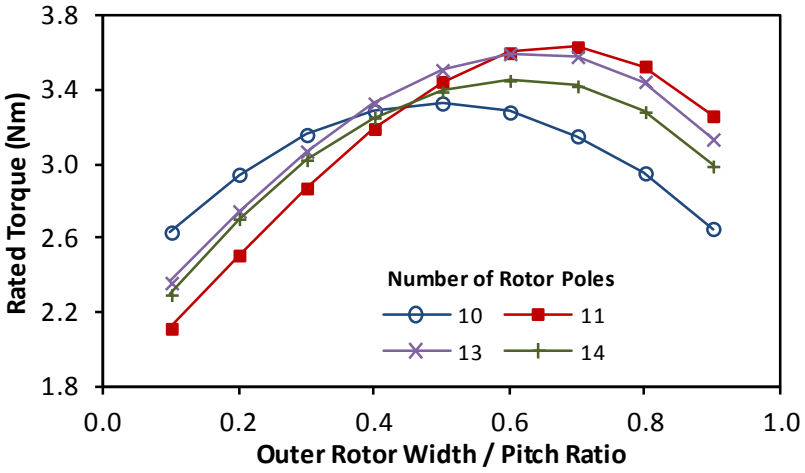

Fig. 2.13. Variation of torque with outer rotor width / pitch ratio for 12 stator teeth with different numbers of rotor poles and optimal inner rotor width / pitch ratio as in Fig 2.14.

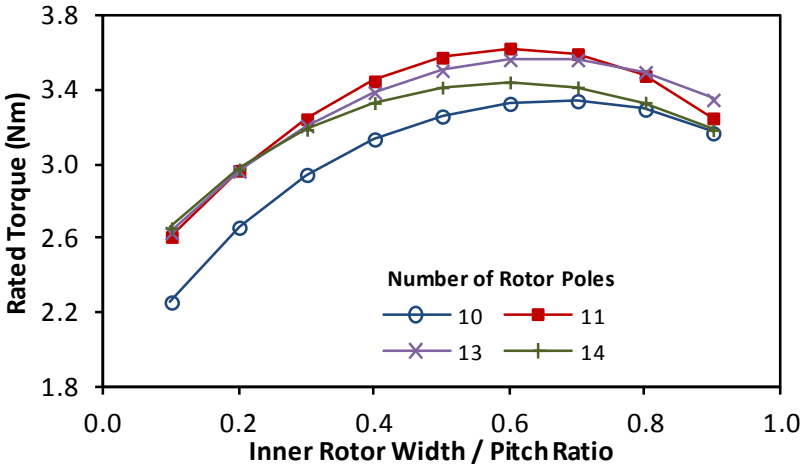

Fig. 2.14. Variation of torque with inner rotor width / pitch ratio for 12 stator teeth with different numbers of rotor poles and optimal outer rotor width / pitch ratio as in Fig 2.13.

If the rotor radial thickness is reduced the torque performance is reduced as the effective saliency and hence switching ability is decreased, also mechanically the rotor structure becomes unfeasible. As the rotor radial thickness increases the torque performance is reduced due to increased effective airgap length, therefore optimal radial thickness is obtained of close to 4mm for all rotor pole numbers Fig. 2.15.

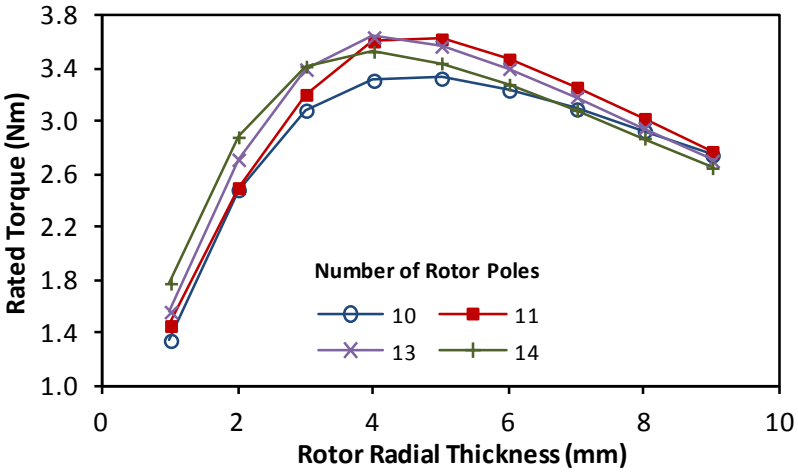

Fig. 2.15. Variation of torque rotor radial thickness for 12 stator teeth with different numbers of rotor poles.

An optimal PM thickness occurs for all rotor poles close to 5.5mm Fig. 2.16 which achieves the highest airgap flux density, increasing further increases the MMF drop across the PM and shortens the radial length of the PM, while decreasing the PM thickness reduces the PM MMF.

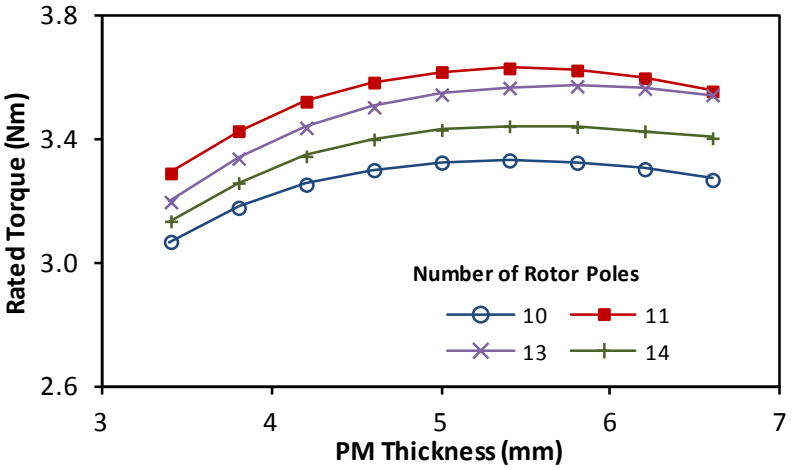

Fig. 2.16. Variation of torque with PM thickness for 12 stator teeth with different numbers of rotor poles.

2.5. Performance Analysis

The performance of PS-SFPM machines with the same inner and outer stators and optimised rotors is now compared. Dimensions of the compared machines are given in Table III.

Table III. Geometric parameters of PS-SFPM machine

Parameter	**Value**			
Rotor Poles	10	11	13	14
Rotor Outer Width/Pitch Ratio	0.5	0.6	0.6	0.5
Rotor Inner Width/Pitch Ratio	0.7	0.7	0.6	0.5
Outer Diameter (mm)	90			
Axial Length (mm)	25			
Stator Slots	12			
Stator PM Pole Pairs	6			
Airgap Length (mm)	0.5			
Split Ratio (Outer airgap)	0.70			
Split Ratio (Inner airgap)	0.58			
Stator Yoke Thickness (mm)	3			
Tooth Width (mm)	4.5			
Tooth Tip Thickness (Body) (mm)	3			
Tooth Tip Thickness (Opening) (mm)	1			
Stator Slot Opening/Pitch Ratio	0.4			
Stator Slot Opening (mm)	6.67			
Rotor Radial Thickness (mm)	5			
PM Thickness (mm)	5			
Inner Diameter (mm)	20.8			

With identical stators, the specification of material volumes and drive conditions are the same with different numbers of rotor poles

Table IV. Specification of PS-SFPM machine

Parameter	Value
Rated Peak Phase Current (A)	14.14
Rated Peak Phase Voltage (V)	20.78
Turns per Phase	72
Copper Packing Factor	0.4
PM Volume (mm^3)	23300
Copper Volume (mm^3)	39958
Slot Area (mm^2)	133.195
Rated Current Density (A/mm^2)	3.82
Rated Copper Loss (W)	15.58
Phase Resistance (Ω)	0.104
End winding length per coil (mm)	38.53

2.5.1. Airgap Flux Density and Machine Distributions

The open-circuit airgap flux density is obtained from FE for both inner and outer airgaps for machines with 10 (Fig. 2.17), 11 (Fig. 2.18), 13 (Fig. 2.19) and 14 (Fig. 2.20) rotor poles. Both distribution and spatial orders are presented, the modulation that occurs between the two airgaps is observed in the spatial order distributions, with the 6^{th} order being dominant in the inner airgap as this is the fundamental PM pole pair order, and modulated orders according to the number of rotor poles being prevalent in the outer airgap adjacent to the wound stator.

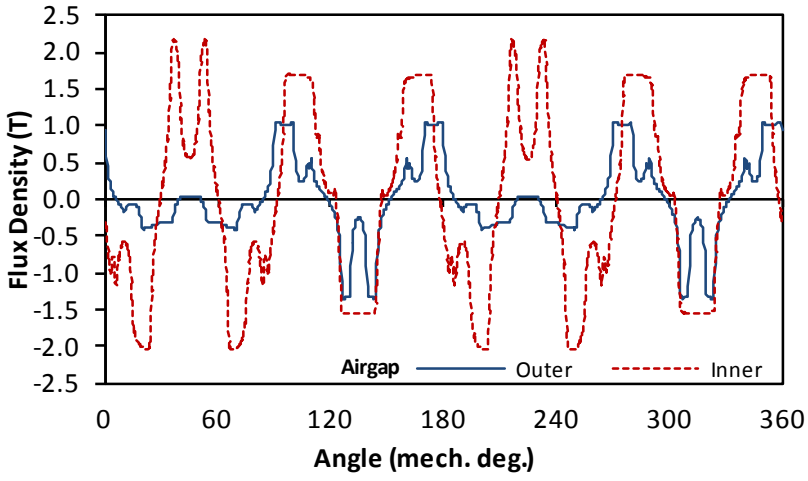

(a)

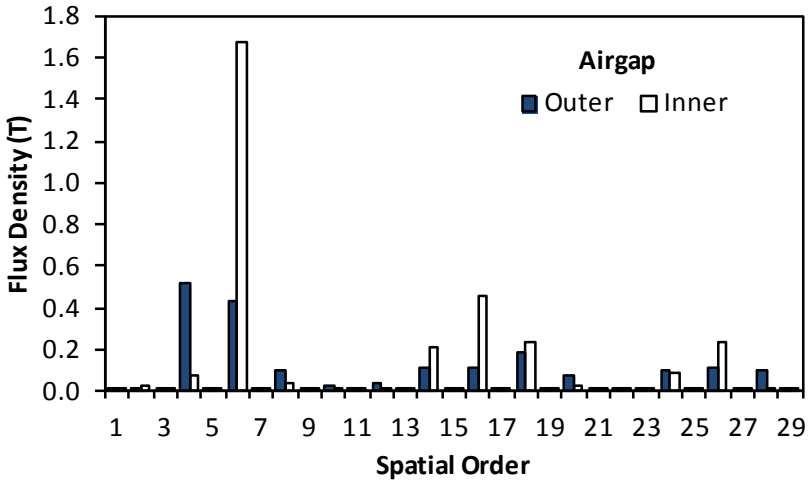

(b)

Fig. 2.17. Open-circuit airgap flux density (a) distribution and (b) spatial orders for 10 rotor poles.

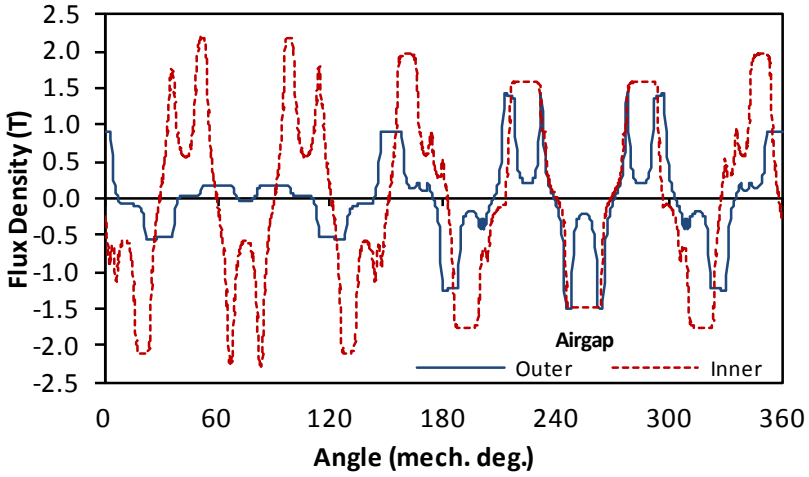

(a)

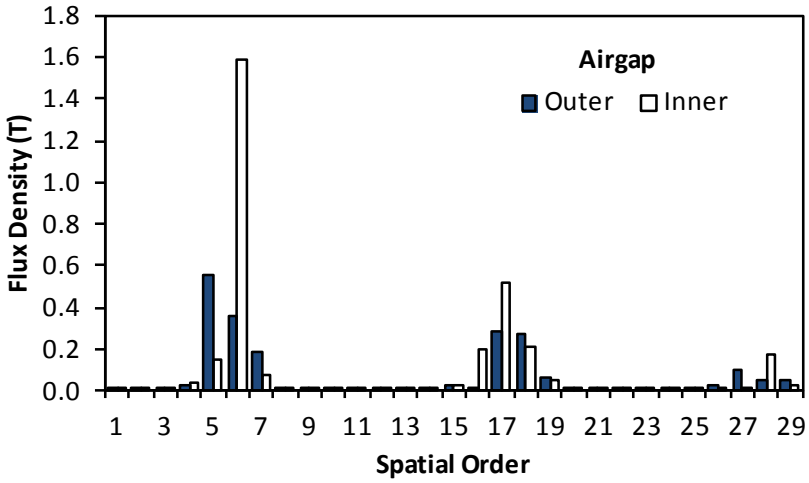

(b)

Fig. 2.18. Open-circuit airgap flux density (a) distribution and (b) spatial orders for 11 rotor poles.

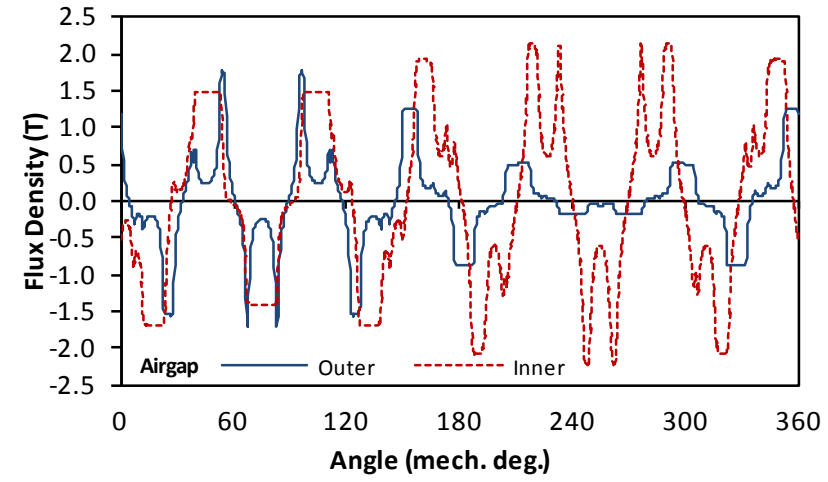

(a)

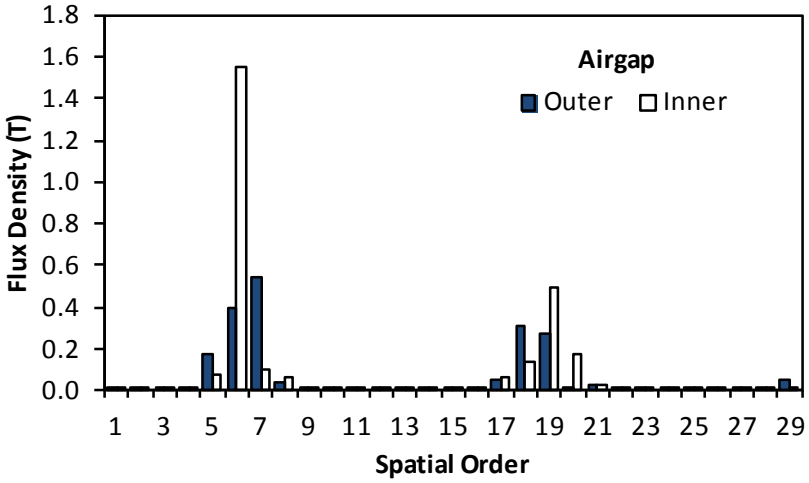

(b)

Fig. 2.19. Open-circuit airgap flux density (a) distribution and (b) spatial orders for 13 rotor poles.

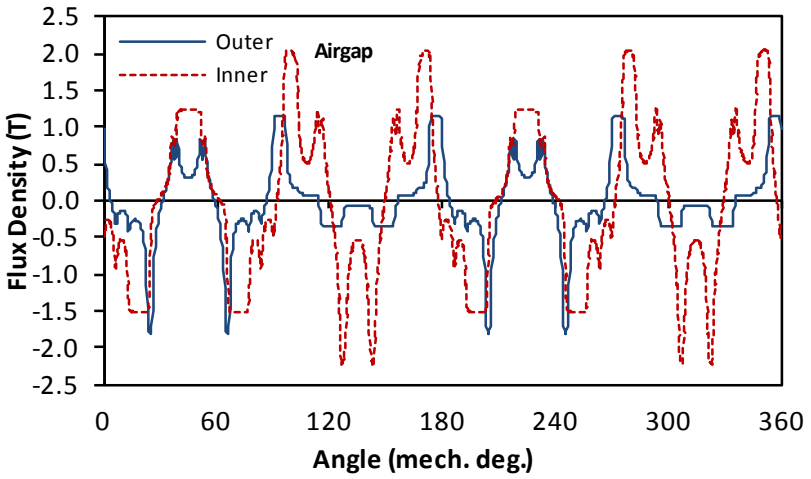

(a)

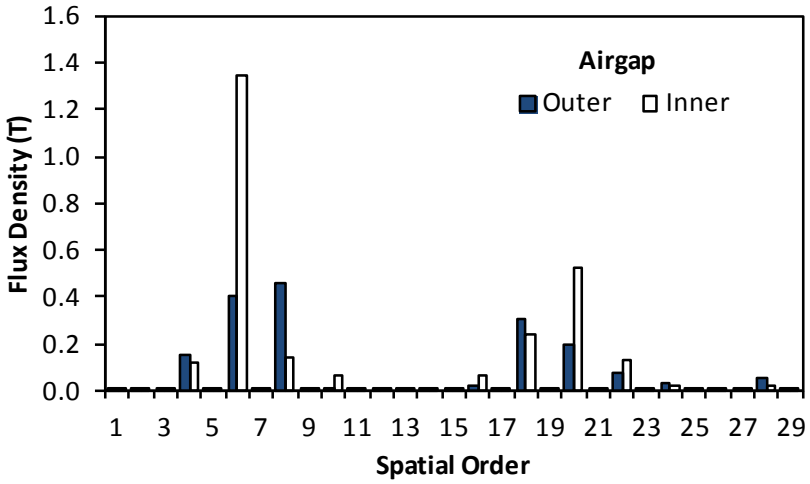

(b)

Fig. 2.20. Open-circuit airgap flux density (a) distribution and (b) spatial orders for 14 rotor poles.

The open-circuit field distributions for PS-SFPM machines with their d-axis aligned with coil 1, with 10, 11, 13 and 14 rotor poles are shown in Fig. 2.21.

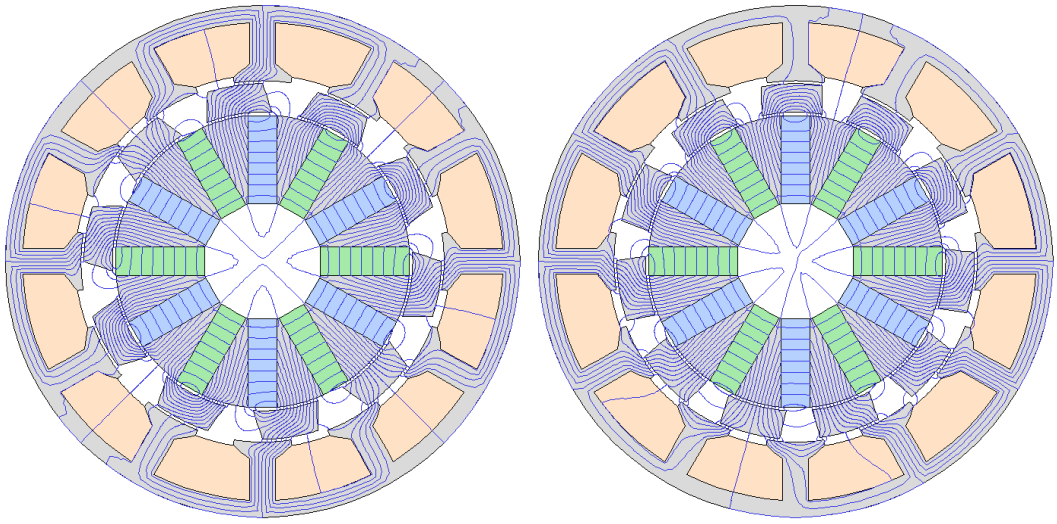

(a) (b)

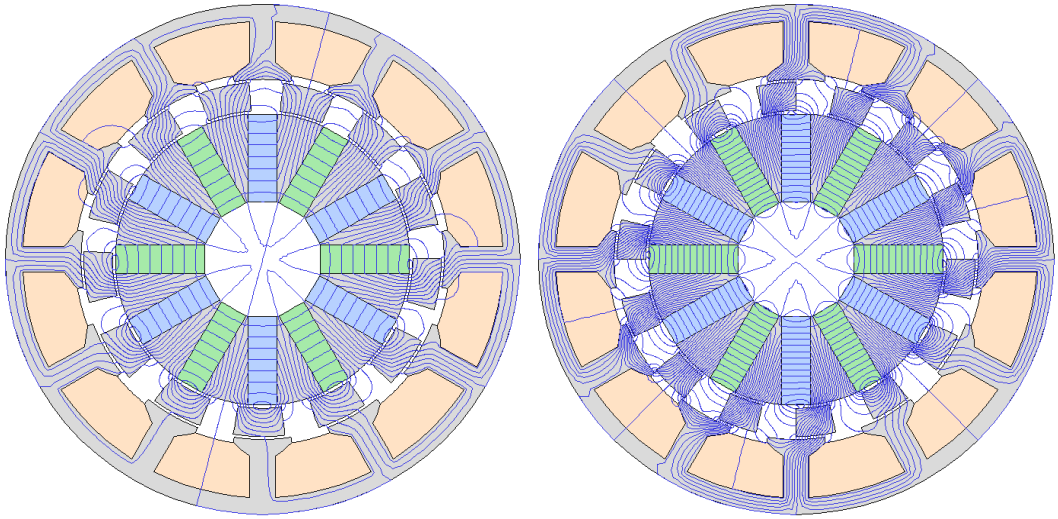

(c) (d)

Fig. 2.21. Field distributions for PS-SFPM machines at d-axis with (a) 10, (b) 11, (c) 13 and (d) 14 rotor poles.

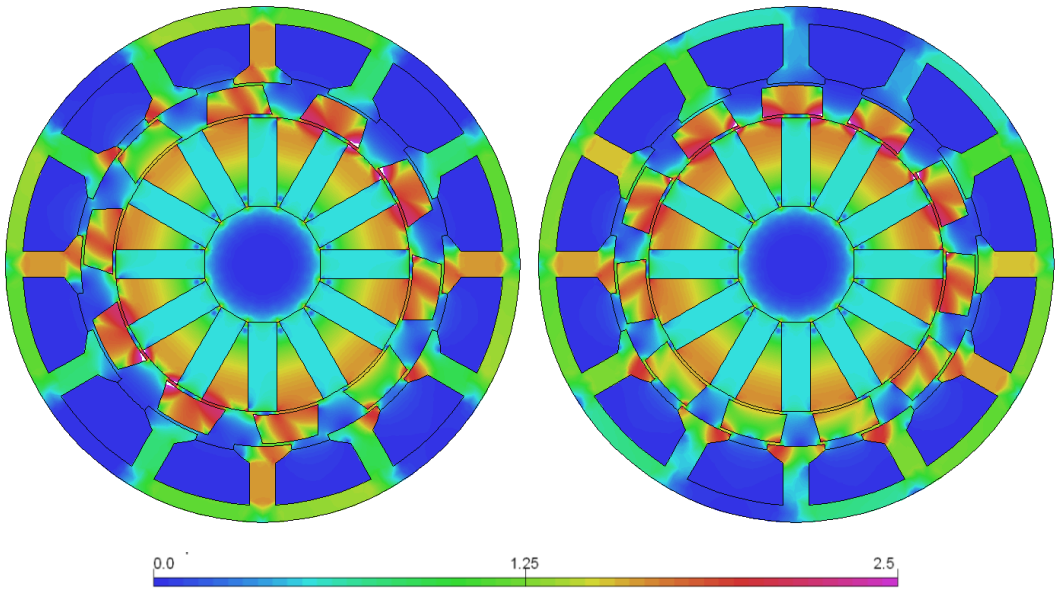

(a) (b)

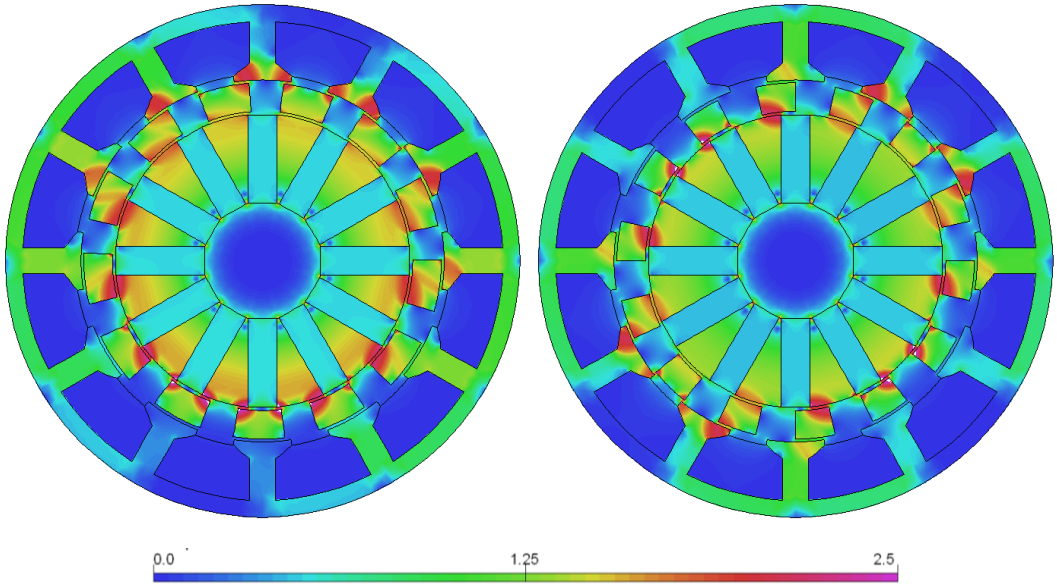

(c) (d)

Fig. 2.22. Flux density distributions for PS-SFPM machines at d-axis with (a) 10, (b) 11, (c) 13 and (d) 14 rotor poles.

2.5.2. Cogging Torque and Torque Ripples

Cogging torque results from the interaction between PM MMF and airgap saliency, in PS-SFPM machines the PM MMF is a stationary field and saliency is experienced from the rotating iron pole rotor. On-load torque ripples in PS-SFPM machines result from the asynchronous armature MMF interaction with the rotating saliency of the rotor poles, observed as back EMF harmonics and also saturation with current excitation [93].

The fundamental order n of the cogging torque waveform during an electrical cycle is dependent on the number of PM poles $2p$ and rotor poles N_r. The lowest common multiple between PM poles and rotor poles determines the fundamental cogging torque order (11), and higher orders general have smaller amplitude [94].

$$n = \frac{\mathrm{LCM}(2p, N_r)}{N_r} \tag{11}$$

Cogging torque orders for the four numbers of rotor poles are given in Table V.

Table V. Cogging torque orders with different rotor poles

Rotor Poles (N_r)	**10**	**11**	**13**	**14**
Electric Cogging Torque Order (n)	6	12	12	6

The machine with 14 rotor poles experiences the highest magnitude of cogging torque Fig. 2.23 while machines with odd numbers of rotor poles have lower cogging torque. The machine with 10 rotor poles has the same cogging torque order as with 14 rotor poles, but due to differing rotor slot opening the cogging torque is reduced.

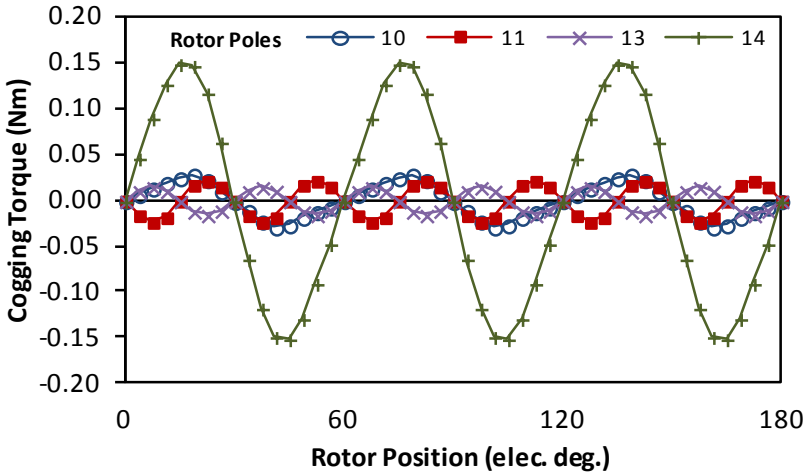

Fig. 2.23. Comparison of cogging torque for PS-SFPM machine with 12 stator slots and different rotor poles.

The variations in torque ripples on-load are most prevalent in machines with 10 and 14 rotor poles Fig. 2.24 with the main contribution occurring for the fundamental cogging torque order. The machine with 10 rotor poles has increasing torque ripple magnitude with q-axis current, while 14 rotor poles torque ripple reduces with q-axis current with double layer windings Fig. 2.24. Machines with 11 and 13 rotor poles experience small increase in torque ripples with q-axis current.

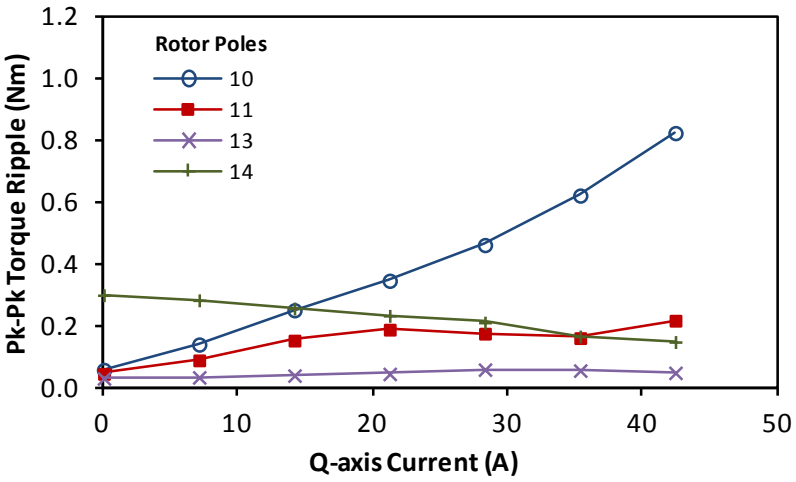

Fig. 2.24. Comparison of torque ripples variation with Q-axis current for different rotor poles.

2.5.3. Electromagnetic Torque

In the absence of reluctance torque the expression for electromagnetic torque *T* in terms of the number of rotor poles N_r, the PM flux linkage along the d-axis φ_m and the q-axis current is given by (12) .

$$T = \frac{3}{2} N_r \psi_m I_q \tag{12}$$

From Maxwell stress tensor method the torque *T* produced on a single body within the airgap surface (13) may be obtained:

$$T = \frac{L_a r^2}{\mu_o} \int_0^{2\pi} B_r B_\alpha d\alpha \tag{13}$$

Where L_a is the active lamination length, *r* is the airgap radius, μ_o is the permeability of free space ($4\pi \times 10^{-7}$ Wb/Am), B_r and B_α are the radial and circumferential airgap flux density. In the PS-SFPM machine there are two airgaps therefore the torque in both airgaps is calculated with subscript *i* and *o* indicating inner and outer airgap (14) and (15):

$$T_i = \frac{L_a r_i^2}{\mu_o} \int_0^{2\pi} B_{ri} B_{\alpha i} d\alpha \tag{14}$$

$$T_o = \frac{L_a r_o^2}{\mu_o} \int_0^{2\pi} B_{ro} B_{\alpha o} d\alpha \tag{15}$$

The output torque *T* on the rotor between the two stationary stators may be expressed as (16):

$$T = T_o - T_i = \frac{L_a}{\mu_o}\left[r_o^2 \int_0^{2\pi} B_{ro} B_{\alpha o} d\alpha - r_i^2 \int_0^{2\pi} B_{ri} B_{\alpha i} d\alpha\right] \quad (16)$$

The electromagnetic torque is obtained with sinusoidal rated peak current of 14.14A (10Arms), the copper loss is fixed for different numbers of rotor poles as identical wound stators are employed for different numbers of rotor poles. The torque variation with rotor position for different numbers of rotor poles with double layer windings are shown in Fig. 2.25, machines with numbers of rotor poles less than 12 have higher rated torque than their counterpart number of rotor poles greater than 12, e.g. 10 poles have higher torque than 14 poles and 11 poles than 13 poles.

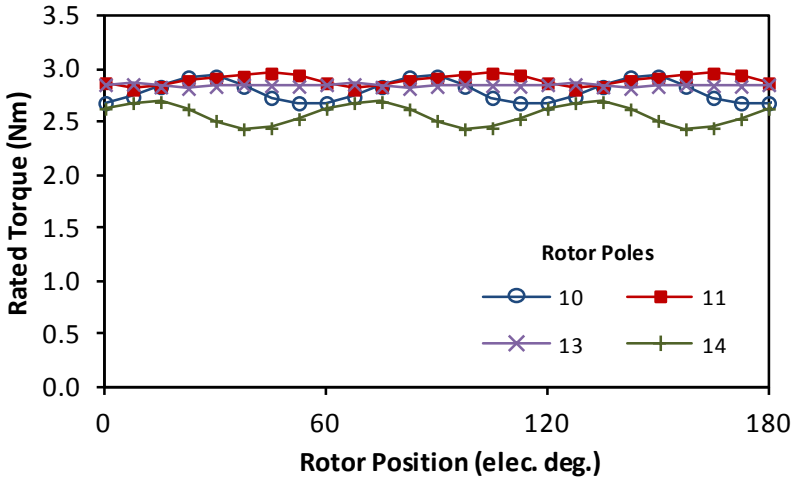

Fig. 2.25. Comparison of rated torque with double layer windings for different rotor poles.

The electromagnetic torque production with q-axis current excitation is compared for different numbers of rotor poles Fig. 2.26, saturation at high q-axis is observed particularly for 11 rotor poles since at rated current 11 rotor poles is operating closest to the saturation point of the wound stator teeth.

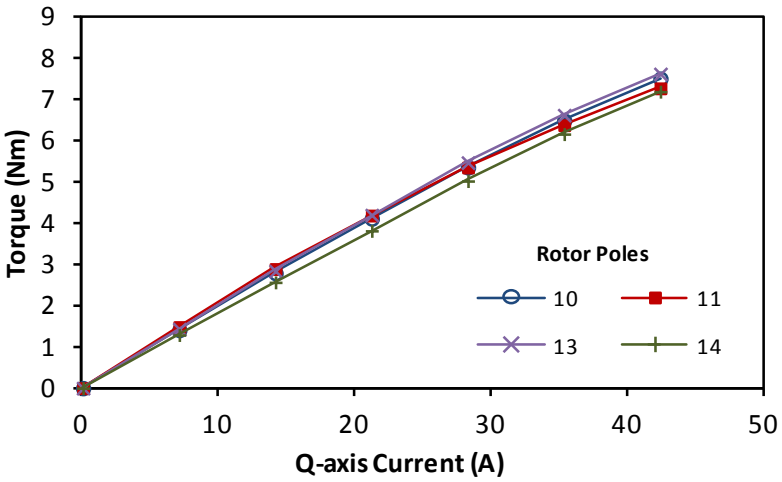

Fig. 2.26. Torque characteristic of PS-SFPM machine with 10, 11, 13 and 14 rotor poles with double layer windings.

2.5.4. Back EMF

The phase back EMF for different numbers of rotor poles Fig. 2.27 are predicted using FE, the greatest back EMF is observed for 11 rotor poles and the smallest with 14 rotor poles. The harmonics of phase back EMF are shown in Fig. 2.28, each number of rotor poles contains minimal higher order harmonics.

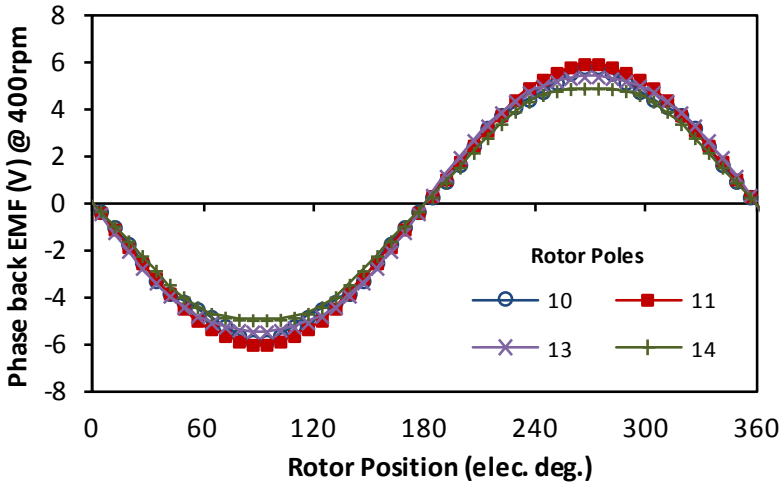

Fig. 2.27. Open-circuit back EMF for PS-SFPM machine with different numbers of rotor poles and double layer windings.

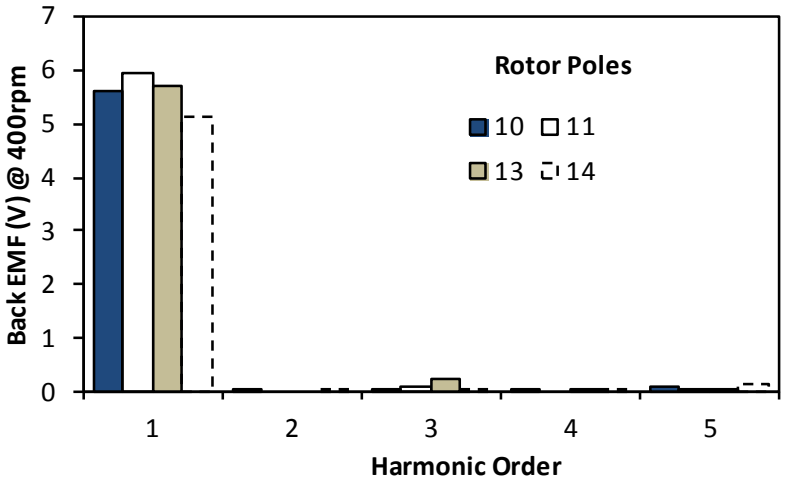

Fig. 2.28. Open-circuit back EMF harmonics for PS-SFPM machine with different numbers of rotor poles and double layer windings.

2.5.5. Winding Inductances and Power Factor

The dq-axis inductances, PM flux linkage and power factor for the PS-SFPM machine while operating with I_d = 0 are shown in Table VI. The constant torque region power factor reduces with increased number of rotor poles as increasing the number of rotor poles decreases the PM flux linkage, increasing the effect of d-axis voltage and reducing the power factor.

Table VI. Average winding inductances and power factor for PS-SFPM machines with different numbers of rotor poles.

	Rotor Poles			
	10	11	13	14
φ_m (mWb)	13.4	12.9	10.5	8.7
L_d (mH)	0.346	0.419	0.375	0.302
L_q (mH)	0.359	0.297	0.279	0.242
P.F	0.98	0.97	0.96	0.95

2.6. Comparison with Iron Bridges

To produce a prototype machine to validate the PS-SFPM machine the geometry has been adapted to ease the process and facilitate the structure required. Principally to strengthen the rotor structure, which ideally would consist of magnetically isolated rotor poles, iron bridges have been introduced to allow the rotor to be produced as one complete lamination stack. The

bridge thickness is 0.5mm and connects the rotor poles and at the surfaces of the PM again to allow for complete PM stator laminations to be produced and to add strength Fig. 2.29.

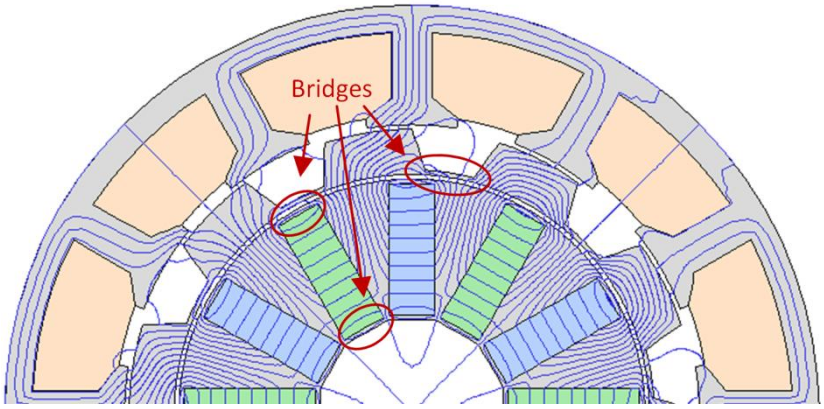

Fig. 2.29. Illustration of rotor bridges included for manufacturing purposes.

The FE predicted static torque for machines with and without 0.5mm iron bridges for machines with 10 and 11 rotor poles are compared in Fig. 2.30, for both numbers of rotor poles the reduction in torque at rated current of 14.14A is 20% due to flux leakage through the bridges.

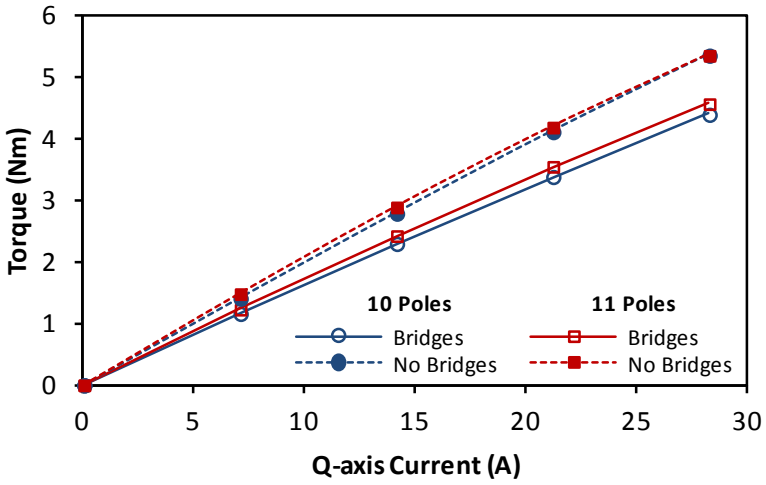

Fig. 2.30. Comparison of torque production with q-axis current variation for 10 and 11 rotor poles with and without bridges.

The back EMFs for 10 and 11 rotor poles with and without bridges are shown in Fig. 2.31 and Fig. 2.32 respectively, again the reduction in flux linking each phase due to flux passing through the bridges around the PM surfaces and rotor bridges, leads to reduced back EMF.

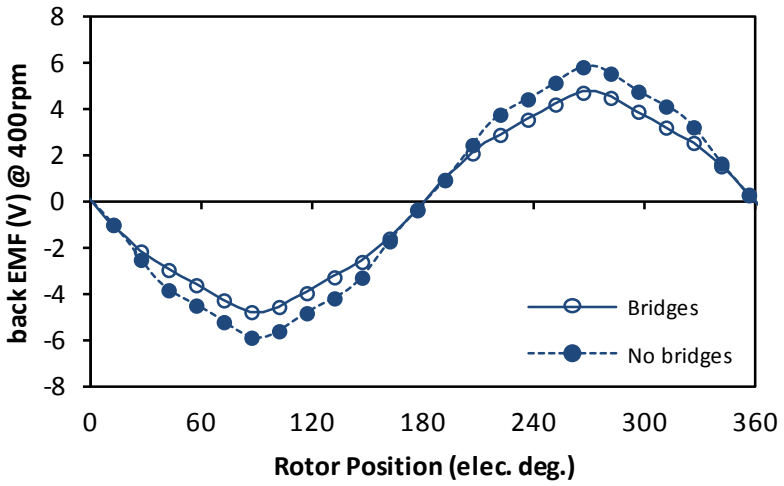

Fig. 2.31. Back EMF at 400rpm for 10 rotor poles with and without bridges.

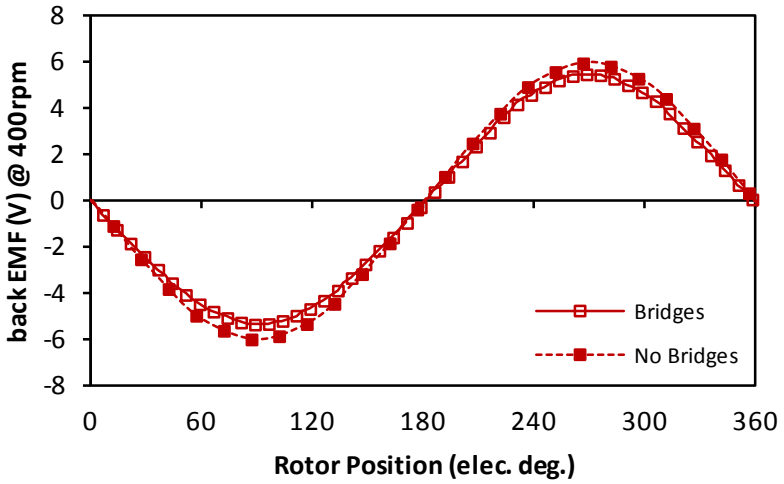

Fig. 2.32. Back EMF at 400rpm for 11 rotor poles with and without bridges.

Inclusion of bridges on both the rotor and PM stator surfaces alters the permeance change as the rotor rotates. Cogging torque is sensitive to these permeance changes and including bridges on the PM surface adjacent to the airgap and on the inner rotor surface alters the permeance. Therefore, the cogging torque with and without inclusion of these bridges is shown for 10 and 11 rotor poles in Fig. 2.33 and Fig. 2.34 respectively. For 10 rotor poles the cogging torque is increased by including bridges but reduced with 11 rotor poles.

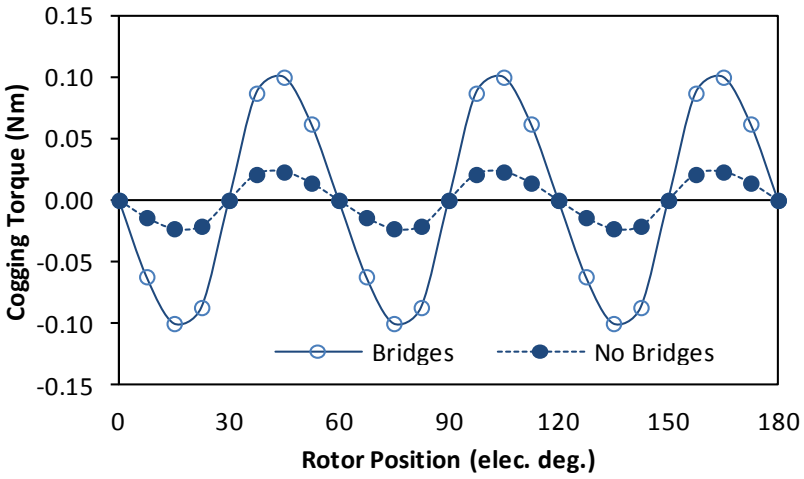

Fig. 2.33. Cogging torque for 10 rotor poles with and without bridges.

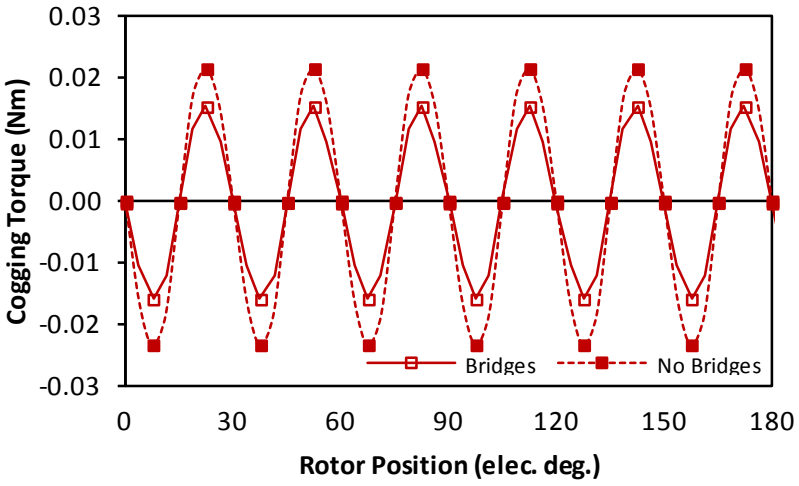

Fig. 2.34. Cogging torque for 11 rotor poles with and without bridges.

While the rotor bridges in Fig 2.29 compromise the torque and back EMF performance of the PS-SFPM machines they are required for a prototype machine in order to ease manufacture and provide suitable structural integrity.

2.7. Experimental Validation

In order to validate the FE predicted performance of the PS-SFPM machine, two prototypes have been produced with 10 and 11 rotor poles. Both designs share wound and PM stator geometry but assume the optimal rotor shaping. The prototype specification is given in Table III, with 0.5mm lamination bridges included between rotor poles adjacent to the inner airgap and on the inner and outer PM surfaces for ease of manufacture. To produce the rotor structure an epoxy resin was used to encapsulate the lamination stack and non-magnetic

aluminium bars used to fix the lamination between the shaft and bottom bearing Fig. 2.35a, negligible eddy current loss in these bars is assumed as the machine speed hence flux density variation frequency is low. During the casting process of the rotor, shrinkage of the resin during curing time introduced bubbles in the final rotor, these bubbles are not detrimental to the design, again at low speed will not produce significant windage loss Fig. 2.35b. A bearing with diameter greater than the inner PM stator was used to facilitate production and testing of multiple rotors with the same stator structure Fig. 2.35c. A double layer concentrated wound stator with all terminals extended outside the machine casing to allow multiple connections required for different numbers of rotor poles Fig. 2.35d was produced.

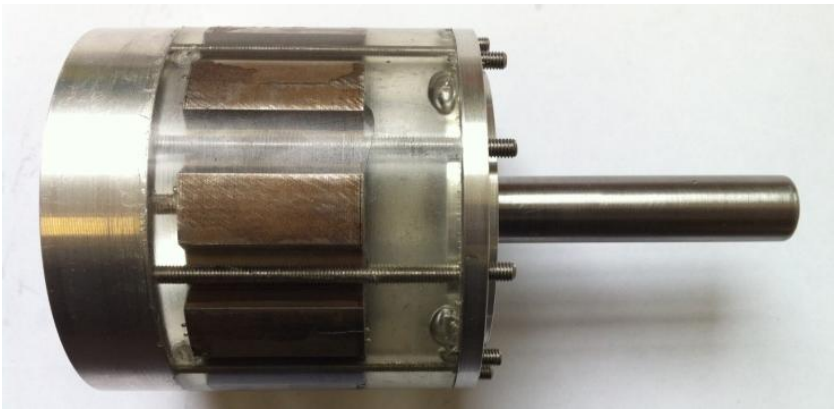

(a)

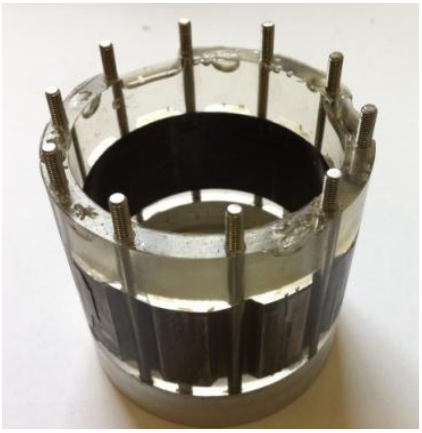

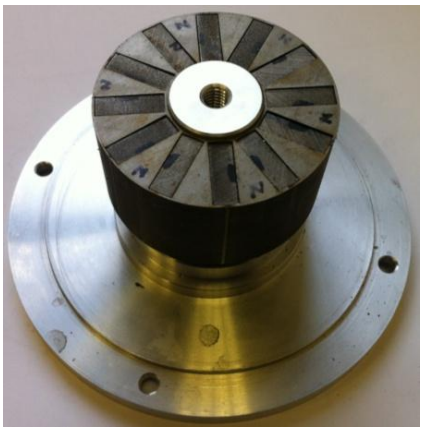

(b) (c)

(d)

Fig. 2.35. Prototype machines (a) complete rotor structure with 10 rotor poles, (b) rotor after resin moulding, (c) PM stator and (d) double layer wound stator.

Measured results for different numbers of rotor poles will be presented and then compared, including cogging torque, back EMF and static torque performance.

2.7.1. 10 Rotor Poles

The cogging torque was measured using the method explained in [95]. During the measurement of cogging torque over an assumed cogging torque period of 6°mech, a complete torque cycle did not present itself and therefore cogging torque over 120°mech was finally obtained and shown in Fig. 2.36.

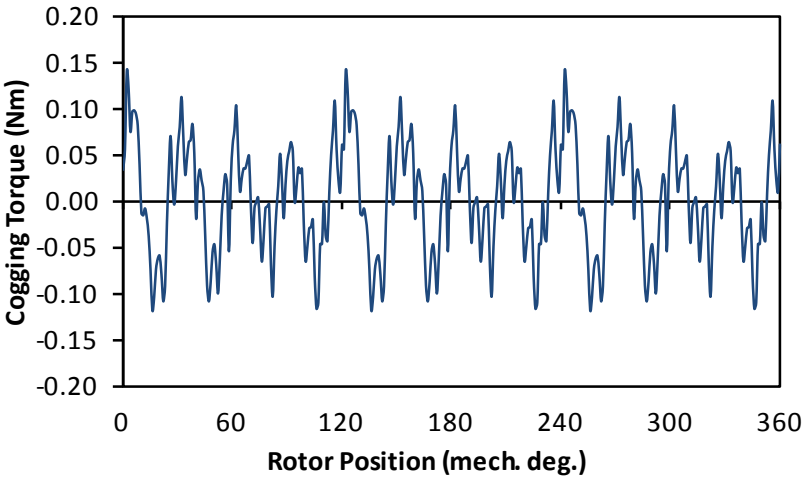

Fig. 2.36. Measured cogging torque for machine with 10 rotor poles.

The measured cogging torque contains lower order torque variation than predicted using FE. As the rotor structure is the most non-conventional and complicated structure the deviation between shaft and bottom bearing was compared using a lathe and comparator Fig. 2.37 finding a 0.2mm peak to peak variation in the bottom bearing position relative to the shaft.

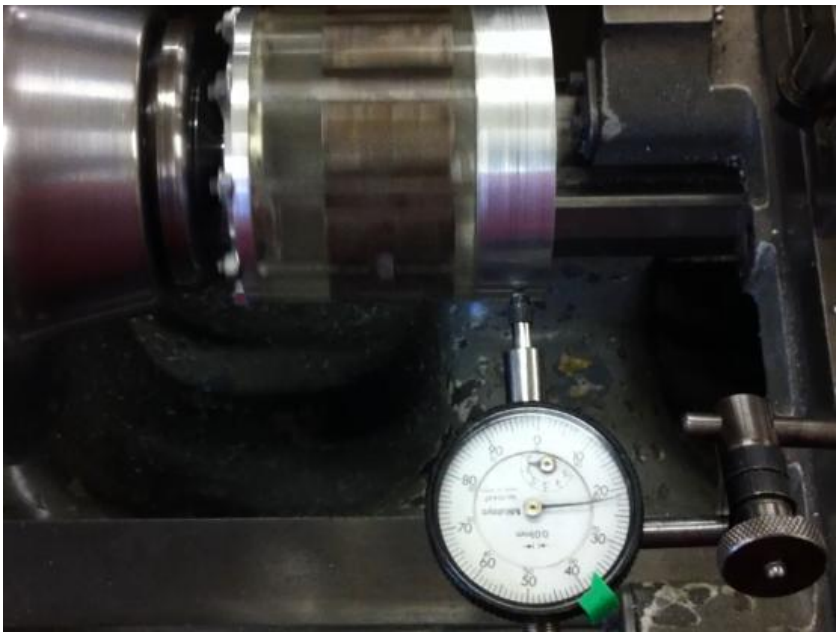

Fig. 2.37. Measurement of rotor eccentricity using a comparator and lathe.

Since a deviation between the shaft and bottom bearing exists, this will present itself as rotational eccentricity of the rotor. Using FE a rotational or dynamic eccentricity simulation was performed and cogging torque harmonics for the ideal FE, FE prediction with 0.1mm eccentricity and measured results are shown in Fig. 2.38.

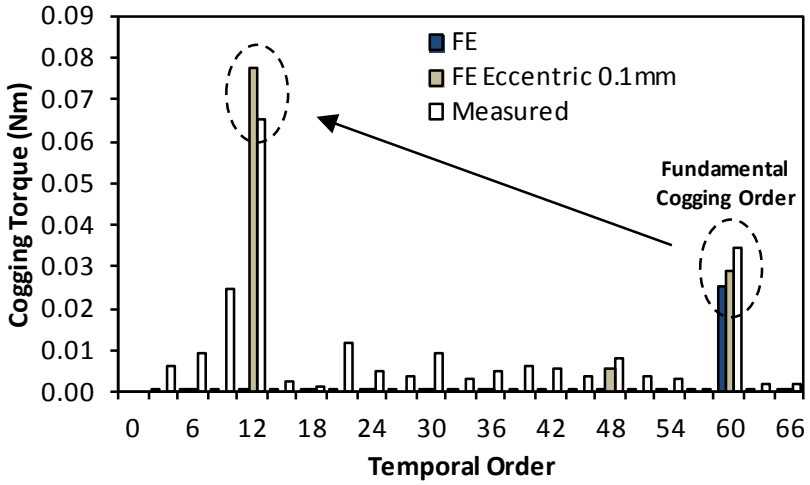

Fig. 2.38. Measured cogging torque harmonics for machine with 10 rotor poles.

There is good agreement between those results measured and simulated with eccentricity from FE, revealing the dominant torque ripple component of 12th mechanical order. Over one electrical cycle the FE, eccentric FE and measured results are shown in Fig. 2.39.

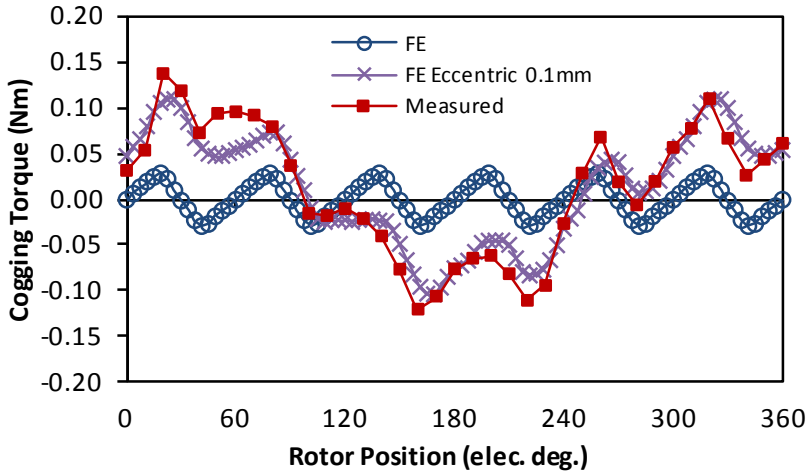

Fig. 2.39. Comparison of measured and FE cogging torque predictions for one electrical cycle.

The three phase back EMF is obtained by driving the rotor and using probes to measure the phase voltage, the EMF is balanced between the three phases Fig. 2.40.

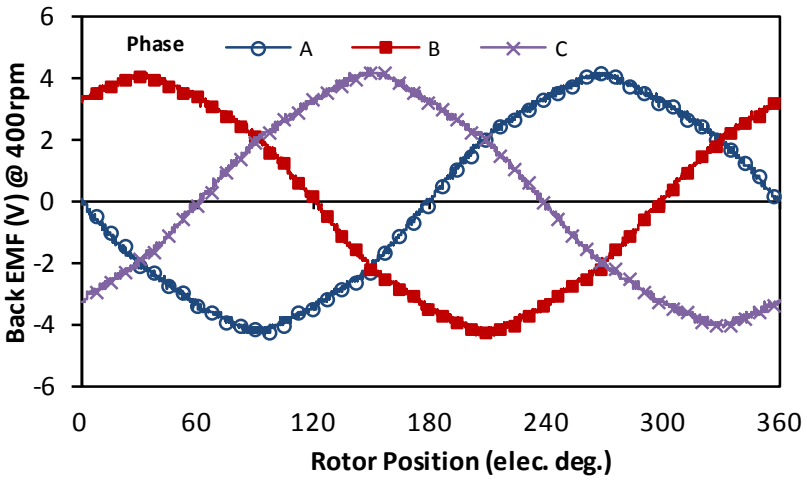

Fig. 2.40. Measured back EMF in all phases for 10 rotor poles.

Comparison of the back EMF with the FE prediction shows a reduction in actual back EMF achieved in the prototype machine. This can be expected since the end effects are neglected, particularly at the PM ends Fig. 2.41.

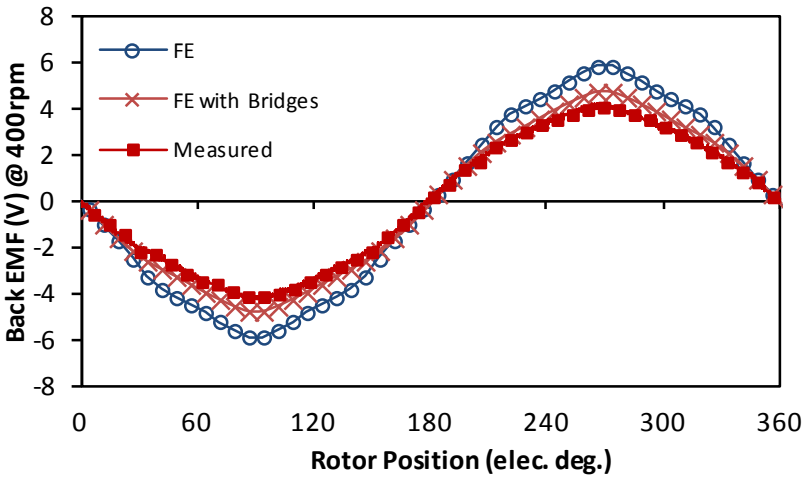

Fig. 2.41. Comparison of measured, ideal FE and FE including prototype bridges back EMF in a single phase.

The harmonics of the phase back EMF from FE and measured are compared in Fig. 2.42 and Table VII, showing reduction in fundamental back EMF in the measured data, small differences in 2nd and 5th harmonics and negligible 3rd and 4th harmonics.

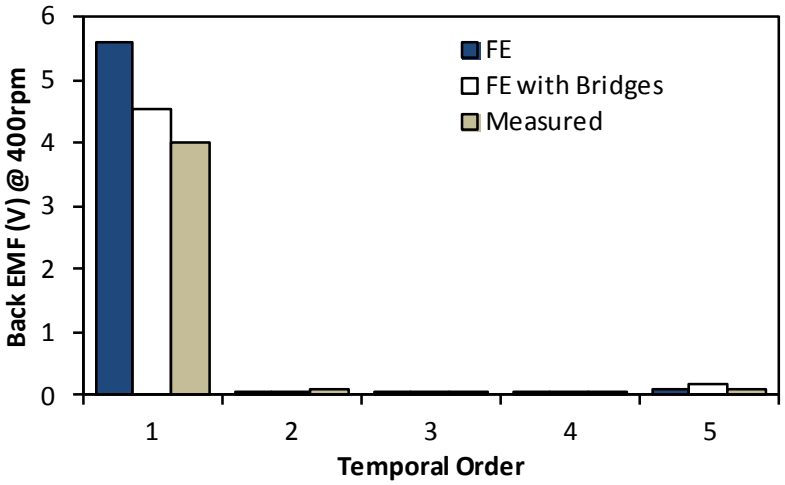

Fig. 2.42. Comparison of measured and FE EMF harmonics for 10 rotor poles.

Table VII. Table of measured and FE EMF harmonics for 10 rotor poles

Temporal Order	**1**	**2**	**3**	**4**	**5**
FE	5.68	0.02	0.02	0.01	0.10
FE with Bridges	4.53	0.01	0.02	0.01	0.19
Measured	3.99	0.11	0.03	0.02	0.11

Static torque characteristics with fixed DC excitation of the phases, ($I_a = I_{pk}$, $I_b = I_c = -I_{pk}/2$), and variation of rotor position is shown for FE and measured results in Fig. 2.43. The measured results agree well with the FE predicted results at lower current loading. As the current is increased the measured results saturate more significantly than the FE predicted results. As can be seen in both the FE and measured results the cogging torque is observed within the static torque result. The cogging torque as a result of eccentricity is low order and therefore has the overall effect of reducing the static torque close to 180°elec as its period is 240°elec.

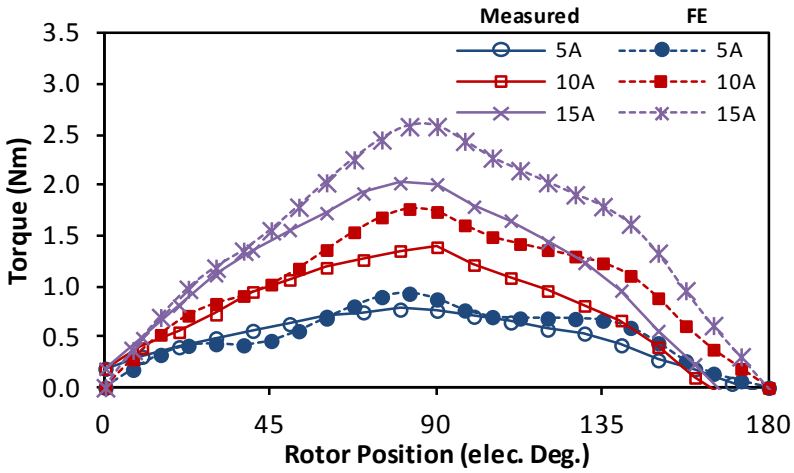

Fig. 2.43. Comparison of measured and FE predictions of static torque with rotor position and DC currents.

The static torque variation with q-axis current is shown in Fig. 2.44, revealing decreased performance in the prototype performance expected due to decreased back EMF from the FE predicted performance.

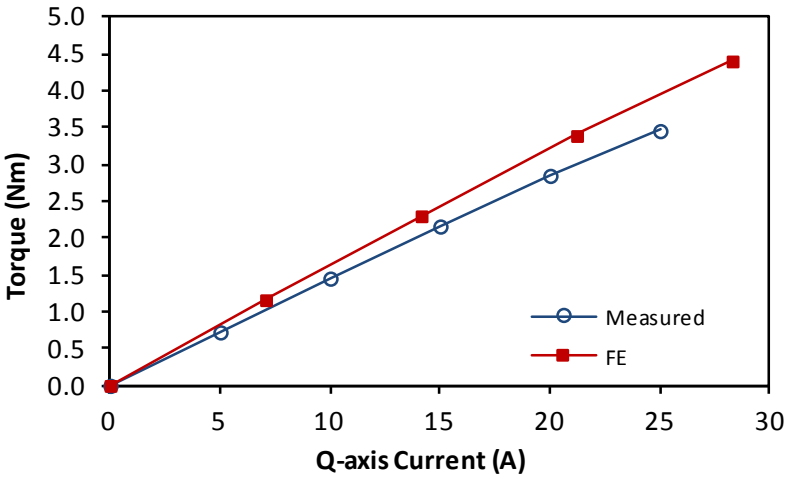

Fig. 2.44. Comparison of measured and FE predictions of static torque with q-axis current.

2.7.2. 11 Rotor Poles

In the measured cogging torque for the machine with 11 rotor poles, as with 10 rotor poles, a lower order of cogging torque than expected was obtained, again with 12th mechanical order Fig. 2.45a. The fundamental mechanical cogging torque order predicted using FE is the 120th mechanical order, can be seen in the harmonics of the cogging torque spectrum Fig. 2.45b.

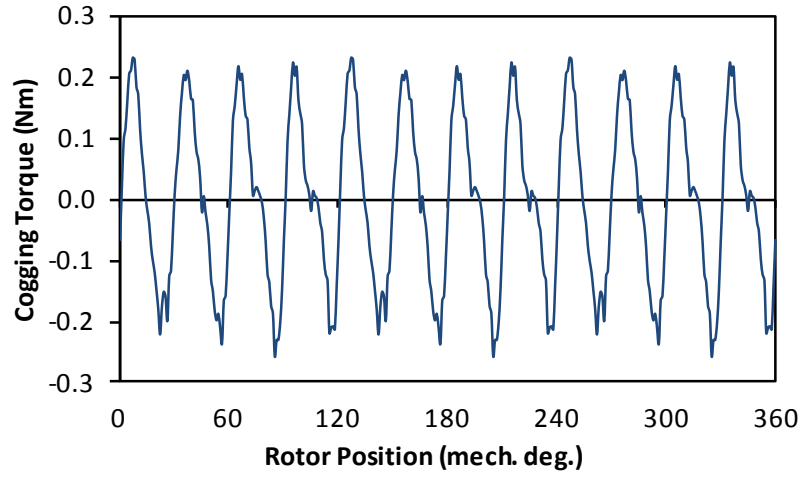

(a)

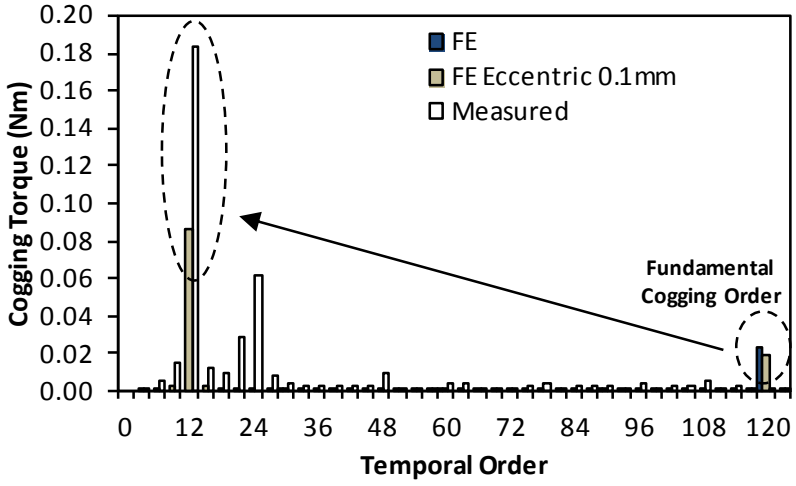

(b)

Fig. 2.45. Measured cogging torque variation and temporal orders for a machine with 11 rotor poles.

The cogging torque with eccentricity is predicted using FE and compared for one electrical cycle with the ideal cogging torque without eccentricity and also with the measured result Fig. 2.46. Again a 12^{th} order cogging is introduced, the FE predicted cogging torque with eccentricity does not correlate with the measured result as for 10 rotor poles but the order of cogging torque due to eccentricity is obtained.

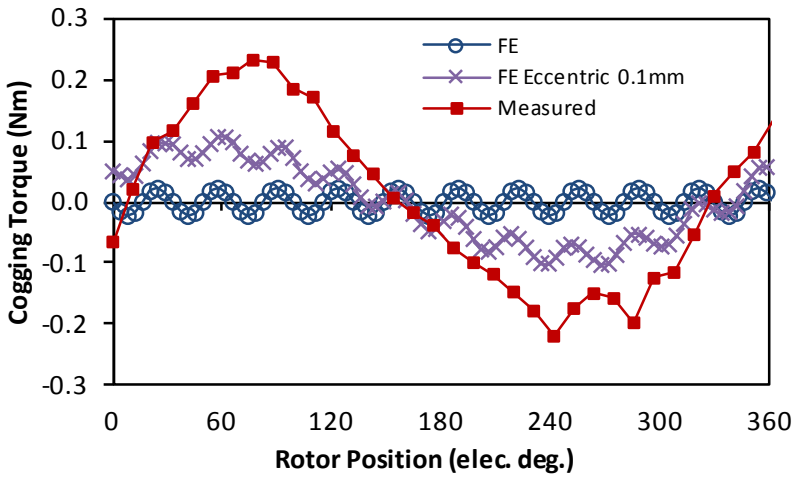

Fig. 2.46. Comparison of measured, FE and FE with eccentricity cogging torque over one electrical cycle.

In an eccentric machine with asymmetry the back EMF also contained lower order harmonics, resulting in discrepancy in magnitude of phases in an electrical cycle [96] Fig. 2.47a. Therefore, over a mechanical cycle the variation in magnitude for each phase can be observed Fig. 2.47b.

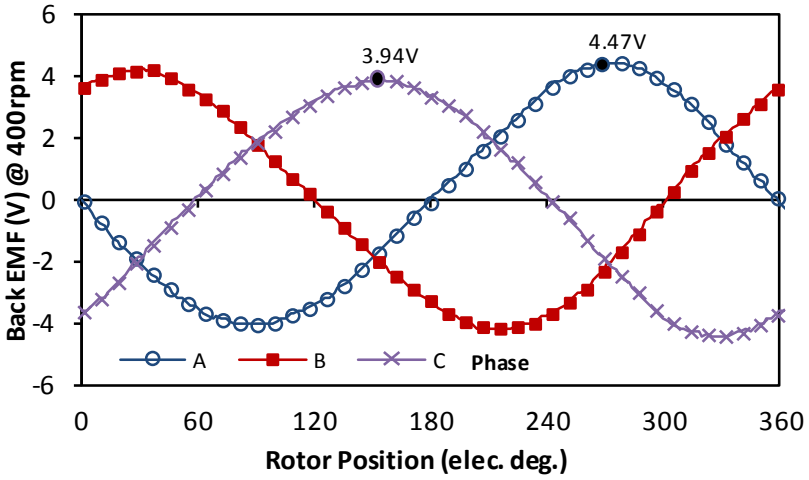

(a)

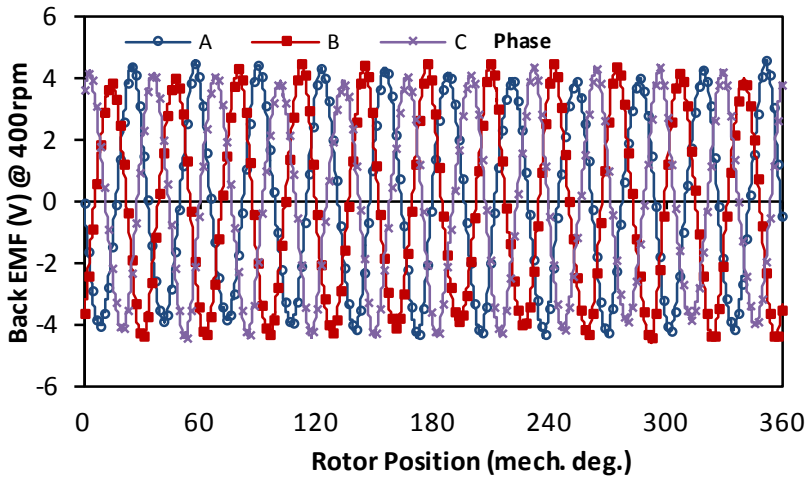

(b)

Fig. 2.47. Measured back EMF at 400rpm over an (a) electrical and (b) mechanical period.

The harmonic content of the FE and measured back EMF is shown in Fig. 2.48 considering a mechanical cycle, the measured result includes increased 23rd order also additional components at 10 and 12 orders.

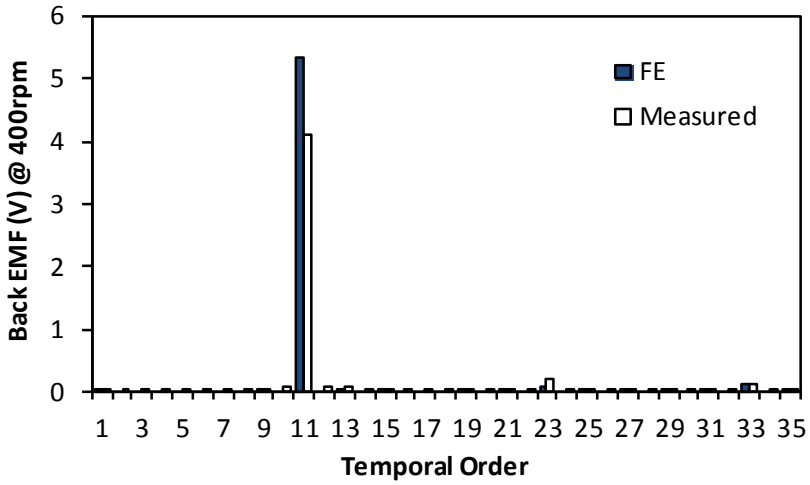

Fig. 2.48. Measured back EMF temporal harmonic orders considering a mechanical cycle.

In the same manner as the machine with 10 rotor poles has a decreased magnitude of back EMF so the 11 rotor poles also has reduced fundamental back EMF due to eccentricity and end effects Fig. 2.49.

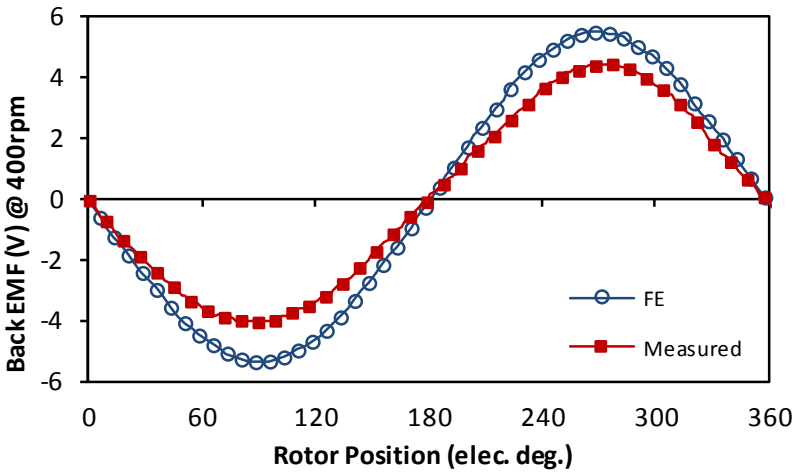

Fig. 2.49. Measured and FE predicted back EMF for one electrical period with 11 rotor poles.

With fixed DC excitation the static torque is obtained with variation in rotor position and compared with FE predicted performance Fig. 2.50. At higher current excitation the measured torque is less than FE predicted, as the ideally predicted cogging torque is low the result both measured and FE are more sinusoidal. As with 10 rotor poles the effect of eccentricity reduces the static torque period, therefore particularly at higher current excitation the static torque reduces to zero before 180°elec.

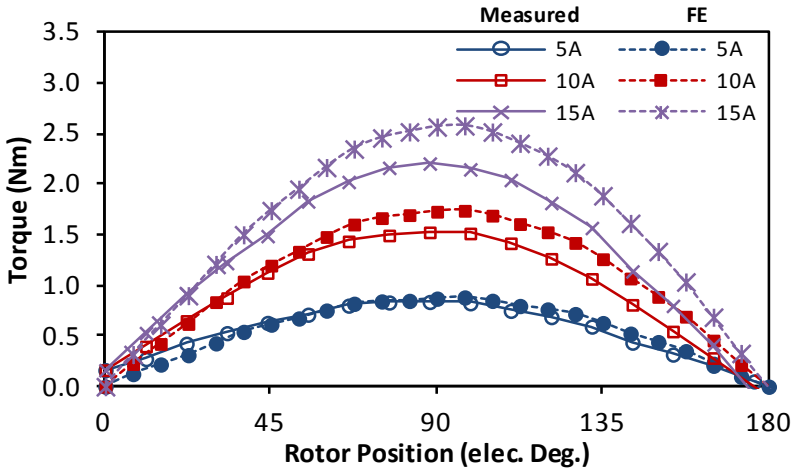

Fig. 2.50. Comparison of measured and FE predictions of static torque with rotor position.

There is good agreement between the static torque predicted using FE and those measured, a reduction in magnitude occurs across the current range due to end effects and expected due to the reduced back EMF observed Fig. 2.51.

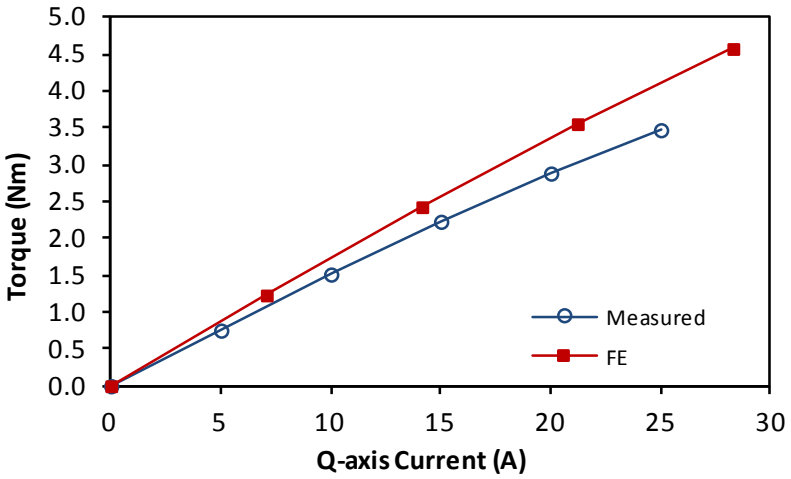

Fig. 2.51. Comparison of measured and FE predictions of static torque q-axis current loading.

2.7.3. Comparison

The back EMF and static torque characteristics for PS-SFPM machines with 10 and 11 rotor poles are compared. The FE predicted and measured results are presented. When analysed using FE the predicted back EMF for 11 rotor poles compared with 10 rotor poles has more significant increase than those observed in the measured results Fig. 2.52, since the eccentricity of the rotors is detrimental to the back EMF in 11 rotor poles as with 11 rotor poles the machine becomes asymmetric.

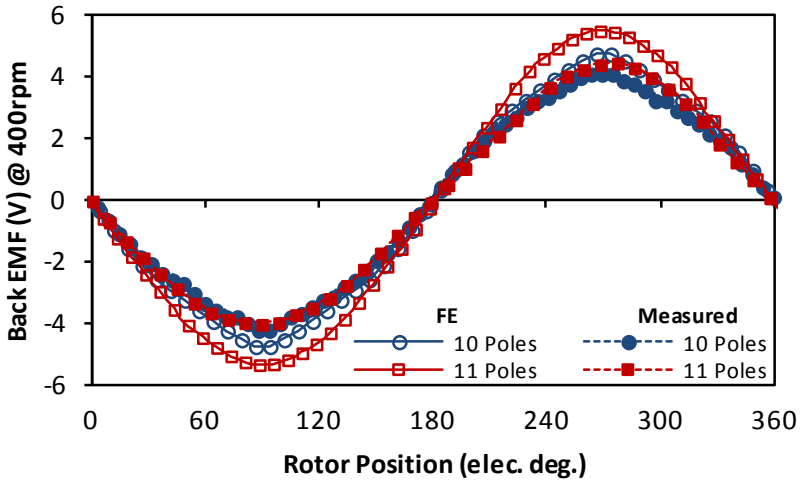

Fig. 2.52. Comparison of measured and FE predictions of back EMF for machines with 10 and 11 rotor poles.

Comparison of the static torque with q-axis current prediction with FE and measured results show that for both 10 and 11 rotor poles there occurs a reduction in performance due to eccentricity and end effects for the PS-SFPM machines. For both FE and measured results

operating at a rated current of 14.14A utilising 11 rotor poles has a higher torque, but the measured results for 11 rotor poles shows greater saturation effects as the current is increased Fig. 2.53.

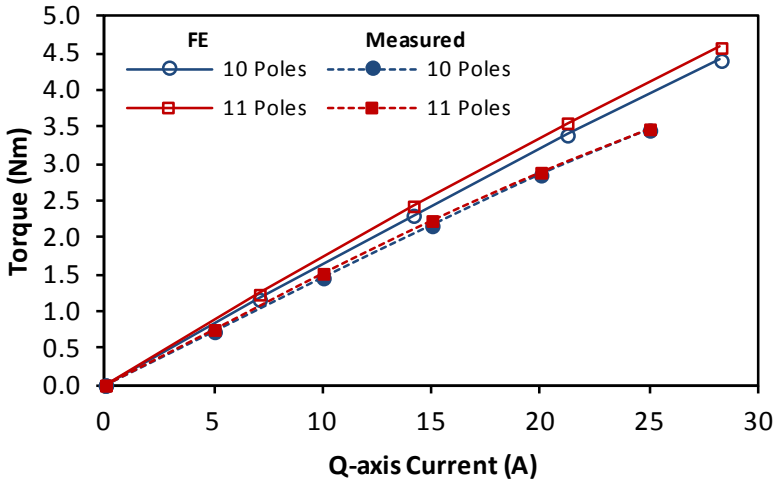

Fig. 2.53. Comparison of measured and FE predictions of static torque with q-axis current loading for machines with 10 and 11 rotor poles.

2.8. Experimental Generator Test

The prototype PS-SFPM machine is tested as a generator, driven by a DC machine with different resistive loads applied to the star connected PS-SFPM machine windings.

The test is initially performed with no resistive load to obtain the back EMF with no current driven. Then the resistive load is introduced and the resistance adjusted to 5.10Ω, 3.65Ω, 2.45Ω and 1.25 Ω to drive a current through the load.

The schematic is shown in Fig. 2.54 with the star connected resistive load, the star connected PS-SFPM machine and shaft coupling to the DC machine. A photograph of the setup is shown in Fig. 2.55. The oscilloscope is a TDS 2004B and the DC source is an IPS-4303.

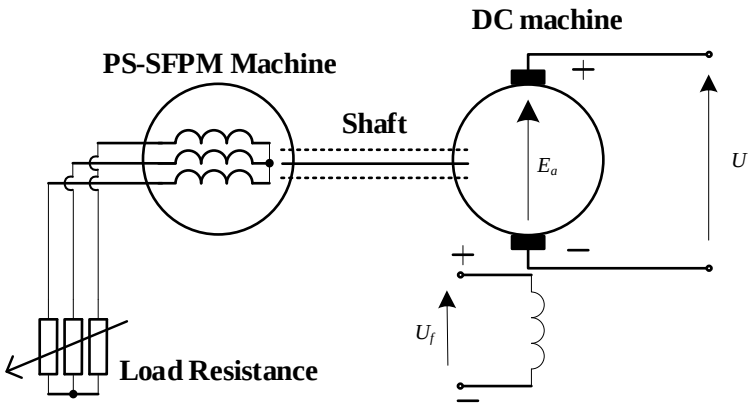

Fig. 2.54. Schematic of test setup with load, PS-SFPM machine and DC machine.

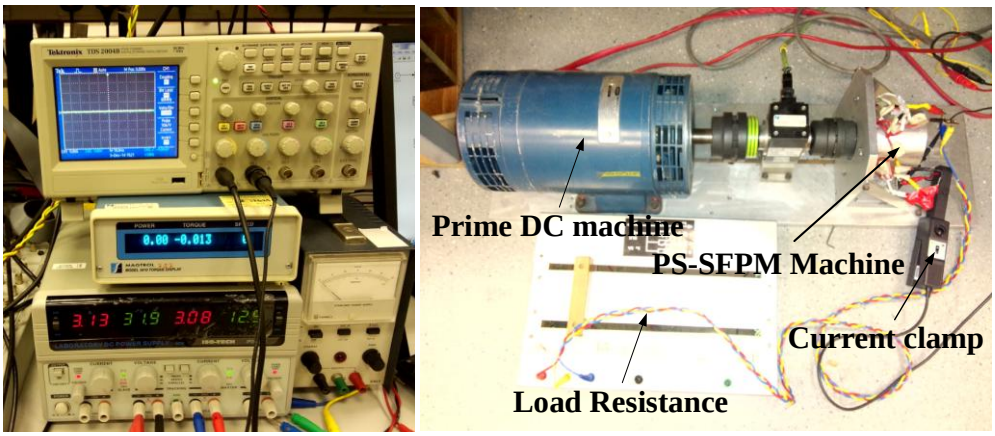

Fig. 2.55. Photographs of test setup with equipment labels.

The test is carried out on the PS-SFPM machine with 10 rotor poles and compared with FE predictions using a coupled circuit model. The peak phase voltage variation with resistance is shown in Fig. 2.56 when operating at 4 different speeds.

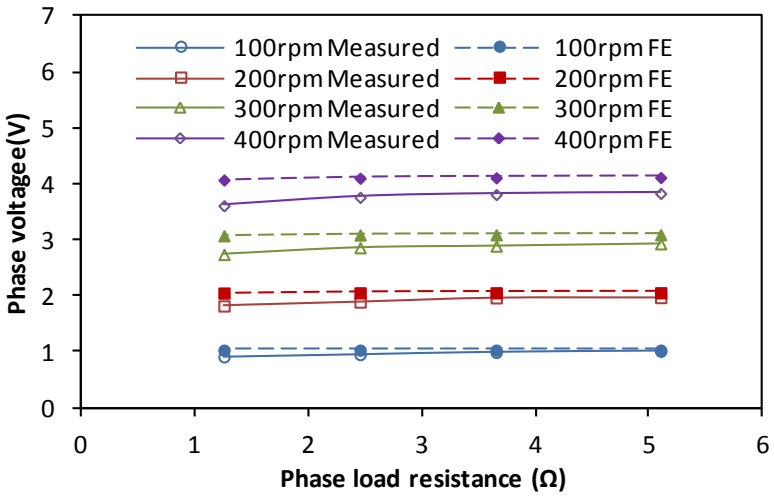

Fig. 2.56. Phase voltage variation with load resistance at different speeds.

As the load resistance is reduced, the current through the load increases and when the current reaches 32% of the rated current the phase voltage reduces by 8.6% Fig. 2.57.

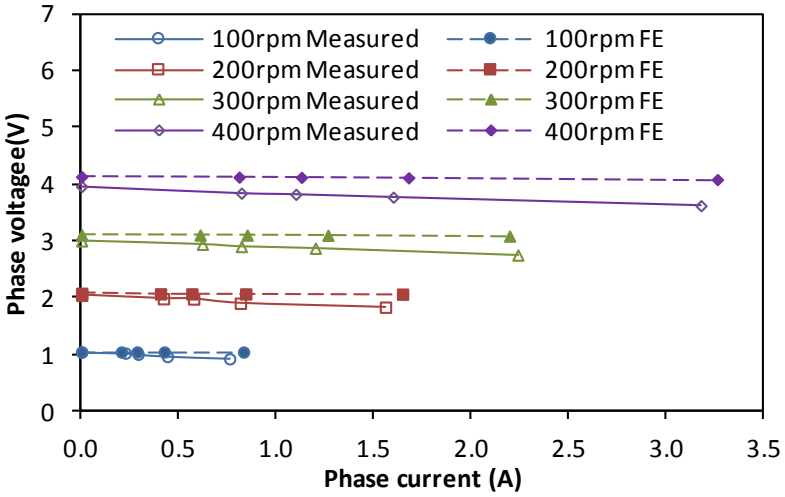

Fig. 2.57. Phase voltage variation with load current at different speeds.

As the load resistance is reduced the load current increases Fig. 2.58, as the back EMF is constant at a given speed, and hence the output power increases as shown in Fig. 2.59 at different speeds.

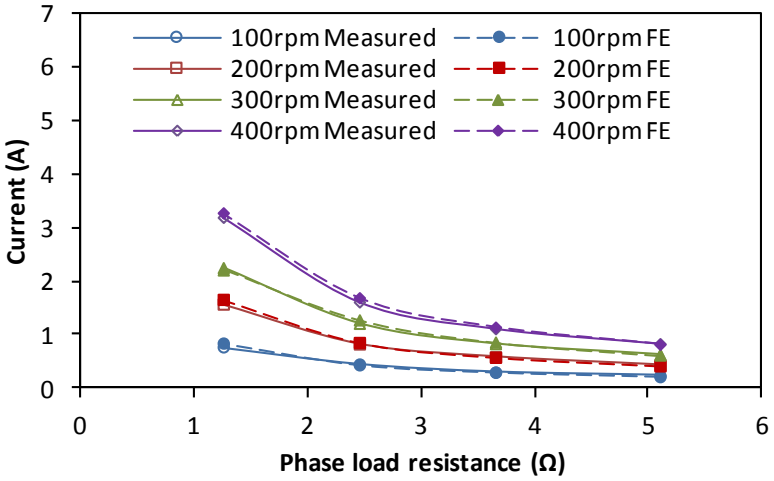

Fig. 2.58. Variation of phase current with load resistance at different speeds.

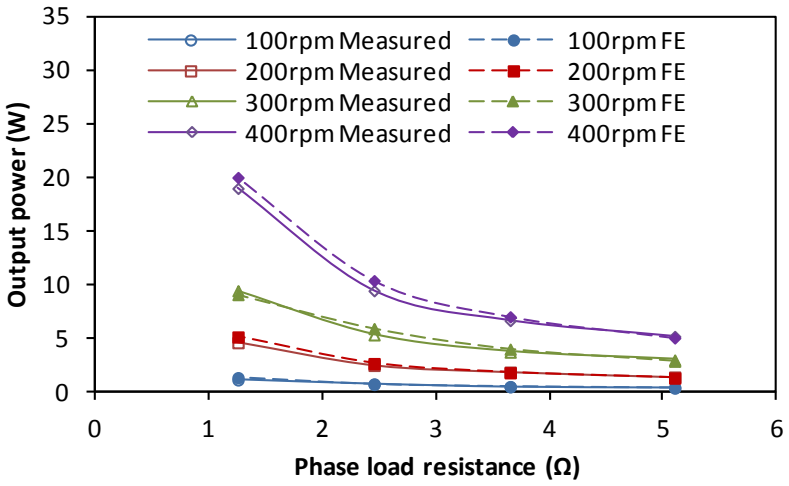

Fig. 2.59. Output power variation with load resistance at different speeds.

The PS-SFPM machine is demonstrated operating up to 32% of its rated phase current to validate that the prototype will operate as expected as a generator with a resistive load. The difference between measured and predicted data is smallest at lower speeds, as the speed increases the measured back EMF is lower than predicted using FE. A reason for this is at higher speeds the magnet temperature increases and hence the remanant flux density will decrease resulting in a reduced back EMF. The measured and FE predicted phase voltage waveforms when the load resistance is 5.10Ω, 3.65Ω, 2.45Ω and 1.25 Ω are shown in Fig. 2.60, Fig. 2.61, Fig. 2.62 and Fig. 2.63 respectively.

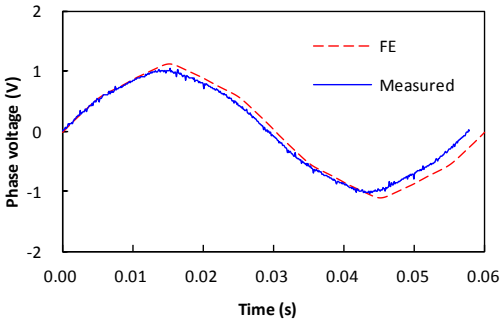

(a) 100 rpm

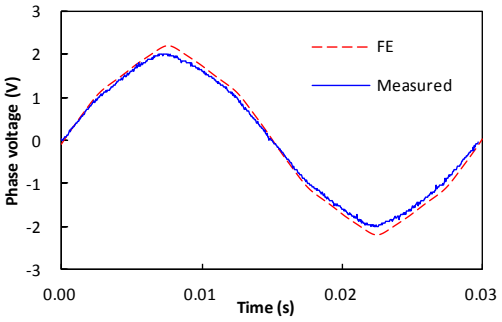

(b) 200 rpm

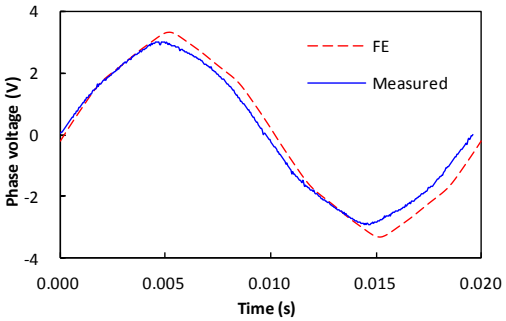

(c) 300 rpm

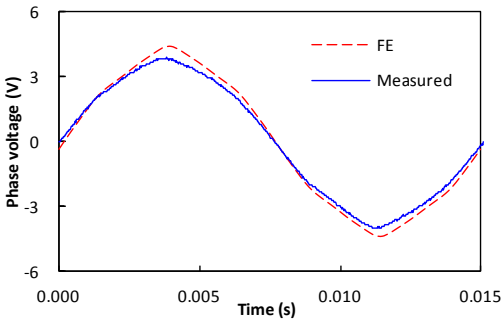

(d) 400 rpm

Fig. 2.60. Phase voltage waveforms with 5.1Ω load resistance.

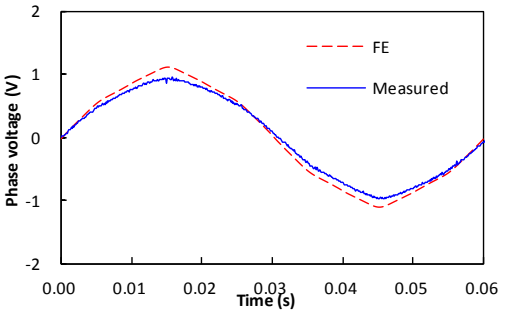

(a) 100 rpm

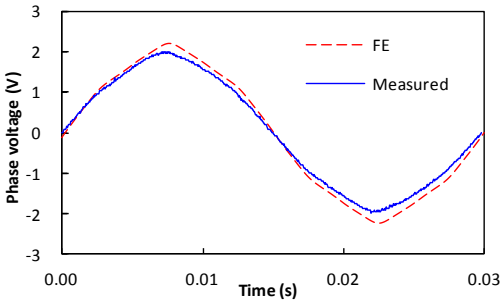

(b) 200 rpm

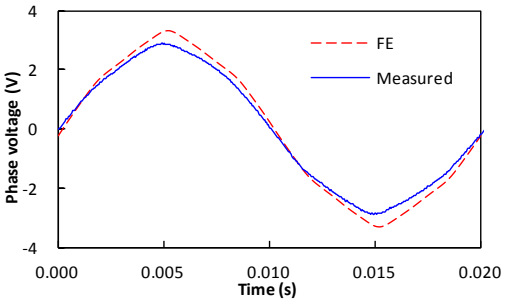

(c) 300 rpm

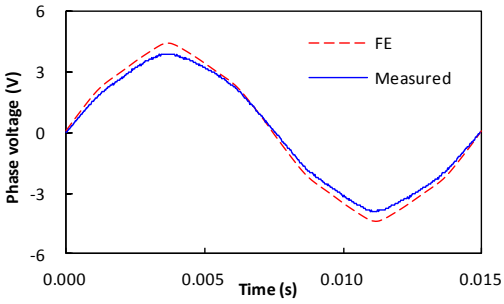

(d) 400 rpm

Fig. 2.61. Phase voltage waveforms with 3.65Ω load resistance.

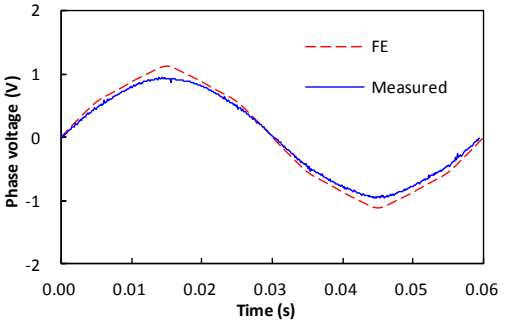

(a) 100 rpm

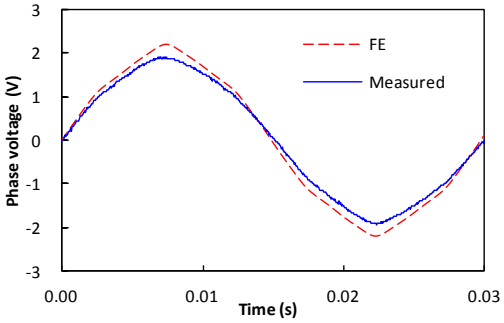

(b) 200 rpm

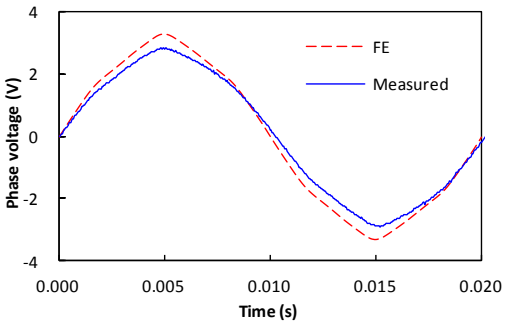

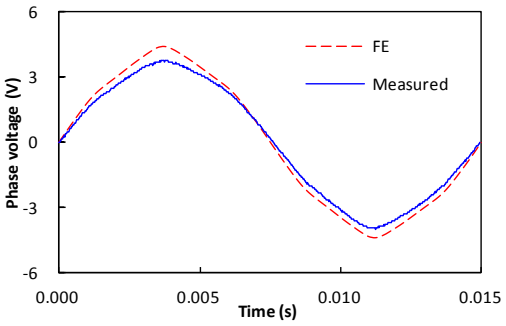

(c) 300 rpm (d) 400 rpm

Fig. 2.62. Phase voltage waveforms with 2.45Ω load resistance.

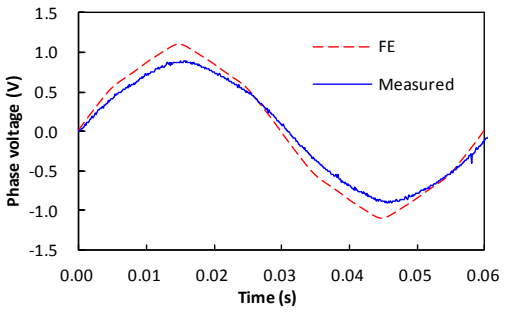

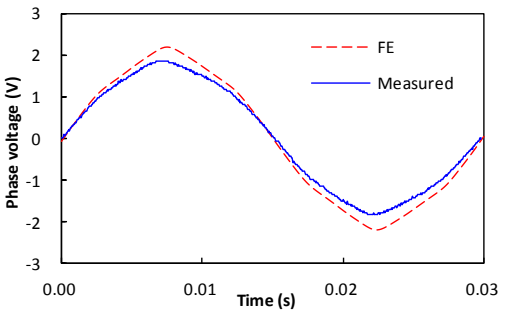

(a) 100 rpm (b) 200 rpm

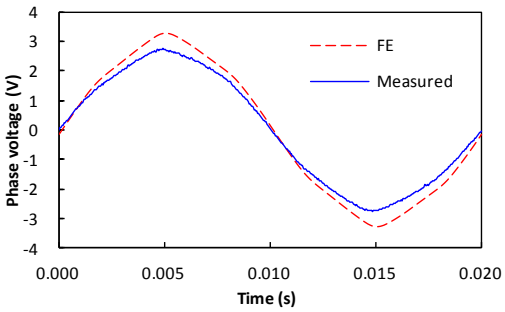

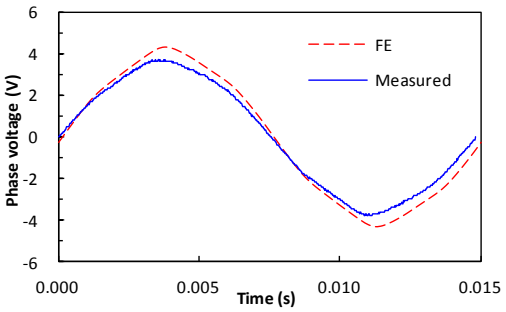

(c) 300 rpm (d) 400 rpm

Fig. 2.63. Phase voltage waveforms with 1.25Ω load resistance.

The measured and FE predicted phase current waveforms when the load resistance is 5.10Ω, 3.65Ω, 2.45Ω and 1.25 Ω are shown in Fig. 2.64, Fig. 2.65, Fig. 2.66 and Fig. 2.67 respectively.

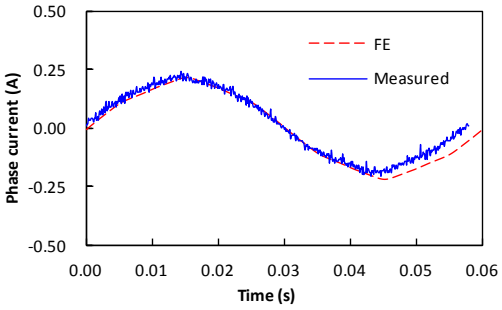

(a) 100 rpm

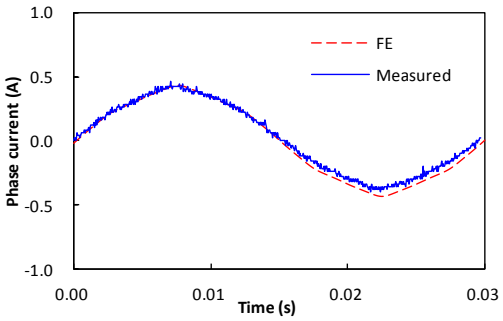

(b) 200 rpm

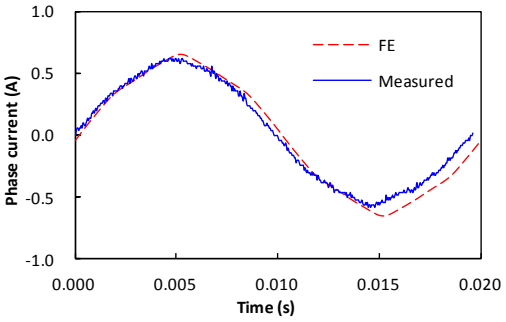

(c) 300 rpm

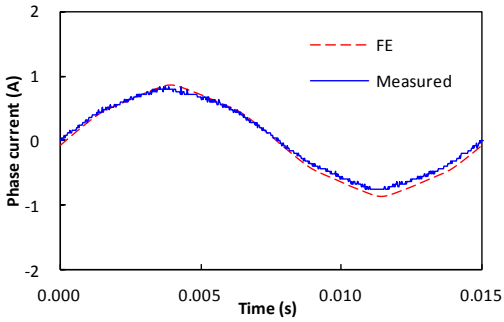

(d) 400 rpm

Fig. 2.64. Phase current waveforms with 5.1Ω load resistance.

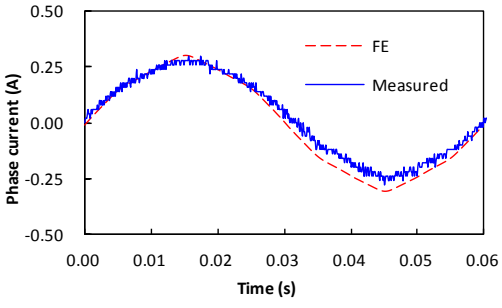

(a) 100 rpm

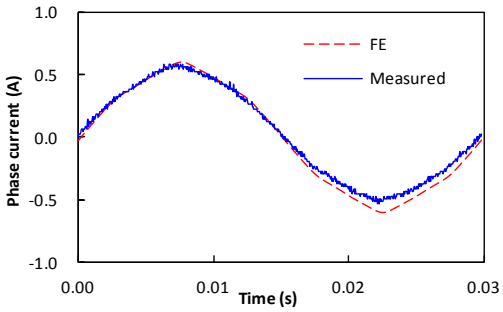

(b) 200 rpm

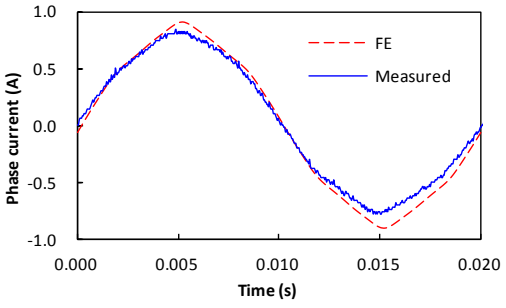

(c) 300 rpm

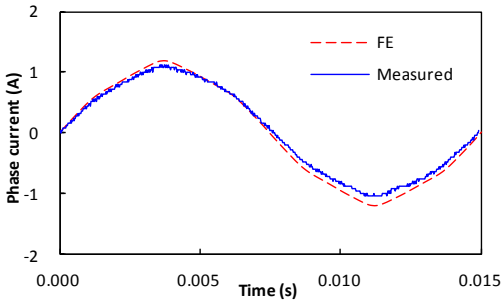

(d) 400 rpm

Fig. 2.65. Phase current waveforms with 3.65Ω load resistance.

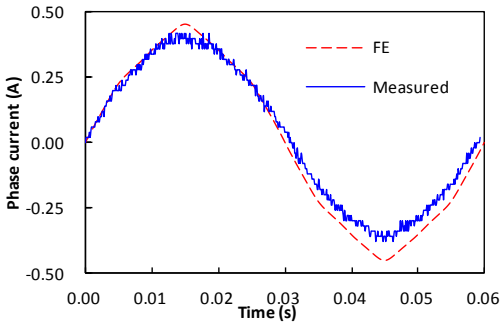

(a) 100 rpm

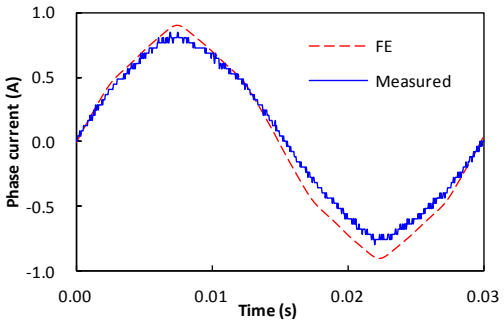

(b) 200 rpm

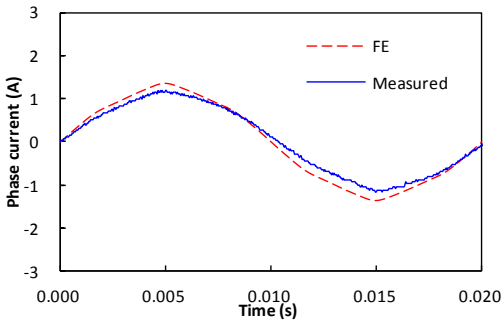

(c) 300 rpm

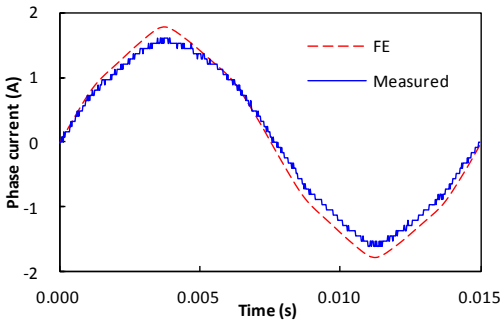

(d) 400 rpm

Fig. 2.66. Phase current waveforms with 2.45Ω load resistance.

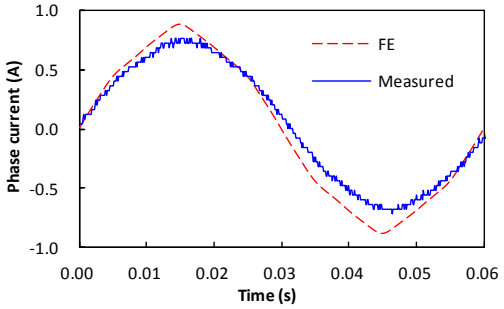

(a) 100 rpm

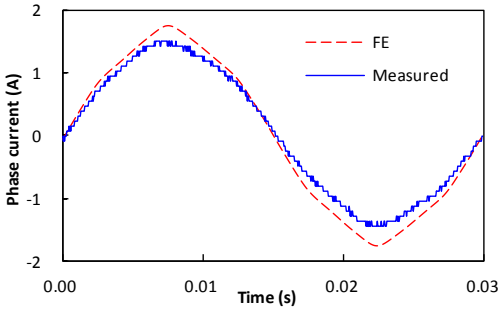

(b) 200 rpm

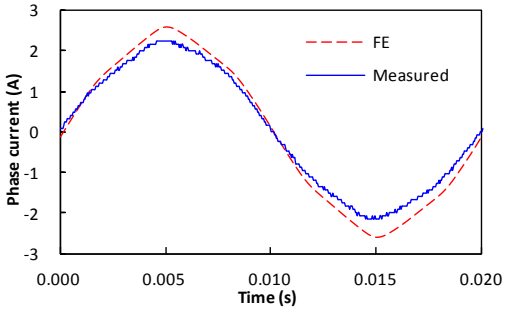

(c) 300 rpm

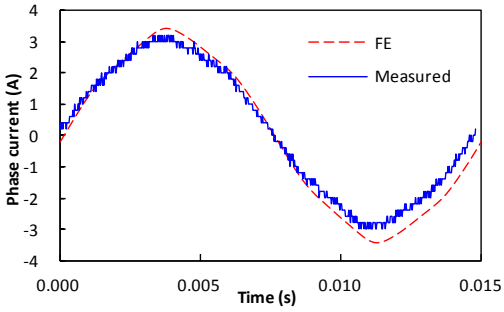

(d) 400 rpm

Fig. 2.67. Phase current waveforms with 1.25Ω load resistance.

2.9. Conclusions

A novel PM switched flux machine with partitioned stator structure has been presented. This machine has been optimised with different numbers of rotor poles and the performance of four machines compared. Electromagnetic torque and torque ripples were investigated, with 11 rotor poles producing the highest rated torque and machines with odd numbers of rotor poles experiencing the lowest cogging and on-load torque ripples. The impact of including rotor and PM bridges for prototyping has been shown to reduce the torque performance and alter the cogging torque magnitude. The power factor under q-axis current control is obtained, showing decreased power factor for increased number of rotor poles due to decreased PM flux linkage. The PS-SFPM machine was then experimentally tested with decreased performance due to end effects while still validating the concept of a PS-SFPM machine.

CHAPTER 3 - PARTITIONED STATOR SWITCHED FLUX PERMANENT MAGNET MACHINES WITH ALTERNATE TOOTH WINDINGS

3.1. Introduction

In the previous chapter a novel permanent magnet (PM) machine which combines switched flux machines and magnetic gearing technology was presented. The PS-SFPM machine enabled increased utilisation of machine volume by separating the copper and PM material of the switched flux machine across two stationary bodies being the wound and PM stators. This evolution of the switched flux machine removed the conflict between volume for copper and PM allowing each to be optimised independently of the other. The PS-SFPM machine was investigated and shown to share features of both a switched flux machine (in the switching nature of the flux in the wound stator with respect to the rotor position) and magnetic geared machines (as the airgap flux density is modulated between airgaps and torque produced from a fractional slot PM machine armature MMF).

In the previous chapter the initial investigation of the PS-SFPM machine focused on developing a fractional slot machine with double layer windings (or all teeth wound) into a partitioned development, this can be further extended to consider the use of single layer windings (alternate tooth wound).

Single layer windings were first explored in the field of conventional fractional slot machines, where employing single layer windings was validated as an alternative concentrated winding topology [4, 92, 97] where double and single layer wound machines are compared revealing for certain combinations of stator teeth and PM poles increased flux linkage was achieved. Often single layer windings are highlighted for their fault tolerance due to increased self and reduced mutual phase inductances enabling reduced phase interaction during fault conditions.

Recently in conventional switched flux machines the single layer or alternate layer windings have been investigated [40-41, 98] revealing that employing this winding technique in switched flux machines has the benefits of increased back EMF, lower mutual inductances and the ability to reduce the width of the non-wound teeth. Particularly the non-sinusoidal nature of the back EMF in single layer windings when even numbers of rotor poles are used is highlighted as a potential issue, but while odd numbers of rotor poles exhibits sinusoidal back EMF they are susceptible to unbalanced magnetic forces acting on the rotor although the number of stator and rotor poles may be further doubled to eliminate the inherent unbalanced magnetic force.

The application of single layer windings to the PS-SFPM machine will be investigated in this chapter, considering its potential benefits and negative features.

3.2. Winding Connections and Specification

PS-SFPM machines with single layer windings will be investigated using FE and experimentally tested. Single layer windings are concentrated windings with phase coils wound on alternate stator teeth not all teeth wound as considered in the previous chapter, where two coils share a single slot. The PS-SFPM machine with double layer windings investigated in the previous chapter is shown with 10 rotor poles in Fig. 3.1, each PM pole has corresponding tooth which has a single coil. With single layer windings now alternate PM poles have a coil associated with them for 10 rotor poles Fig. 3.2 and 11 rotor poles Fig. 3.3. Each phase for single and double layer windings have the same slot area available but single layer windings will have longer end windings due to the increased coil span (resulting from utilisation of a complete slot area instead of sharing the slot area with an adjacent coil).

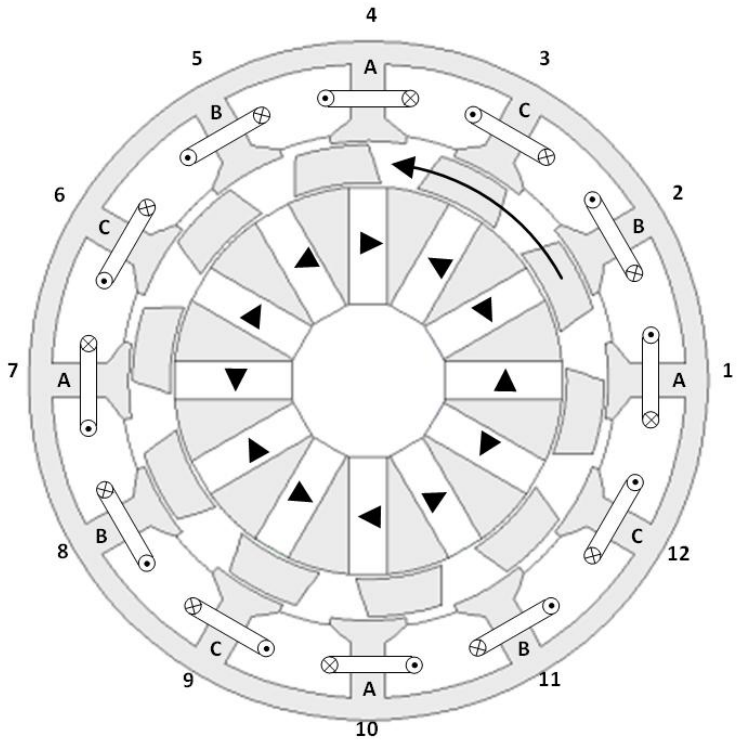

Fig. 3.1. PS-SFPM machine with double layer windings and 10 rotor poles

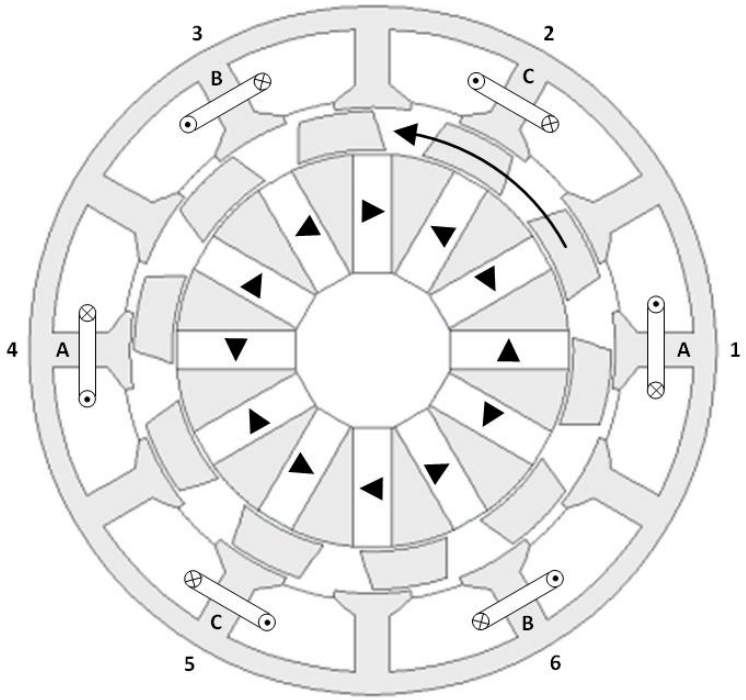

Fig. 3.2. PS-SFPM machine with 10 rotor poles and single layer windings

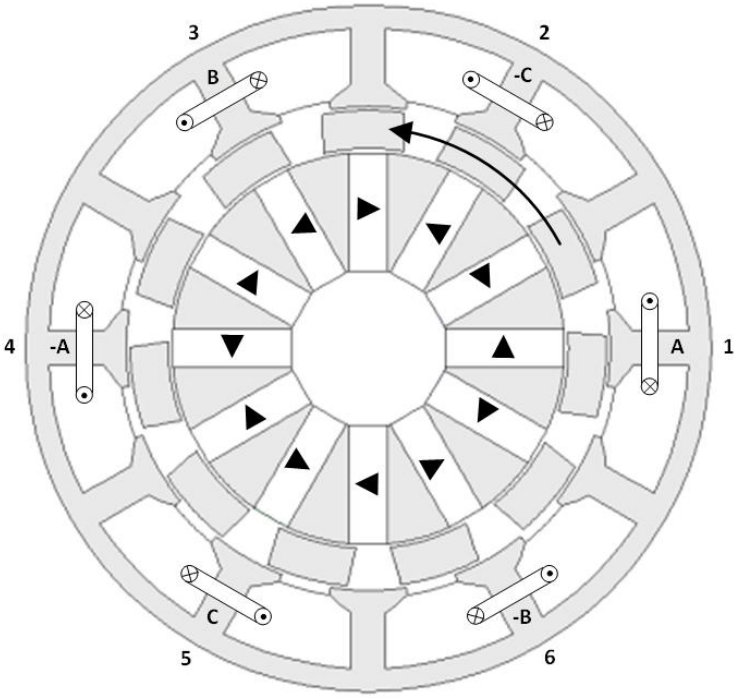

Fig. 3.3. PS-SFPM machine with 11 rotor poles and single layer windings

The winding connection again may be determined in the same manner as with double layer windings, either considering the winding connection in terms of a switched flux machine or a magnetic geared machine. For single layer windings back EMF vectors for each tooth are now alternate teeth and therefore only half the numbers of coils per phase are employed. The coil EMF vector diagrams for 10 (Fig. 3.4) and 11 (Fig. 3.5) rotor poles are shown with coils in phase electrically with each other grouped and attributed to a phase.

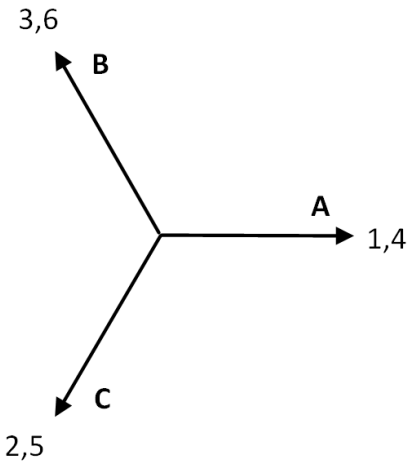

Fig. 3.4. Coil EMF vectors for machine with 10 rotor poles and single layer windings

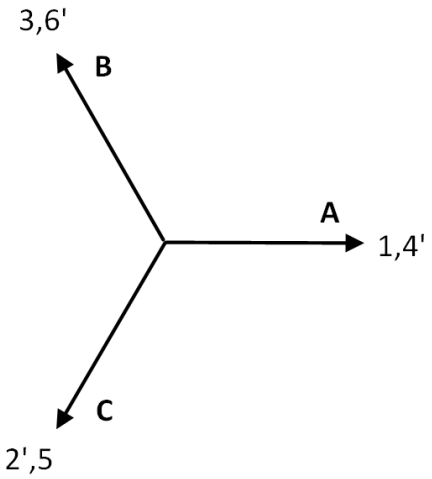

Fig. 3.5. Coil EMF vectors for machine with 11 rotor poles and single layer windings

It is observed that the winding connections are identical for 10 and 14 rotor poles with the B and C phases reversed, and likewise for 11 and 13 rotor poles. Unlike double layer windings all the coils of a single phase are electrically in phase and therefore a unity distribution factor is achieved with all combinations of rotor poles.

In order to provide comparison with the investigation of the machines with double layer windings the dimensions of the machines with single layer windings are constrained to those used for double layer windings, the geometric parameters are given in

Table III.

Table VIII. Geometric parameters of PS-SFPM machine

Parameter	**Value**			
Rotor Poles	10	11	13	14
Rotor Outer Width/Pitch Ratio	0.5	0.6	0.6	0.5
Rotor Inner Width/Pitch Ratio	0.7	0.7	0.6	0.5
Outer Diameter (mm)	90			
Axial Length (mm)	25			
Stator Slots	12			
Stator PM Pole Pairs	6			
Airgap Length (mm)	0.5			
Split Ratio (Outer airgap)	0.70			
Split Ratio (Inner airgap)	0.58			
Stator Yoke Thickness (mm)	3			
Tooth Width (mm)	4.5			
Tooth Tip Thickness (Body) (mm)	3			
Tooth Tip Thickness (Opening) (mm)	1			
Stator Slot Opening/Pitch Ratio	0.4			
Stator Slot Opening (mm)	6.67			
Rotor Radial Thickness (mm)	5			
PM Thickness (mm)	5			
Inner Diameter (mm)	20.8			

The drive parameters used are shown in Table IX, with the difference between double and single layer highlighted, that due to different end winding length the phase resistance is increased and hence at rated current it exhibits greater copper loss.

Table IX. Specification of PS-SFPM machine

Parameter	Value	
Rated Peak Phase Current (A)	14.14	
Rated Peak Phase Voltage (V)	20.78	
Turns per Phase	72	
Copper Packing Factor	0.4	
PM Volume (mm^3)	23300	
Copper Volume (mm^3)	39958	
Slot Area (mm^2)	133.195	
Rated Current Density (A/mm^2)	3.82	
Winding Configuration	Double Layer	Single Layer
Rated Copper Loss (W)	15.58	21.43
Phase Resistance (Ω)	0.104	0.143
End winding length per coil (mm)	38.53	62.41

3.3. Performance Analysis

The performance of the PS-SFPM machine with single layer windings will be compared with different numbers of rotor poles in terms of the back EMF production, on-load torque production (as cogging torque has been investigated in the previous chapter for the same machine geometry) and inductances. The performance will then be compared with the results for double layer windings.

3.3.1. Back EMF

The back EMF of machines with single layer windings is predicted using FE and shown for different numbers of rotor poles in Fig. 3.6. Even numbers of rotor poles exhibit asymmetric back EMF in a single phases with different positive and negative peaks. The phase back EMF harmonics are obtained in Fig. 3.7, with even orders observed in machines with even numbers of rotor poles being 10 and 14. These even orders in the back EMF are the same as those observed in conventional switched flux machines with even numbers of rotor poles is observed.

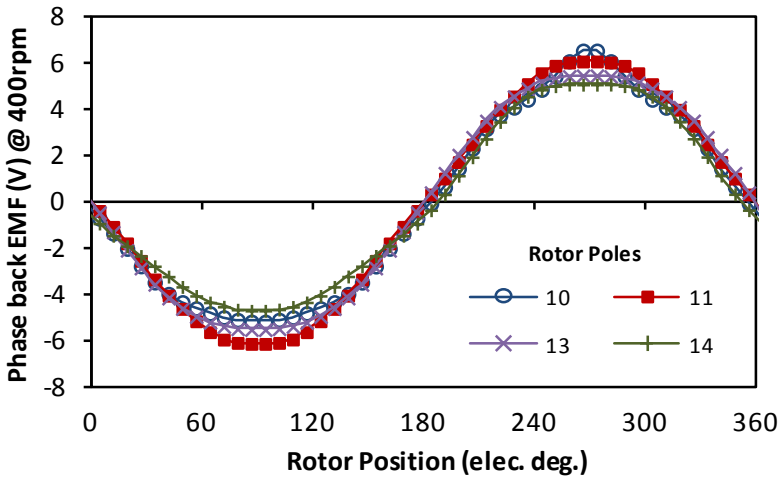

Fig. 3.6. Open-circuit back EMF variation with rotor position with different numbers of rotor poles and single layer windings

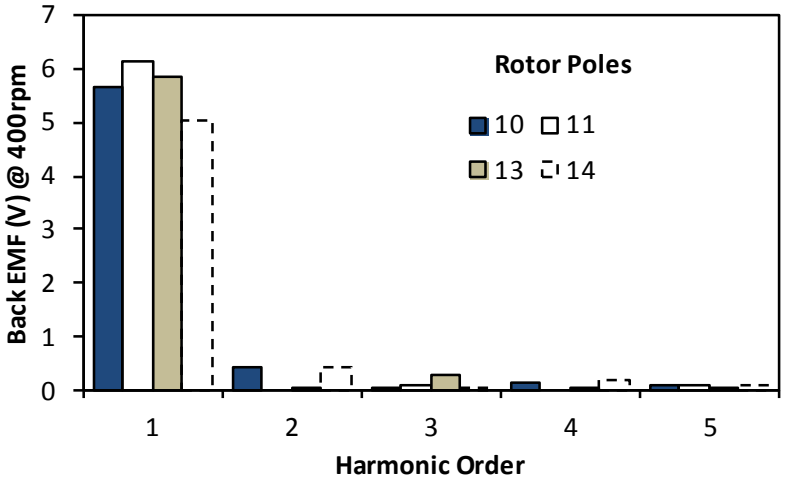

Fig. 3.7. Open-circuit back EMF harmonics with different numbers of rotor poles and single layer windings

PS-SFPM machines with 10 rotor poles, with double layer windings each phase contains 4 individual coils but with single layer windings each phase contains 2. From Fig. 3.8 the back EMFs for two coils of the single layer winding are asymmetric and identical, whereas with double layer windings both coils are asymmetric but reversed polarity. With single layer windings and even numbers of rotor poles, each coil of the same phase experiences the same rotor pole situation, resulting in asymmetric phase back EMF. With odd numbers of rotor poles each coil of the same phase experiences different rotor pole situations i.e. one positive and one negative, therefore cancelling harmonics which result in asymmetric back EMF.

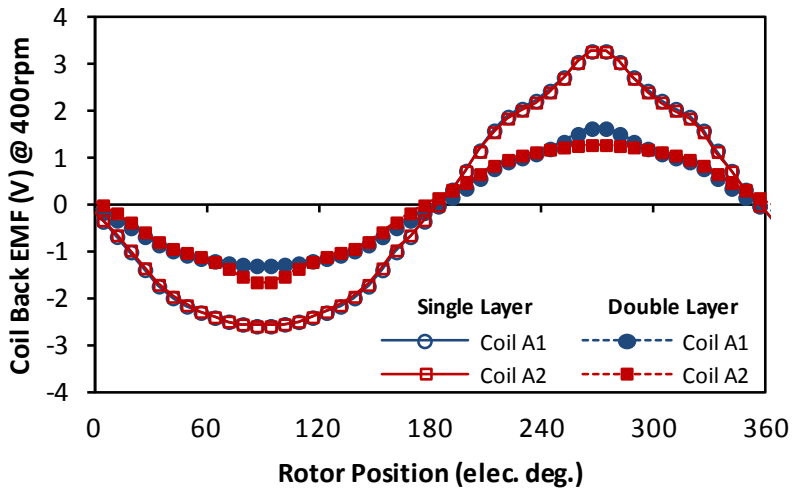

Fig. 3.8. Individual coil back EMF for 10 rotor poles with single and double layer windings

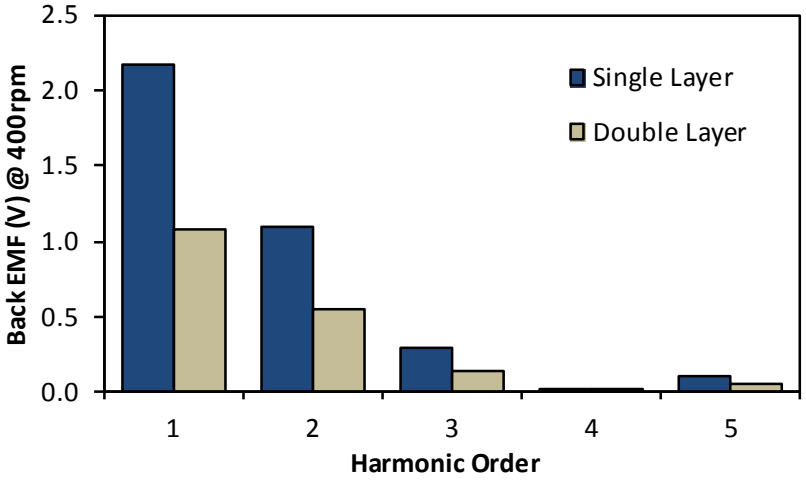

Fig. 3.9. Individual coil back EMF harmonics for 10 rotor poles with single and double layer windings

With asymmetric back EMF for PS-SFPM machines with single layer windings when excited with sinusoidal currents, additional torque ripples will be produced.

3.3.2. Torque

The rated torque for PS-SFPM machines with single layer windings and different numbers of rotor poles is shown in Fig. 3.10. As the rotor position changes there occurs greater torque ripples in those machines with even numbers of rotor poles due to asymmetric back EMF, 11 rotor poles has the highest average torque.

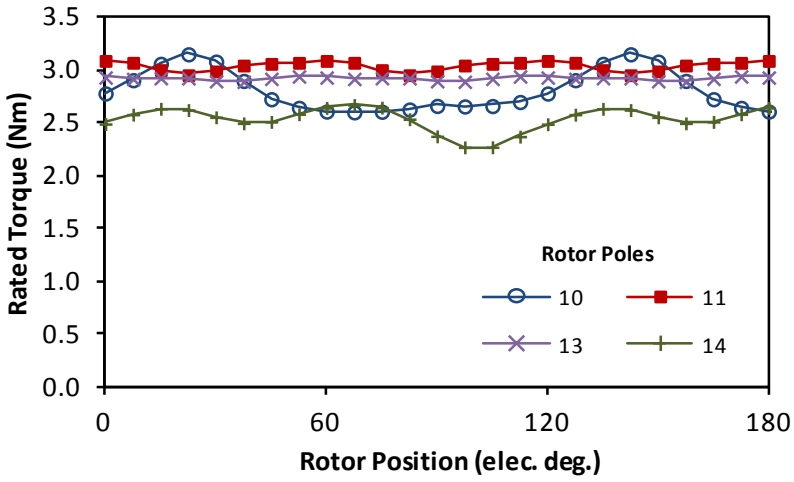

Fig. 3.10. Comparison of rated torque with single layer windings for different rotor poles

Increasing the q-axis current, the variations in peak to peak torque ripples are obtained for different numbers of rotor poles. As previously stated, machines with even numbers of rotor poles being 10 and 14 exhibit asymmetric back EMF therefore incur increased torque ripples with q-axis current increase. For machines with 11 and 13 rotor poles as their back EMF is very sinusoidal therefore increasing the armature reaction field in the q-axis does not significantly increase the on-load torque ripples.

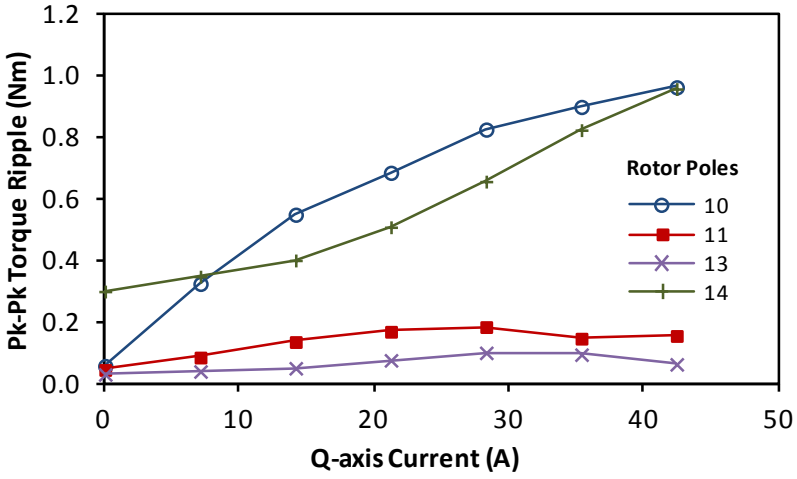

Fig. 3.11. Comparison of torque ripples variation with Q-axis current and single layer windings for different rotor poles

For increased q-axis current, the machine with 11 rotor poles has the highest torque production compared with 10, 13 and 14 rotor poles, with 14 having the lowest. As the q-axis current is increased saturation reduces the overload performance for all combinations of rotor poles Fig. 3.12.

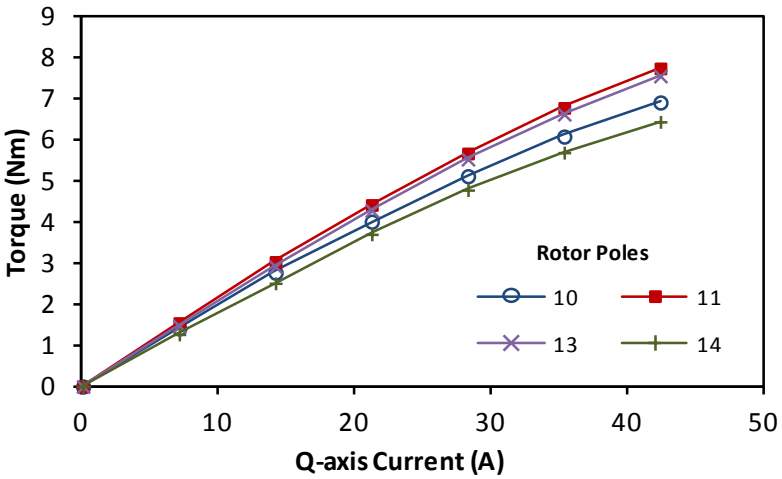

Fig. 3.12. Torque characteristic of PS-SFPM machine with 10, 11, 13 and 14 rotor poles with single layer windings

3.4. Inductances

The self inductance L_a is obtained through two FE solutions with PM only and when I_a is dc excited with the peak current I_{pk} (17). Where $\varphi_{a(Ia=Ipk)}$ is the flux linkage in phase A when phase A is dc excited with I_{pk} and PM excitation, and $\varphi_{a(Ia=0)}$ is the flux linkage in phase A with only PM excitation.

$$L_a = \frac{\psi_{a(I_a=I_{pk})} - \psi_{a(I_a=0)}}{I_{pk}} \tag{17}$$

The mutual inductance between phase A and B, M_{ab} is again obtained through FE using two solutions with PM only and when I_a is dc excited with the peak current I_{pk} (18). Where $\varphi_{b(Ia=Ipk)}$ is the flux linkage in phase B when phase A is dc excited with I_{pk} and PM excitation, and $\varphi_{b(Ia=0)}$ is the flux linkage in phase B with only PM excitation.

$$M_{ab} = \frac{\psi_{b(I_a=I_{pk})} - \psi_{b(I_a=0)}}{I_{pk}} \tag{18}$$

Using FE the self and mutual inductances with different numbers of rotor poles are obtained Fig. 3.13, due to the salient nature of the rotor structure both self and mutually the inductance contains significant variation with rotor position. Machines with odd numbers of rotor poles have higher self inductance and lower mutual inductance than those with even

numbers of rotor poles increasing their fault tolerance through short circuit limitation with larger self inductances. The mutual inductance for even numbers of rotor poles is negative as the flux linking a phase from another phase's current excitation is negative.

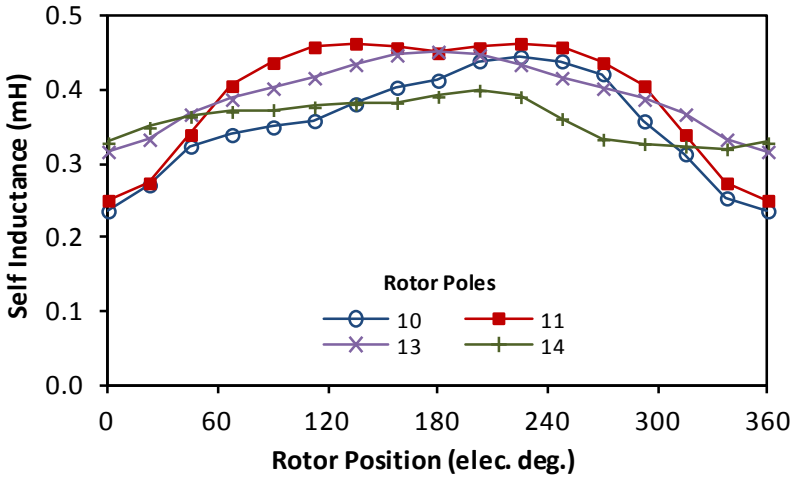

(a)

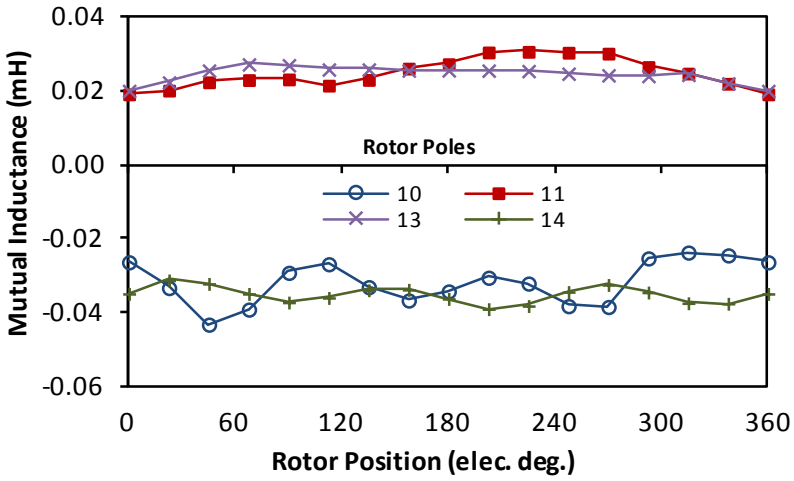

(b)

Fig. 3.13. (a) Self and (b) mutual inductances with different numbers of rotor poles at rated current 14.14A

3.5. Comparison of Double and Single Layer Windings

Comparison of single layer and double layer windings for the same machine geometry is now performed, to provide insight into selection of winding layout.

3.5.1. Back EMF

The back EMF variation with rotor position for both single and double layer windings have been shown and now the harmonic components of both are compared Fig. 3.14. Single layer windings with 11 and 13 rotor poles have greater fundamental back EMF than those with double layer, but the converse is observed for those with 10 and 14. The reduction in fundamental back EMF for machines with 10 and 14 rotor poles with single layer winding may be expected as their back EMF is asymmetric and second order harmonics occur.

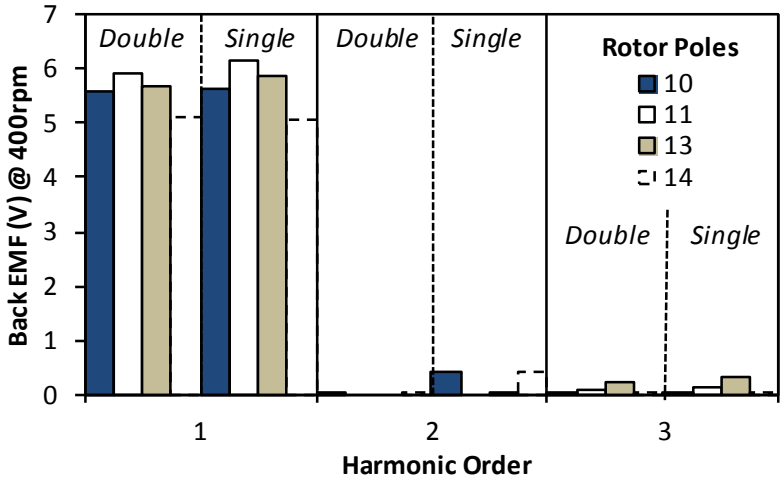

Fig. 3.14. Open-circuit back EMF harmonics for PS-SFPM machine with different numbers of rotor poles and single and double layer windings

3.5.2. Torque

As the reluctance torque in PSFPMMs is negligible, as a result of minimal difference between d-and q-axis inductances, zero d-axis current control is utilised in the constant torque region. In PSFPMMs numbers of rotor poles close to the number of stator teeth produces optimal torque production. Average electromagnetic torque variation, predicted using FE, with q-axis current having double and single layer concentrated windings are shown in Fig. 3.15.

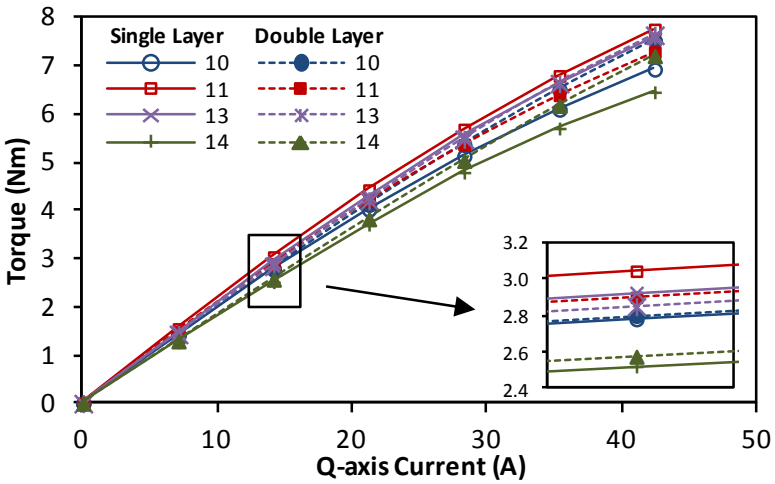

Fig. 3.15. Torque characteristic of PSFPMM with 10, 11, 13 and 14 rotor poles with single and double layer windings

From Table X it can be seen that 11 rotor poles produce maximum rated torque with both double and single layer windings. Employing single layer windings increases the rated torque density for odd numbers of rotor poles but with large q-axis current the magnetic circuit saturates quicker, Fig. 3.15. While for single layer windings greater torque density is achieved, this must be considered with respect to additional copper loss and the impact on total machine power density. The average rated torque for machines with different numbers of rotor poles and with single and double layer windings is shown in Table X

Table X. Rated torque of PSFPMMs with different numbers of rotor poles

	Winding Layers	Rotor Poles			
		10	11	13	14
Torque (Nm)	Single	2.78	3.04	2.93	2.52
	Double	2.80	2.90	2.85	2.58

In Fig. 3.16 the torque for 11 rotor poles is higher for all q-axis current for single rather than double layer windings and the opposite is true for 10 rotor poles. As the magnetic circuit is saturated at higher q-axis currents the d-axis inductance decreases because of decreased stator iron permanence, therefore the PM flux linkage is reduced with increased q-axis current. This results in reduced overload torque from the possible torque performance if φ_m is considered independent of I_q.

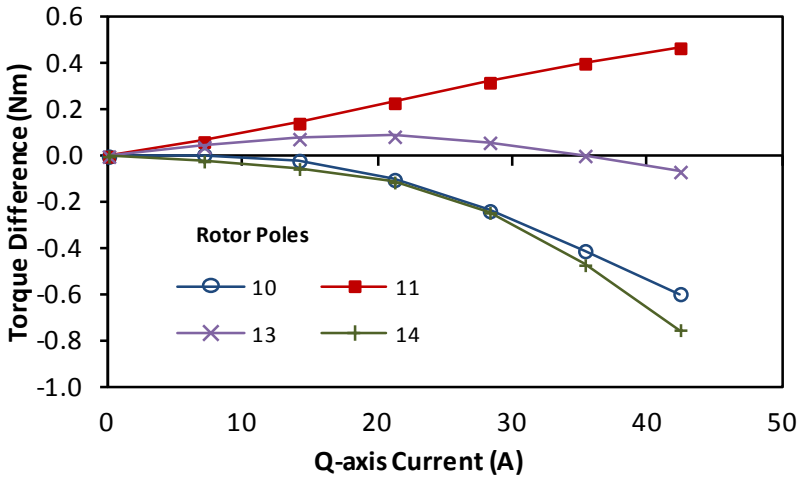

Fig. 3.16. Difference between single and double layer average torque production

For machines with 11 rotor poles their peak tooth flux density is higher with double layer windings Fig. 3.18 therefore higher saturation in the d-axis and hence reduction in PM flux linkage for higher q-axis current. The opposite is true for a machine with 10 rotor poles where single layer windings have the higher tooth flux density Fig. 3.17 and decreased torque performance.

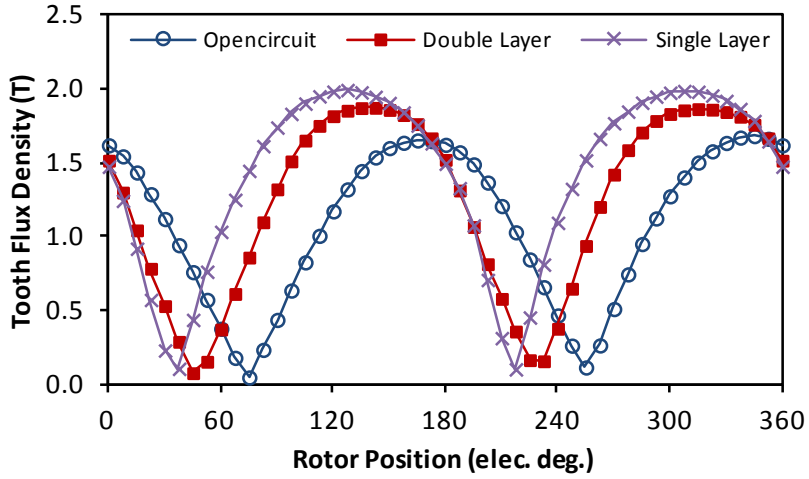

Fig. 3.17. Single tooth flux density variation for 10 rotor poles where Iq = 42.42A for double and single layer excitation

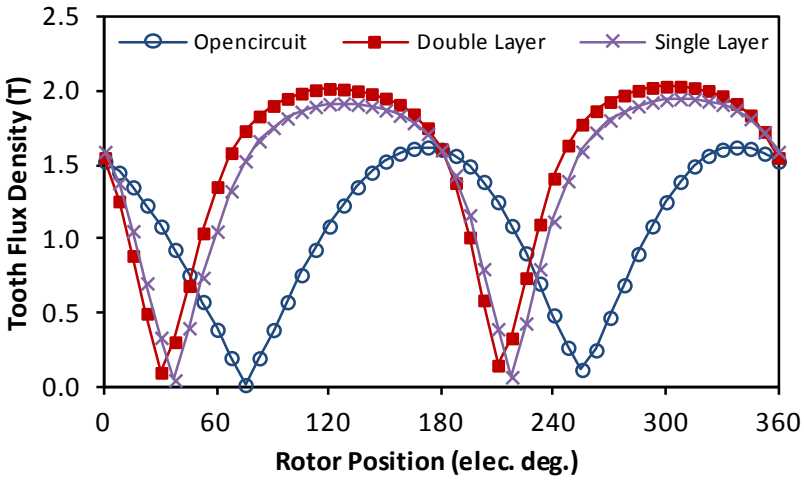

Fig. 3.18. Single tooth flux density variation for 11 rotor poles where Iq = 42.42A for double and single layer excitation

With significant back EMF harmonics and flux density harmonics due to winding excitation at rated current, the on-load torque ripples are increased for machines with 10 rotor poles Fig. 3.19 for single layer windings compared with double layer windings. The difference between on-load torque ripples for machines with 11 rotor poles is minimal as the back EMF for both single and double layer windings is very sinusoidal.

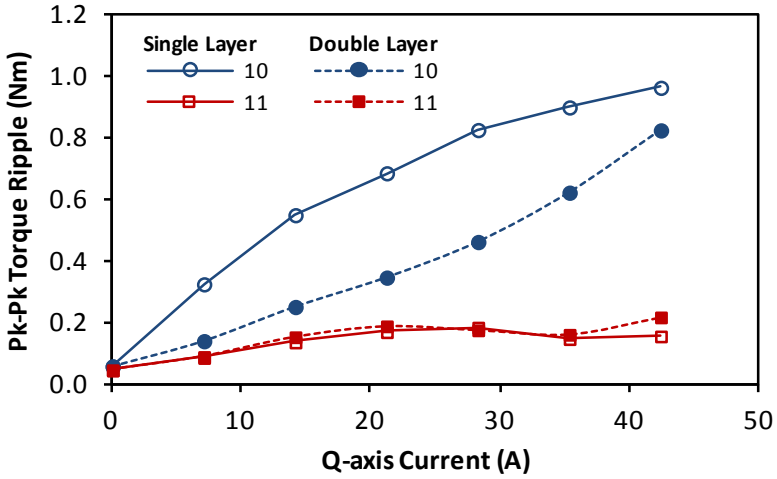

Fig. 3.19. Comparison of torque ripples with q-axis current for double and single layer windings with 10 and 11 rotor poles

The armature reaction field for machines with 10, 11, 13 and 14 rotor poles are shown in Fig. 3.20, Fig. 3.21, Fig. 3.22 and Fig. 3.23 respectively.

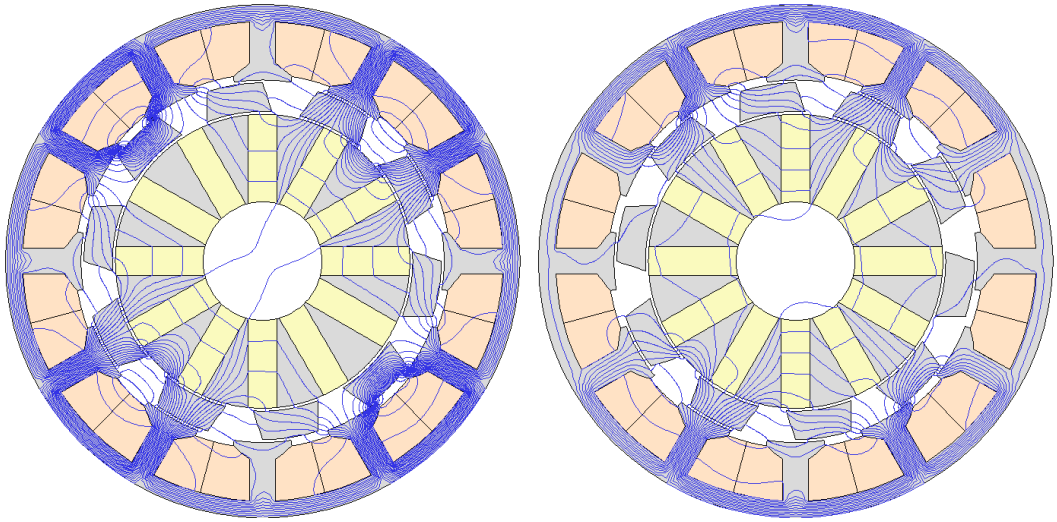

(a) (b)

Fig. 3.20. Armature reaction field with 10 rotor poles (a) double layer and (b) single layer

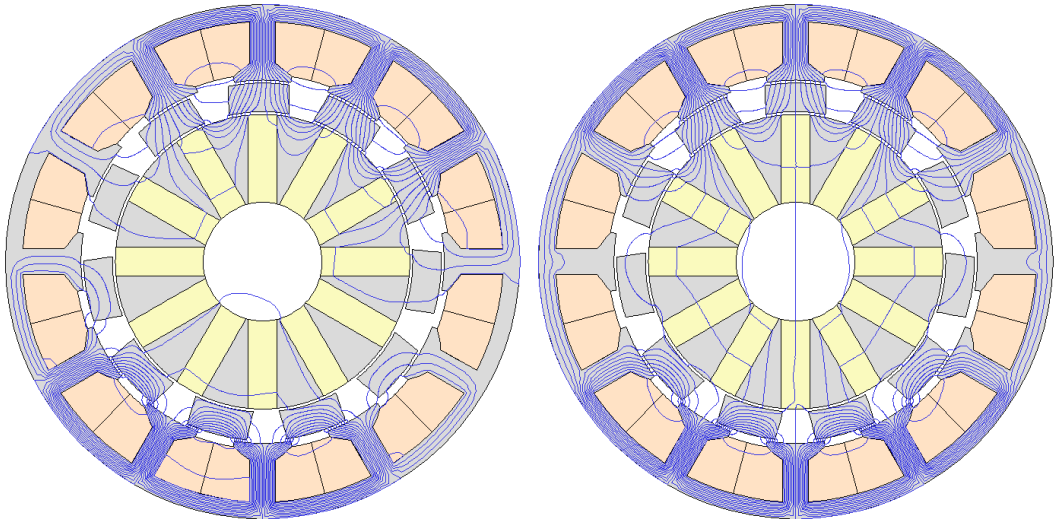

(a) (b)

Fig. 3.21. Armature reaction field with 11 rotor poles (a) double layer and (b) single layer

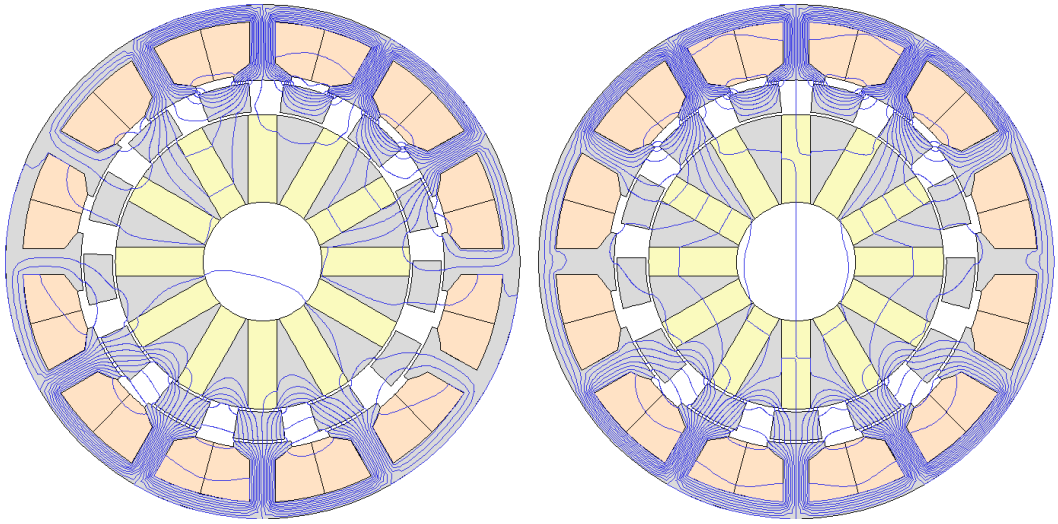

(a) (b)

Fig. 3.22. Armature reaction field with 13 rotor poles (a) double layer and (b) single layer

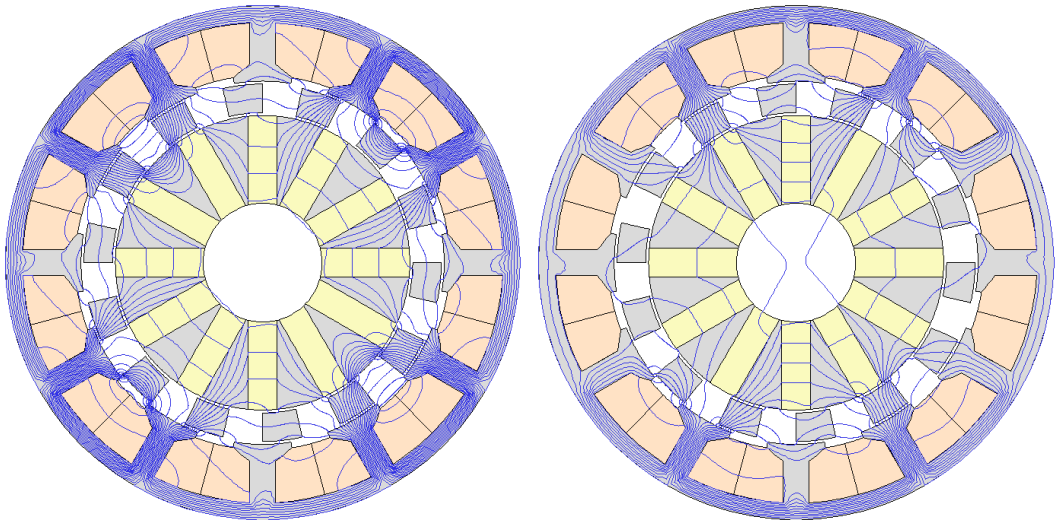

(a) (b)

Fig. 3.23. Armature reaction field with 14 rotor poles (a) double layer and (b) single layer

3.6. Inductances

Self and mutual inductances for the PS-SFPM machine with double and single layer windings are now compared when the rated DC value of current is applied to a phase. The FE model is initially solved at rated current in all phases and PM present, to attain the saturation of the iron, the PM remanance is then removed and the permeance of each FE mesh element is maintained and a single phase DC excited to attain the inductance. The variation of inductance with rotor position is shown, to observe the change in flux in a phase which will

vary saturation of each phase at different positions. For single layer windings the average self inductance Fig. 3.24 for all numbers of rotor poles increases compared with double layer windings providing limitation of short circuit currents during faulty operation. Employing machines with odd numbers of rotor poles i.e. 11 or 13, will result in higher self inductance than those with even numbers of rotor poles i.e. 10 and 14.

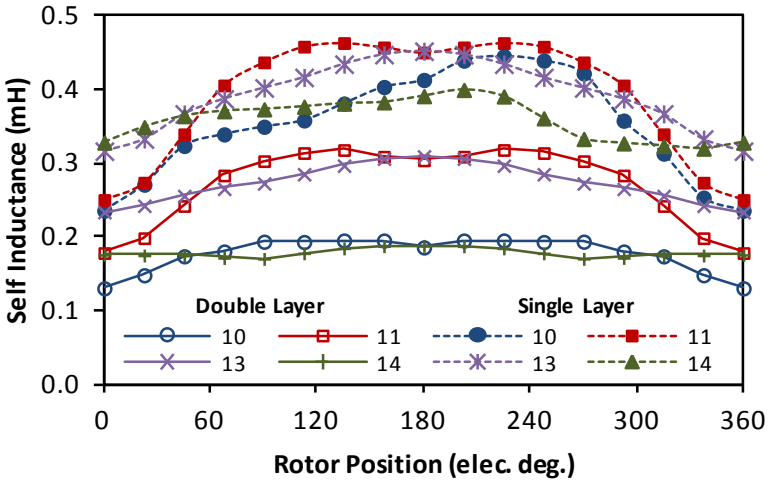

Fig. 3.24. Variation of self inductance with rotor position with different numbers of rotor poles employing single and double layer windings

The mutual inductance between phases for double and single layer windings is shown in Fig. 3.25. Employing single layer the mutual inductance is inverted as the flux linking B and C phases is in the opposite direction for odd numbers of rotor poles, due to the coil orientation change from double to single layer windings. The magnitude of mutual inductance remains very similar for double and single layer windings with 11 and 13 rotor poles. But for even numbers of rotor poles the polarity of mutual inductance remains the same and decreases with single layer windings.

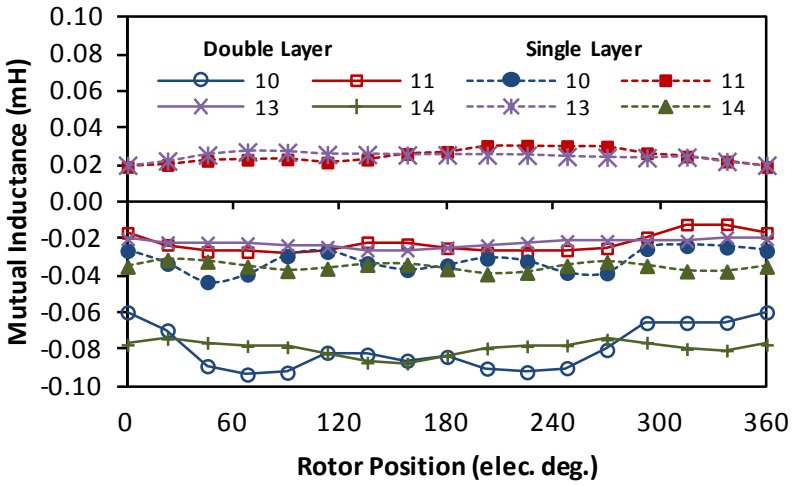

Fig. 3.25. Variation of mutual inductance with rotor position with different numbers of rotor poles employing single and double layer windings

The average values of self and mutual inductances with single and double layer windings are presented in Table XI along with the ratio of mutual to self inductance at rated currents. Machines with single layer windings and odd numbers of rotor poles have lowest mutual to self inductance ratio and are therefore favourable for fault tolerance.

Table XI. Average inductances with different numbers of rotor poles employing single and double layer windings

	Winding	Rotor Poles			
		10	11	13	14
L_d (mH)	Single Layer	0.649	0.569	0.470	0.469
	Double Layer	0.346	0.419	0.375	0.302
L_q (mH)	Single Layer	0.385	0.369	0.356	0.379
	Double Layer	0.359	0.297	0.279	0.242
L_a (mH)	Single Layer	0.353	0.390	0.393	0.360
	Double Layer	0.177	0.271	0.273	0.178
M_{ab} (mH)	Single Layer	-0.032	0.025	0.025	-0.035
	Double Layer	-0.079	-0.022	-0.022	-0.079
M_{ab}/L_q (%)	Single Layer	9.0	6.4	6.3	9.8
	Double Layer	44.7	8.3	8.2	44.5

3.7. Torque and Power-Speed Characteristic

To predict the PS-SFPM machine torque-speed relationship the inverter voltage limit determines the maximum speed, the phase voltage is calculated using (19) where the DC voltage limit of the convertor is (20):

$$V_{pha} = \sqrt{\left(R_{ph}I_d - \omega_{elec}L_qI_q\right)^2 + \left(R_{ph}I_q + \omega_{elec}L_dI_d + \omega_{elec}\psi_m\right)^2} \tag{19}$$

$$V_{pha} = \frac{V_{dc}}{\sqrt{3}} \tag{20}$$

The electrical angular frequency ω_{elec} is N_r times the mechanical angular frequency ω_{mech} which is the rotational velocity of the rotor. The phase resistance is determined by the slot area and end winding length for different winding configurations. The inductances change with different d and q axis currents, therefore the inductance is calculated using FE at different combinations of I_d and I_q.

From the results for double Fig. 3.26 and single Fig. 3.27 layer windings, machines with single layer windings have larger speed range resulting from their higher d-axis inductance than those with double layer windings.

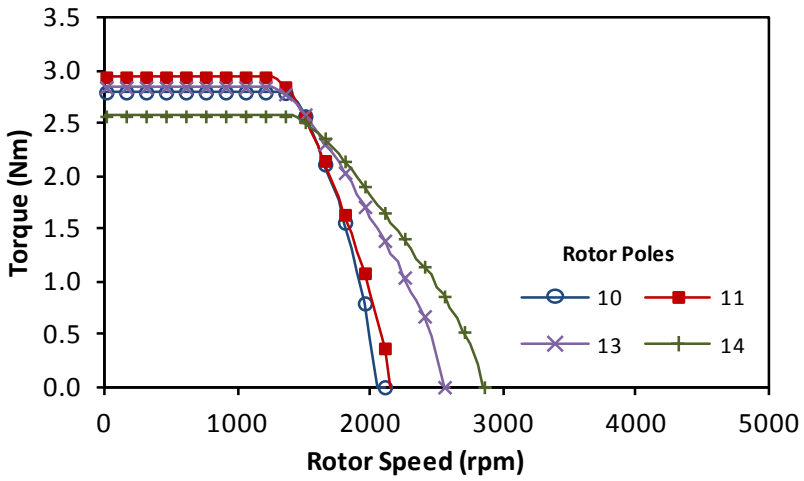

Fig. 3.26. Torque-speed characteristic with different numbers of rotor poles and double layer windings

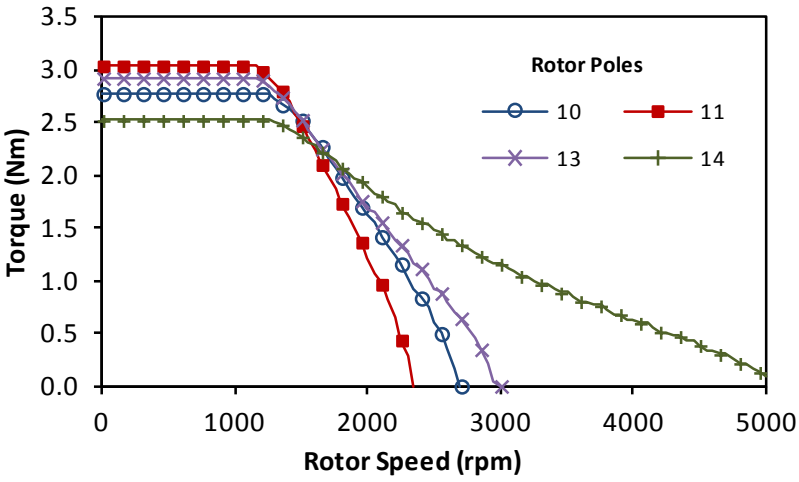

Fig. 3.27. Torque-speed characteristic with different numbers of rotor poles and single layer windings

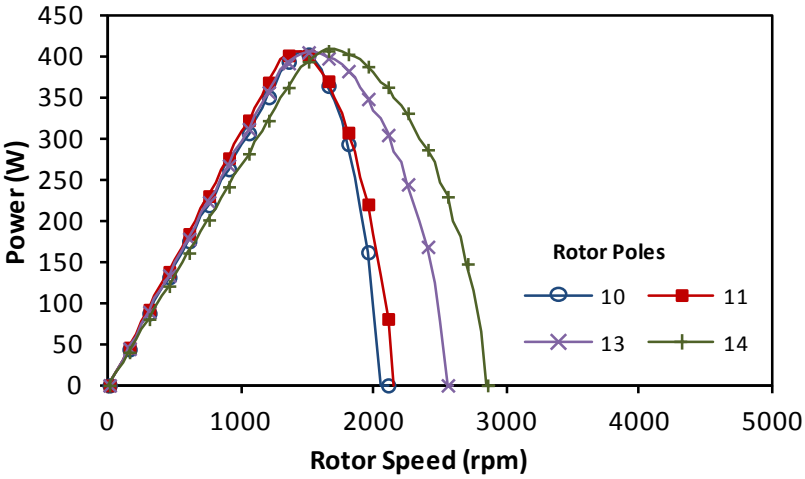

Fig. 3.28. Power-speed characteristic with different numbers of rotor poles and double layer windings

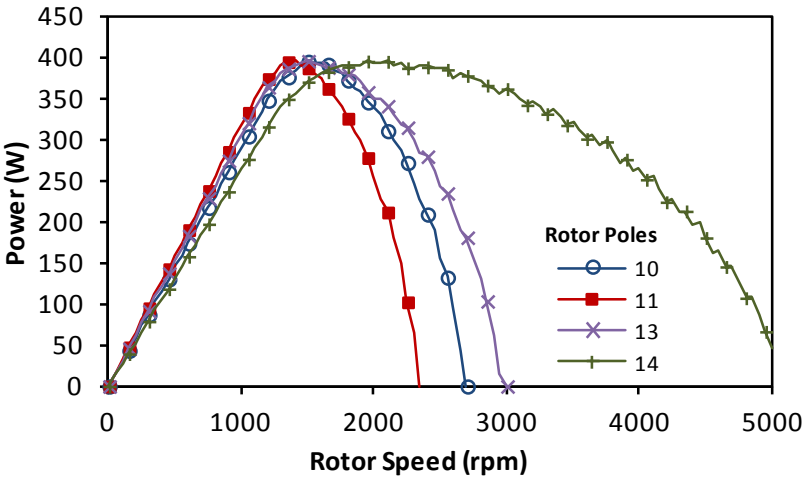

Fig. 3.29. Power-speed characteristic with different numbers of rotor poles and single layer windings

The ability of d-axis current to suppress the PM flux may be quantified by a flux weakening factor. This factor (21) indicates the potential of a machine's speed range beyond the rated

speed. A value which is equal to 1 may feature an 'infinite' flux weakening region, with larger values having the larger field weakening ranges.

$$K_{fw} = \frac{L_d I}{\psi_m} \tag{21}$$

From the PM flux linkage φ_m and dq-axis inductances the field weakening factor K_{fw} may be determined for different numbers of rotor poles with single and double layer windings Table XII.

Table XII. Flux linkage, flux weakening factor and rated power factor with different numbers of rotor poles

	Winding	**Rotor Poles**			
		10	11	13	14
φ_m (mWb)	Single Layer	13.5	13.4	10.8	8.6
	Double Layer	13.4	12.9	10.5	8.7
K_{fw}	Single Layer	0.68	0.60	0.62	0.77
	Double Layer	0.37	0.46	0.51	0.49
P.F	Single Layer	0.96	0.96	0.94	0.91
	Double Layer	0.98	0.97	0.96	0.95

The power factor variation with speed is calculated, as negative d-axis current is injected during field weakening operation the power factor increases until the current leads the voltage and then power factor reduces. The power factors for double Fig. 3.30 and single Fig. 3.31 layer windings are shown. With double layer windings the power factor during the constant torque region is greater than those with single layer windings.

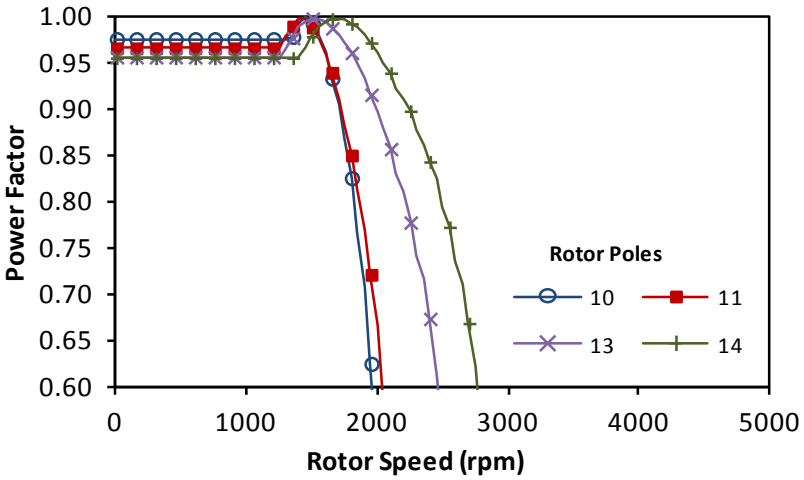

Fig. 3.30. Power factor-speed characteristic with different numbers of rotor poles and double layer windings

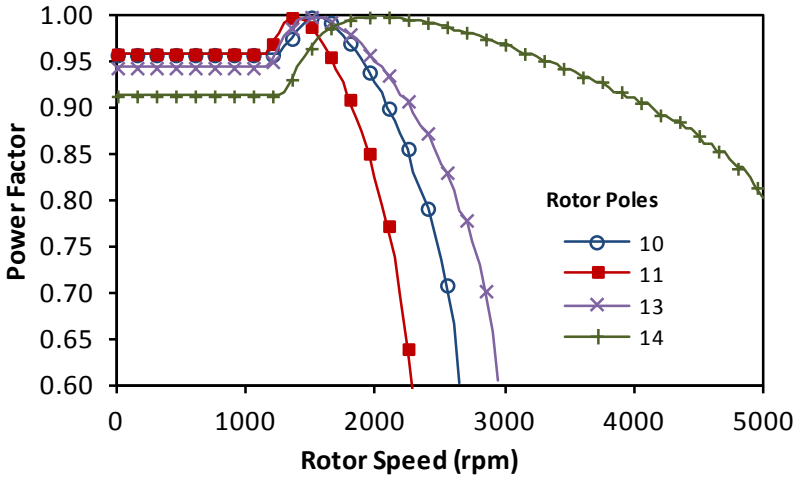

Fig. 3.31. Power factor-speed characteristic with different numbers of rotor poles and single layer windings

3.8. Experimental Validation

In order to obtain measured results for single layer windings the prototype stator with double layer windings is utilised with alternate coils. The measured single layer results assume half the number of turns per coil therefore in static torque operation lower q-axis current measurement is performed as the current density is doubled. Static operating conditions will be measured and compared for both double and single layer windings.

3.8.1. Back EMF

The measured and FE predicted back EMF at 400rpm is presented in Fig. 3.32 for the prototype machine with 10 rotor poles and double layer windings. In the measured back EMF even order harmonics are observed due to prototypical compromise and error, but a large fundamental back EMF is obtained validating the machine principle.

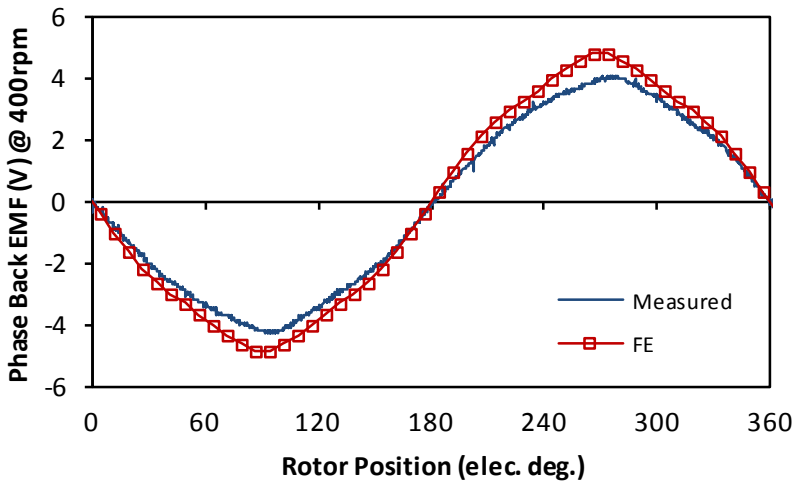

Fig. 3.32. Measured and FE back EMF for 10 rotor poles with double layer windings

With single layer windings with 10 rotor poles, as explained previously, asymmetric back EMF is expected due to the lack of cancelation of even order harmonics between coils in the same phase. This asymmetry of back EMF can be observed in both the FE and experimental results presented in Fig. 3.33, albeit with a similar reduction in back EMF magnitude between measured and FE results which may be attributed to manufacturing variances or that in FE the 3D end field effects are not considered.

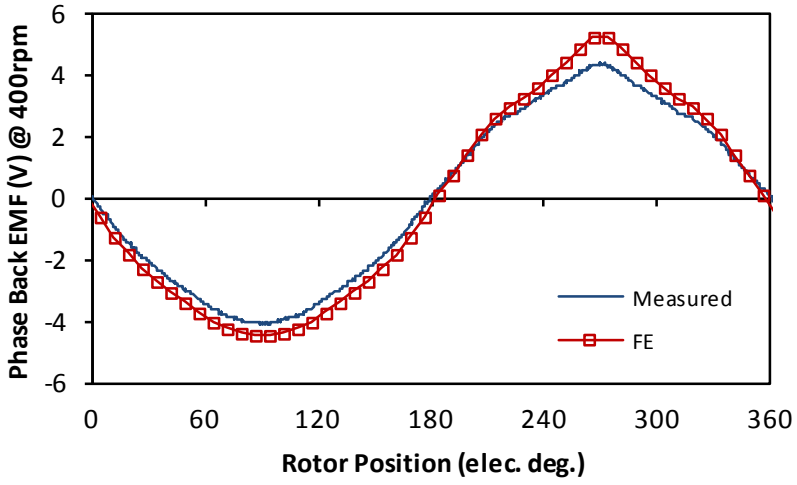

Fig. 3.33. Measured and FE back EMF for 10 rotor poles with single layer windings

A second rotor with 11 rotor poles is produced for comparison with 10 rotor poles with the same wound and PM stators. From FE calculation utilising 11 rotor poles rather than 10 will result in a higher phase back EMF and ultimately higher torque density with the same wound and PM stators. The back EMF for an 11 pole rotor with double layer windings is presented in Fig. 3.34. As with the 10 rotor poles comparison between FE and measured results with double layer windings, ideally from FE all even order harmonics in the back EMF in different coils of the same phase would be cancelled, therefore resulting in only odd order harmonics with greatest fundamental order, again in the measured results there occurs even order harmonics which skew the back EMF waveform. A similar reduction in back EMF magnitude occurs between FE and measured results as occurred in 10 rotor poles.

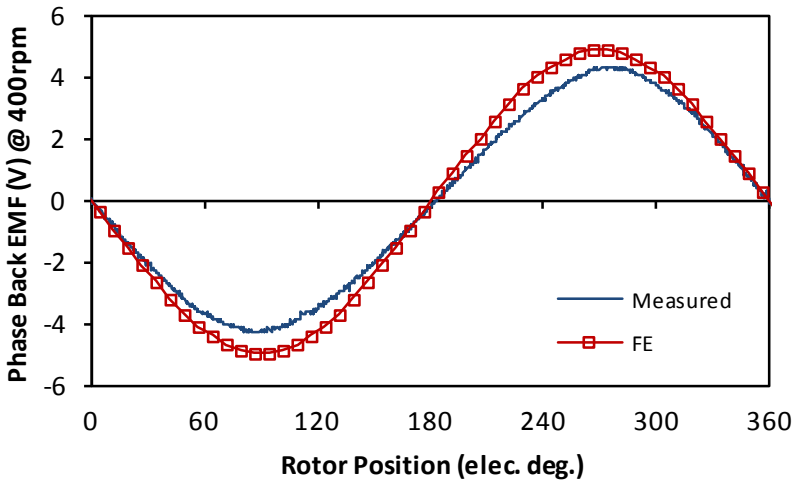

Fig. 3.34. Measured and FE predicted back EMF for 11 rotor poles with double layer windings

For 11 rotor poles with single layer winding the measured and FE predicted back EMF is compared in Fig. 3.35, again due to the difficult construction of a prototype rotor for this machine deformities occur thus resulting in additional parasitic back EMF harmonics.

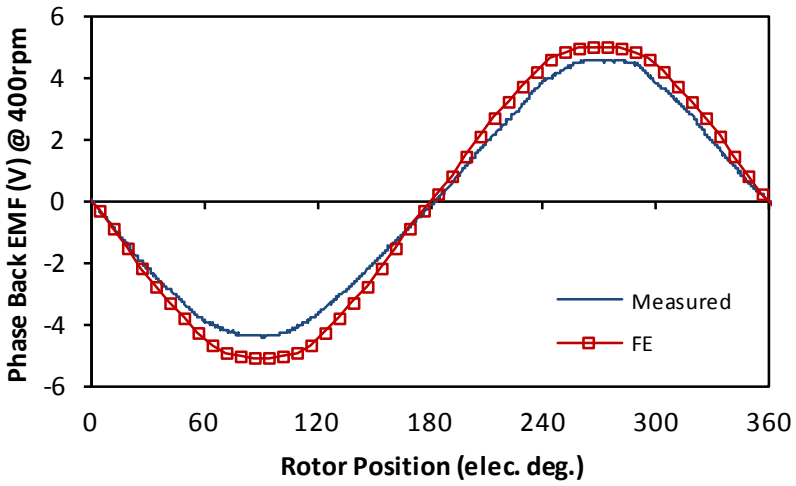

Fig. 3.35. Measured and FE back EMF for 11 rotor poles with single layer windings

In all the back EMF results there has been a reduction in measured back EMF which could be expected due to prototype procedure and end effects which have not been considered. But the measured back EMF validated that with 10 and 11 rotor poles now employing single layer winding are able to produce fundamental order back EMF when rotated to ultimately produce constant torque when supplied with sinusoidal phase current.

3.8.2. Static Torque

The static torque variation with q-axis current is compared between FE and measured results, with double layer windings Fig. 3.36. Both FE and measured confirm that with 11 rotor poles a higher torque is achieved than when 10 rotor poles are utilised.

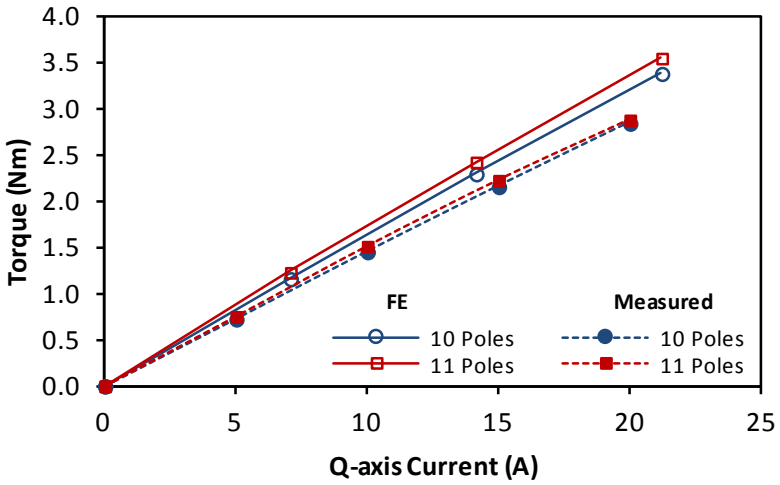

Fig. 3.36. Measured and FE back torque with q-axis current with double layer windings

Further with single layer windings also 11 rotor poles have higher constant torque production than with 10 rotor poles, again a reduction between FE and measured results is observed but is expected Fig. 3.37.

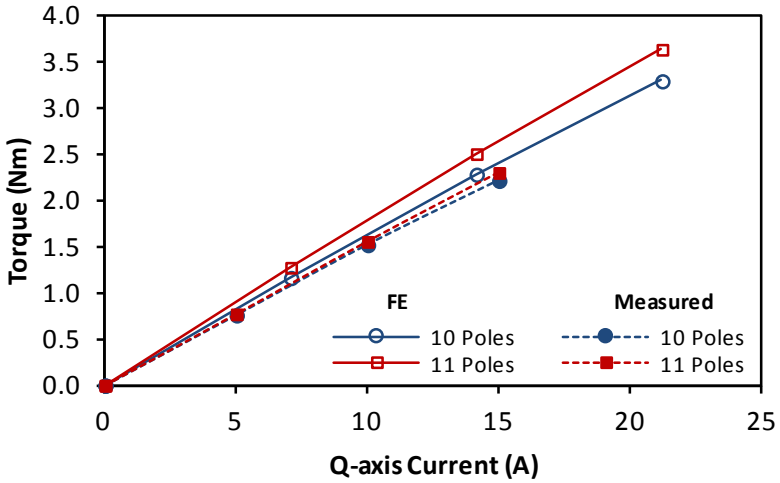

Fig. 3.37. Measured and FE back torque with q-axis current with single layer windings

3.8.3. Comparison

Single and double layer wound machines are now compared with the same number of rotor poles. In Fig. 3.38 machines with 10 rotor poles have their torque measured with different q-axis current applied, with 10 rotor poles minimal increase in torque is expected between single and double layer windings at rated q-axis current due to the asymmetry of the single layer winding back EMF causing reduced overall fundamental back EMF resulting in reduced overall torque performance. The measured and FE results feature the same characteristics for 10 rotor poles with single layer windings having a slight increase in torque production at rated current.

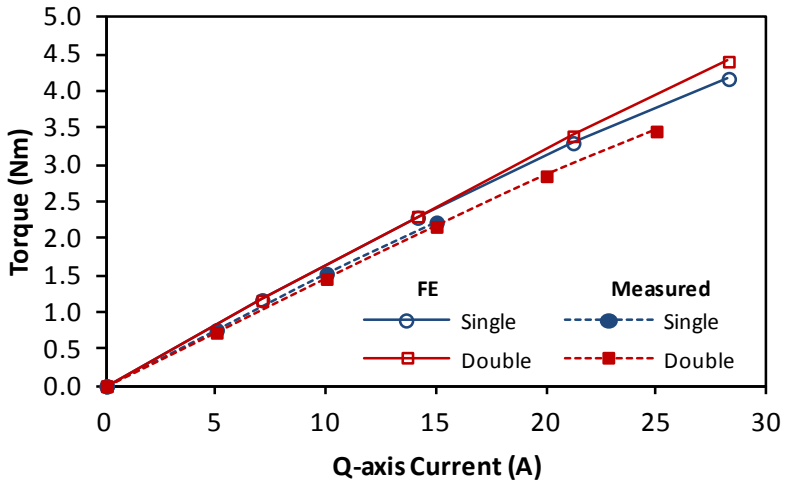

Fig. 3.38. FE predicted and measured torque for machine with 10 rotor poles for double and single layer windings

From FE with single layer windings and 11 rotor poles there is expected a greater increase between double to single layer windings. This can be seen in Fig. 3.39 for FE results, but the measured results display less increase but still increased slightly by employing single layer windings. In the measured back EMF for single layer windings with 11 rotor poles there was observed an amount of asymmetry which could account for the reduction in increase between measured double to single layer windings.

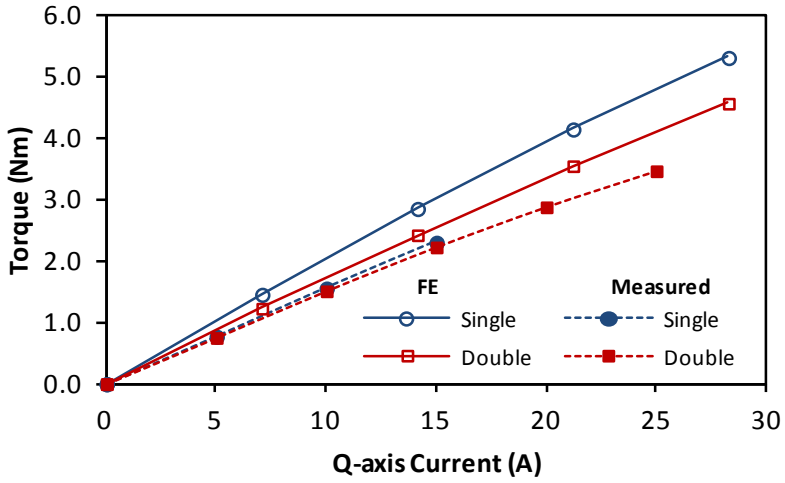

Fig. 3.39. FE predicted and measured torque for machine with 11 rotor poles for double and single layer windings

Measured static torque with double and single layer windings having 10 and 11 rotor poles are compared in Fig. 3.40 which as predicted using FE the machine having the same wound and PM stators with 11 rotor poles with single layer windings has the highest torque

production with 10 rotor poles with double layer windings having the minimum. These measured results validate that a machine utilising the magnetic gearing/switched flux principle in a PS-SFPM format is possible.

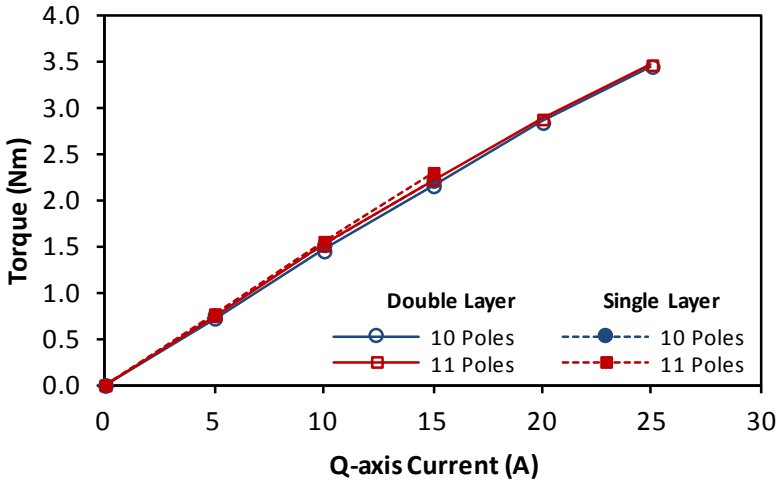

Fig. 3.40. Measured torque comparison with double and single layer windings with 10 and 11 rotor poles

3.9. Conclusions

An alternative winding configuration with single layers has been presented for the PS-SFPM machines which in the previous chapter was presented with double layers windings within a single slot area.

As with double layer windings, for PS-SFPM machines with single layer windings having 11 rotor poles is optimal for maximum torque production. Particularly single layer machines with even numbers of rotor poles experience even harmonics in their coil back EMF which due to the coil layout feature no cancelation of such harmonics which occurs in those machines with double layer windings. A possible solution to the even harmonics which occur in single layer wound machines would be to skew the rotor in order to reduce or remove these undesirable harmonics.

For the purposes of fault tolerant design the single layer exhibits lower self to mutual inductance ratios compared with double layer windings which is favourable for fault tolerance.

The torque/power speed characteristic of machines with double and single layer windings has been presented, revealing that single layer windings may achieve a wider speed range than those employing double layer windings.

CHAPTER 4 – MECHANICAL FLUX WEAKENING OF PARTITIONED STATOR SWITCHED FLUX PERMANENT MAGNET MACHINES

4.1. Introduction

The speed range of a permanent magnet (PM) machine is determined by the machine's PM flux and the d-axis inductance for a given maximum power supplied to the machine. Large PM flux linkage is preferable for high torque performance at low speed, but lower PM flux allows higher speed operation based on a maximum power delivered from the power convertor. Adjustment of the current angle from q-axis current to include negative d-axis current weakens the PM flux and is a common method of achieving higher speeds [99-100]. In order to extend the operating region of a machine various methods of varying the flux have been proposed through introduction of DC field excitation coils [101] or by mechanically adjusting or short circuiting the PM field [102-103]. The area of mechanical flux weakening is of particular interest as the PS-SFPM machine while previously having fixed PM stator within the rotor may be adjusted mechanically without altering the wound stator or rotor. In variable flux machines with mechanical adjustment, compromise to the machine geometry is required to include flux adjustment through alteration of the rotor structure [101] and airgap length variation [104].

4.2. Permanent Magnet Alignment Definition

The PS-SFPM machine as investigated in the previous chapters is illustrated as the aligned PS-SFPM machine in Fig. 4.1 since each PM pole is aligned with a single stator tooth. From the switched flux machine perspective, the PM is removed from within the stator teeth and placed on a stator inside the rotor poles. In PS-SFPM machines the PM and windings are separated, hence free to assume different relative positions than only with the PM aligned with stator teeth. A new PS-SFPM machine with the PM aligned to the wound stator slot openings, or unaligned from the stator teeth, is shown as unaligned in Fig. 4.1.

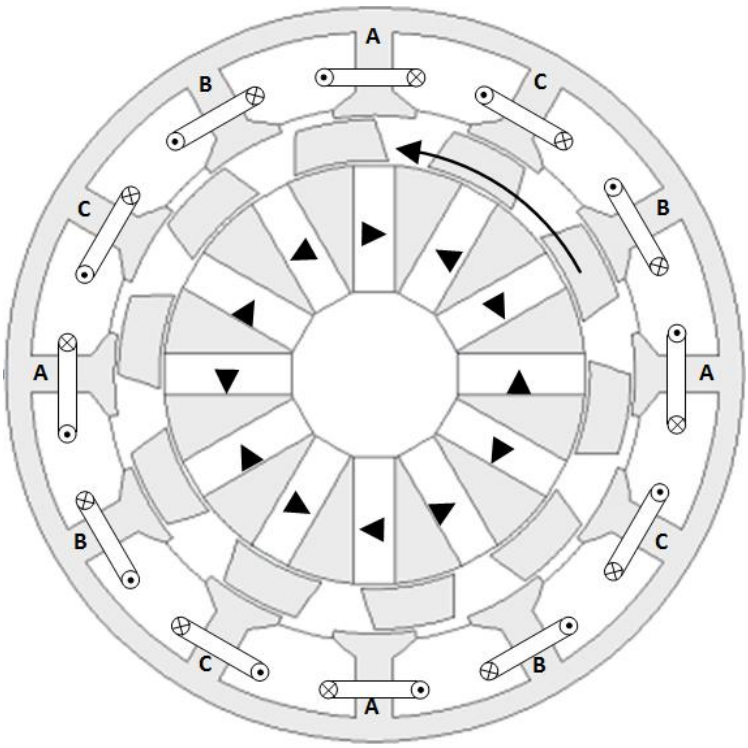

(a) Aligned

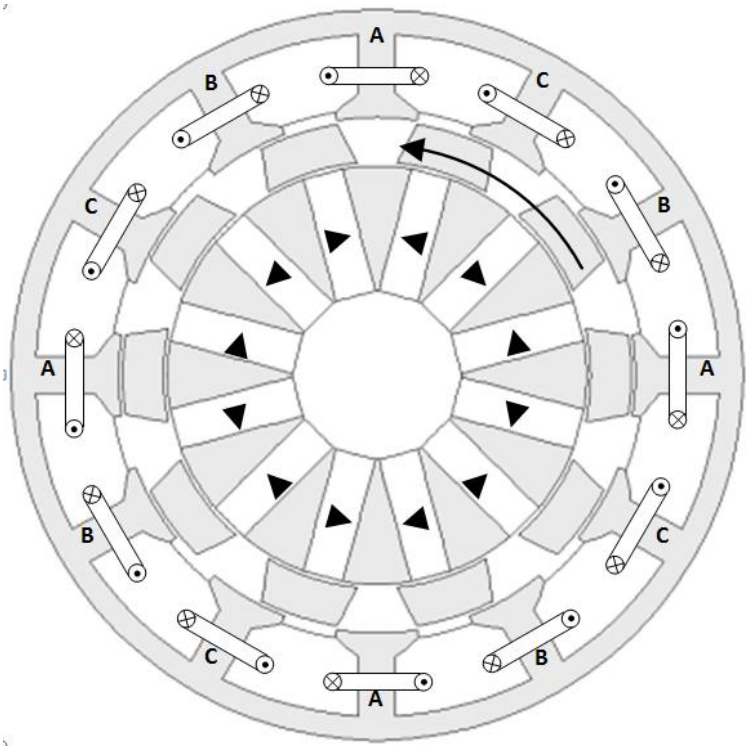

(b) Un-aligned

Fig. 4.1. Illustration of PS-SFPM machines with (a) aligned and (b) unaligned PM stator with respect to the wound stator

Positioning the PM to be unaligned from the stator teeth may be considered as a 90° electrical shift in terms of the number of PM pole pairs. Therefore, the d-axis rotor position is

shifted by 90° electrical in terms of the number of rotor poles. For a machine with 10 rotor poles the d-axis aligned with phase A with the PM aligned and unaligned from the wound stator are shown in Fig. 4.2. The flux focusing effect of interior mounted PM is maintained, rather than each tooth being presented with both north and south poles of a PM, each tooth only has a single pole.

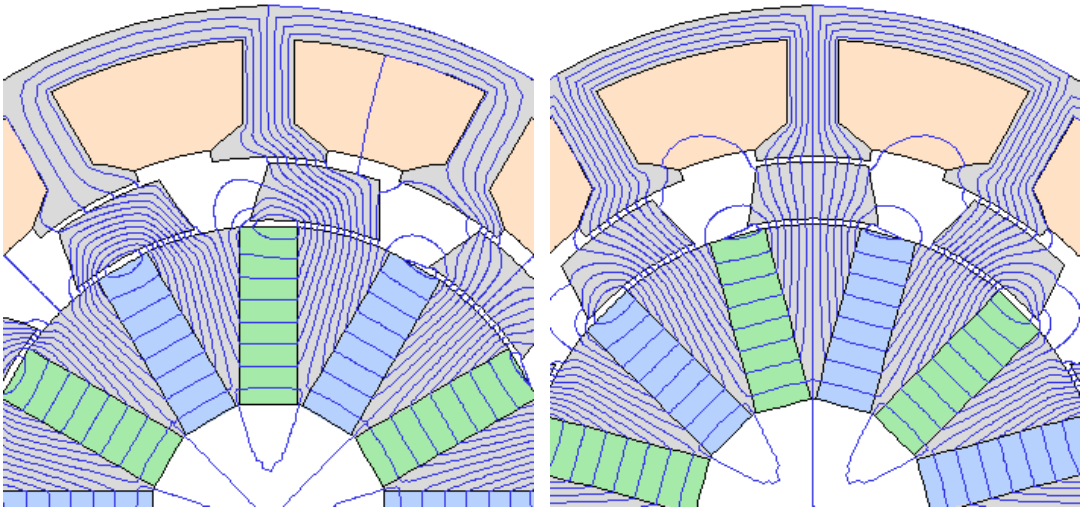

(a) Aligned (b) Un-aligned

Fig. 4.2. Flux lines through single tooth with (a) PM aligned with stator teeth and (b) PM un-aligned with stator teeth

4.3. Cogging Torque

Cogging torque results from variations in permeance around the airgap surfaces, i.e. slots, and the tendency of magnetising MMF to align in stable positions of zero net torque on open circuit [105]. The cogging torque is influenced by the choice of slot/pole combination, PM and slot geometry and airgap length [94], methods of reducing cogging torque have been proposed through skewing, PM shifting and additional notches on teeth [106]. For PS-SFPM machines with 12 slots, 10, 11, 13 and 14 rotor poles and 6 PM pole pairs the cogging torque was presented in chapter 2 showing the fundamental order of cogging torque for each number of rotor poles. This cogging torque for PS-SFPM machines with the PM stator aligned with the wound stator teeth is shown in Fig. 2.23, also for identical machine geometry with unaligned PM stator, the cogging torque is shown in Fig. 4.4.

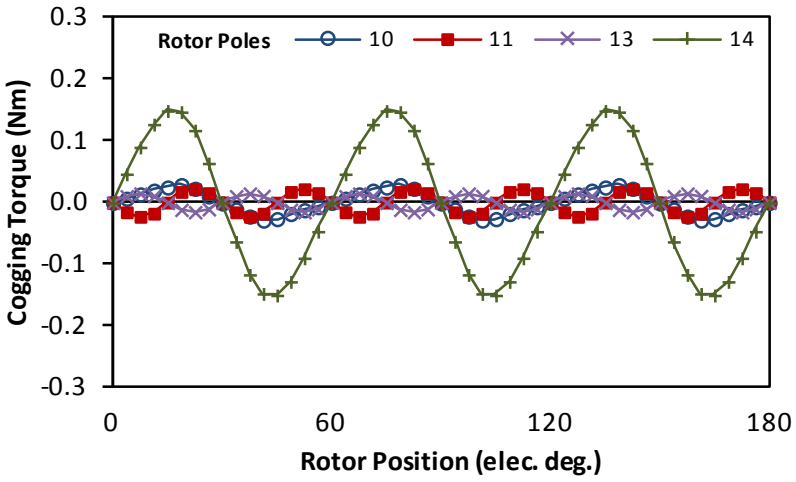

Fig. 4.3. Comparison of cogging torque for PS-SFPM machine with 12 stator slots and different rotor poles with PM aligned with stator teeth

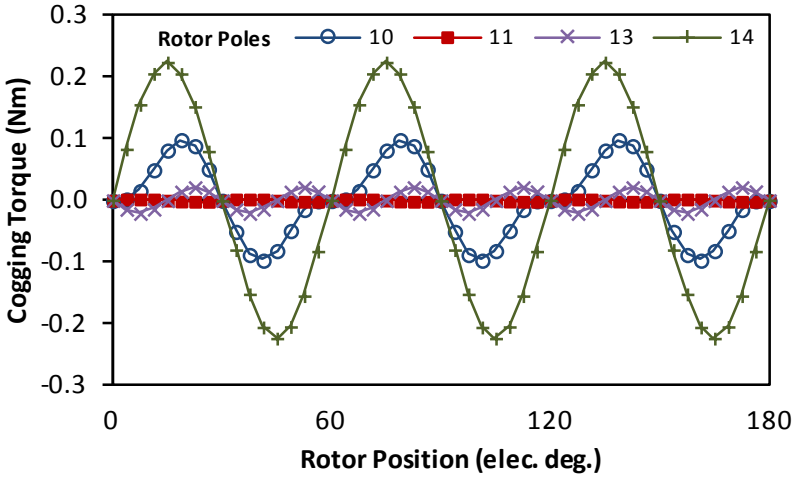

Fig. 4.4. Comparison of cogging torque for PS-SFPM machine with 12 stator slots and different rotor poles with PM unaligned with stator teeth

For both aligned and unaligned PM stator positioning the cogging torque fundamental order remains unchanged Fig. 2.23 and Fig. 4.4, although the magnitude of cogging torque changes as the relative position of the PM and wound stators vary, given in Table XIII. Machines with 10, 13 and 14 rotor poles the cogging torque increases as the PM stator is unaligned, while for 11 rotor poles with unaligned PM with stator teeth decreases the cogging torque.

Table XIII. Comparison of cogging torque with different numbers of rotor poles with aligned and unaligned PM

	PM Position	Rotor Poles			
		10	11	13	14
Pk-Pk Cogging Torque (Nm)	Aligned	**0.058**	0.045	**0.030**	**0.301**
	Unaligned	0.196	**0.004**	0.043	0.450

To provide understanding of the changed cogging torque magnitudes with PM stator position, the torque between the three machine bodies is considered. The rotor torque T_r may be expressed in terms of the torque on the inner PM stator T_i and outer wound stator T_o (7):

$$T_r = T_i + T_o \tag{22}$$

As the most dramatic difference in cogging torque between aligned and unaligned PM stator occurs for 10 and 11 rotor poles these are analysed further, for 10 rotor poles the cogging torque increases and 11 it decreases. For 10 rotor poles the torque on the inner and outer stator at aligned and unaligned PM position is shown in Fig. 4.5. The inner torque remains relatively unchanged for different PM positioning as the interaction between rotor slots and PM MMF is largely unaffected by the wound stator relative position. As the rotor position changes the magnetisation of rotor poles varies as a function of angle between rotor pole and PM, this field creates cogging torque between the rotor poles and wound stator slots. For unaligned PM stator with 10 rotor poles the torque experienced on the wound stator is reduced and hence the cogging torque on the rotor increases as the inner and outer torque are of opposite polarity (7).

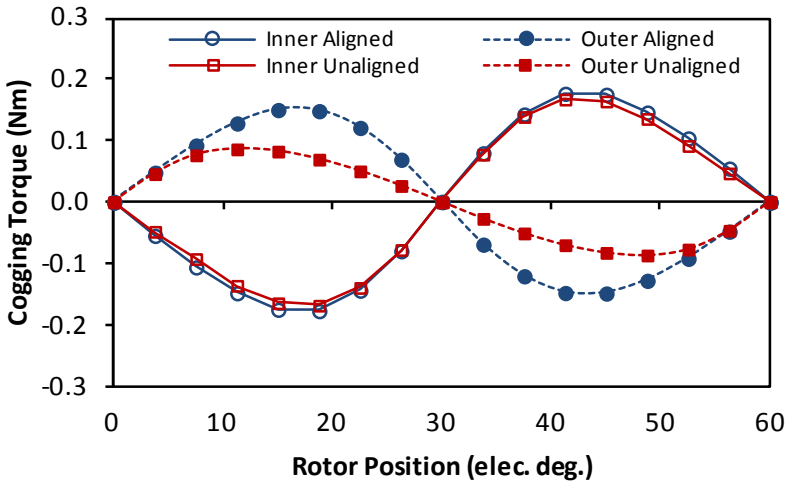

Fig. 4.5. Cogging torque on inner PM stator and outer wound stator for machines with aligned and unaligned PM with 10 rotor poles

Likewise for machines with 11 rotor poles the inner cogging remains almost unchanged with PM positioning. The torque on the wound stator again reduces, but its polarity is reversed, hence with unaligned PM the cogging torque now reduces Fig. 4.6.

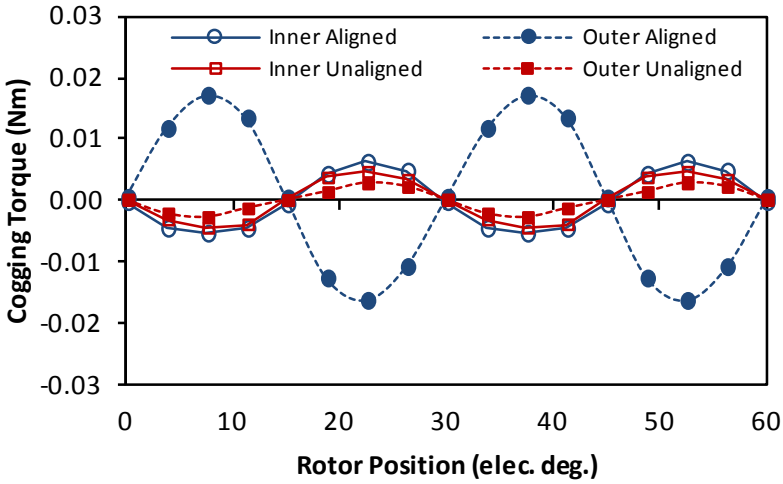

Fig. 4.6. Cogging torque on inner PM stator and outer wound stator for machines with aligned and unaligned PM with 11 rotor poles

In PS-SFPM machines there occur two contributions to cogging torque, the interaction of PM MMF and rotor slotting and the position varying MMF of the rotor poles interaction with the wound stator slots. The second causes difference in cogging torque with modified PM alignment relative to the wound stator.

4.4. Electromagnetic Performance

As the relative position between the inner PM stator and wound stator is changed to align a single PM with a stator tooth the flux direction in an individual tooth is biased, either positive or negative, as a rotor pole passing a wound stator tooth will not reverse the polarity of the flux through the tooth. This is illustrated by a machine with 10 rotor poles, two individual coils from the same phase (1 and 4) are considered with aligned and unaligned PM stator positioning. The flux linkage variation is DC shifted in each coil, for two coils of the same phase one is positive and the other negatively shifted, as the FE data for an example 10 rotor pole machine demonstrates in Fig. 4.7

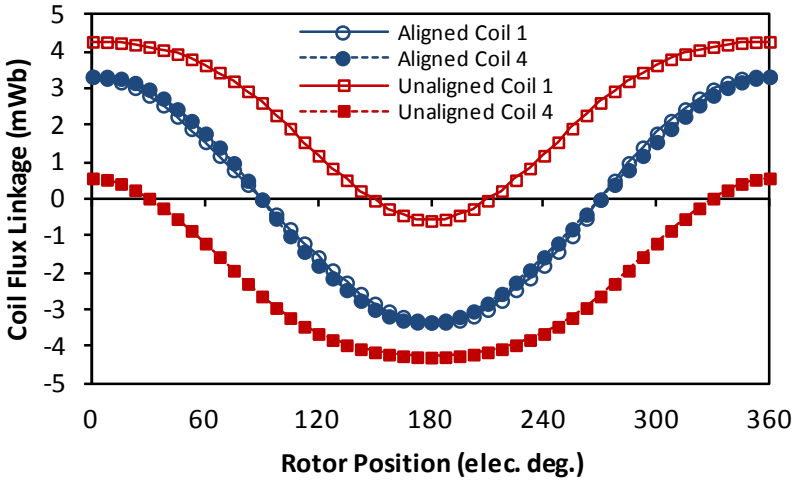

Fig. 4.7. Open-circuit flux linkage of a PS-SFPM machine individual coils of one phase with aligned and unaligned PM with 10 rotor poles

The flux linkage variation in a single coil is DC shifted but its magnitude is also limited due to saturation in a single tooth, this can be seen in Fig. 4.8 as the PM is unaligned from the wound stator teeth the flux density in a single tooth with a rotor pole aligned is saturated (Iron material BH knee point 1.8T).

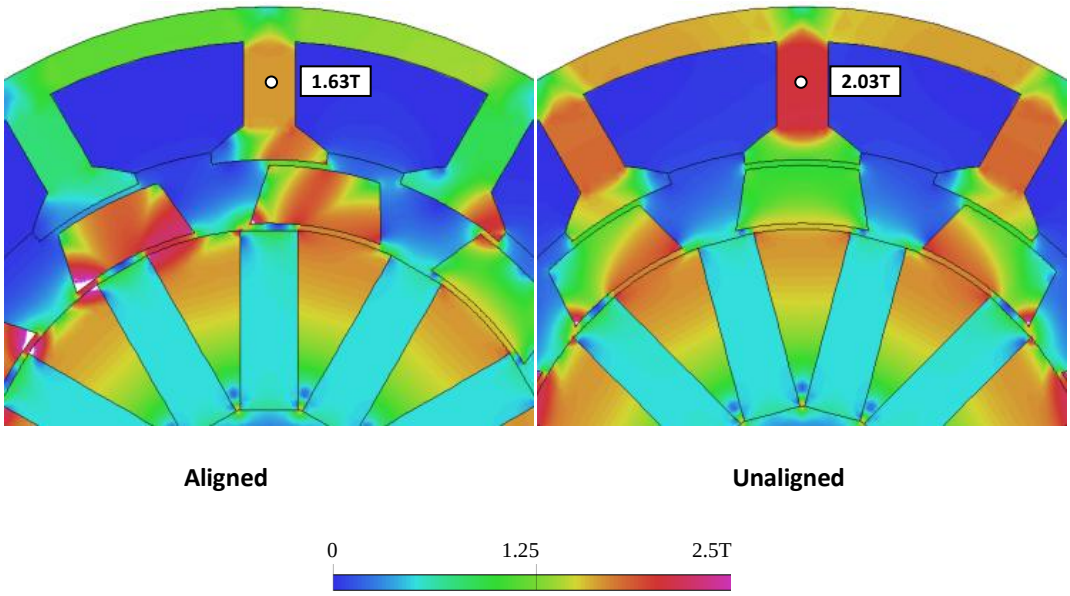

Fig. 4.8. Open-circuit flux density in coil 1 of PS-SFPM machine with 10 rotor poles at 0 degrees with aligned and unaligned PM

This saturation of stator teeth results in reduced overall phase flux linkage variation and hence the phase back EMF is reduced from the aligned PM position Fig. 2.27. The stator iron is saturated in this unaligned position without the addition of armature reaction field, therefore the armature reaction and PM field have been adjusted from a parallel configuration which is assumed in a switched flux PM machines and now are in series with each other, thus reducing the torque production in this position.

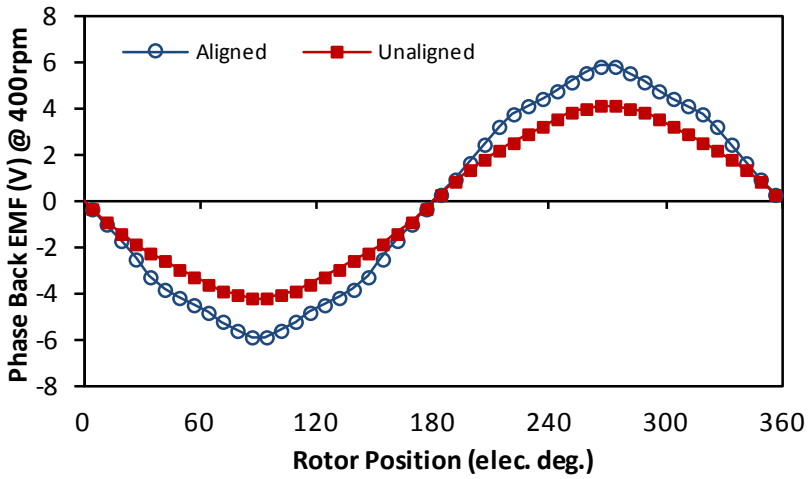

Fig. 4.9. Open-circuit back EMF for PS-SFPM machine with 10 rotor poles with aligned and unaligned PM

At rated current the torque with rotor position is obtained for different numbers of rotor poles with PM stator aligned and unaligned Fig. 4.11. As previously found the cogging torque and hence the on-load torque ripple changes as a different PM stator position is assumed.

Machines with 10, 11, 13 and 14 rotor poles feature a reduction in rated torque as the back EMF is reduced in each case because of the uni-polar flux link variation causing saturation in the wound stator teeth.

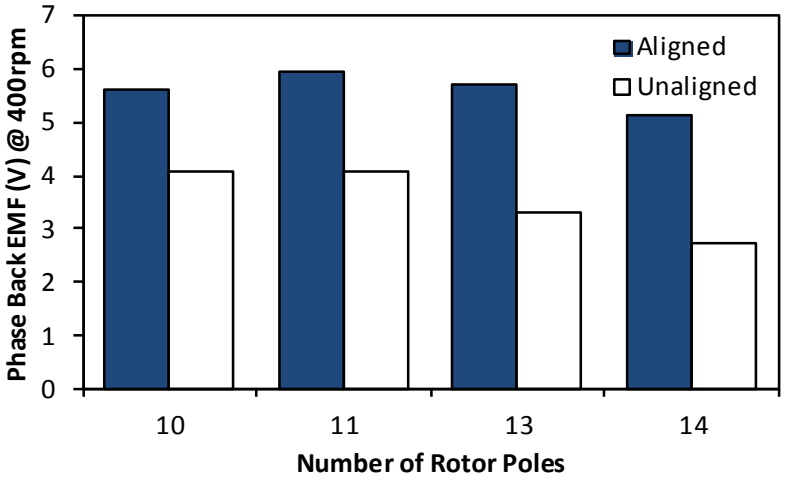

Fig. 4.10. Fundamental order of phase back EMF comparison with aligned and unaligned PM at 400rpm with different numbers of rotor poles

As the back EMF has been reduced the machine may be operated to a higher speed before the maximum supply voltage is reached, and therefore the potential to increase the speed range in this configuration is observed.

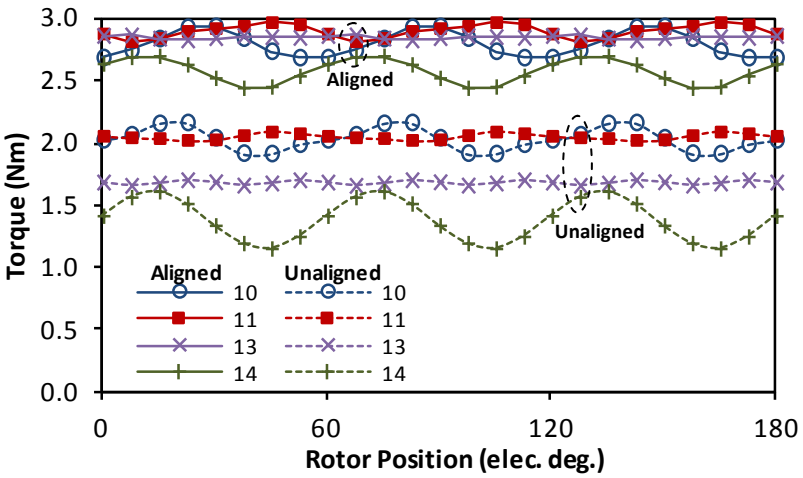

Fig. 4.11. Torque variation with rotor position for PS-SFPM machine with 10, 11, 13 and 14 rotor poles with aligned and unaligned PM

The variation of torque for different q-axis current for different numbers of rotor poles with the PMs aligned and unaligned from the wound rotor is shown in Fig. 4.12, those machines

with 13 and 14 rotor pole exhibit a considerable drop in torque from the aligned PM positioning.

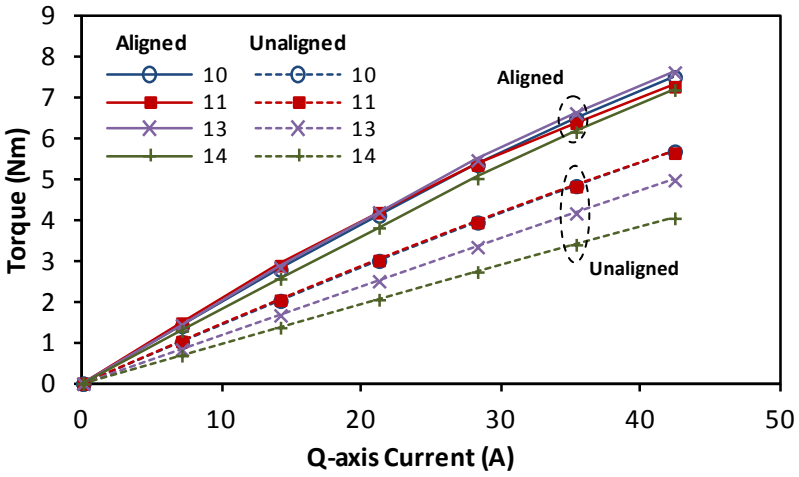

Fig. 4.12. Torque characteristic of PS-SFPM machine with 10, 11, 13 and 14 rotor poles with aligned and unaligned PM and q-axis current

In this case, the optimised stator and rotor, for torque production at the aligned position, are used to show a decrease in torque when the PM stator is unaligned. A further comparison could be made if optimised for the unaligned position.

4.5. Single and Double Layer Windings

In the previous two chapters the PS-SFPM machine with PM aligned with the wound stator was first presented with double layer windings, and then followed by a comparison with a PS-SFPM machine with single layer windings. The winding terminology resulting from the number of coils sharing a single slot area.

In a similar manner to the cancellation of even order harmonics in single layer windings in the aligned PS-SFPM machine, due to the reduced number of coils per phase from 4 to 2 in single layer windings, machines with even numbers of rotor poles experience a DC shift in their phase flux linkage. In double layer windings, even though the flux linking individual coils has a DC offset (as one tooth as one PM pole) there are other coils in the same phase of negative orientation which provides cancellation of the DC offset. In single layer windings for even numbers of rotor poles both coils of the same phase may have the same DC offset in flux linkage, as shown in Fig. 4.13.

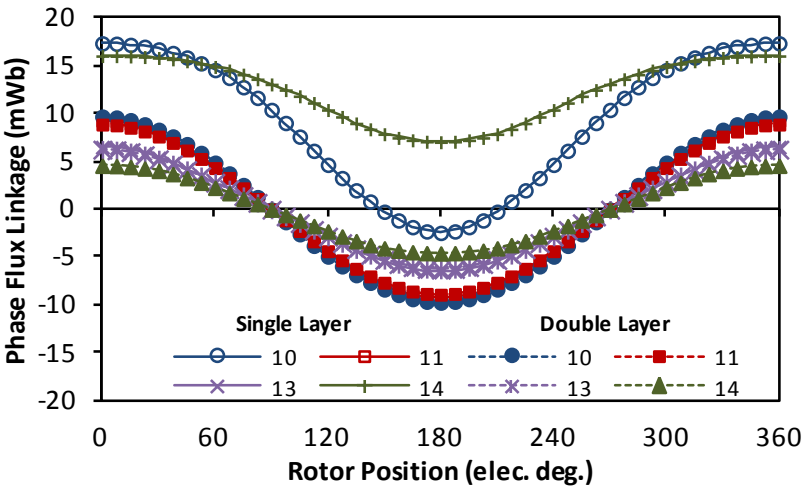

Fig. 4.13. Phase flux linkage for PS-SFPM machines with unaligned PM for different numbers of rotor poles with double and single layer windings

The effect of this DC offset in phase flux linkage presents itself in the back EMF, Fig. 4.14, since a single coil only experiences flux in a single direction for machines with even numbers of coils no cancelation of even harmonics occurs, and as the flux is in a single direction the stator teeth the iron saturates introducing even order harmonics in the back EMF.

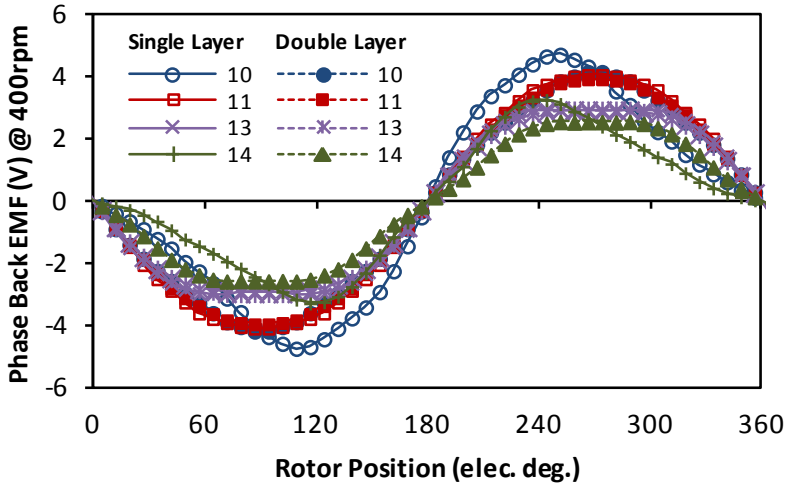

Fig. 4.14. Phase Back EMF for PS-SFPM machines with unaligned PM for different numbers of rotor poles with double and single layer windings

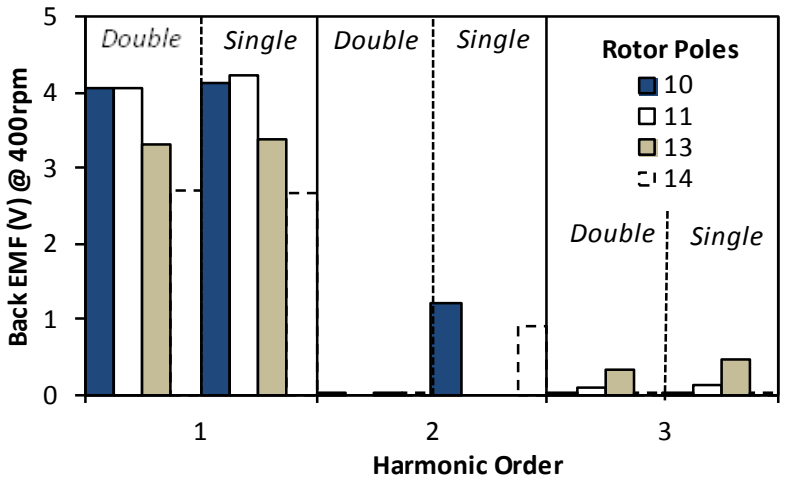

Fig. 4.15. Phase Back EMF harmonics for PS-SFPM machines with unaligned PM for different numbers of rotor poles with double and single layer windings

Due to the introduction of even order harmonics in the back EMF of PS-SFPM machines with single layer windings with un-aligned stators (10 and 14 rotor poles), the on-load torque ripples are significantly increased compared with those with double layer windings. This is as a result of the interaction between the sinusoidal phase current and the non-sinusoidal nature of the back EMF creating additional torque variation around the constant torque production Fig. 4.16.

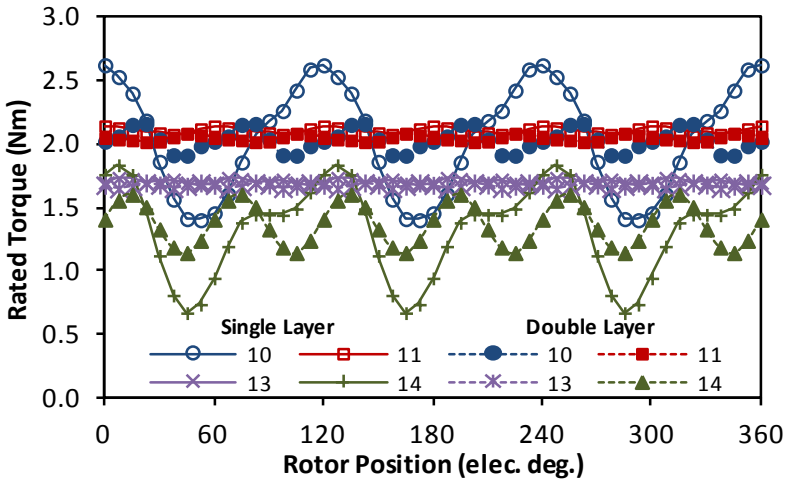

Fig. 4.16. Rated torque for PS-SFPM machines with unaligned PM for different numbers of rotor poles with double and single layer windings

Neglecting the effect of additional torque ripples created by additional harmonics in the back EMF the sinusoidal component remains to produce constant torque when excited by a

sinusoidal phase current. The difference between average torque with q-axis current injection for double and single layer windings with un-aligned stators is shown in Fig. 4.17.

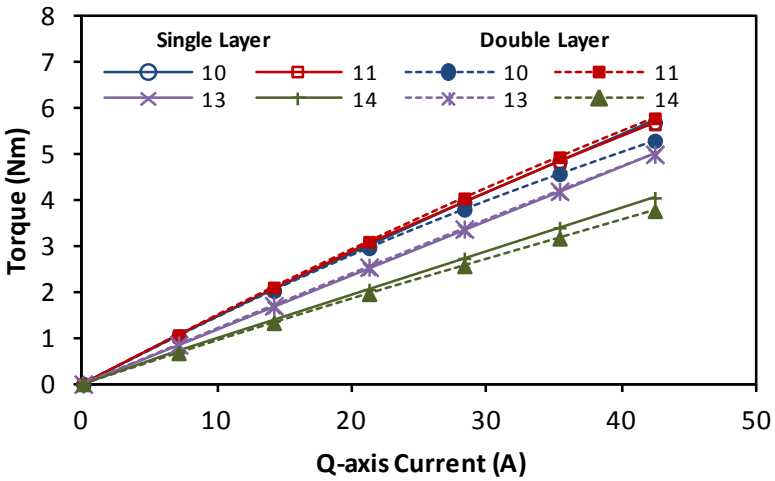

Fig. 4.17. Static torque variation with q-axis current for PS-SFPM machines with unaligned PM for different numbers of rotor poles with double and single layer windings

4.6. Mechanical Flux Weakening

For this machine, with optimised geometry for the aligned position, the effect of changing the PM angle is shown to reduce the EMF and hence torque capability. This provides potential improvement to the speed range of the PS-SFPM machine, by weakening the PM flux linkage by changing the PM stator angle. As can be seen for a PS-SFPM machine with 10 rotor poles varying the PM angle reduces the constant torque performance but increases the overall speed capability Fig. 4.21. The PM within the centre of the PS-SFPM machine is considered adjustable through means of mechanical actuation rather than stationary, the torque-speed relationship of the partitioned switch flux machine with the PM aligned with the wound stator may be adjusted to achieve greater speed range. A PM angle of 90° elec. will achieve the highest PM flux weakening as increasing further restores the PM flux linkage to the situation at 0° elec. with negative phase. Considering the torque-speed relationship at 0° elec. and 90° elec. and between the base speeds the PM angle is varied to achieve the torque for maximum power. As magnetic circuit saturation is increased with unaligned PM therefore the inductance reduces Table XIV.

Table XIV. DQ Axis inductances and PM flux linkage for PS-SFPM machines with aligned and unaligned PM with different numbers of rotor poles

	PM Position	Rotor Poles			
		10	11	13	14
D-axis Inductance (mH)	Aligned	0.35	0.42	0.37	0.30
	Unaligned	0.30	0.35	0.26	0.21
Q-axis Inductance (mH)	Aligned	0.26	0.30	0.28	0.24
	Unaligned	0.23	0.26	0.23	0.19
PM Flux Linkage (mwb)	Aligned	13.40	12.86	10.45	8.74
	Unaligned	9.71	8.83	6.08	4.46

To predict the PS-SFPM machine torque-speed relationship the inverter voltage limit determines the maximum speed, the phase voltage is calculated using (19) where the DC voltage limit of the convertor is (20):

$$V_{pha} = \sqrt{\left(R_{ph}I_d - \omega_{elec}L_qI_q\right)^2 + \left(R_{ph}I_q + \omega_{elec}L_dI_d + \omega_{elec}\psi_m\right)^2} \tag{23}$$

$$V_{pha} = \frac{V_{dc}}{\sqrt{3}} \tag{24}$$

The electrical angular frequency ω_{elec} is N_r times the mechanical angular frequency ω_{mech} which is the rotational velocity of the rotor. The phase resistance is determined by the slot area and end winding length for different winding configurations.

In general, the torque speed and power speed curves are represented in 4.18 and Fig. 4.19, with 4 key speeds indicated and their relationship to PM angle shown in Table XV. The constant power region with the inclusion of PM angle has two components determined by the flux weakening due to PM angle between ω_1 and ω_2, and increased conventional flux weakening range by reduction of ψ_m and less variation in L_d with PM angle. If a flux weakening ratio of 1 is achieved with 90° elec. there is possibility of infinite speed range. Adjusting the position of the PM at low speed to achieve the highest constant torque region and at high speed to weaken the flux to allow the highest speed operation.

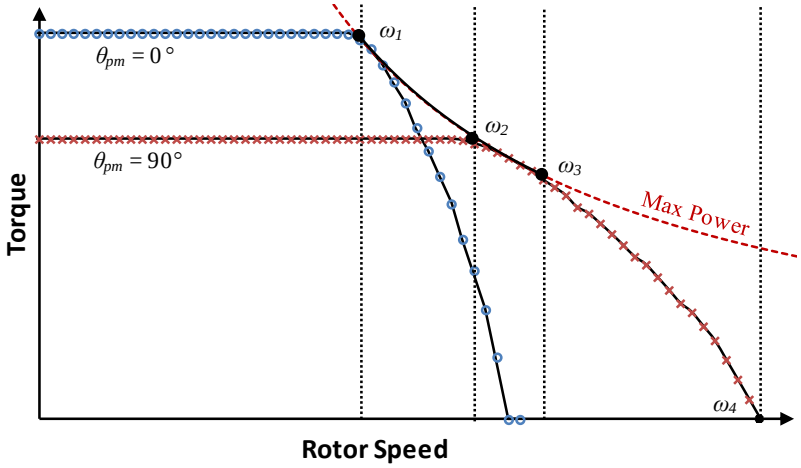

Fig. 4.18. Torque - Speed relationship including effect of PM angle

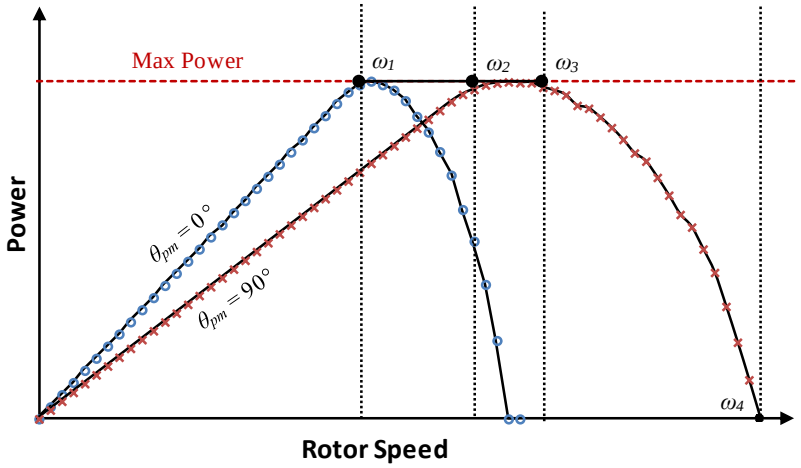

Fig. 4.19. Power - Speed relationship including effect of PM angle

Table XV. Description of speeds presented in Fig. 4.19

Speed	PM Angle (elec. deg.) ϑ_{pm}	Description
ω_1	0°	Base speed
ω_2	90°	Base speed
ω_3	90°	Maximum constant power speed
ω_4	90°	Maximum speed

The constant power region between ω_1 and ω_2 is dependent on the decrease of φ_m by changing the PM angle, the second constant power region is the more typical constant power region which is determined by the field weakening ability of the machine with the PM angle at 90° elec. The maximum rotor speed depends on the maximum speed with the PM at 90° elec.

In order to achieve high constant torque $\psi_m(\vartheta_{pm} = 0°)$ must be maximised, and to maximise the effect of PM angle then $\psi_m(\vartheta_{pm} = 90°)$ must be minimised to increase ω_2. In order to increase the flux weakening region between ω_3 and ω_2 the flux weakening factor when $\vartheta_{pm} = 90°$ must be closer to 1, therefore as $\varphi_m(\vartheta_{pm} = 90°)$ is reduced, then higher $L_d(\vartheta_{pm} = 90°)$ is favourable.

The torque speed and power speed relationships are presented for single and double layer wound machines as investigated in the previous chapter with 10, 11, 13 and 14 rotor poles. Each combination of rotor poles compares the difference in torque speed range with the PM fixed in the aligned position (providing highest constant torque) and when the PM angle is permitted to change to the un-aligned angle allowing greater speed range.

Increasing the number of rotor poles increases the speed range possibility when employing mechanical flux weakening as the reduction in d-axis inductance between the aligned and un-aligned position increases as the number of rotor poles increases. Single layer windings have greater speed range with fixed and variable PM angles, with 14 rotor poles by un-aligning the PM poles infinite flux weakening is achieved.

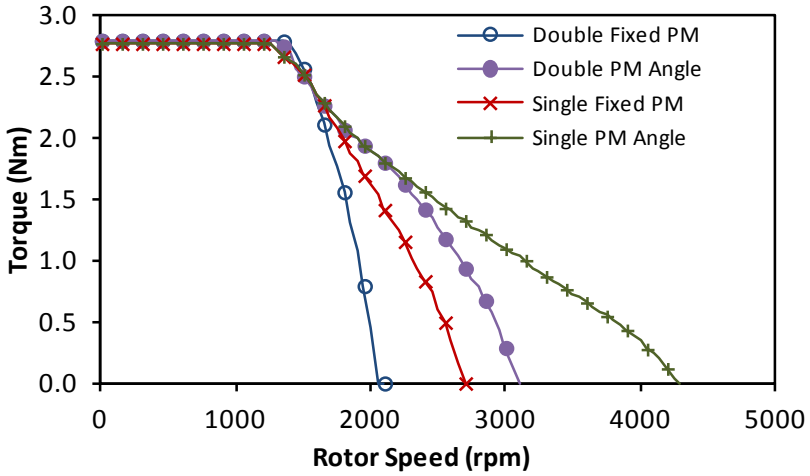

Fig. 4.20. Torque -Speed relationship for 10 rotor poles comparison of single and double layer winding

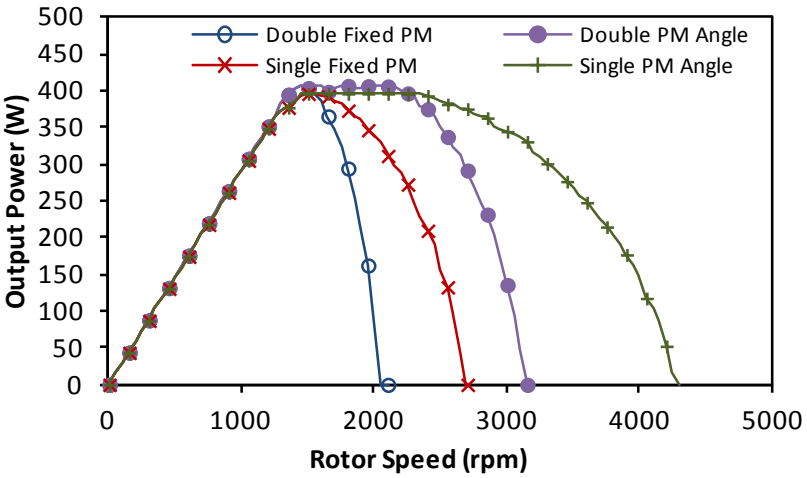

Fig. 4.21. Power-Speed relationship for 10 rotor poles comparison of single and double layer winding

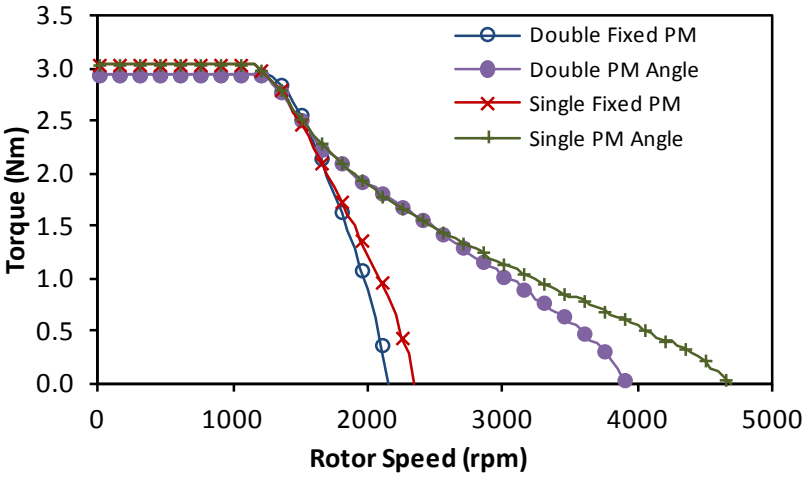

Fig. 4.22. Torque -Speed relationship for 11 rotor poles comparison of single and double layer winding

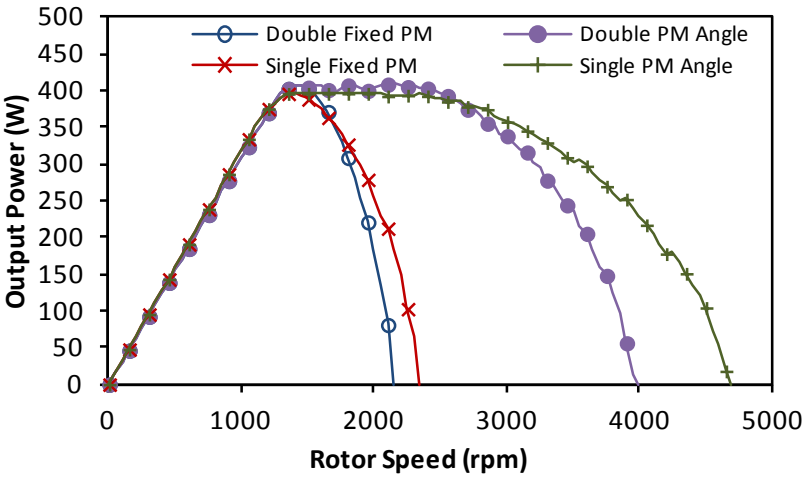

Fig. 4.23. Power-Speed relationship for 11 rotor poles comparison of single and double layer winding

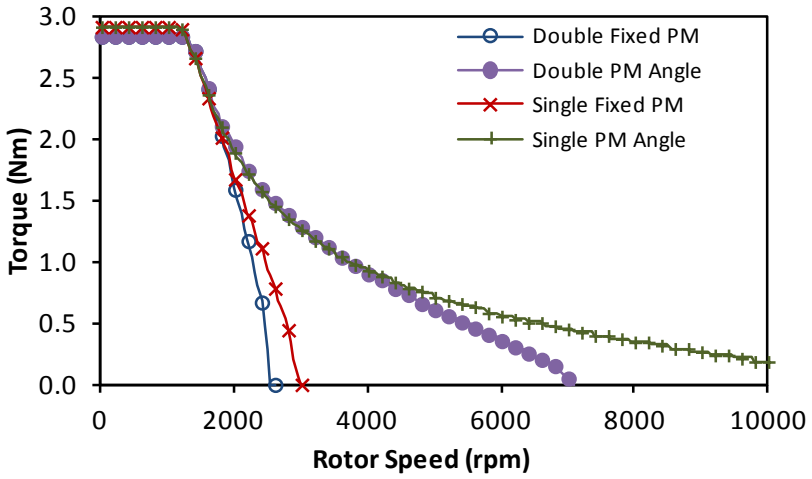

Fig. 4.24. Torque -Speed relationship for 13 rotor poles comparison of single and double layer winding

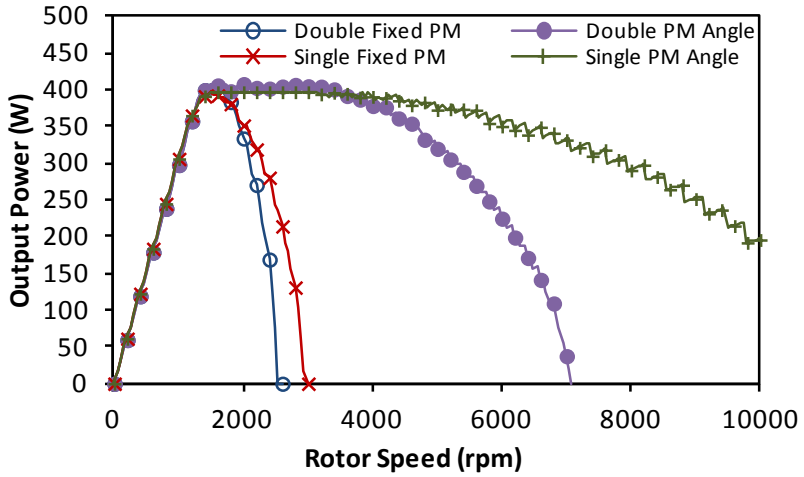

Fig. 4.25. Power-Speed relationship for 13 rotor poles comparison of single and double layer winding

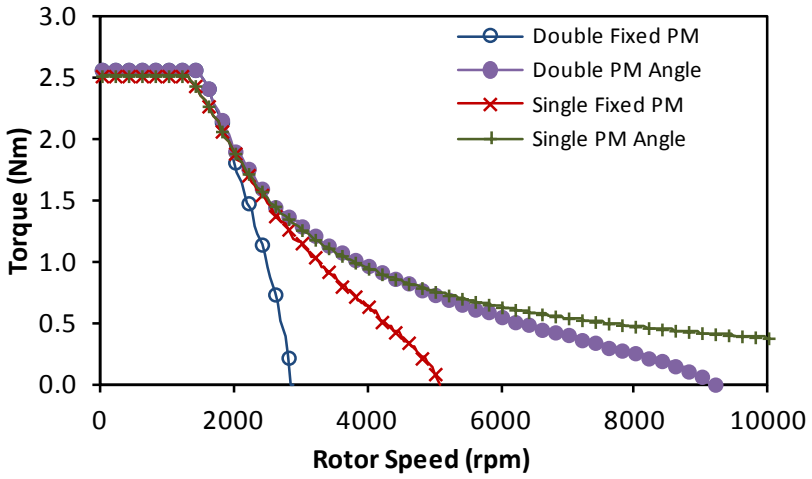

Fig. 4.26. Torque -Speed relationship for 14 rotor poles comparison of single and double layer winding

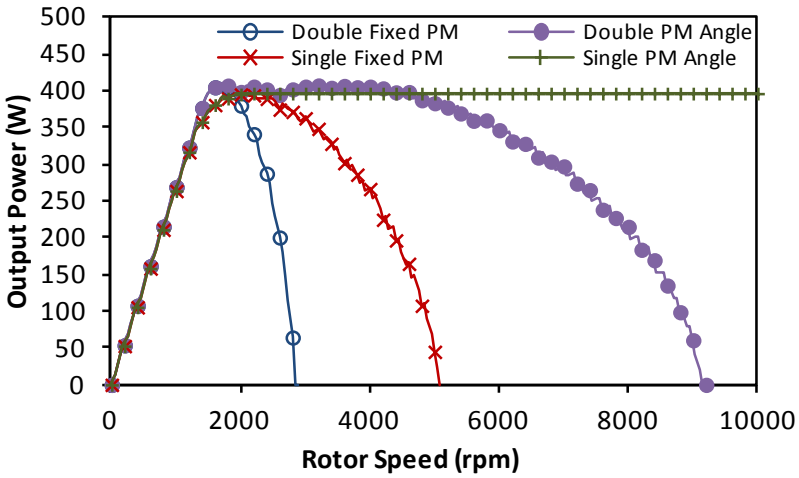

Fig. 4.27. Power-Speed relationship for 14 rotor poles comparison of single and double layer winding

In all combinations of rotor poles (10, 11, 13 and 14) mechanically flux weakening the flux through rotation of the central PM stator achieves greater speed range than moving from a double to single layer winding, and maintains the higher torque production at lower speeds.

While the mechanical implementations of this scheme require further investigation, the advantage of increased speed range is obvious. In terms of mechanical flux weakening the arrangement of the independent wound stator on the outside and PM rotor on the inside of the rotor poles provides a good opportunity to realise mechanical flux weakening with this machine.

4.7. Experimental Results

Measured results for the PS-SFPM machine prototype with 10 and 11 rotor poles are collected and compared with FE predictions. The back EMF and static torque is measured with aligned and un-alignment positions of the inner PM rotor. The compromises for building a prototype such as the introduction of rotor bridges must be considered as a reduction in performance is expected, but the results show agreement with the FE and confirm the differences between aligned and un-aligned PM poles from the wound stator teeth.

4.7.1. Back EMF

The measured and FE predicted back EMF at 400rpm is compared for 10 rotor poles with the PM poles aligned and un-aligned from the wound stator teeth and double layer windings.

There is a reduction in the measured back EMF compared with the FE in both cases, but the reduction between aligned and unaligned in the FE and measured is consistent in both cases Fig. 4.28.

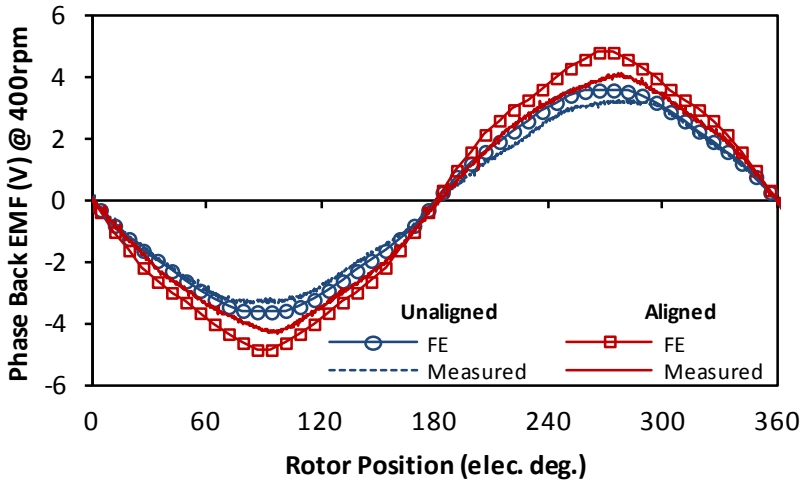

Fig. 4.28. Measured and FE predicted phase back EMF at 400rpm with aligned and unaligned PM with 10 rotor poles and double layer windings

For 10 rotor poles with single layer windings the aligned back EMF is non-sinusoidal due to the non-cancellation of higher order harmonics from coils in the same phase with reverse polarity, this can be seen in the measured results. When the PM poles are un-aligned the even order harmonics, which are created as the flux linkage becomes uni-polar, become more prevalent and are observed in both the FE and measured back EMF Fig. 4.29.

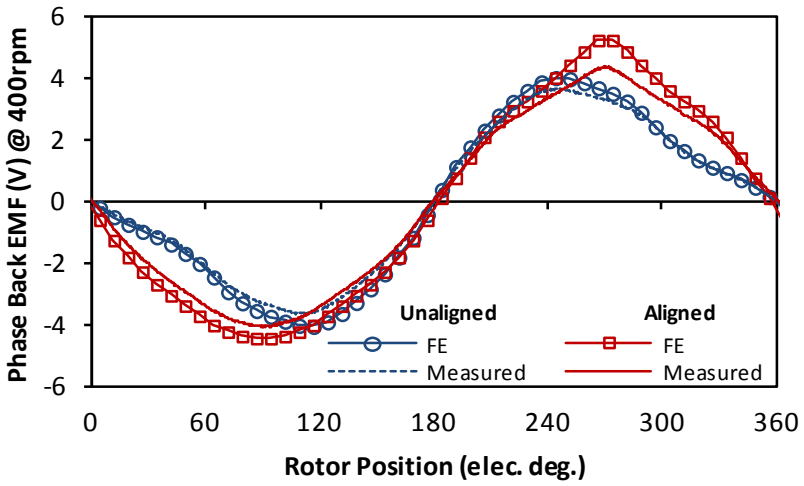

Fig. 4.29. Measured and FE predicted phase back EMF at 400rpm with aligned and unaligned PM with 10 rotor poles and single layer windings

A second rotor was prototyped with 11 rotor poles allowing comparison with 10 rotor poles. The FE predicted and measured back EMF results with double layer windings and 11 rotor poles are presented where the PM poles are aligned and un-aligned from the wound stator teeth. Again as for 10 rotor poles the obvious reduction in back EMF due to the alignment of the PM poles is seen in both the FE predicted and measured data Fig. 4.30.

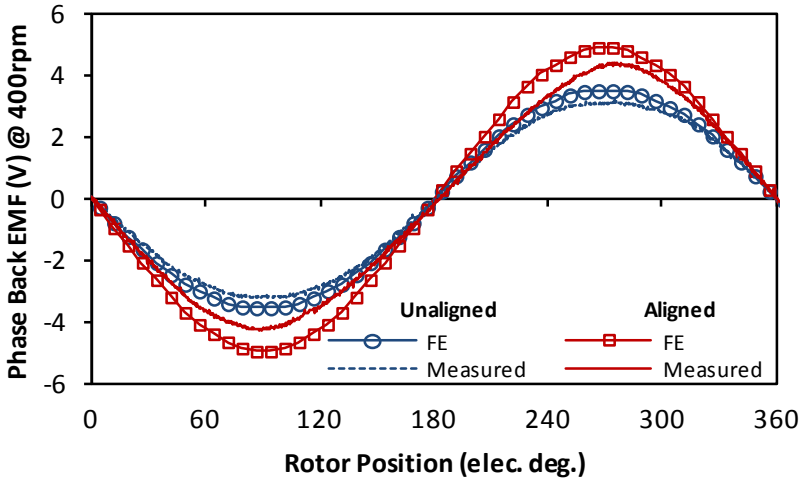

Fig. 4.30. Measured and FE predicted phase back EMF at 400rpm with aligned and unaligned PM with 11 rotor poles and double layer windings

With single layer windings the back EMF is measured Fig. 4.31. The EMF predicted by FE is identical for both positive and negative, whereas the measured results shows differing magnitudes of EMF in the positive and negative cycles. This difference could be due to

eccentricities introduced by the prototyping of the rotor poles, creating non-cancellation of harmonics between individual coil EMF's of the same phase.

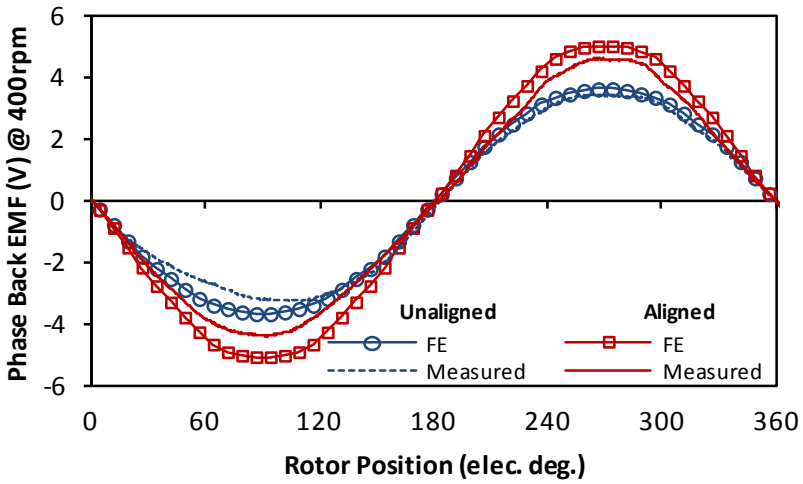

Fig. 4.31. Measured and FE predicted phase back EMF at 400rpm with aligned and unaligned PM with 11 rotor poles and single layer windings

4.7.2. Static Torque

Static torque characteristics with fixed DC excitation of the phases, ($I_a = I_{pk}$, $I_{b,c} = -I_{pk}/2$), providing the maximum torque angle relative to the rotor position, equating to q-axis current injection. Increasing torque without significant saturation of the motor up to 20A, is predicted with FE and measured for 10 rotor poles with the alignment of the PM poles altered Fig. 4.32.

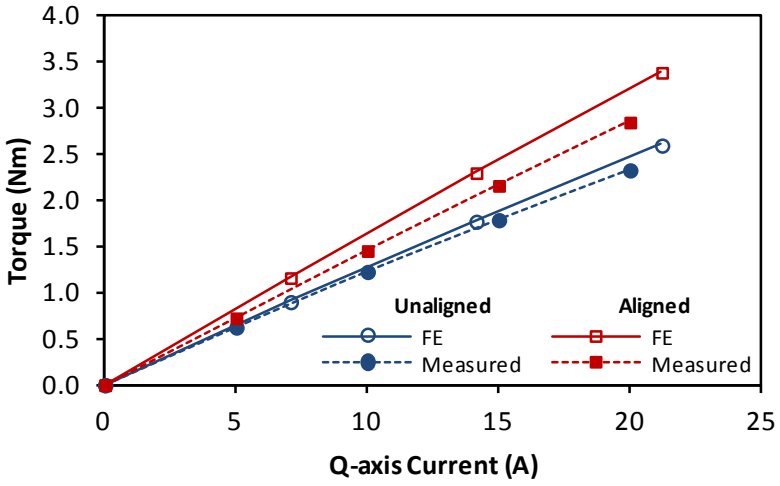

Fig. 4.32. Measured and FE predicted phase static torque with aligned and unaligned PM with 10 rotor poles and double layer windings

The discrepancy between FE predicted and measured values when the PM poles are unaligned increases with single layer windings Fig. 4.33, with single layer windings and 10 rotor

poles unaligned PM the back EMF waveform contains even order harmonics thus increasing the possibility of reduced torque measurements when a static torque position is considered with DC winding excitation.

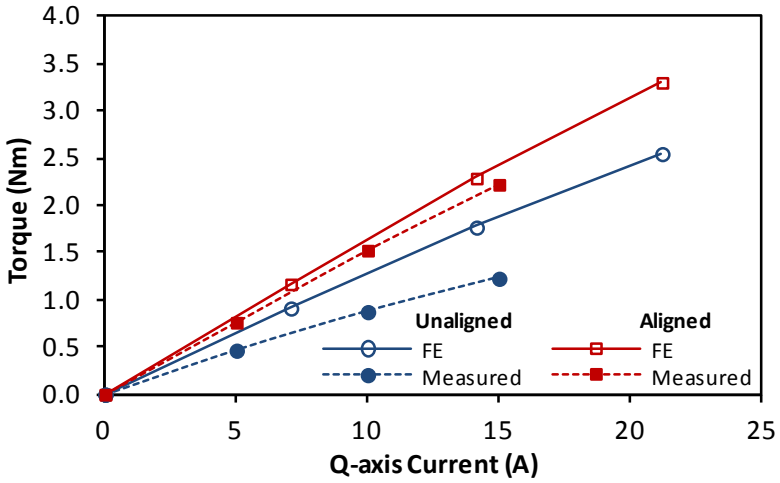

Fig. 4.33. Measured and FE predicted phase static torque with aligned and unaligned PM with 10 rotor poles and single layer windings

For the 11 rotor pole machine the measured and FE predicted static torque is compared with aligned and un-aligned PM poles with double layer windings. Good agreement between FE and measurements is achieved with unaligned PM poles Fig. 4.34.

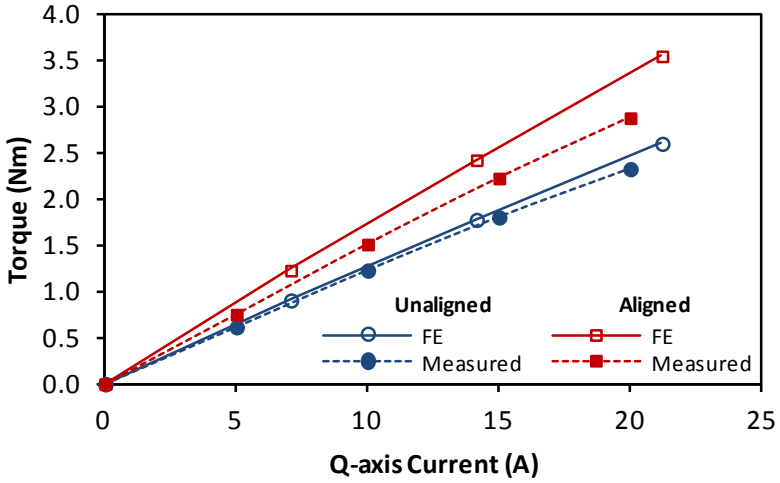

Fig. 4.34. Measured and FE phase static torque with aligned and unaligned PM with 11 rotor poles and double layer windings

With single layer windings there is again a reduction between FE and measured results, but the reduction in torque production between aligned and unaligned PM poles can be observed in both FE and measured results Fig. 4.35.

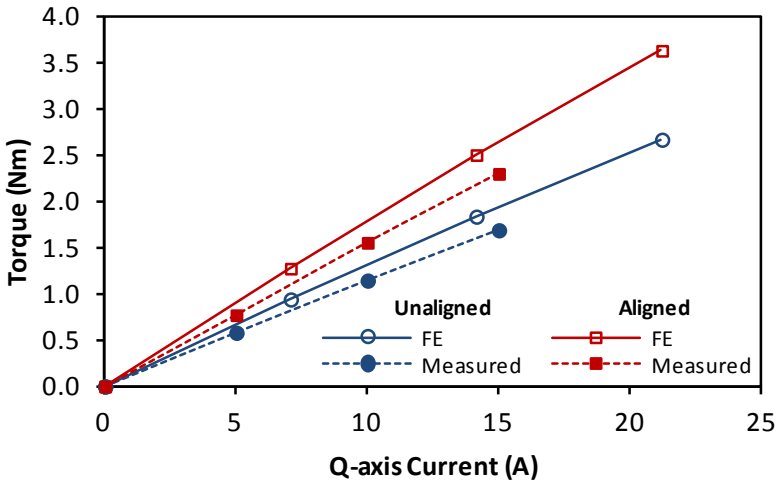

Fig. 4.35. Measured and FE predicted phase static torque with aligned and unaligned PM with 11 rotor poles and single layer windings

4.7.3. Comparison

The measured prototype values for 10 and 11 rotor poles, with double and single layer windings are compared for the PS-SFPM machine Fig. 4.36. The difference between 10 and 11 rotor poles back EMF is minimal, but the reduction when the inner PM are rotated to 90° is shown for both pole combinations. In the prototyping of the PS-SFPM machine, ensuring the inner PM was exactly aligned or unaligned from the wound stator teeth was difficult particularly as the cogging torque between the PM and the wound stator teeth forced them into the unaligned position. Further development of the mechanical system is required to ensure the PM may exactly assume the aligned position to achieve maximum back EMF and ultimately torque at low speeds.

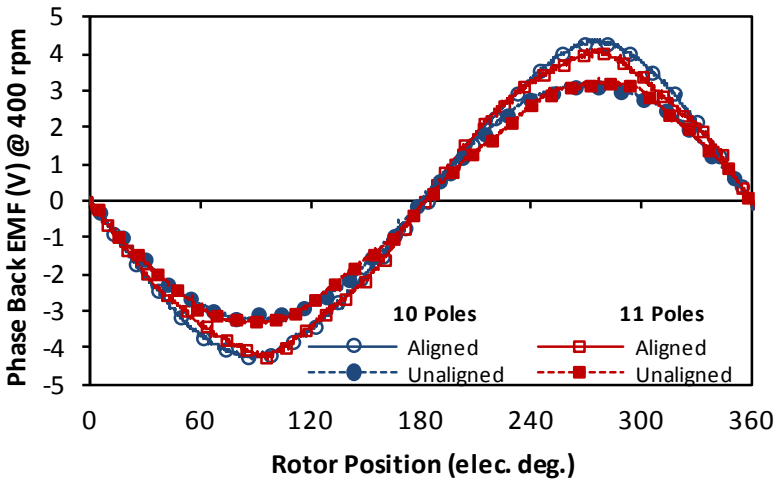

Fig. 4.36. Measured phase back EMF at 400rpm with aligned and unaligned PM with 10 and 11 rotor poles and double layer windings

When employing single layer windings in the PS-SFPM machine, 10 rotor poles are not favourable due to their asymmetric back EMF in the aligned position and even order harmonics when unaligned, while for 11 rotor poles in the aligned position a sinusoidal back EMF is achieved and good reduction in EMF as the PM are unaligned while avoiding additional EMF harmonics. The measured single layer winding results for 10 and 11 rotor poles are shown in Fig. 4.37.

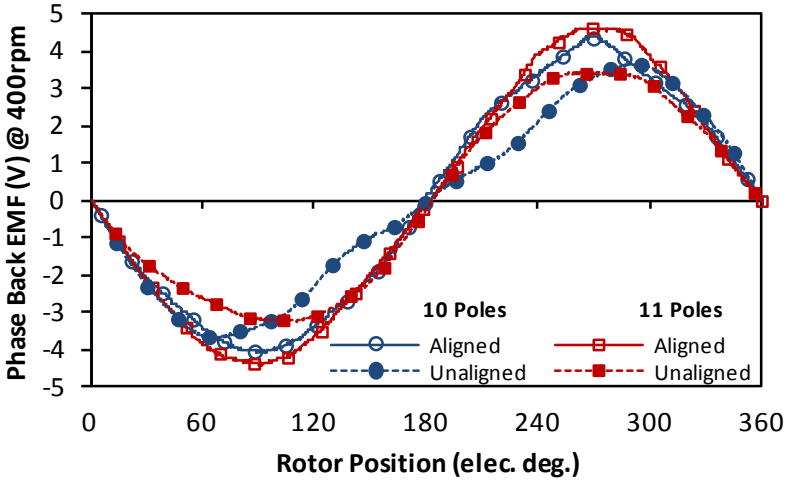

Fig. 4.37. Measured phase back EMF at 400rpm with aligned and unaligned PM with 10 and 11 rotor poles and single layer windings

Between 10 and 11 rotor poles measured static torque of the prototype machine there is very little difference, but the 11 rotor pole variant saturates quicker with increased current loading than the 10 rotor pole combination. The reduction in torque is greater for 10 rotor

poles and therefore favourable for mechanical flux weakening to achieve larger speed range Fig. 4.38.

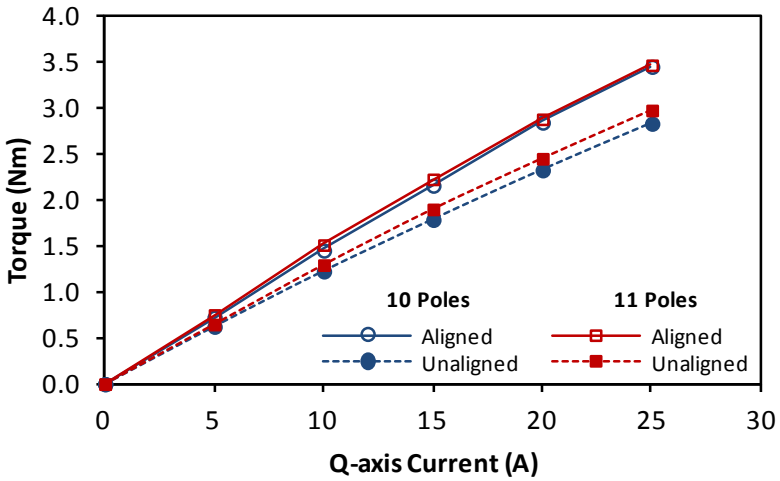

Fig. 4.38. Measured static torque with aligned and unaligned PM with 10 and 11 rotor poles and double layer windings

Additional to the previous conclusions about the 10 rotor poles having non-fundamental EMF harmonics resulting in torque ripples, the measured static torque in both the aligned and unaligned positions with single layer windings is less than using 11 rotor poles Fig. 4.39

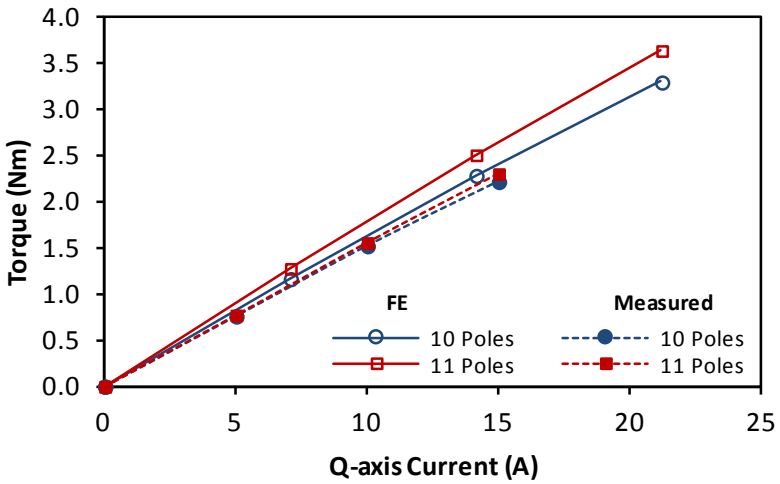

Fig. 4.39. Measured static torque with aligned and unaligned PM with 10 and 11 rotor poles and single layer windings

Both single and double layer windings have been tested on the prototype PS-SFPM machines and shown that particularly 10 rotor poles will incur additional back EMF harmonics which are not favourable as they will produce undesirable torque ripple components.

4.8. Conclusions

As the PS-SFPM machine has two stationary bodies and a single rotating body, the potential to adjust the angle between the two stationary bodies was realised. Furthermore, while adjustment of this angle was found to be undesirable for increased low speed torque production, adjustment of the angle between the two bodies provided opportunity to reduce the PM flux mechanically. From this reduction of PM flux linkage the speed range of the PS-SFPM machine could be increased. The impact of this adjustment of PM position relative to wound stator on cogging torque for different numbers of rotor poles was investigated, showing that depending on the addition of cogging torque components between the rotor and two stators resulted in increased or decreased cogging torque in the unaligned position depending on the number of rotor poles. Double and single layer windings were compared in terms of their performance with aligned and unaligned stators, particularly with single layer windings combinations with even numbers of rotor poles suffered from additional EMF harmonics and hence torque ripples, while odd numbers of rotor poles produced greater static torque without even order back EMF harmonics. The torque/power-speed performance for the PS-SFPM machine without adjustment of the PM angle and when the PM angle was freed to assume different relative angles to the wound stator was compared. This comparison revealed that higher numbers of rotor poles would achieve a larger speed range, and single layer windings will achieve greater speed range than double layer windings for the same supply power limit. A prototype machine was produced to test the performance of the PS-SFPM machine with aligned and unaligned PM stator. Two combinations of 10 and 11 rotor poles rotors were produced for the same PM and wound stator design, with double and single layer windings investigated. The asymmetric back EMF in 10 rotor poles was observed and better performance from 11 rotor poles as predicted from FE. The mechanical aspect of the prototype machine requires further refinement to ensure correct alignment and un-alignment between stationary bodies. The static performance was measured on the prototype machine, but further work into the true dynamic performance is required.

The PS-SFPM machine, while initially developed to enhance the torque density of the machine by separation of the copper and PM materials across the airgap, has presented its self as an arrangement that naturally lends itself to mechanical flux weakening to increase its speed range, while maintaining high torque at low speeds.

CHAPTER 5 – PARASITIC EFFECTS IN PARTITIONED STATOR SWITCHED FLUX PERMANENT MAGNET MACHINES

5.1. Introduction

The PS-SFPM permanent magnet (PM) machine culminates in a machine that maintains the switching flux action of switched flux machines [16, 24-25, 41] and employs a magnetic gear rotor structure [15, 58]. In the previous chapters the machine topology has been introduced, different numbers of rotor poles and winding configurations analysed and the opportunity of mechanical field weakening explored. This chapter will further investigate more parasitic effects in PM machines applied to the PS-SFPM machines, being losses and unbalanced forces.

The efficiency of a machine is determined by its power and losses, therefore predicted loss across different speeds with varying electric loading is investigated in this chapter. Three loss contributions in PS-SFPM machines are considered, being copper, iron and PM loss. As the copper loss, based on DC resistance, is independent of frequency it is generally assumed to dominate the total loss at low speeds, whereas hysteresis and eddy current losses in the iron and PM increase with operating speed [107].

Eddy current losses in the PM result from slotting harmonics [108] and stator MMF harmonics of significant magnitude and frequency [109]. Such losses in the PM may cause significant heating and hence potential partial reversible demagnetisation [110]. In PS-SFPM machines the slot opening along the surface of the PM stator are those of the salient iron pole rotor, which for optimal torque, with higher numbers of rotor poles, will feature large slot openings as shown in the previous chapters. The eddy current loss in conventional switched flux machines reduces when the PM material adjacent to the airgap is removed and PM segmentation reduces the eddy current loss inversely proportionally to the number of segments employed [36].

Hysteresis and eddy loss in the soft ferromagnetic iron are a result of irreversible changes in the magnetisation process and eddy currents induced in the laminations respectively [107],

both resulting from time varying magnetic fields. In conventional switched flux machines the complex nature of the flux density variation highlights the necessity to consider higher order flux density harmonics [35], simple models considering only fundamental order are insufficient [111].

PS-SFPM machines achieve highest torque density with numbers of rotor poles and stator teeth differing by one achieving highest back EMF, as in conventional brushless PM machines [9, 112-113] and switched flux machines [114]. Therefore, odd numbers of rotor poles may be favourable for optimal torque production, but due to asymmetric disposition around the airgap surface [115] unbalanced magnetic force (UMF) occurs, resulting in noise and vibration causing decreased bearing life [116]. The magnetic pull on a body may be calculated using the Maxwell tensor theory [115] where the relationship with airgap flux density distribution was expanded in [116].

5.2. Permanent Magnet Eddy Current Loss

The eddy current losses induced in the PS-SFPM machines PMs are predicted using FE methods and analysed for different numbers of rotor poles with single and double layer windings.

5.2.1. Open-circuit

PS-SFPM machines include interior mounted PM within an inner stationary body and rotating salient iron pole rotor. The PM poles are subjected to a time varying permeance along the airgap surface as the rotor poles rotate, therefore incurring time varying flux within the PM material, resulting in induced eddy currents, ultimately causing loss in the PM. Transient 2D FE is used to predict eddy currents induced in the PM, assuming a PM conductivity of $6.67\times10^{5}(\Omega m)^{-1}$. The open-circuit eddy current loss considering a single PM is minimal when the PM airgap surface is aligned with the rotor slot opening Fig. 5.1, for 10 and 14 rotor poles this occurs at 270°elec with 11 and 13 rotor shifted ±15°elec due to distribution factor less than one resulting in shifted initial rotor position (relative to q-axis current excitation).

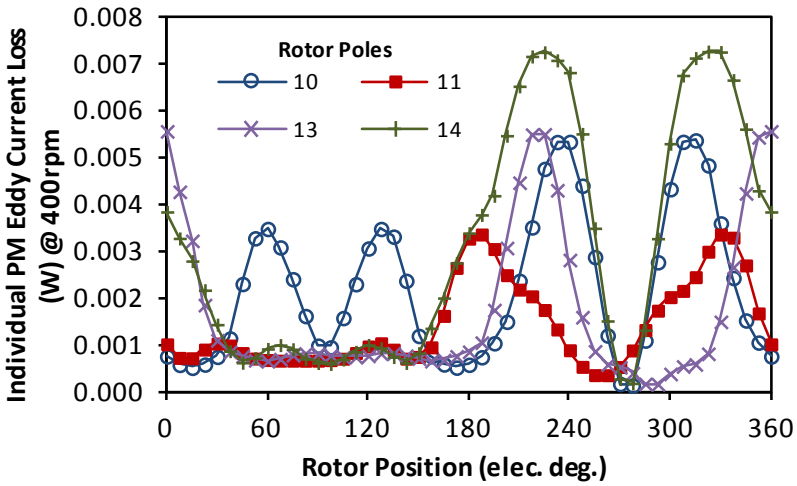

Fig. 5.1. Open-circuit PM eddy current loss in a single PM through one electrical cycle

Due to the asymmetry of the rotor poles in machines with 11 and 13 rotor poles the combined total PM eddy current loss of all the PM poles contains minimal variation with rotor position compared with machines with even numbers of rotor poles Fig. 5.2.

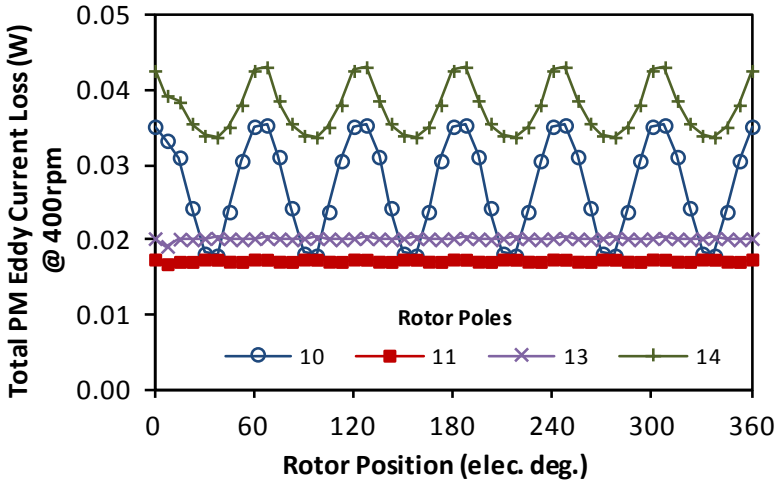

Fig. 5.2. Open-circuit total PM eddy current loss through one electrical cycle

The open-circuit induced eddy current distribution and loss distribution for a machine with 10 rotor poles is shown in Fig. 5.3, revealing concentration of eddy current loss occurs at the PM surface adjacent to the airgap resulting from greatest flux density variation as the rotor poles pass the PM surface.

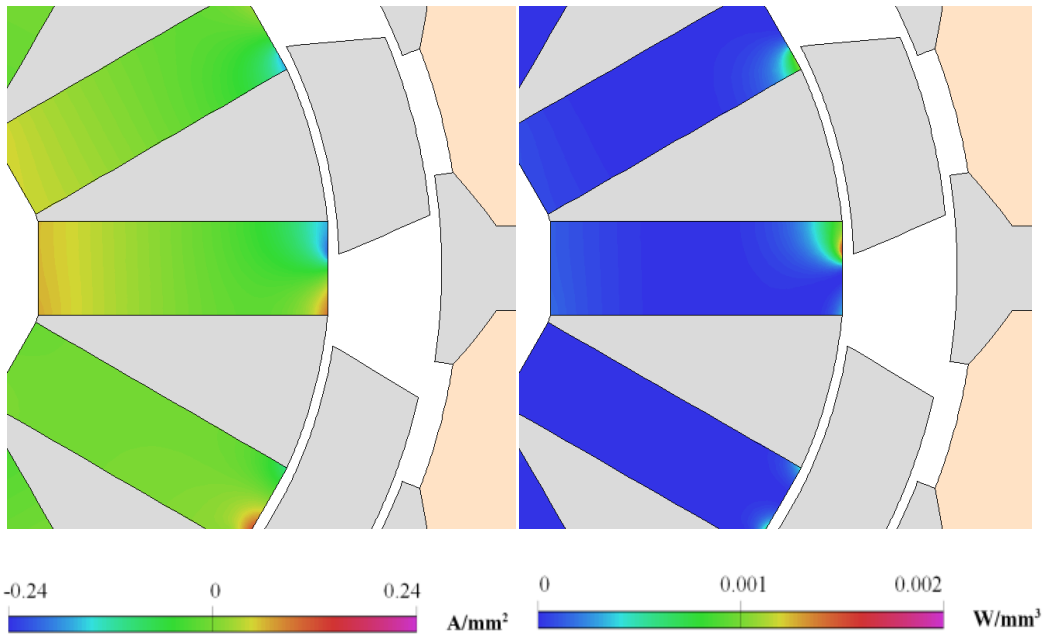

(Current distribution) (Loss distribution)

Fig. 5.3. Maximum PM eddy current loss position with 10 rotor poles

Radial and circumferential flux density variation with rotor position within the PM surface close to the airgap is modelled using FE for different numbers of rotor poles Fig. 5.4. While the radial fundamental flux density variation decreases with number of rotor poles, 13 and 14 have higher circumferential fundamental variation compared with 10 and 11. The eddy current loss is frequency dependant and that increasing the number of rotor poles will increase the fundamental frequency, hence increase the loss independently of the flux density variation magnitude.

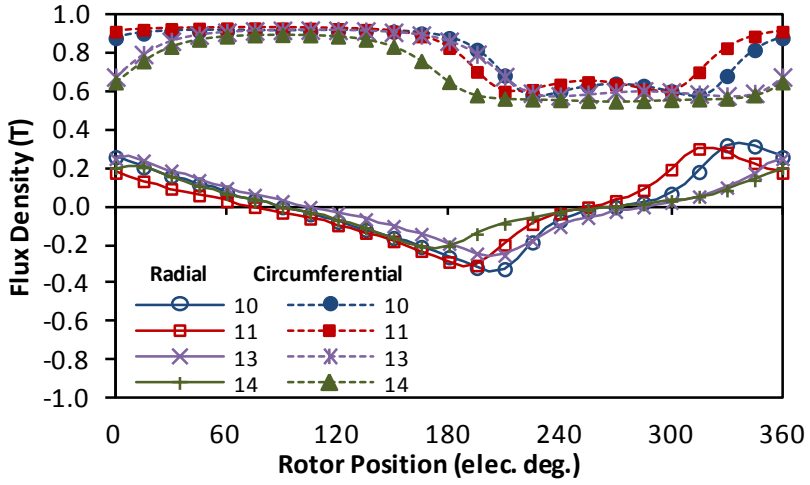

(a)

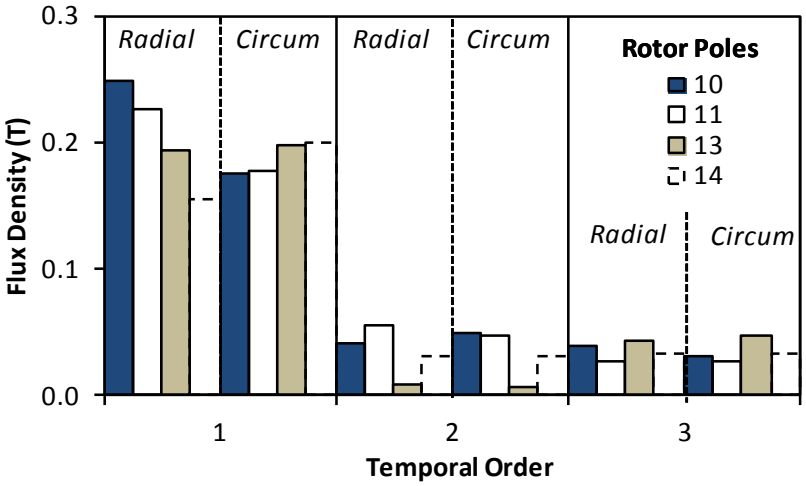

(b)

Fig. 5.4. Open-circuit flux density with rotor position close to airgap of single PM (a) flux density variation with rotor position, (b) flux density variation harmonics

As the rotor speed increases the PM eddy current increases with the square of speed for all combinations of rotor poles Fig. 5.5. Average open-circuit PM eddy current loss is shown in Table XVI with 10 and 14 having the highest eddy current loss due to their magnitude of flux density variation and high frequency respectively.

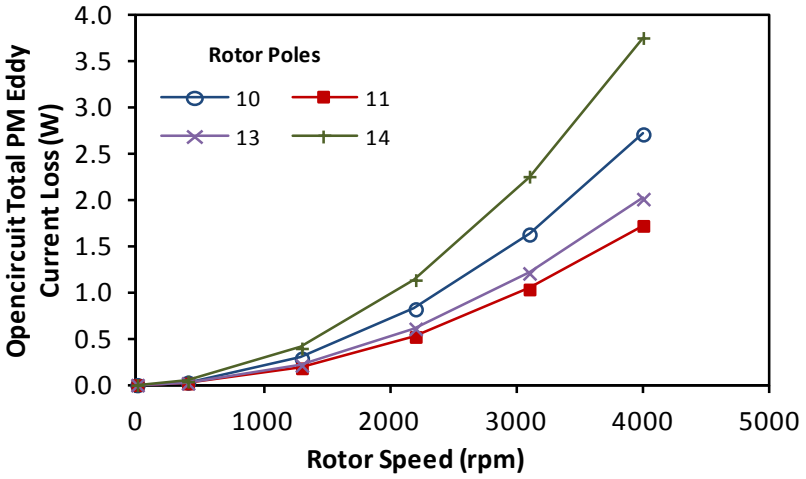

Fig. 5.5. Variation of PM eddy current loss with increased rotor speed and different numbers of rotor poles

5.2.2. On-load

With winding current excitation the field within the PM is altered depending on the armature reaction field magnitude which is dependent on the current magnitude and winding topology. Two winding topologies are considered with double and single layer concentrated

windings termed according to the number of winding layers in a single slot. The PM eddy current loss at rated current with double and single layer windings, compared with the open-circuit loss is shown in Table XVI.

Table XVI. PM eddy current loss – open-circuit and at rated current

PM Eddy Current Loss (W)	Rotor Poles			
	10	11	13	14
Open-circuit	0.027	0.017	0.020	0.038
Double Layer, load	0.030	0.024	0.023	0.042
Single Layer, load	0.035	0.024	0.030	0.054

With 10 rotor poles the eddy current distribution in one PM is shown in Fig. 5.6 with double and single layer windings at the same rotor position.

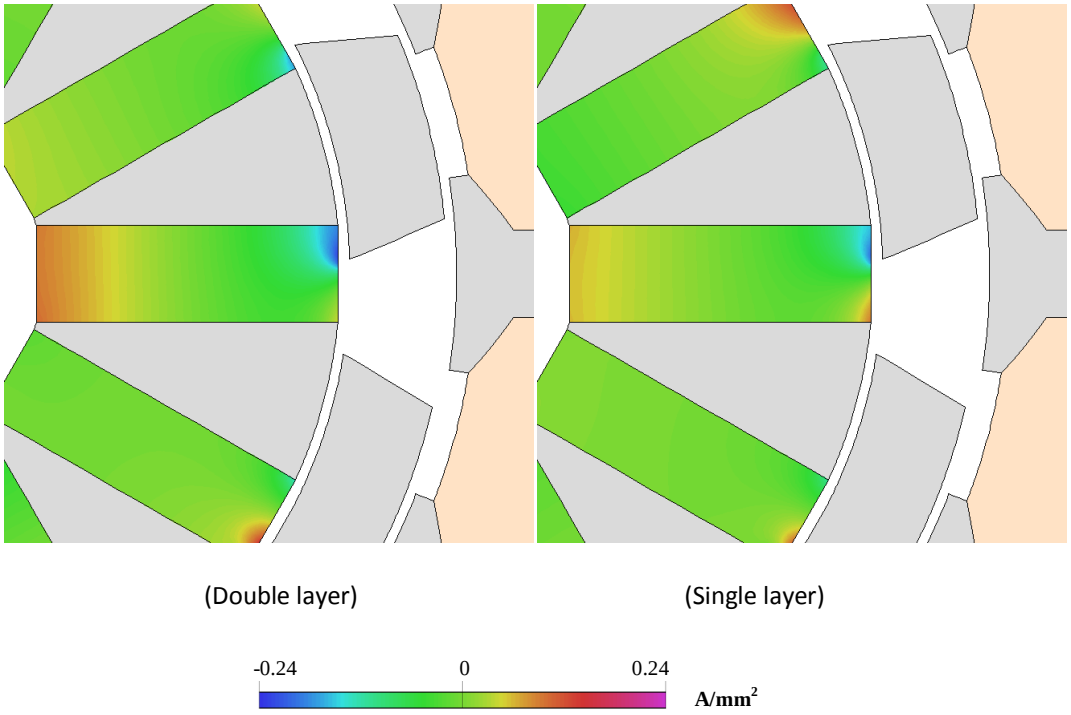

Fig. 5.6. PM eddy current distribution with 10 rotor poles with rotor at 240°elec (I_q = 14.14A)

The loss associated with the eddy currents in Fig. 5.6 are shown in Fig. 5.7 for the same machine with double and single layer windings. At this instantaneous rotor position the loss with double layers in this individual PM is greater than the loss with single layer windings, but the overall average loss increases with single layer windings for all numbers of rotor poles.

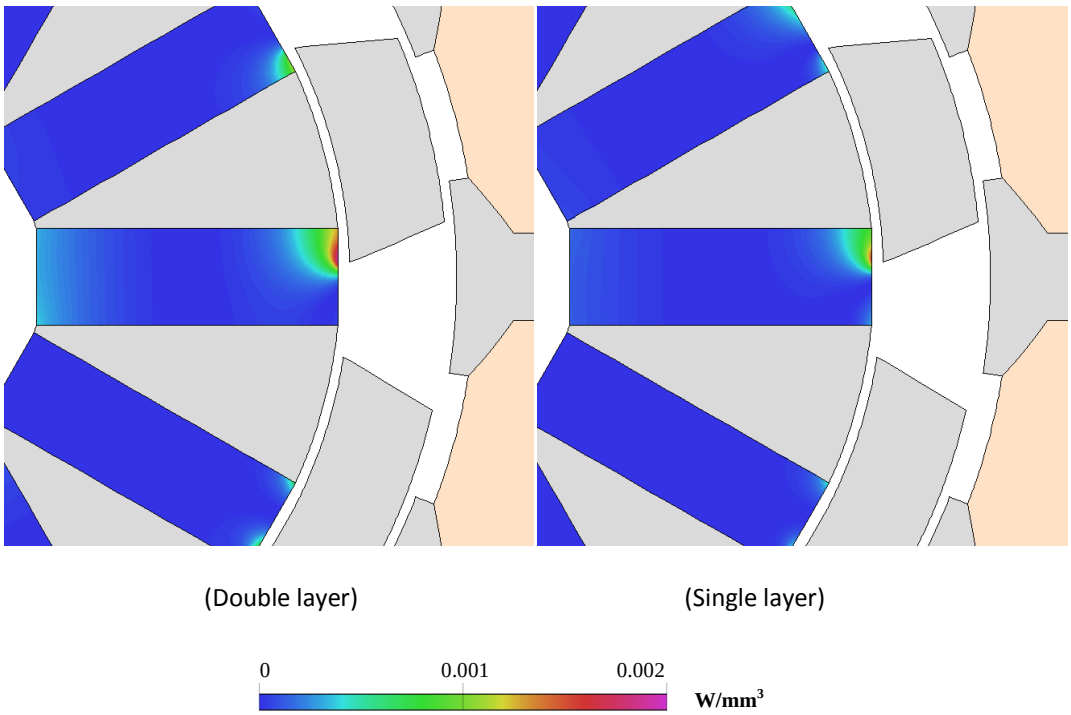

Fig. 5.7. PM eddy current loss distribution with 10 rotor poles with rotor at 240°elec (I_q = 14.14A)

The armature reaction field is shown in Fig. 5.8 for machines having 10 rotor poles with double and single layer windings, with the airgap radial flux density of the inner airgap shown in Fig. 5.9.

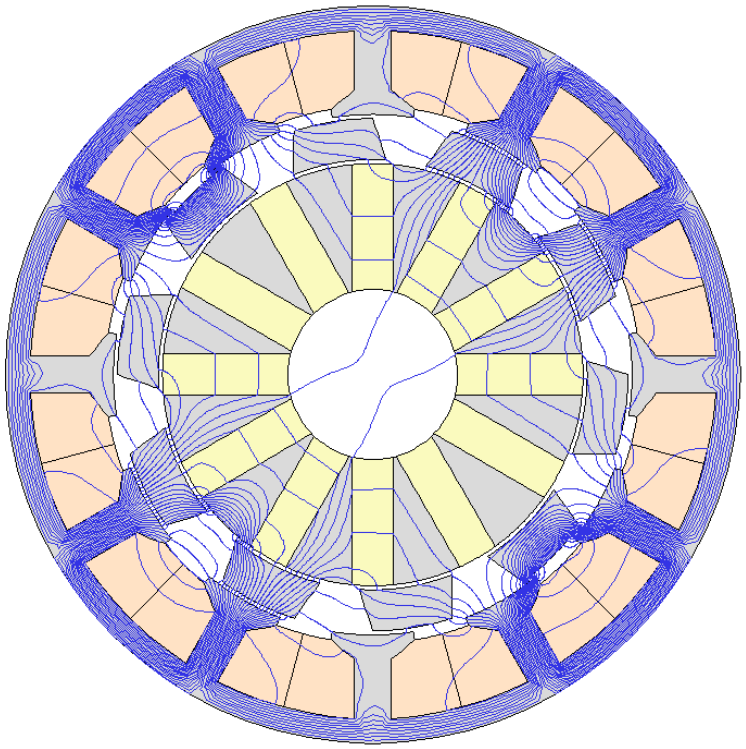

(a)

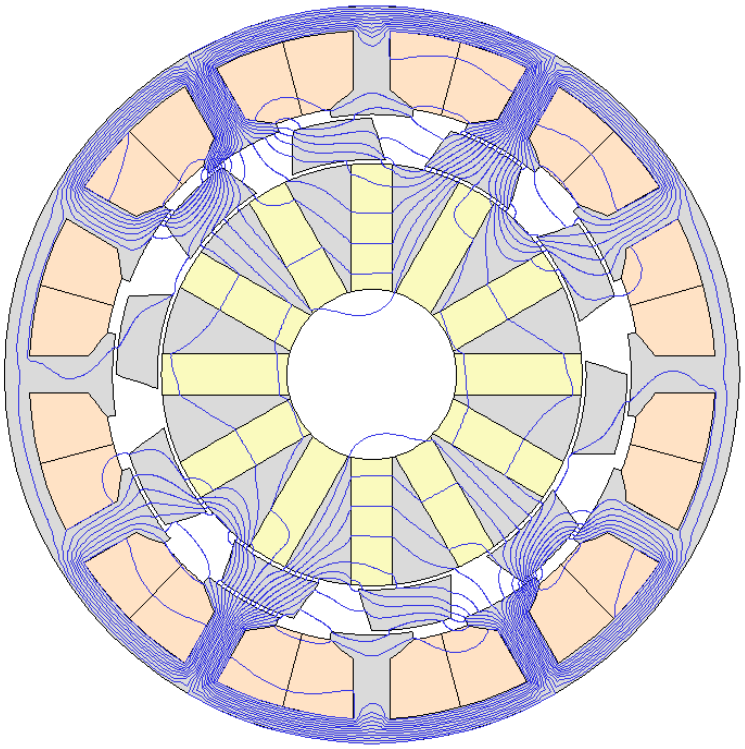

(b)

Fig. 5.8. Armature reaction field with (a) double and (b) single layer concentrated windings at rated current of 14.14A

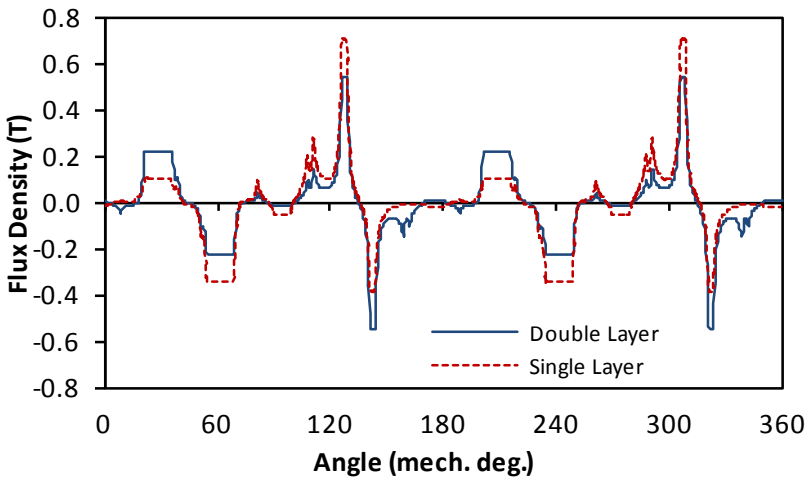

Fig. 5.9. Radial armature reaction flux density inner airgap with double and single layer windings

By employing single layer windings airgap flux density sub-harmonic magnitudes are increased Fig. 5.10, thus increasing the flux density variation in the PM material causing additional eddy current loss to the open-circuit loss.

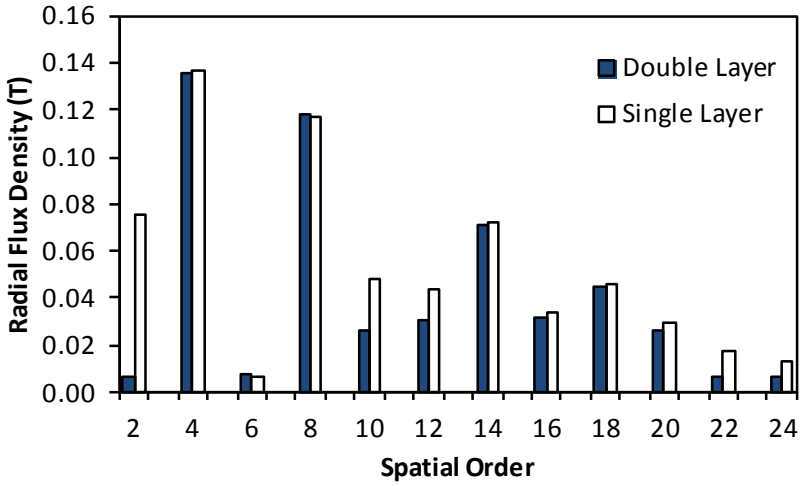

Fig. 5.10. Radial armature reaction flux density harmonics inner airgap with double and single layer windings

By employing single layer windings the additional armature reaction field harmonics introduced cause eddy current loss, therefore with any number of rotor poles the PM eddy current loss is increased. The smallest increase between double and single layer windings PM eddy current loss is with 11 rotor poles and the greatest is with 14 rotor poles.

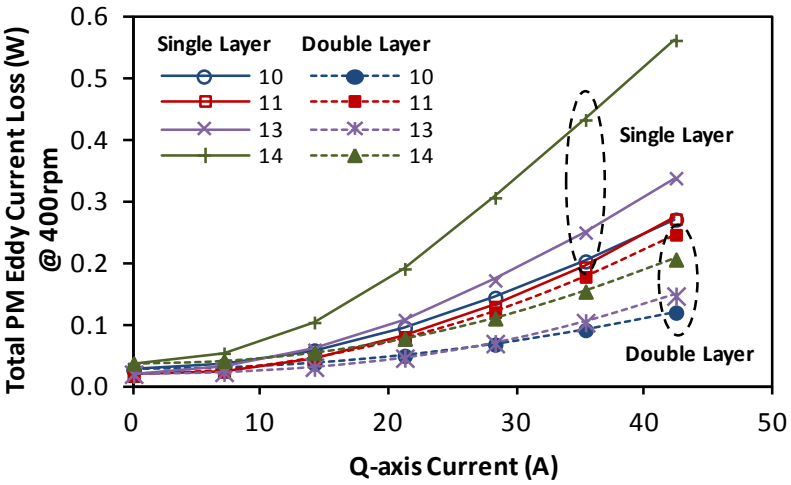

Fig. 5.11. Variation in PM eddy current loss with different numbers of rotor poles at 400rpm with single and double layer windings

The flux density variation with rotor position close to the inner airgap surface of the PM, an identical position to that used in Fig. 5.4, the open-circuit, rated double and single layer flux density variation are compared in Fig. 5.12 with 10 rotor poles. The major difference in flux density variation occurs in the radial flux density around 90°elec with increased flux density with single layer windings compared with double and open-circuit.

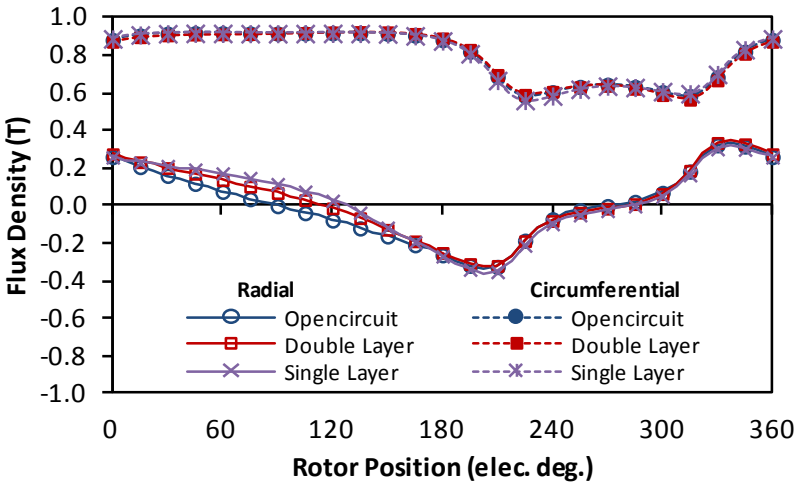

Fig. 5.12. Flux density close to airgap surface of PM with 10 rotor poles

Considering the harmonics that occur in the radial flux density, the fundamental and 2nd order harmonics increase as double layer and then single layer windings are employed compared with open-circuit condition Fig. 5.13, therefore the increased PM eddy current loss when single layer windings are employed is validated by an increased harmonic content of the airgap field resulting in increased variation in flux density within the PM surface.

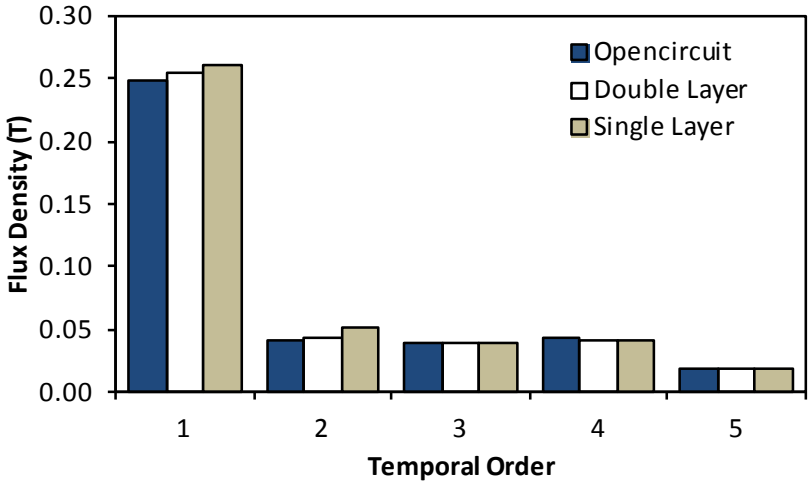

Fig. 5.13. Radial flux density harmonics close to airgap surface of PM with 10 rotor poles

As the current loading is increased the variation of flux density in a single PM is shown in Fig. 5.14 for a machine with 10 rotor poles.

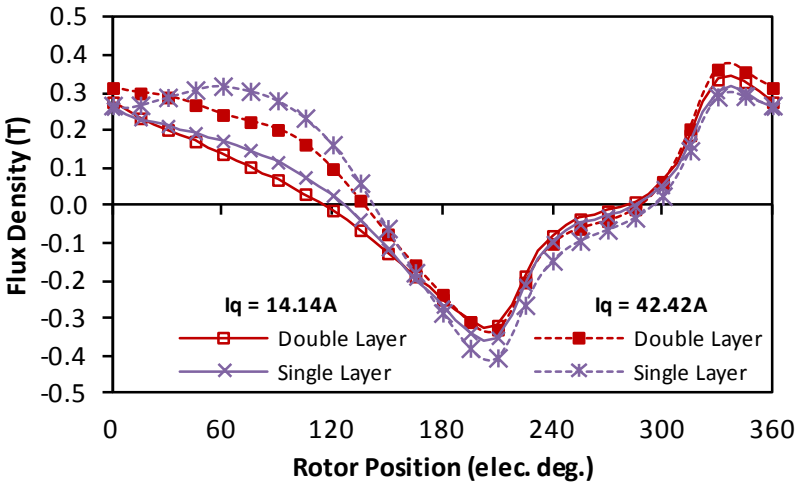

Fig. 5.14. Radial flux density harmonics close to airgap surface of PM with 10 rotor poles

Increasing the number of rotor poles increases the frequency of flux density variation in the PM for the same output rotor speed, therefore higher numbers of rotor poles increase the PM eddy current loss. But 11 and 13 rotor poles contain less armature reaction harmonics resulting in PM eddy current loss hence reducing the loss, Fig. 5.15. The PM eddy current loss increased with the square of rotor speed, as may be expected.

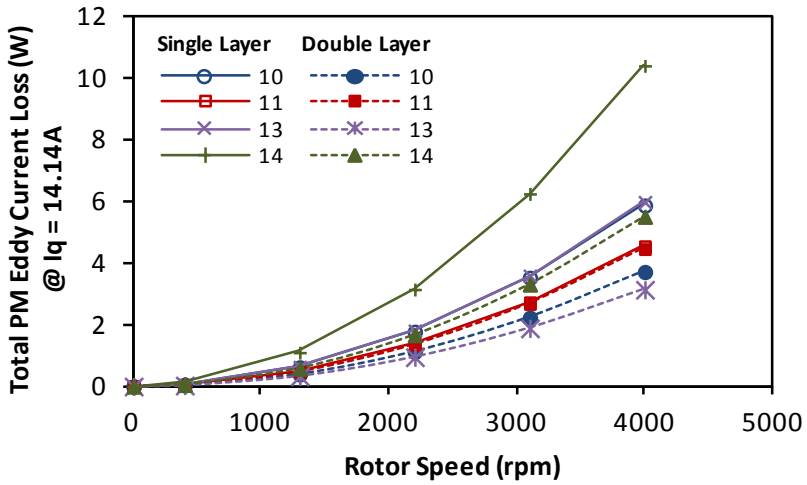

Fig. 5.15. Variation in PM eddy current loss with different numbers of rotor poles at rated current with single and double layer windings

5.3. Hysteresis and Eddy Iron Loss

Iron loss in soft ferromagnetic materials in a machine may be decomposed into hysteresis and dynamic or eddy current loss [107]. Due to the complexity of the flux density variation in

PS-SFPM machines minor hysteresis loops must be considered. A general expression for iron loss (25) is given in [117] that considers hysteresis and eddy current loss components:

$$P_{loss} = f\left(k_{h1}\Delta B_{pp} + k_{h2}\Delta B_{pp}^2\right) + f k_e \int_0^T \left(\frac{\partial B}{\partial t}\right)^2 dt \qquad (25)$$

where the coefficients are shown in TABLE XVII, with coefficients obtained from the material data in [131] .

Table XVII. Specification of PS-SFPM machine

Description	**Symbol**
Fundamental flux density frequency	f
Peak to peak flux density	B_{pp}
Material	Transil300_16T
Hysteresis loss coefficient 1	$k_{h1} = 1.55\times10^{-2}$
Hysteresis loss coefficient 2	$k_{h2} = 2.45$
Eddy current loss coefficient	$k_e = 1\times10^{-4}$

Iron loss models are limited by the accurate prediction of loss coefficients based on material data, as the impact of machining on materials has a significant effect on the material structure and hence the losses produced. As the flux density variation in the laminations is complex and many harmonics occur, the accurate prediction of iron loss is further complicated. Accepting these limitations, the iron loss of the PS-SFPM machine is predicted to compare different rotor pole combinations and provide an estimation of the loss expected.

Fig. 5.16 compares the iron loss calculated using (25) with a 2D FE analysis, collecting flux density data in each mesh element and obtaining iron loss considering 10 harmonic orders of flux density variation. Machines with 10, 11, 13 and 14 rotor poles are compared with single and double layer windings, 10 and 11 rotor poles have the highest open-circuit iron loss with 14 having the lowest. Typically increasing the number of rotor poles would increase iron loss as the flux density frequency is increased, in PS-SFPM machines the peak to peak variation in flux density for higher numbers of rotor poles is reduced, therefore even with increased fundamental frequency of flux density variation the iron loss is reduced.

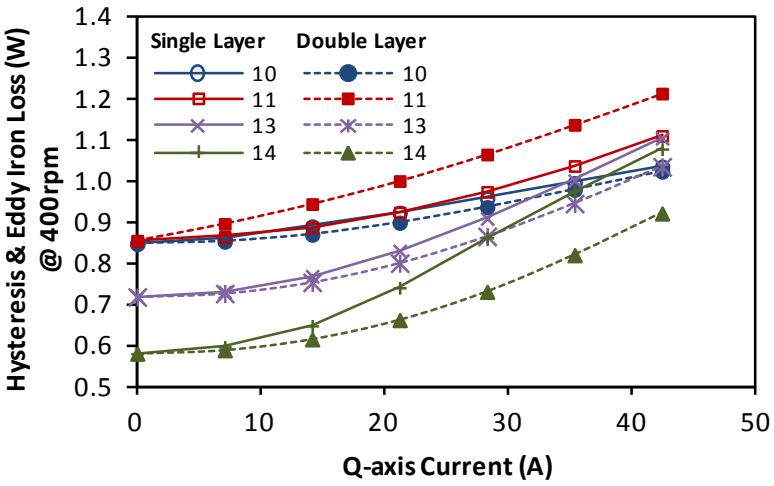

Fig. 5.16. Variation in iron loss with different numbers of rotor poles at 400rpm with single and double layer windings

The hysteresis and eddy current loss components are shown in Fig. 5.17, as the armature reaction field is considered the peak to peak flux density increases, as the hysteresis loss is proportional to B^2 the hysteresis loss increases more significantly with q-axis loading than the eddy current loss Fig. 5.17a. Conversely the eddy current loss is proportional to f^2 therefore with increasing rotor speed the eddy current loss increases with squared relationship whereas the hysteresis loss increases linearly Fig. 5.17b.

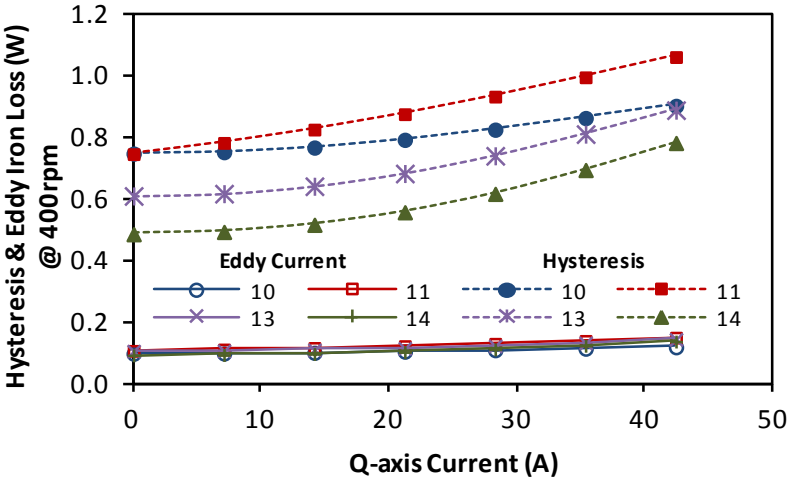

(a)

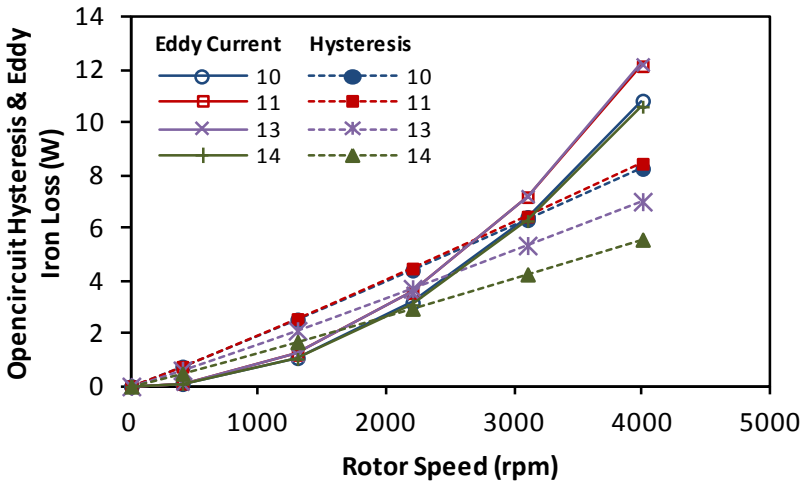

(b)

Fig. 5.17. Variation in hysteresis and eddy current loss with double layer windings with (a) q-axis current loading and (b) rotor speed

The variation of iron loss for different numbers of rotor poles with rotor speed is shown for open-circuit and with double and single layer windings at rated current Fig. 5.18b, with 11 rotor poles having the highest iron loss.

Compared with conventional switched flux machines with double and single layer windings the PS-SFPM machine has lower iron loss compared with the switched flux machine in [37] at 4000rpm, due to decreased saturation thus reducing the flux density variation from the conventional switched flux machine [35].

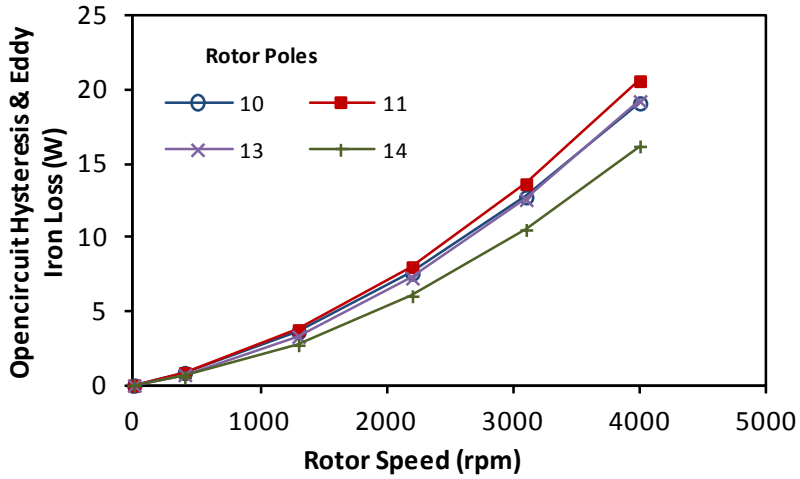

(a)

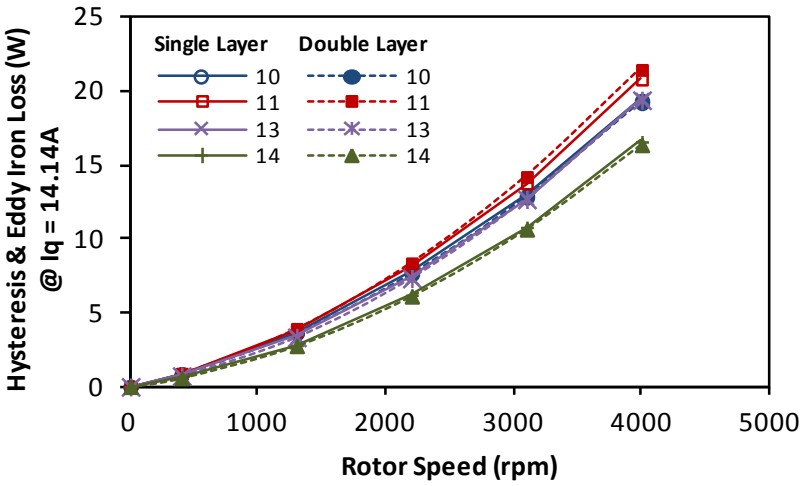

(b)

Fig. 5.18. Variation in iron loss with different numbers of rotor poles (a) opencircuit and (b) rated current with single and double layer windings

To provide understanding of the iron loss presented in Fig. 5.16, the flux density variations at example points within the PS-SFPM machine with different numbers of rotor poles are investigated. Points A-D in the outer wound stator, E-F in the rotor poles and H in the stationary PM, as shown in Fig. 5.19.

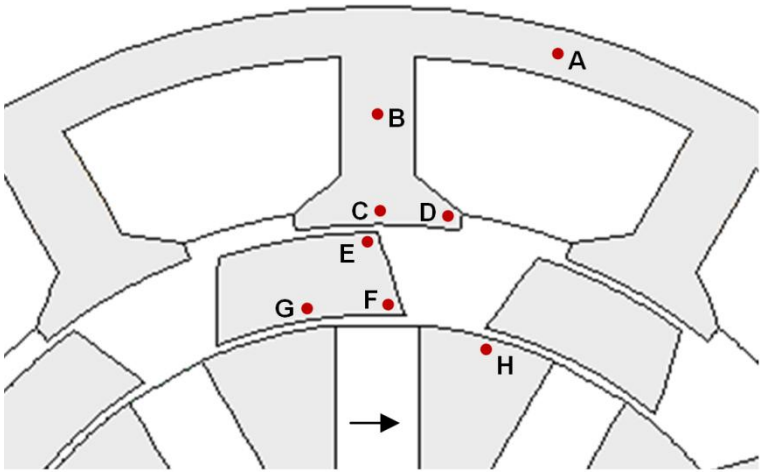

Fig. 5.19. Positioning of flux density probes (A-D) Outer Stator, (E-G) Rotor and (H) Inner Stator

In the stator yoke the radial and circumferential variation over one electrical period, Fig. 5.20, shows the variation is in the circumferential direction and that in open-circuit conditions the magnitude of variation is greatest with 10 rotor poles. The fundamental period of flux density variation is one electrical period in the outer stator.

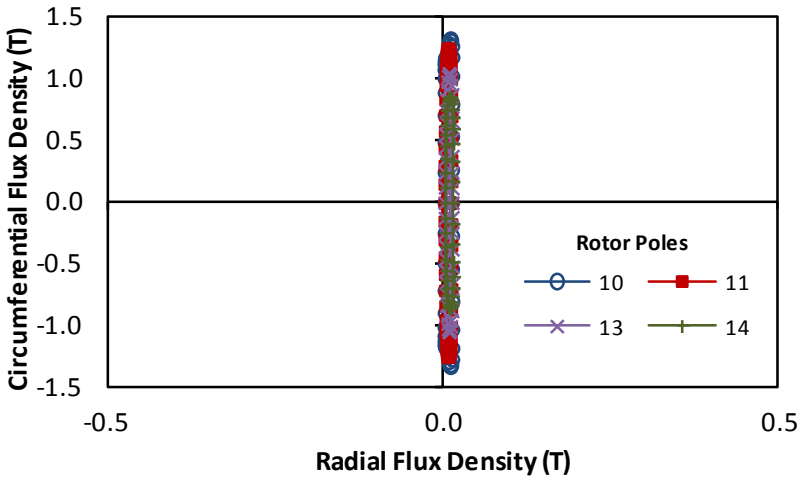

Fig. 5.20. Open-circuit circumferential and radial flux density for one electrical cycle in the outer stator yoke for different numbers of rotor poles (A)

Conversely in the stator tooth body the majority of flux variation is in the radial direction, Fig. 5.21, as the stator yoke is half the tooth body width the flux density magnitude is almost the same in both tooth and yoke.

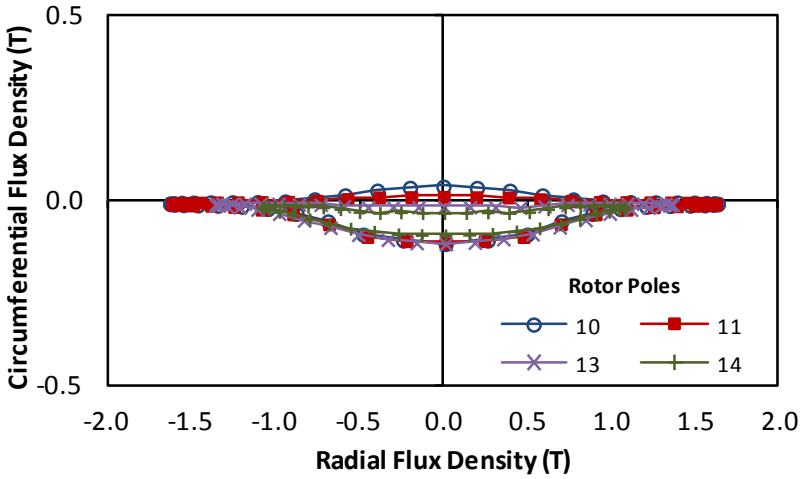

Fig. 5.21. Open-circuit circumferential and radial flux density for one electrical cycle in an outer stator tooth for different numbers of rotor poles (B)

The outer stator tooth tip centre experiences circumferential biasing of flux density as the inner PM is aligned with a single tooth, therefore net flux circumferentially occurs, Fig. 5.22. Radially the flux alternates as the rotor passes the PM pole, the maximum variation in flux density is with 11 rotor poles.

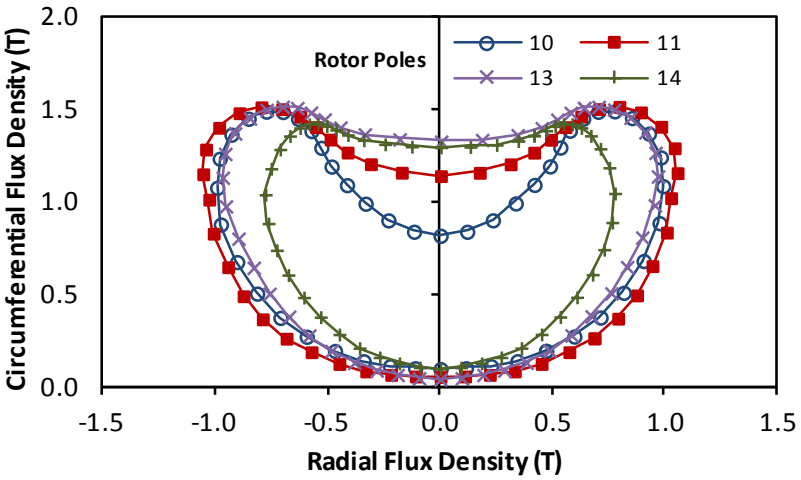

Fig. 5.22. Open-circuit circumferential and radial flux density for one electrical cycle in an outer stator centre tooth tip for different numbers of rotor poles (C)

In the stator tooth tip edge the flux density is circumferentially and radially bias according to the PM orientation Fig. 5.23.

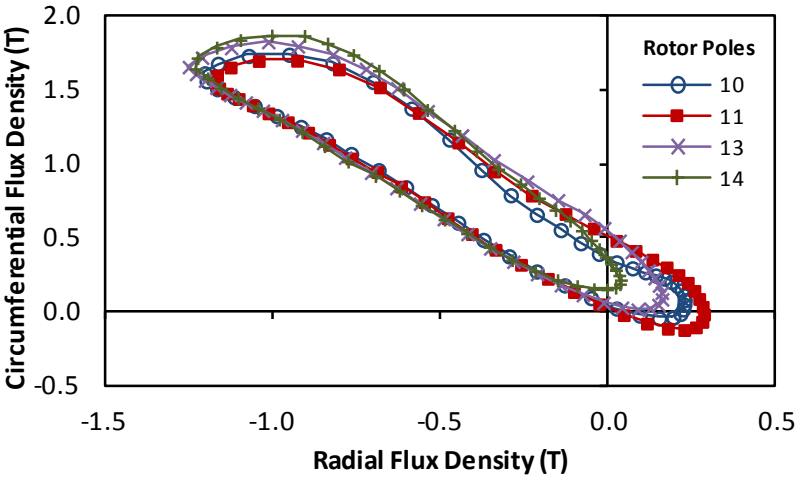

Fig. 5.23. Open-circuit circumferential and radial flux density for one electrical cycle in an outer stator tooth tip for different numbers of rotor poles (D)

Unlike the stator, the fundamental period of flux density variation in the rotor iron is dependent on the number of PM poles, as passing a single rotor pole through one electrical cycle is not sufficient for a full cycle in flux density variation. Therefore, the angle may be considered as the PM electrical angle, rather than rotor pole electrical angle, the PS-SFPM machines investigated have 6 pole pairs. As this angle is obtained from the number of PM poles, the frequency is independent of the number of rotor poles.

The flux density variation for one PM electrical period is shown for three points within the rotor, outer corner, inner corner and inner centre Fig. 5.24. For each point in a rotor pole, the variation in flux density decreases with increased number of rotor poles.

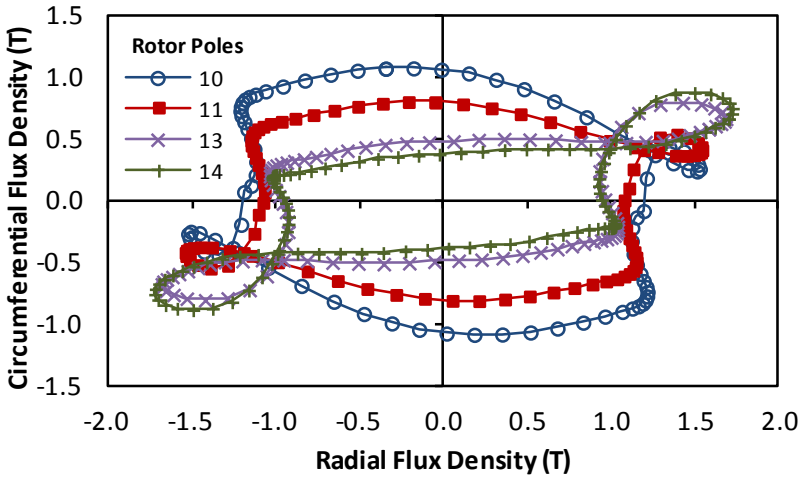

(Point E)

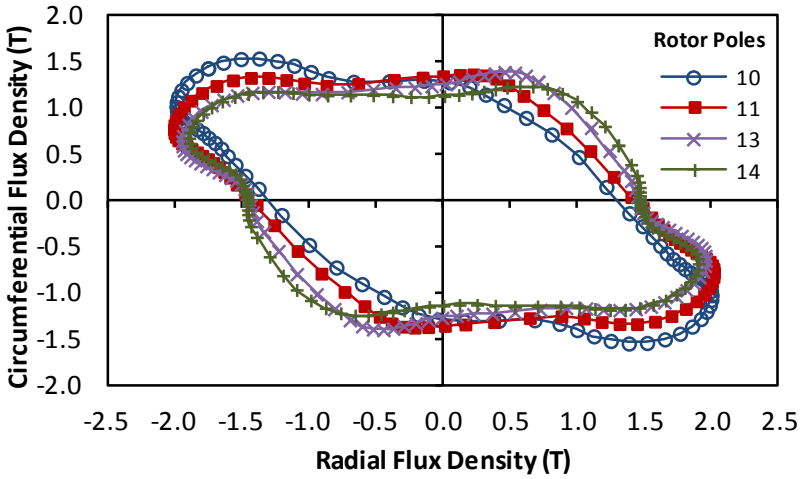

(Point F)

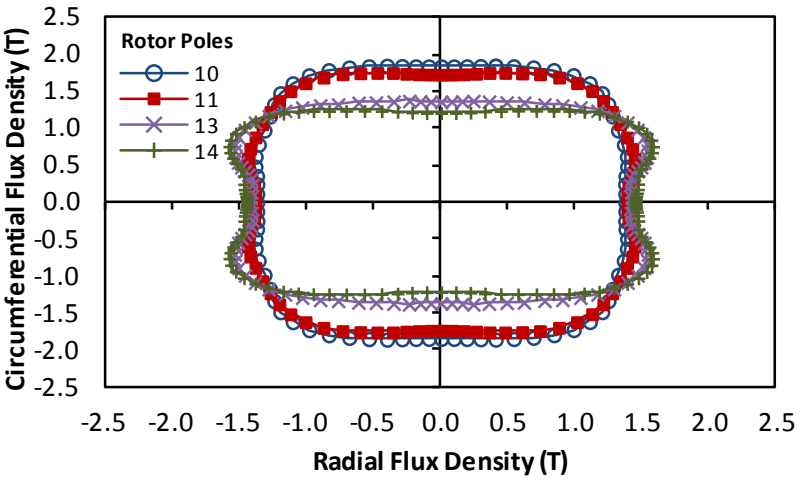

(Point G)

Fig. 5.24. Open-circuit circumferential and radial flux density for one 6th of a mechanical cycle in rotor pole inner centre for different numbers of rotor poles at points E-G

In the stationary PM iron the flux density is obtained Fig. 5.25 and compared with the outer stator and rotor the flux density variation is smaller, also the volume of iron is smaller.

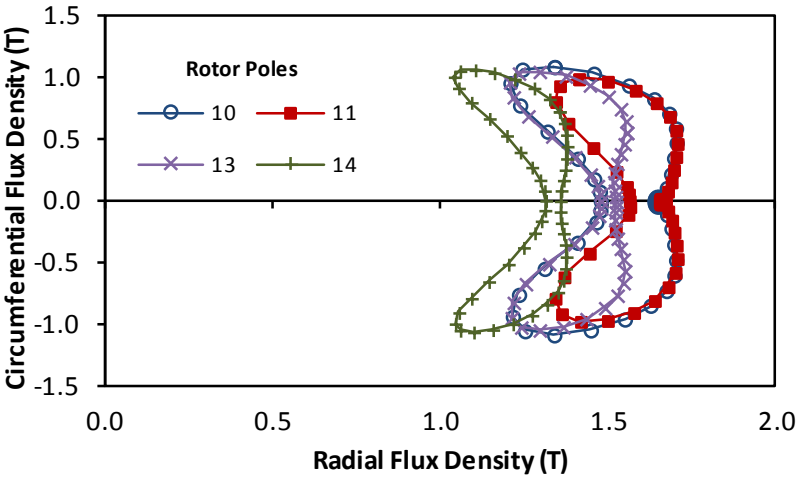

Fig. 5.25. Open-circuit circumferential and radial flux density for one electrical cycle in inner stator centre for different numbers of rotor poles (H)

As the flux in the inner PM stator iron has minimal variation with rotor position and lower volume of iron than the rotor and wound stator, its iron loss is negligible compared to iron loss in the rotor and wound stator. The number of rotor poles has no effect on the frequency of flux density in the rotor poles, therefore as 11 rotor poles has the largest peak to peak flux density it incurs the greatest loss. The armature reaction field only minimally affects the flux

density in the rotor poles, resulting in almost constant rotor loss with different q-axis current loadings.

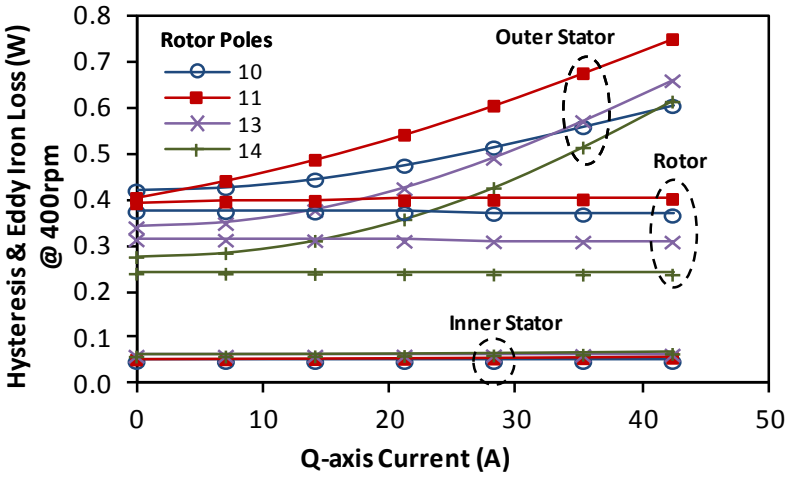

(a)

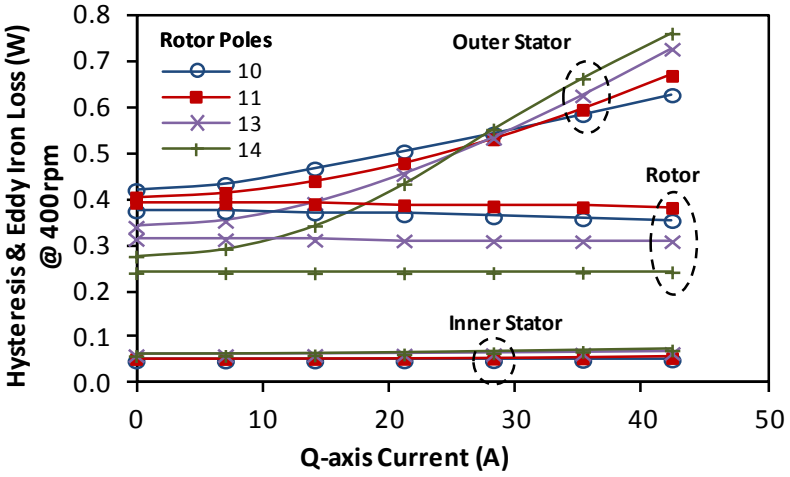

(b)

Fig. 5.26. Variation in iron loss in machine sections with different numbers of rotor poles at rated current with double (a) and single (b) layer windings

The outer wound stator loss is most affected by q-axis current loading. Comparison between double and single layer windings and q-axis current dependency reveals that single layer windings increase the on load iron loss in the wound stator for machines with 13 and 14 rotor poles, while reducing with 10 and 11 rotor poles. The change between double and single layer windings has very little effect on the loss in the rotor and inner PM stator.

To compare machines with different numbers of rotor poles having double and single layer windings the copper, iron and magnet losses are obtained using 2D FE and presented in Table

XVIII. The copper loss dominates the loss in the constant torque region as at lower speed the frequency dependant losses are less, therefore the efficiency with single layer windings is reduced as employing single layer windings increases the end winding length, hence the copper loss. While 11 rotor poles incurs the greatest iron loss it has the low PM loss with high output power it achieves the highest rated efficiency.

Table XVIII. Losses and efficiency at 1300rpm (Constant torque region)

	Winding Layers	**Rotor Poles**			
		10	11	13	14
Copper Loss (W)	Single	21.43	21.43	21.43	21.43
	Double	15.58	15.58	15.58	15.58
Iron Loss (W)	Single	3.68	3.81	3.37	2.81
	Double	3.65	3.94	3.36	2.77
Magnet Loss (W)	Single	0.37	0.26	0.32	0.57
	Double	0.31	0.26	0.25	0.44
Input Power (W)	Single	406.6	420.4	413.1	375.5
	Double	398.1	434.2	417.6	362.2
Output Power (W)	Single	378.6	414.5	398.4	343.4
	Double	381.1	394.9	388.0	350.7
Efficiency (%)	Single	93.69	94.20	94.07	93.26
	Double	95.12	95.23	95.29	94.91

5.4. Losses with Mechanical Flux Weakening

PS-SFPM machines have been shown in the previous chapters to be able to assume different relative angles between their windings and PM, resulting in the ability to mechanically weaken the PM flux, ultimately providing a larger operational speed range. Comparison of the PM eddy current losses in a single PM for different rotor positions with the PM aligned with the wound stator teeth and un-aligned, reveals that for the same speed (400rpm) the unaligned PM position experiences less eddy current loss for both 10 rotor poles Fig. 5.27 and 11 rotor poles Fig. 5.28.

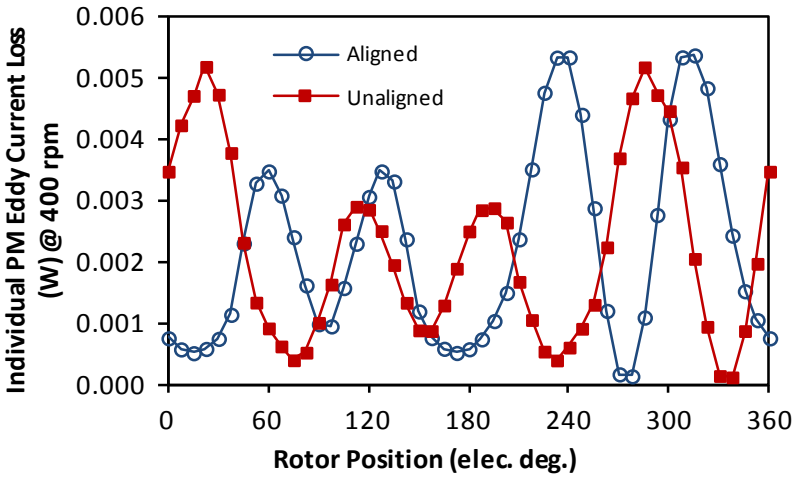

Fig. 5.27. Individual PM eddy current losses for PS-SFPM machines with aligned and unaligned PM with 10 rotor poles

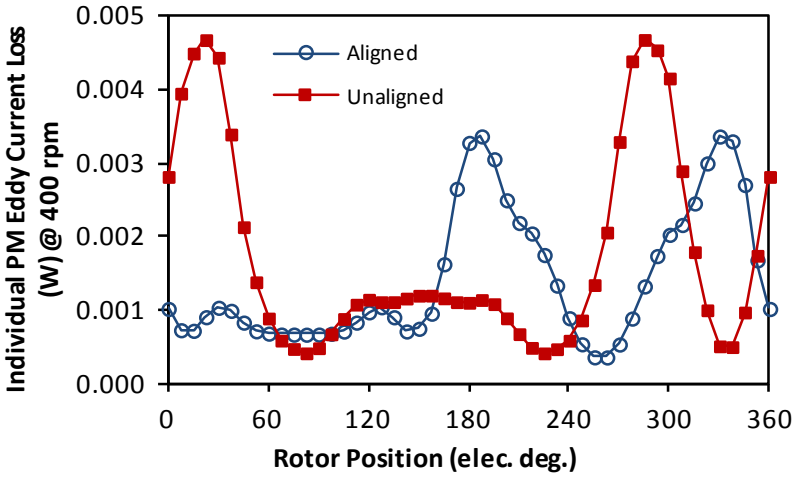

Fig. 5.28. Individual PM eddy current losses for PS-SFPM machines with aligned and unaligned PM with 11 rotor poles

The PM eddy current losses on load increase for all numbers of rotor poles with q-axis current excitation. For even numbers of rotor poles the aligned eddy current losses are greater than when the PM's are unaligned, but for odd numbers of rotor poles the armature reaction field when unaligned is more significant and therefore at higher current loading the unaligned losses are greater. At the rated current, for all numbers of rotor poles the eddy current losses are higher when the PM is aligned with the wound stator teeth Fig. 5.29.

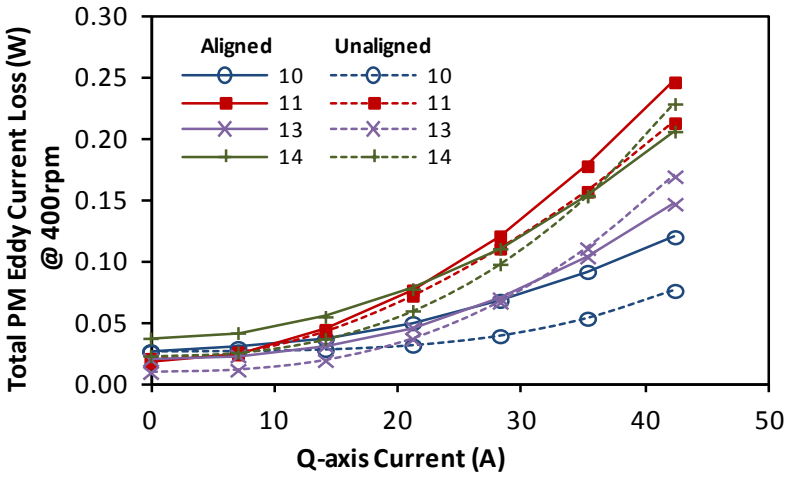

Fig. 5.29. Total PM eddy current losses for PS-SFPM machines with aligned and unaligned PM with different numbers of rotor poles

While this is the conclusion for eddy current losses aligned and unaligned at the same speed, as the speed increases the eddy current losses increase with a squared relationship. Therefore when the unaligned condition is used at higher speeds, for field weakening purposes, the eddy current losses will increase accordingly.

Similarly considering the iron hysteresis and eddy current losses, the unaligned position has smaller losses compared to the aligned position with the same number of rotor poles Fig. 5.30.

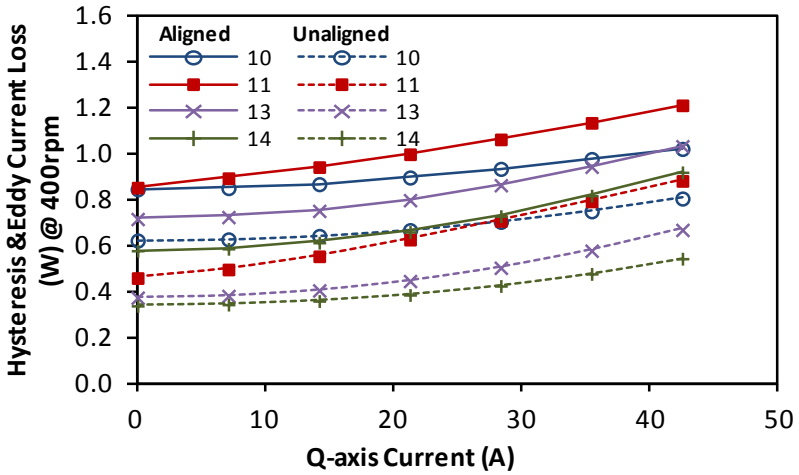

Fig. 5.30. Iron losses for PS-SFPM machines with aligned and unaligned PM with different numbers of rotor poles

As the PM are moved from the aligned to unaligned the variation in flux density throughout the machine changes, resulting in the change in iron loss. The centre of the tooth tip (Fig. 5.19 Point C) demonstrates this change between aligned and unaligned flux density variation Fig.

5.31. In the aligned position the flux density variation is bi-polar in the radial plain, as the flux passes through the tooth both positive and negative for both PM poles, and the circumferential variation is only positive as the leakage flux from the PM is field is fixed. Once the PMs have been unaligned, the radial variation becomes only positive as one PM pole (N or S) is aligned with the stator tooth, and the circumferential flux density is both positive and negative as the rotor passes the stator tooth.

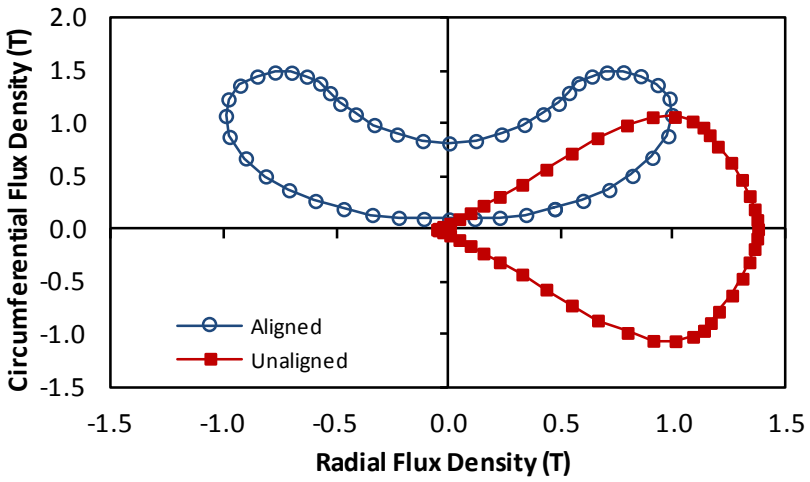

Fig. 5.31. Flux density variation in outer stator tooth tip for one electrical period with 10 rotor poles with aligned and unaligned PM

The unipolar variation of flux when the PM are unaligned can be observed in the flux density variation in the stator yoke Fig. 5.32, the alignment of a single PM pole (N or S) with a single tooth biases the variation of flux through the stator.

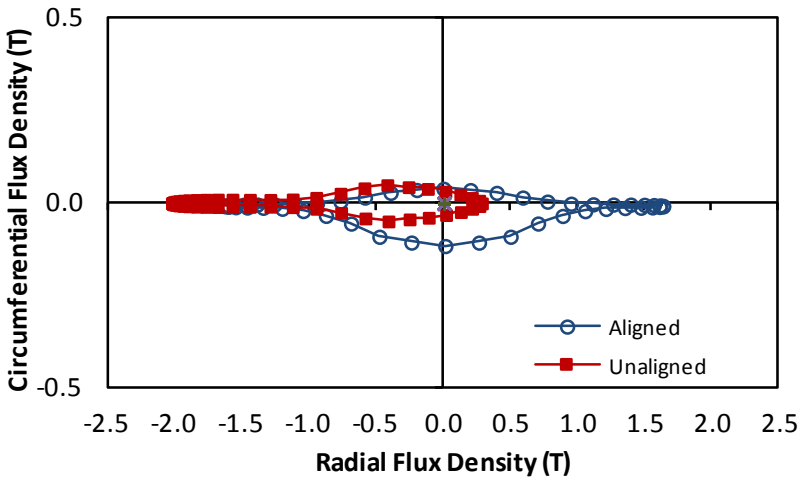

Fig. 5.32. Flux density variation in outer stator yoke for one electrical period with 10 rotor poles with aligned and unaligned PM

When the PM are unaligned from the wound stator teeth the variation of flux through the rotor poles shifts from being predominately circumferential with the PM aligned to a reduced time of circumferential flux density to more radial flux as the rotor pole passes between the PM pole (N or S) and a single stator tooth Fig. 5.33.

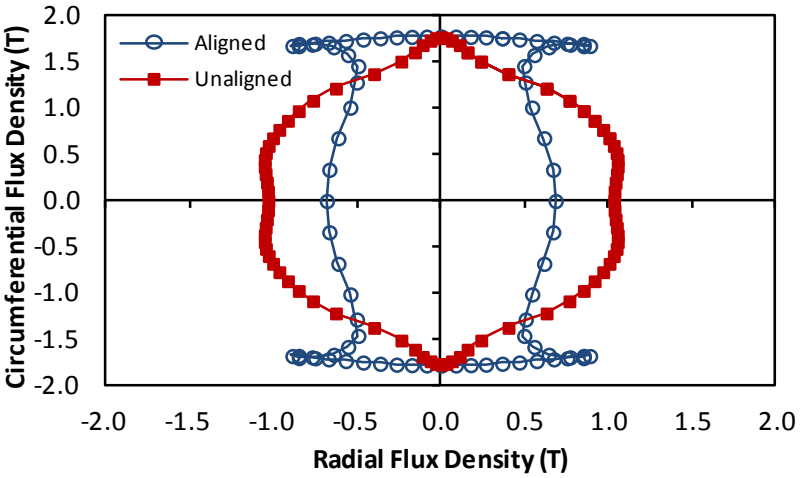

Fig. 5.33. Flux density variation in rotor pole for 6th of a mechanical period with 10 rotor poles with aligned and unaligned PM

The un-alignment of the PM from the wound stator teeth, decreases the flux linking the coils by adjustment of the flux path through the machine. This causes reduction of PM flux linkage, through saturation of iron within the magnetic circuit, but does not incur an increase in PM eddy current and iron losses. Although there is a reduction when the unaligned position is assumed, the significance of this is reduced as the influence of rotor speed affects the losses.

5.5. Unbalanced Magnetic Forces

For a PS-SFPM machine with odd numbers of rotor poles, the flux density distribution around the airgap surface is asymmetric and therefore will feature unbalanced magnetic forces (UMF). The magnetic pull on a body may be calculated using the Maxwell tensor theory [115] where the relationship with airgap flux density distribution was expanded in [116]. From the opencircuit flux potential plots for 11 (Fig. 5.34) and 13 (Fig. 2.21) rotor poles it can be seen that the alignment of each rotor pole does not have a balancing opposite rotor pole with

respect to the arrangement of PM on the stator, this may lead to unbalanced forces acting on the rotor.

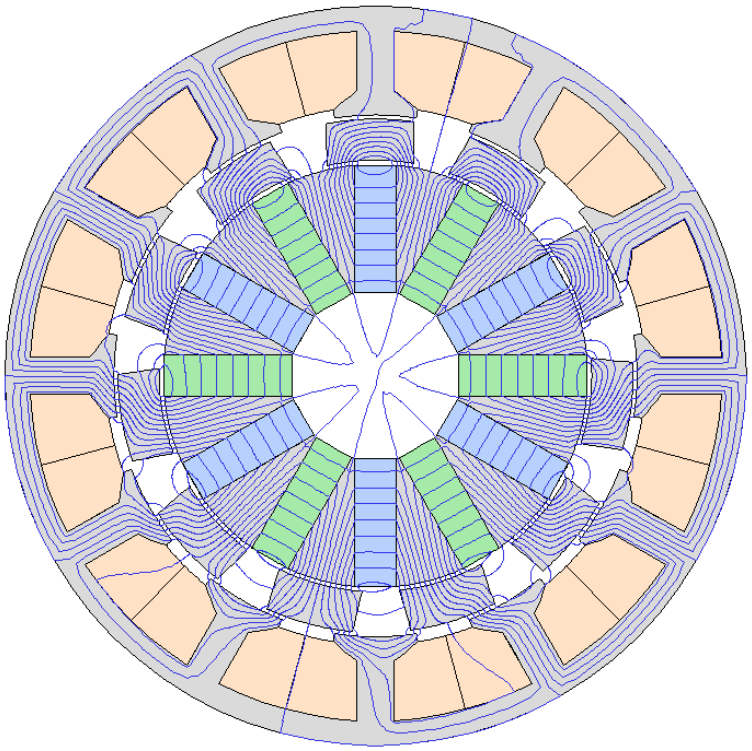

Fig. 5.34. Field distributions for PS-SFPM machines at d-axis with 11 rotor poles

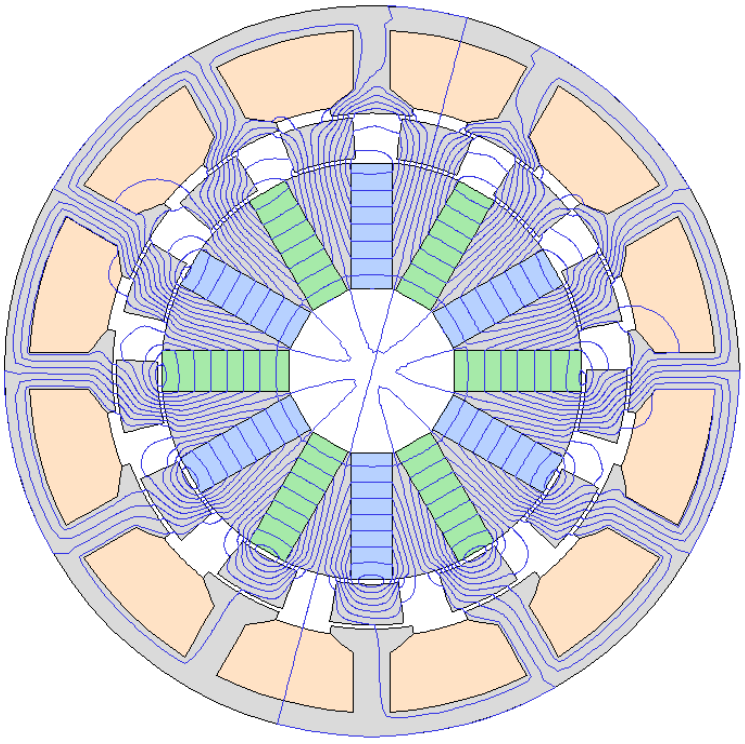

Fig. 5.35. Field distributions for PS-SFPM machines at d-axis with 13 rotor poles

The airgap flux density for odd numbers of rotor poles does not display rotational symmetry as that for even numbers of rotor poles shown in chapter 2. For 11 rotor poles the

radial (Fig. 5.36) and tangential (Fig. 5.37) airgap flux densities are shown for the inner and outer airgaps on both rotor surfaces and again for 13 rotor poles the radial (Fig. 5.38) and tangential (Fig. 5.39) flux densities.

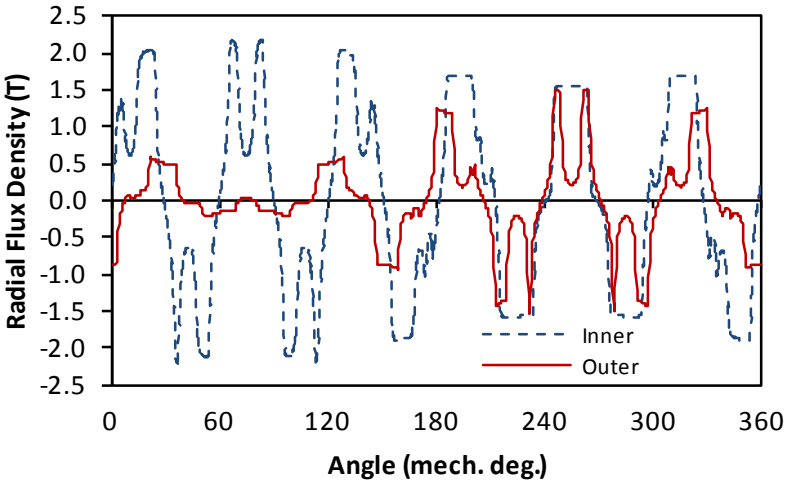

Fig. 5.36. Open-circuit radial flux density for 11 rotor poles

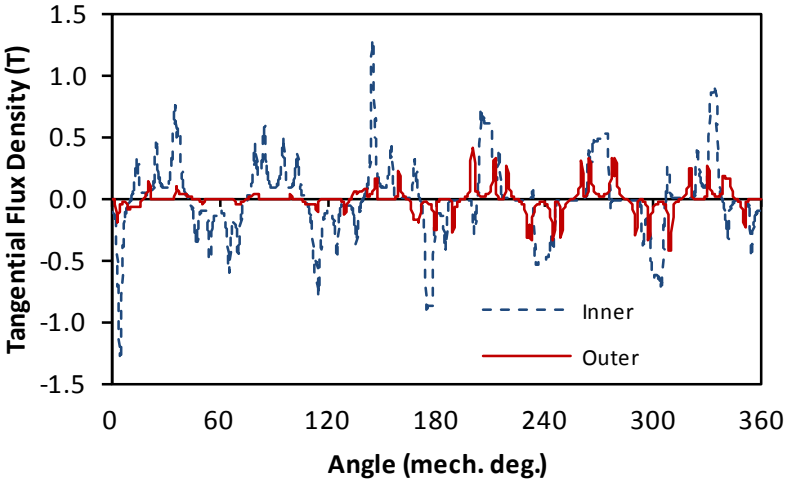

Fig. 5.37. Open-circuit tangential flux density for 11 rotor poles

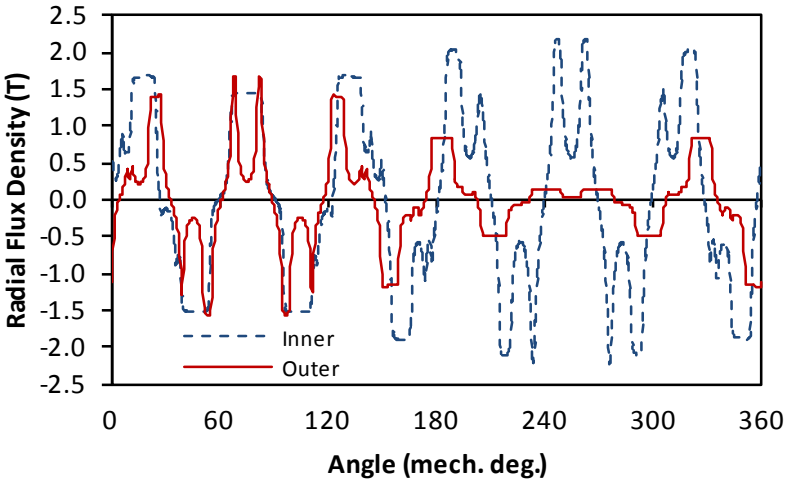

Fig. 5.38. Open-circuit radial flux density for 13 rotor poles

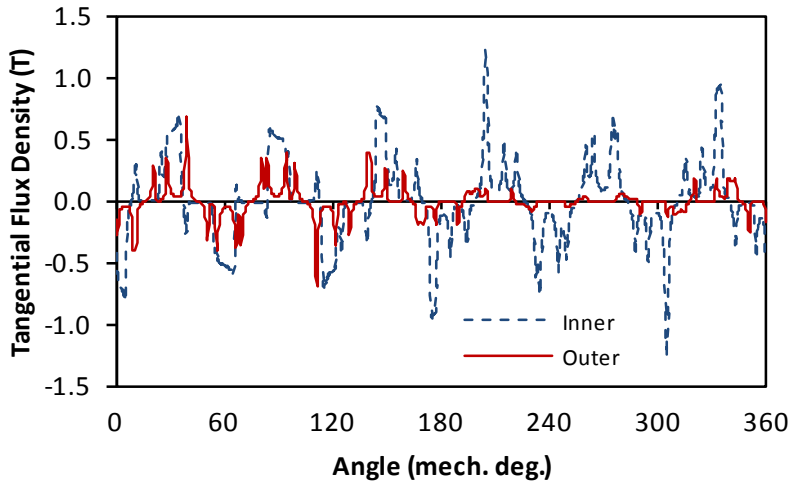

Fig. 5.39. Open-circuit tangential flux density for 13 rotor poles

The contribution of radial and tangential forces to unbalanced magnetic force was shown for conventional switched flux machines in [114]. Unbalanced x-axis force F_{mx} and y-axis force F_{my} for a machine with single airgap are expressed in (26) and (27):

$$F_{mx} = \frac{rL_a}{2\mu_o}\int_0^{2\pi} [(B_\alpha^2 - B_r^2)\cos(\alpha) + 2B_r B_\alpha \sin(\alpha)]\, d\alpha \tag{26}$$

$$F_{my} = \frac{rL_a}{2\mu_o}\int_0^{2\pi} [(B_\alpha^2 - B_r^2)\sin(\alpha) - 2B_r B_\alpha \cos(\alpha)]\, d\alpha \tag{27}$$

where r is the radius at the middle of the airgap, L_a is the active lamination length, μ_o is the permeability of free space ($4\pi\times10^{-7}$ Wb/Am), B_r and B_α are the radial and circumferential components of airgap flux density.

$$S_n = -\frac{1}{2\mu_0}\left(B_n{}^2 - B_t{}^2\right) \tag{28}$$

$$S_t = -\frac{1}{\mu_0}(B_n B_t) \tag{29}$$

For a PS-SFPM machine there are two airgaps, therefore the force acting on the internal PM stator is obtained from the inner airgap flux density with the subscript *i* denoting the inner airgap (30) and (31):

$$F_{mxi} = \frac{r_i L_a}{2\mu_o} \int_0^{2\pi} [(B_{\alpha i}^2 - B_{ri}^2)\cos(\alpha) + 2B_{ri}B_{\alpha i}\sin(\alpha)]\, d\alpha \tag{30}$$

$$F_{myi} = \frac{r_i L_a}{2\mu_o} \int_0^{2\pi} [(B_{\alpha i}^2 - B_{ri}^2)\sin(\alpha) - 2B_{ri}B_{\alpha i}\cos(\alpha)]\, d\alpha \tag{31}$$

While the force on the iron pole rotor and internal PM stator is obtained by the force in the outer airgap denoted as *o* in (32) and (33):

$$F_{mxo} = \frac{r_o L_a}{2\mu_o} \int_0^{2\pi} [(B_{\alpha o}^2 - B_{ro}^2)\cos(\alpha) + 2B_{ro}B_{\alpha o}\sin(\alpha)]\, d\alpha \tag{32}$$

$$F_{myo} = \frac{r_o L_a}{2\mu_o} \int_0^{2\pi} [(B_{\alpha o}^2 - B_{ro}^2)\sin(\alpha) - 2B_{ro}B_{\alpha o}\cos(\alpha)]\, d\alpha \tag{33}$$

Hence, the x and y unbalanced magnetic force components acting on the whole rotor is (34) and (35):

$$F_{mx} = F_{mxo} - F_{mxi} \tag{34}$$

$$F_{my} = F_{myo} - F_{myi} \tag{35}$$

The open-circuit UMF for two PS-SFPM machines with 11 and 13 rotor poles, over one mechanical rotation, is shown in Fig. 5.40. For the two machines with 11 and 13 rotor poles both wound and PM stators geometries are constrained, but the rotor poles are optimised for maximum torque production. In these two combinations of rotor poles with the same stators the machine with 13 rotor poles experiences larger UMF.

Unbalanced forces in the x-axis and y-axis for double layer winding PS-SFPM machines with 11 and 13 rotor poles with no current loading is shown in Fig. 5.40 for an electrical period.

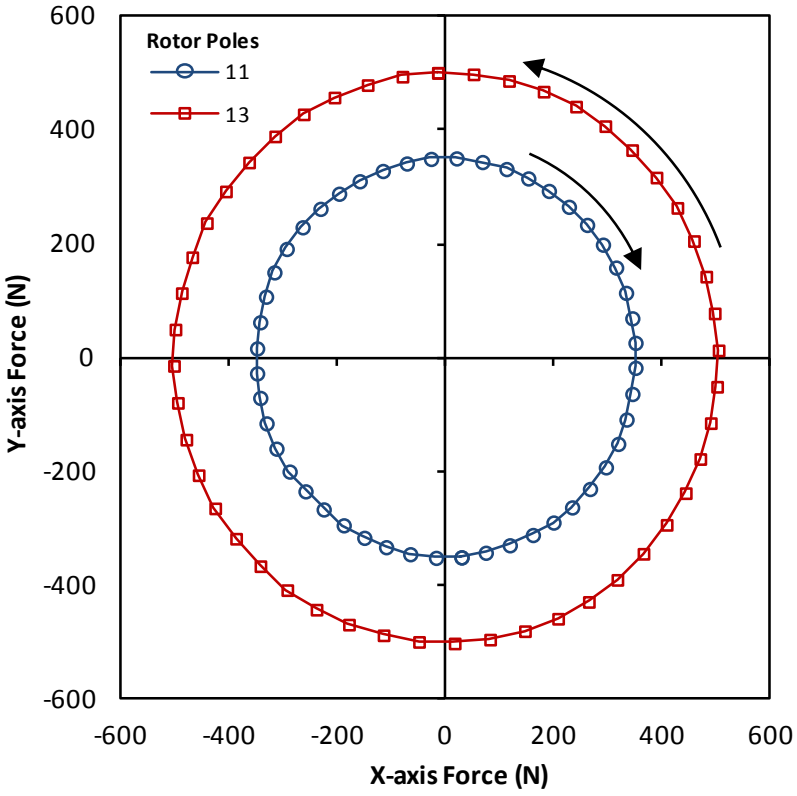

Fig. 5.40. Open-circuit unbalanced magnetic for PS-SFPM machines with 11 and 13 rotor poles

The forces acting on the unbalanced rotor may be further investigated by the force contribution based on the influence of the radial and tangential components of the forces acting upon the rotor. For both 11 and 13 rotor poles it can be seen that the major contributing force is that of the radial unbalanced force, Fig. 5.41 and Fig. 5.42 respectively.

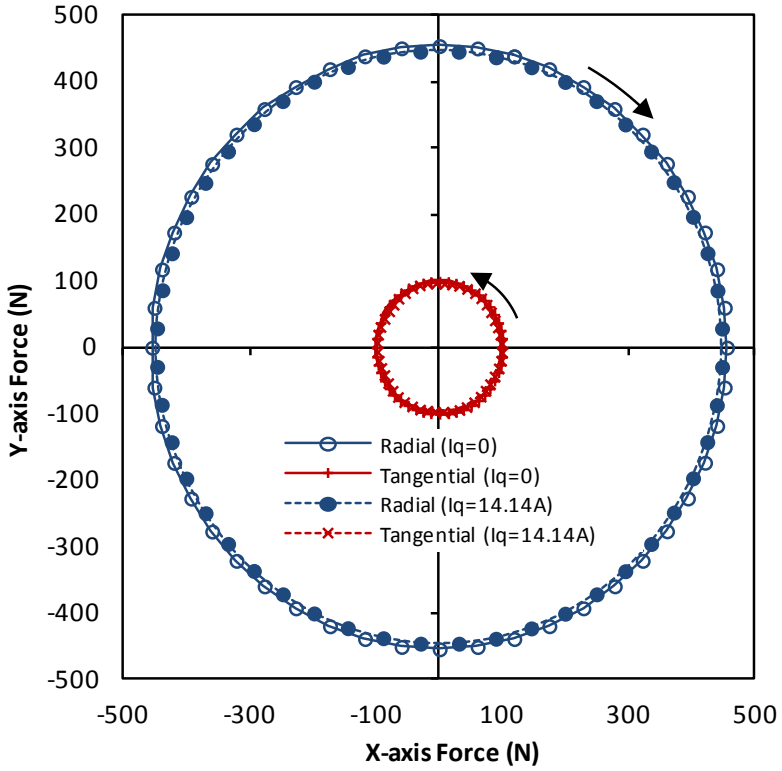

Fig. 5.41 Unbalanced magnetic forces for open-circuit and rated current conditions for a PS-SFPM machine with 11 rotor poles

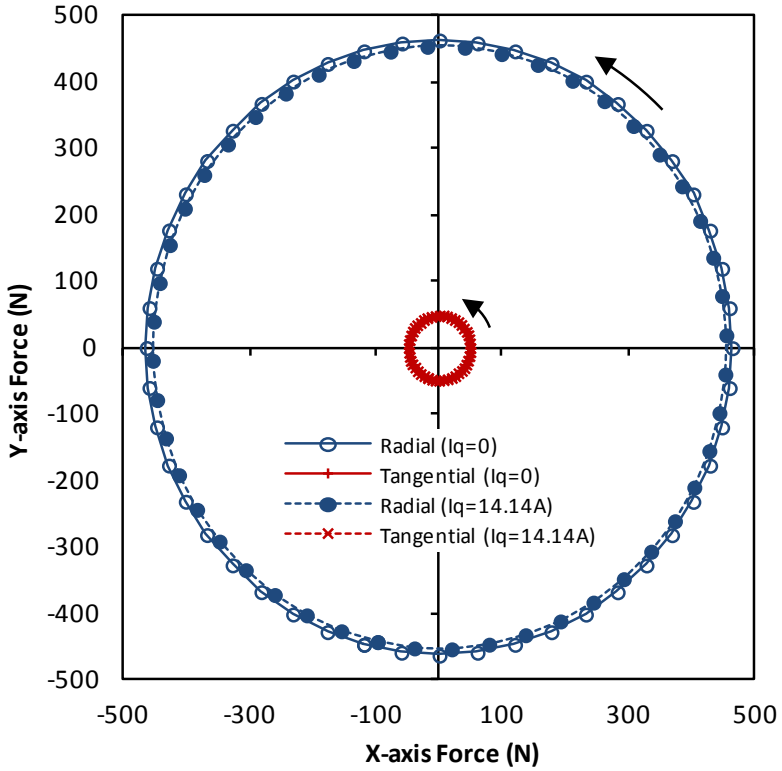

Fig. 5.42. Unbalanced magnetic forces for open-circuit and rated current conditions for a PS-SFPM machine with 13 rotor poles

The open-circuit UMF created between the rotor and interior PM dominates the total UMF experienced by the rotor, Fig. 5.43. Up to three times the rated current the UMF reduces slightly with both 11 and 13 rotor poles, the effect of increasing q-axis current is to oppose the force created by the PM. As the armature reaction field has minimal effect on the overall UMF and the difference between double and single layer windings is negligible.

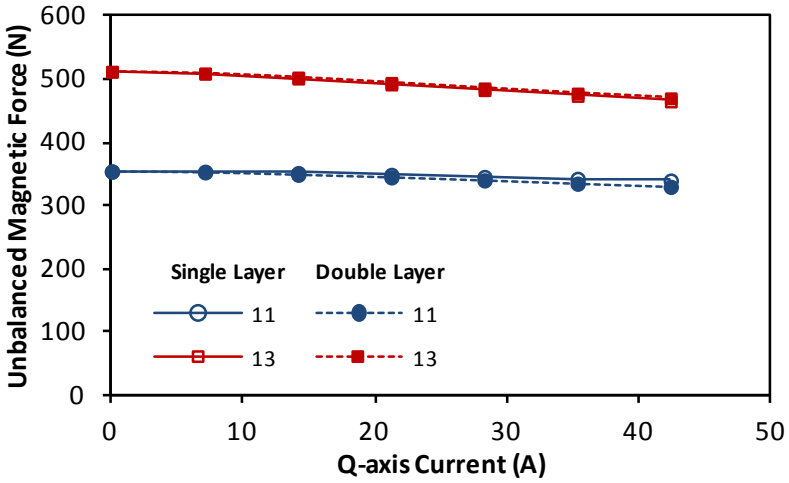

Fig. 5.43. Unbalanced magnetic force variation with q-axis current excitation with 11 and 13 rotor poles, double and single layer windings

While compared to the overall unbalanced forces including the forces with open-circuit winding, the change in unbalanced force due to armature reaction fields for double and single layer windings is shown in Fig. 5.44. The effect of the armature field is greater with 13 rotor poles, while the difference between single and double layer effects of armature field is reversed between 11 and 13 rotor poles.

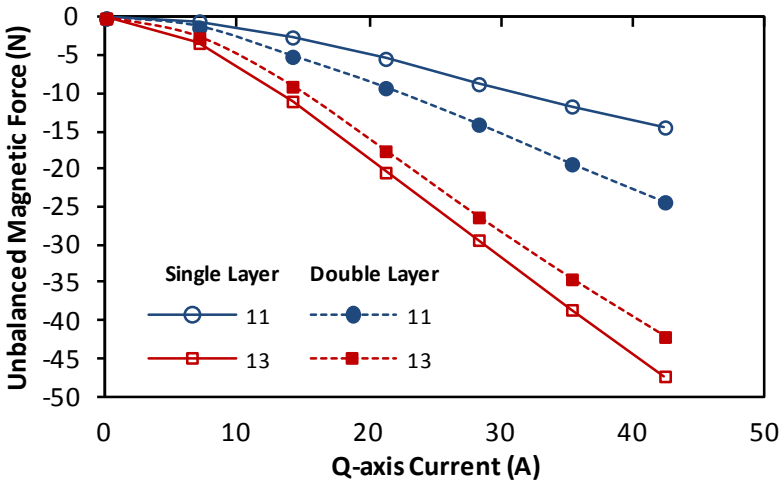

Fig. 5.44. Unbalanced magnetic force due to armature reaction with 11 and 13 rotor poles, double and single layer windings

Observing the influence of radial and tangential components the polarity of the tangential unbalanced forces changes with increasing current, while the radial forces dominate so as to reduce the total unbalanced force acting on the rotor as the current is increased Fig. 5.45.

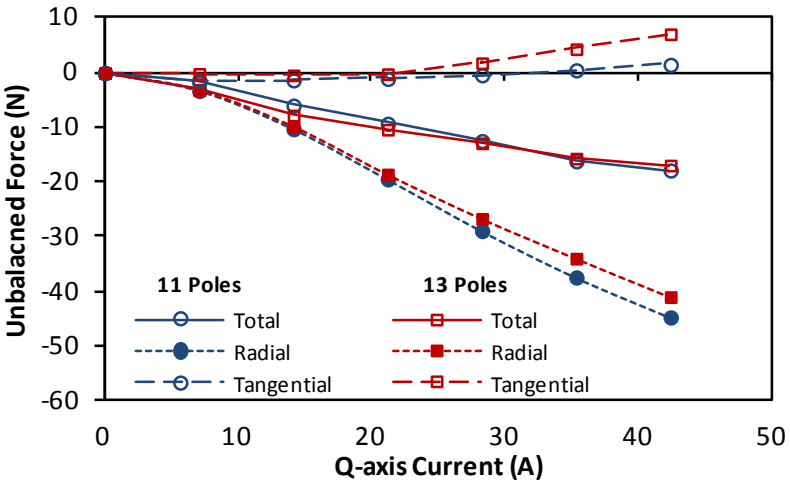

Fig. 5.45. Unbalanced magnetic force radial and tangential components for 11 and 13 rotor poles with double layer windings due to armature reaction

As the PS-SFPM machine has been shown to have the opportunity to mechanically weaken the PM flux through adjustment of the inner PM stator, the effect this has upon the unbalanced forces experienced by the rotor is investigated.

In the open-circuit condition as the PM stator is unaligned for 11 rotor poles this reduces the UMF, while for 13 rotor poles the UMF is increased Fig. 5.46. As the q-axis current is increased there is a greater change in UMF in the unaligned position than when the PM stator

is aligned with the wound stator. With 11 rotor poles and unaligned PM stator the UMF reduces as the q-axis current increases and the UMF increases for 13 rotor poles in the unaligned position.

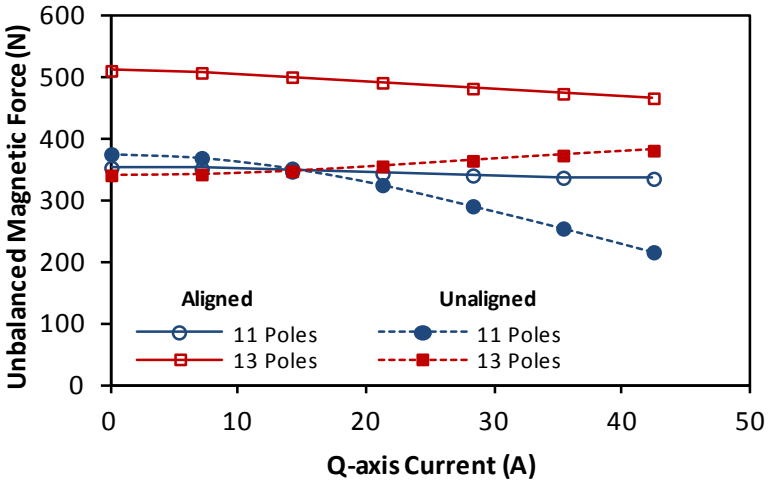

Fig. 5.46. Unbalanced magnetic force with 11 and 13 rotor poles variation with q-axis current with aligned and unaligned PM

The difference between the UMF in the unaligned position for 11 and 13 rotor poles variation with q-axis current occurs due to the difference in UMF in the radial and tangential components. For 11 rotor poles there is a significant reduction in UMF for the radial component which does not exist in the 13 rotor poles Fig. 5.47.

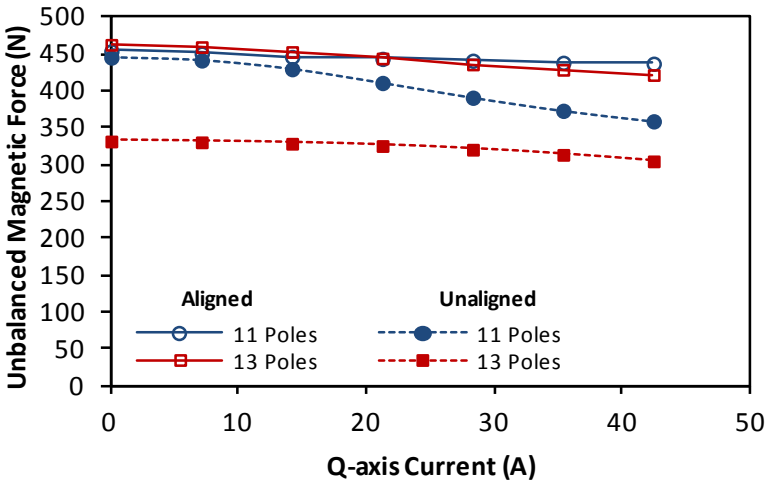

Fig. 5.47. Radial component of unbalanced magnetic force with 11 and 13 rotor poles variation with q-axis current with aligned and unaligned PM

The relationship between UMF and q-axis current for 11 and 13 rotor poles considering the tangential components are very similar Fig. 5.48, therefore the total UMF experienced by the

rotor reduces for 11 rotor poles and increases for 13 rotor poles in the unaligned PM stator position.

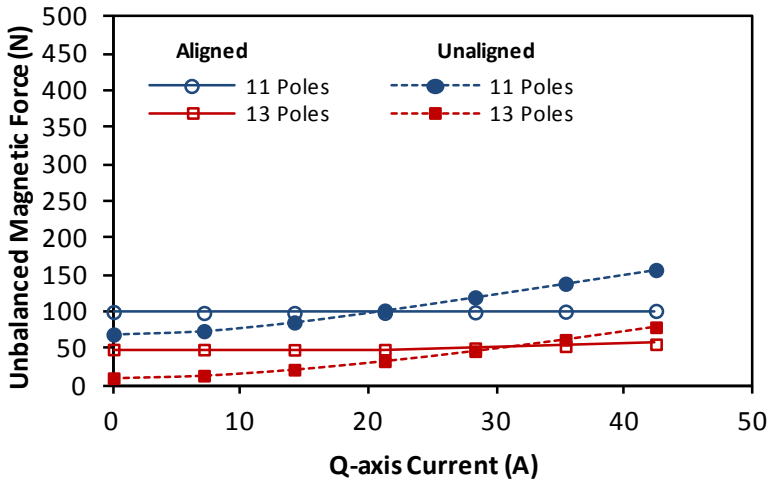

Fig. 5.48. Tangential component of unbalanced magnetic force with 11 and 13 rotor poles variation with q-axis current with aligned and unaligned PM

For PS-SFPM machines with odd numbers of rotor poles, the major contribution to unbalance magnet force occurs due to the interaction between the PM and iron rotor poles rather than the armature reaction field and the iron poles. This is evident from the magnitude of UMF occurring in open-circuit and the comparative minimal impact of q-axis current on these forces. The difference between double and single layer windings on UMF is small, while the un-alignment of the PM stator for 13 rotor poles is favourable in terms of UMF, but for 11 rotor poles the UMF is increased.

5.6. Conclusions

The PS-SFPM machine has been investigated in terms of parasitic effects that occur in the machine. Losses in the PM material due to eddy currents induced in the PM have been analysed, revealing that even numbers of rotor poles have greater losses than those with odd numbers of poles and that those with more rotor poles (13 and 14) have higher losses compared to those with less (10 and 11). Single layer windings cause greater on-load PM eddy current loss than double layer due to their armature reaction field's penetration into the PM particularly at the PM airgap surface. Iron losses in the wound stator, rotor poles and PM

stator iron have been investigated as the number of rotor poles increases the frequency of flux density variation increases, also the magnitude of variation reduces, therefore the maximum iron loss in opencircuit occurs for 11 rotor poles. The hysteresis loss in the iron is greater than the eddy current losses, with the majority of loss occurring in the rotor and outer stator. A feature of the PS-SFPM machine is that the PM field may be reduced mechanically in order to increase to the operational speed range, therefore the losses in this condition has been investigated. Further due to the potential use of odd numbers of rotor poles the PS-SFPM machine may experience unbalanced magnetic forces acting upon its rotor, this may be removed by doubling the number of rotor poles, but as for this geometry it increases the torque density by employing odd numbers of rotor poles these combinations have been considered. The effect of armature reaction field on the unbalanced force is minimal, therefore use of single or double layer windings has little effect on this force, particular attention of this force is required as these odd numbers of rotor poles will experience unbalanced forces and the effect on vibration and bearing life should be considered.

CHAPTER 6 – GENERAL CONCLUSIONS

6.1. Conclusions

This research has generated and developed a novel brushless permanent magnet machine which builds upon previous research in the areas of magnetic gearing and switched flux machines. The machine termed the partitioned stator switched flux machine itself presents a machine topology competitive with other permanent magnet machines, but also opens the potential to apply this principle of partitioning permanent magnets and windings to other machine types.

6.2. Machine Concept

Based on the investigation of magnetic gearing and switched flux machine principles the connection between these two areas of research was identified, based on the combinations of permanent magnets, winding configurations and rotor poles used in switched flux machines matching the requirements of a magnetic gear. From this connection the ability to share machine geometries and features was observed, primarily the separation of windings and permanent magnets in the switched flux machine topology by using a magnetic gears modulating rotor geometry. This new arrangement from the switched flux machines perspective could be described as having its windings and permanent magnets partitioned throughout the machine and hence the name partitioned stator switched flux (PS-SFPM) machine was born.

6.2.1. Magnetic Gearing

Fundamental to magnetic gearing is that a combination of two magnetic fields of different spatial and temporal order (whether from electrical excitation or permanent magnet fields) could be coupled by modulation through the medium of a spatial variation in permeance. Connecting this concept with the Vernier machine, or the exploitation into new magnetic geared machines has been previously investigated, but this research extends this connection

particularly to switched flux machines by identifying the combinations of stator teeth, permanent magnet pole pairs and rotor teeth used in switched flux machines.

6.2.2. Switched Flux

Switched flux machines base their operation on a time varying permanence creating switching flux linking its coils. This machine benefits from focusing of flux from a single permanent magnet to a single coil, but is limited by saturation of the stator iron and complex stator structure. Applying the magnetic gears modulating structure, the time varying permeance is maintained and the separation of windings and permanent magnets possible.

6.3. Machine Investigation

Once the PS-SFPM machine concept was recognised, an investigation into machine features and details was required to identify the validity of this machine topology compared to conventional permanent magnet machines. The research into this machine can be split into two headings being the machines performance characteristics and undesirable parasitic effects.

6.3.1. Performance Characteristics

The initial idea was investigated and its operation presented from both the perspective of a switched flux machine and a magnetic geared machine. The following main conclusions concerning the PS-SFPM machines performance observed during this research are outlined:

- *Optimisation* – Determining the optimal number of rotor poles is particularly important in machine design and for PS-SFPM machines with 12 stator slots and 6 PM pole pairs an optimal number of rotor poles of 11 was determined. Individual parameters with for different numbers of rotor poles were optimised and demonstrating the importance of the rotor pole design for maximum torque production, as from a switched flux point of view this determines the amount of flux linking individual coils and from the magnetic gears perspective this alters the modulating effect of the poles. (Chapter 2)

- *Performance* – The winding layouts for both double and single layer windings were presented, the benefits of utilising single layer windings was seen to be increased for those machines with odd numbers of rotor poles at low speed operation. As could be expected, but confirmed for PS-SFPM machines, with single layer windings the self to mutual inductance ratio is reduced thus presenting themselves as a more favourable fault tolerant design (Chapter 2 and Chapter 3)

- *Different Speed Operation* – As those machines with single layer windings yield a higher flux weakening factor, than their double layer winding counterparts with the same number of rotor poles, they achieve higher torque across a larger speed range. The potential to mechanically weaken the flux was seen in the PS-SFPM machine by virtue of the separated PM on the inner stator, for all combinations of rotor poles and windings the lower speed with high torque could be maintained and the speed range extended. Especially for 14 rotor poles with single layer windings an "infinite" speed range could be achieved. (Chapter 3 and Chapter 4)

6.3.2. Parasitic Effects

As for any machine design there occurs parasitic effects which are undesirable, these factors need to be quantified to assess their implications on design, whether they may be mitigated or accepted. The following effects that occur in the PS-SFPM machine are explored and conclusions presented:

- *Torque ripples* – Cogging torque and on-load ripples, due to back EMF harmonics, were predicted using FE, generally odd numbers of rotor poles experienced the lowest torque ripples. Single layer windings with even numbers of rotor poles have large on-load torque ripples since their back EMF is asymmetric containing even order harmonics. When the relative angle of the inner PM stator is adjusted for mechanical flux weakening the contributions of cogging torque varies for different numbers of rotor poles, with even numbers of rotor poles having increased cogging

torque and 11 rotor poles experiencing a reduction in cogging torque. (Chapter 2, Chapter 3 and Chapter 4)

- *Losses* – PM eddy current losses were predicted for the PS-SFPM machine, the smallest loss occurs in 11 rotor poles design, employing single layer windings increases the loss compared to double layer windings. The majority of iron loss occurs in the rotor and outer stator compared with the inner stator with 11 rotor poles having the highest total iron loss as it has the largest variation in flux density magnitude and the frequency of variation is greater than 10 rotor poles.
- *Unbalanced forces* – Unbalanced forces on the rotor occur for odd numbers of rotor poles, for the PS-SFPM machine using 13 rotor poles has the largest unbalanced forces. As the PM stator is adjusted to the unaligned position, to facilitate flux weakening, at lower currents the unbalanced force is reduced, but with increased current excitation the unbalanced forces increase.

6.4. Future Work

Based on the work performed during this thesis, there are possible future avenues of research to extend understanding and design of the PS-SFPM permanent magnet machine, but also additional applications of the link between magnetic gears and switched flux machines to other machine types.

6.4.1. Mechanical Structure

Key to the design of magnetic gears is the mechanical structure of the modulating pole pieces, in this research this has been the greatest compromise to the electromagnetic design with the inclusion of iron bridges. Further research into the mechanical design of this geometry of rotor would increase understanding of the potential and limits when designing magnetic gears and PS-SFPM machines.

6.4.2. Switched Flux Machines

In the area of switched flux machines there have been multiple variations in design to E-core, C-core, Multi PM, Multi-tooth, hybrid and wound field variants. All of these derivations of the switched flux machine may be applied to the partitioned design to find if they provide any benefits.

6.4.3. Stator Permanent Magnet Machines

From a wider view the potential to partitioned PM and windings across two stationary bodies is applicable to any machine with stationary PM and windings, therefore this theory provides potential for further developments of new partitioned stator flux reversal and partitioned stator doubly salient machines.

REFERENCES

[1] M. Sagawa, S. Fujimura, N. Togawa, H. Yamamoto, and Y. Matsuura, "New material for permanent magnets on base of Nd and Fe," *J. Appl. Phys.,* vol. 55, no. 6, pp. 2083-2087, 1985.

[2] R. Misutani and N. Matsui, "Design and analysis of low-speed, high-torque permanent magnet motors," *Electrical Engineering in Japan,* vol. 132, no. 3, pp. 48-56, 2000.

[3] Z. Q. Zhu, K. Ng, and D. Howe, "Design and analysis of high-speed brushless permanent magnet motors," in *EMD*, 1997, pp. 381-385.

[4] N. Bianchi, S. Bolognani, M. D. Pre, and G. Grezzani, "Design considerations for fractional-slot winding configurations of synchronous machines," *IEEE Trans. Ind. Appl.,* vol. 42, no. 4, pp. 997-1006, 2006.

[5] A. M. El-Refaie, T. M. Jahns, and D. W. Novotny, "Analysis of surface permanent magnet machines with fractional-slot concentrated windings," *IEEE Trans. Energy Convers.,* vol. 21, no. 1, pp. 34-43, 2006.

[6] H. Jussila, P. Salminen, M. Niemela, and J. Pyrhonen, "Guidelines for designing concentrated winding fractional slot permanent magnet machines," in *POWERENG*, 2007, pp. 191-194.

[7] P. Salminen, J. Pyrhonen, H. Jussila, and M. Niemela, "Concentrated wound permanent magnet machines with different rotor designs," in *POWERENG*, 2007, pp. 514-517.

[8] K. T. Chau, C. C. Chan, and L. Chunhua, "Overview of permanent-magnet brushless drives for electric and hybrid electric vehicles," *IEEE Trans. Ind. Elec.,* vol. 55, no. 6, pp. 2246-2257, 2008.

[9] Z. Q. Zhu, "Fractional slot permanent magnet brushless machines and drives for electric and hybrid propulsion systems," *COMPEL,* vol. 30, no. 1, pp. 9-31, 2009.

[10] H. Polinder, F. F. A. van der Pijl, G. J. de Vilder, and P. J. Tavner, "Comparison of direct-drive and geared generator concepts for wind turbines," *IEEE Trans. Energy Convers.,* vol. 21, no. 3, pp. 725-733, 2006.

[11] D. Yao and R. G. Harley, "Present and future trends in wind turbine generator designs," in *PEMWA*, 2009, pp. 1-6.

[12] E. V. Kazmin, E. A. Lomonova, and J. J. H. Paulides, "Brushless traction PM machines using commercial drive technology, Part I: Design methodology and motor design," in *ICEMS,* 2008, pp. 3801-3809.

[13] E. V. Kazmin, E. A. Lomonova, and J. J. H. Paulides, "Brushless traction PM machines using commercial drive technology, Part II: Comparative study of the motor configurations," in *ICEMS,* 2008, pp. 3772-3780.

[14] C. Ming, H. Wei, Z. Jianzhong, and Z. Wenxiang, "Overview of stator-permanent magnet brushless machines," *IEEE Trans. Ind. Elec.,* vol. 58, no. 11, pp. 5087-5101, 2011.

[15] K. Atallah and D. Howe, "A novel high-performance magnetic gear," *IEEE Trans. Magn.,* vol. 37, no. 4, pp. 2844-2846, 2001.

[16] S. E. Rauch and L. J. Johnson, "Design principles of flux-switch alternators," *Transactions of the Amer. Inst. of Elect. Engineers Power App. and Syst.,* vol. 74, no. 3, pp. 1261-1268, 1955.

[17] L. Yuefeng, L. Feng, and T. A. Lipo, "A novel permanent magnet motor with doubly salient structure," *IEEE Trans. Ind. Appl.,* vol. 31, no. 5, pp. 1069-1078, 1995.

[18] C. Ming, K. T. Chau, C. C. Chan, E. Zhou, and X. Huang, "Nonlinear varying-network magnetic circuit analysis for doubly salient permanent-magnet motors," *IEEE Trans. Magn.,* vol. 36, no. 1, pp. 339-348, 2000.

[19] M. Cheng, K. T. Chau, and C. C. Chan, "Design and analysis of a new doubly salient permanent magnet motor," *IEEE Trans. Magn.,* vol. 37, no. 4, pp. 3012-3020, 2001.

[20] M. Lin, M. Cheng, and E. Zhou, "Design and performance analysis of new 12/8-pole doubly salient permanent-magnet motor," in *ICEMS,* 2003, pp. 21-25 vol.1.

[21] R. P. Deodhar, S. Andersson, I. Boldea, and T. J. E. Miller, "The flux-reversal machine: a new brushless doubly-salient permanent-magnet machine," in *IAS,* 1996*,* pp. 786-793 vol.2.

[22] C. Wang, S. A. Nasar, and I. Boldea, "Three-phase flux reversal machine (FRM)," *IEE Proc. Elec. Power. App.,* vol. 146, no. 2, pp. 139-146, 1999.

[23] C. X. Wang, I. Boldea, and S. A. Nasar, "Characterization of three phase flux reversal machine as an automotive generator," *IEEE Trans. Energy Convers.,* vol. 16, no. 1, pp. 74-80, 2001.

[24] E. Hoang, B. Ahmed, and J. Lucidarme, "Switching flux permanent magnet polyphased synchronous machines," in *EPE,* pp. 903-908, 1997.

[25] Z. Q. Zhu, Y. Pang, D. Howe, S. Iwasaki, R. Deodhar, and A. Pride, "Analysis of electromagnetic performance of flux-switching permanent-magnet Machines by nonlinear adaptive lumped parameter magnetic circuit model," *IEEE Trans. Magn.,* vol. 41, no. 11, pp. 4277-4287, 2005.

[26] N. K. Sheth and K. R. Rajagopal, "Improved torque profile of a doubly salient permanent magnet motor using skewed rotor teeth and sinusoidal excitation," in *PEDES,* 2006, pp. 1-6.

[27] K. T. Chau, S. Qiang, F. Ying, and C. Ming, "Torque ripple minimization of doubly salient permanent-magnet motors," *IEEE Trans. Energy Convers.,* vol. 20, no. 2, pp. 352-358, 2005.

[28] W. Hua, Z. Q. Zhu, M. Cheng, Y. Pang, and D. Howe, "Comparison of flux-switching and doubly-salient permanent magnet brushless machines," in *ICEMS,* 2005, pp. 165-170 Vol. 1.

[29] I. Boldea, Z. Jichun, and S. A. Nasar, "Theoretical characterization of flux reversal machine in low-speed servo drives-the pole-PM configuration," *IEEE Trans. Ind. Appl.,* vol. 38, no. 6, pp. 1549-1557, 2002.

[30] D. S. More and B. G. Fernandes, "Analysis of flux-reversal machine based on fictitious electrical gear," *IEEE Trans. Energy Convers.,* vol. 25, no. 4, pp. 940-947, 2010.

[31] Z. Q. Zhu, Y. Pang, J. T. Chen, Z. P. Xia, and D. Howe, "Influence of design parameters on output torque of flux-switching permanent magnet machines," in *VPPC,* 2008, pp. 1-6.

[32] B. L. J. Gysen, E. Ilhan, K. J. Meessen, J. J. H. Paulides, and E. A. Lomonova, "Modeling of flux switching permanent magnet machines with fourier analysis," *IEEE Trans. Magn.,* vol. 46, no. 6, pp. 1499-1502, 2010.

[33] A. S. Thomas, Z. Q. Zhu, and G. W. Jewell, "Comparison of flux switching and surface mounted permanent magnet generators for high-speed applications," *IET Elec. Syst. Trans.,* vol. 1, no. 3, pp. 111-116, 2011.

[34] H. Wei, C. Ming, Z. Q. Zhu, and D. Howe, "Analysis and optimization of back EMF waveform of a flux-switching permanent magnet motor," *IEEE Trans. Energy Convers.,* vol. 23, no. 3, pp. 727-733, 2008.

[35] Y. Pang, Z. Q. Zhu, D. Howe, S. Iwasaki, R. Deodhar, and A. Pride, "Investigation of iron loss in flux-switching PM machines," in *PEMD,* 2008, pp. 460-464.

[36] Z. Q. Zhu, Y. Pang, J. T. Chen, R. L. Owen, D. Howe, S. Iwasaki, R. Deodhar, and A. Pride, "Analysis and reduction of magnet eddy current loss in flux-switching permanent magnet machines," in *PEMD,* 2008, pp. 120-124.

[37] J. T. Chen, Z. Q. Zhu, S. Iwasaki, and R. Deodhar, "Comparison of losses and efficiency in alternate flux-switching permanent magnet machines," in *ICEM*, 2010, pp. 1-6.

[38] J. Zhang, M. Cheng, and Z. Chen, "Investigation of a new stator interior permanent magnet machine," *IET Proc. Elec. Power. App.,* vol. 2, no. 2, pp. 77-87, 2008.

[39] Z. Q. Zhu, A. S. Thomas, J. T. Chen, and G. W. Jewell, "Cogging torque in flux-switching permanent magnet machines," *IEEE Trans. Magn.,* vol. 45, no. 10, pp. 4708-4711, 2009.

[40] J. T. Chen and Z. Q. Zhu, "Comparison of all- and alternate-poles-wound flux-switching PM machines having different stator and rotor pole numbers," *IEEE Trans. Ind. Appl.,* vol. 46, no. 4, pp. 1406-1415, 2010.

[41] J. T. Chen and Z. Q. Zhu, "Winding configurations and optimal stator and rotor pole combination of flux-switching PM brushless AC machines," *IEEE Trans. Energy Convers.,* vol. 25, no. 2, pp. 293-302, 2010.

[42] J. T. Chen, Z. Q. Zhu, S. Iwasaki, and R. P. Deodhar, "A novel E-core switched-flux PM brushless AC machine," *IEEE Trans. Ind. Appl.,* vol. 47, no. 3, pp. 1273-1282, 2011.

[43] J. T. Chen, Z. Q. Zhu, S. Iwasaki, and R. Deodhar, "Influence of slot opening on optimal stator and rotor pole combination and electromagnetic performance of flux-switching PM brushless AC machines," in *ECCE,* 2010, pp. 3478-3485.

[44] Z. Q. Zhu, J. T. Chen, Y. Pang, D. Howe, S. Iwasaki, and R. Deodhar, "Analysis of a novel multi-tooth flux-switching PM brushless AC machine for high torque direct-drive applications," *IEEE Trans. Magn.,* vol. 44, no. 11, pp. 4313-4316, 2008.

[45] J. T. Chen, Z. Q. Zhu, and D. Howe, "Stator and rotor pole combinations for multi-tooth flux-switching permanent-magnet brushless AC machines," *IEEE Trans. Magn.,* vol. 44, no. 12, pp. 4659-4667, 2008.

[46] J. T. Chen, Z. Q. Zhu, S. Iwasaki, and R. P. Deodhar, "A novel hybrid-excited switched-flux brushless AC machine for EV/HEV applications," *IEEE Trans. Vehicular Tech.,* vol. 60, no. 4, pp. 1365-1373, 2011.

[47] Z. Q. Zhu and J. T. Chen, "Advanced flux-switching permanent magnet brushless machines," *IEEE Trans. Magn.,* vol. 46, no. 6, pp. 1447-1453, 2010.

[48] W. Z. Fei and J. X. Shen, "Novel permanent magnet switching flux motors," in *UPEC,* 2006, pp. 729-733.

[49] Z. Q. Zhu, "Switched flux permanent magnet machines - Innovation continues," in *ICEMS,* 2011, pp. 1-10.

[50] Z. Q. Zhu, D. Howe, and C. C. Chan, "Improved analytical model for predicting the magnetic field distribution in brushless permanent-magnet machines," *IEEE Trans. Magn.,* vol. 38, no. 1, pp. 229-238, 2002.

[51] Z. Q. Zhu and D. Howe, "Instantaneous magnetic field distribution in permanent magnet brushless DC motors. IV. magnetic field on load," *IEEE Trans. Magn.,* vol. 29, no. 1, pp. 152-158, 1993.

[52] M. M. Liwschitz, "Field harmonics in induction motors," *Trans. of the Amer. Inst. of Elect. Engineers,* vol. 61, no. 11, pp. 797-803, 1942.

[53] S. Salon, D. Burow, M. DeBortoli, and C. Slavik, "Effects of slot closure and magnetic saturation on induction machine behavior," *IEEE Trans. Magn.,* vol. 30, no. 5, pp. 3697-3700, 1994.

[54] A. Canova and C. Ragusa, "Calculation of slot harmonic effects in induction motors by finite element method," in *EMD, 1995*, pp. 82-87.

[55] Z. Q. Zhu and D. Howe, "Instantaneous magnetic field distribution in brushless permanent magnet DC motors. III. effect of stator slotting," *IEEE Trans. Magn.,* vol. 29, no. 1, pp. 143-151, 1993.

[56] J. T. B. Martin, "Magnetic transmission," U.S. Patent 3378710, Apr. 16, 1968.

[57] D. E. Hesmondhalgh and D. Tipping, "A multielement magnetic gear," *IEE Proc. Elec. Power. App.,* vol. 127, no. 3, pp. 129-138, 1980.

[58] K. Atallah, S. D. Calverley, and D. Howe, "Design, analysis and realisation of a high-performance magnetic gear," *IEE Proc. Elec. Power. App.,* vol. 151, no. 2, pp. 135-143, 2004.

[59] E. P. Furlani, "A two-dimensional analysis for the coupling of magnetic gears," *IEEE Trans. Magn.,* vol. 33, no. 3, pp. 2317-2321, 1997.

[60] E. Gouda, S. Mezani, L. Baghli, and A. Rezzoug, "Comparative study between mechanical and magnetic planetary gears," *IEEE Trans. Magn.,* vol. 47, no. 2, pp. 439-450, 2011.

[61] Y. Li, J. Xing, K. Peng, and Y. Lu, "Principle and simulation analysis of a novel structure magnetic gear," in *ICEMS,* 2008, pp. 3845-3849.

[62] N. W. Frank and H. A. Toliyat, "Gearing ratios of a magnetic gear for marine applications," in *ESTS*, 2009, pp. 477-481.

[63] P. O. Rasmussen, T. O. Andersen, F. T. Joergensen, and O. Nielsen, "Development of a high performance magnetic gear," in *IAS*, 2003, pp. 1696-1702.

[64] K. Atallah, J. Rens, S. Mezani, and D. Howe, "A novel 'pseudo' direct-drive brushless permanent magnet machine," *IEEE Trans. Magn.,* vol. 44, no. 11, pp. 4349-4352, 2008.

[65] K. T. Chau, Z. Dong, J. Z. Jiang, L. Chunhua, and Z. Yuejin, "Design of a magnetic-geared outer-rotor permanent-magnet brushless motor for electric vehicles," *IEEE Trans. Magn.,* vol. 43, no. 6, pp. 2504-2506, 2007.

[66] L. L. Wang, J. X. Shen, P. C. K. Luk, W. Z. Fei, C. F. Wang, and H. Hao, "Development of a magnetic-geared permanent-magnet brushless motor," *IEEE Trans. Magn.,* vol. 45, no. 10, pp. 4578-4581, 2009.

[67] W. N. Fu and S. L. Ho, "A quantitative comparative analysis of a novel flux-modulated permanent-magnet motor for low-speed drive," *IEEE Trans. Magn.,* vol. 46, no. 1, pp. 127-134, 2010.

[68] C. H. Lee, "Vernier motor and its design," *IEEE Trans. on Power App. and Syst.,* vol. 82, no. 66, pp. 343-349, 1963.

[69] A. Toba and T. A. Lipo, "Generic torque-maximizing design methodology of surface permanent-magnet vernier machine," *IEEE Trans. Ind. Appl.,* vol. 36, no. 6, pp. 1539-1546, 2000.

[70] L. Jiangui, K. T. Chau, and L. Wenlong, "Harmonic analysis and comparison of permanent magnet vernier and magnetic-geared machines," *IEEE Trans. Magn.,* vol. 47, no. 10, pp. 3649-3652, 2011.

[71] J. Li and K. T. Chau, "Design and analysis of a HTS vernier PM machine," *IEEE Trans. on Appl. Superconductivity,* vol. 20, no. 3, pp. 1055-1059, 2010.

[72] R. Qu, D. Li, and J. Wang, "Relationship between magnetic gears and vernier machines," in *ICEMS,* 2011, pp. 1-6.

[73] K. Atallah, S. Calverley, R. Clark, J. Rens, and D. Howe, "A new PM machine topology for low-speed, high-torque drives," in *ICEM,* 2008, pp. 1-4.

[74] J. Wang and K. Atallah, "Modeling and control of 'pseudo' direct-drive brushless permanent magnet machines," in *IEMDC,* 2009, pp. 870-875.

[75] K. Atallah, W. Jiabin, S. D. Calverley, and S. Duggan, "Design and operation of a magnetic continuously variable transmission," *IEEE Trans. Ind. Appl.,* vol. 48, no. 4, pp. 1288-1295, 2012.

[76] J. Linni, X. Guoqing, C. C. Mi, K. T. Chau, and C. C. Chan, "Analytical method for magnetic field calculation in a low-speed permanent-magnet harmonic machine," *IEEE Trans. Energy Convers.,* vol. 26, no. 3, pp. 862-870, 2011.

[77] F. J. Allen, C. E. Miller, J. E. Parton, L. J. Stone, and S. A. Swann, "A magnetic gear," in *UPEC*, vol. 8, 1969.

[78] R. Wang, E. P. Furlani, and Z. J. Cendes, "Design and analysis of a permanent magnet axial coupling using 3D finite element field computations," *IEEE Trans. Magn.,* vol. 30, no. 4, pp. 2292-2295, 1994.

[79] L. Jian and K.T. Chau, "Analytical calculation of magnetic field distribution in coaxial magnetic gears," in *PIER,* vol. 92, pp. 1-16, 2009.

[80] N. W. Frank and H. A. Toliyat, "Gearing ratios of a magnetic gear for wind turbines," in *IEMDC,* 2009, pp. 1224-1230.

[81] N. W. Frank and H. A. Toliyat, "Analysis of the concentric planetary magnetic gear with strengthened stator and interior permanent magnet inner rotor," *IEEE Trans. Ind. Appl.,* vol. 47, no. 4, pp. 1652-1660, 2011.

[82] L. Xianglin, K. T. Chau, C. Ming, H. Wei, and D. Yi, "An improved coaxial magnetic gear using flux focusing," in *ICEMS,* 2011, pp. 1-4.

[83] K. Atallah, J. Wang, and D. Howe, "A high-performance linear magnetic gear," *J. Appl. Phys.,* vol. 97, no. 10, 2005.

[84] A. Reinap and F. Marquez, "Development of a modular linear magnetic gear as a project in the electrical engineering education," in *ICEM,* 2008, pp. 1-5.

[85] S. Mezani, K. Atallah, and D. Howe, "A high-performance axial-field magnetic gear," *J. Appl. Phys.,* vol. 99, no. 8, 2006.

[86] P. O. Rasmussen, H. H. Mortensen, T. N. Matzen, T. M. Jahns, and H. A. Toliyat, "Motor integrated permanent magnet gear with a wide torque-speed range," in *ECCE*, 2009, pp. 1510-1518.

[87] F. Ying, H. Xuedong, X. Zhongbing, and J. Hehe, "Design, analysis and control of a permanent magnet in-wheel motor based on magnetic-gear for electric vehicles," in *ICEMS,* 2011, pp. 1-6.

[88] J. Hongyun, C. Ming, H. Wei, Y. Zhengzhuan, and Z. Yunqian, "Compensation of cogging torque for flux-switching permanent magnet motor based on current harmonics injection," in *IEMDC,* 2009, pp. 286-291.

[89] Y. Pang, Z. Q. Zhu, D. Howe, S. Iwasaki, R. Deodhar, and A. Pride, "Comparative study of flux-switching and interior permanent magnet machines," *ICEMS,* 2007, pp. 757-762.

[90] Z. Gan, C. Ming, H. Wei, and D. Jianning, "Analysis of the oversaturated effect in hybrid excited flux-switching machines," *IEEE Trans. Magn.,* vol. 47, no. 10, pp. 2827-2830, 2011.

[91] Y. Pang, Z. Q. Zhu, and D. Howe, "Analytical determination of optimal split ratio for permanent magnet brushless motors," *IEE Proc. Elec. Power. App.,* vol. 153, no. 1, pp. 7-13, 2006.

[92] D. Ishak, Z. Q. Zhu, and D. Howe, "Comparison of PM brushless motors, having either all teeth or alternate teeth wound," *IEEE Trans. Energy Convers.,* vol. 21, no. 1, pp. 95-103, 2006.

[93] M. S. Islam, S. Mir, T. Sebastian, and S. Underwood, "Design considerations of sinusoidally excited permanent-magnet machines for low-torque-ripple applications," *IEEE Trans. Ind. Appl.,* vol. 41, no. 4, pp. 955-962, 2005.

[94] Z. Q. Zhu and D. Howe, "Influence of design parameters on cogging torque in permanent magnet machines," *IEEE Trans. Energy Convers.,* vol. 15, no. 4, pp. 407-412, 2000.

[95] Z. Q. Zhu, "A simple method for measuring cogging torque in permanent magnet machines," in *PES,* 2009, pp. 1-4.

[96] Z. Zhu, L. Wu, and M. Mohd Jamil, "Distortion of back-EMF and torque of PM brushless machines due To eccentricity," *IEEE Trans. Magn.,* vol. 49, no. 8, pp. 4927-4936, 2013.

[97] A. M. El-Refaie and T. M. Jahns, "Impact of winding layer number and magnet type on synchronous surface PM machines designed for wide constant-power speed range operation," *IEEE Trans. Energy Convers.,* vol. 23, no. 1, pp. 53-60, 2008.

[98] R. L. Owen, Z. Q. Zhu, A. S. Thomas, G. W. Jewell, and D. Howe, "Alternate poles wound flux-switching permanent-magnet brushless AC machines," *IEEE Trans. Ind. Appl.,* vol. 46, no. 2, pp. 790-797, 2010.

[99] J. R. Hendershot Jr, and T. J. E. Miller, *Design of brushless permanent magnet motors*. Oxford, UK: Clarendon, 1994.

[100] W. L. Soong and T. J. E. Miller, "Field-weakening performance of brushless synchronous AC motor drives," *IEE Proc. Elec. Power. App.,* vol. 141, no. 6, pp. 331-340, 1994.

[101] J. A. Tapia, F. Leonardi, and T. A. Lipo, "Consequent-pole permanent-magnet machine with extended field-weakening capability," *IEEE Trans. Ind. Appl.,* vol. 39, no. 6, pp. 1704-1709, 2003.

[102] L. Del Ferraro, F. Caricchi, and F. G. Capponi, "Analysis and comparison of a speed-dependant and a torque-dependant mechanical device for wide constant power speed range in AFPM starter/alternators," *IEEE Trans. Power Electron.,* vol. 21, no. 3, pp. 720-729, 2006.

[103] F. G. Capponi, R. Terrigi, F. Caricchi, and L. Del Ferraro, "Active output voltage regulation for an ironless axial-flux PM automotive alternator with electromechanical flux weakening," *IEEE Trans. Ind. Appl.,* vol. 45, no. 5, pp. 1785-1793, 2009.

[104] M. Lei, M. Sanada, S. Morimoto, Y. Takeda, and N. Matsui, "High efficiency adjustable speed control of IPMSM with variable permanent magnet flux linkage," in *IAS,* 1999, pp. 881-887 vol.2.

[105] Z. Q. Zhu and D. Howe, "Analytical prediction of the cogging torque in radial-field permanent magnet brushless motors," *IEEE Trans. Magn.,* vol. 28, no. 2, pp. 1371-1374, 1992.

[106] N. Bianchi and S. Bolognani, "Design techniques for reducing the cogging torque in surface-mounted PM motors," *IEEE Trans. Ind. Appl.,* vol. 38, no. 5, pp. 1259-1265, 2002.

[107] K. Atallah, Z. Q. Zhu, and D. Howe, "An improved method for predicting iron losses in brushless permanent magnet DC drives," *IEEE Trans. Magn.,* vol. 28, no. 5, pp. 2997-2999, 1992.

[108] B. C. Mecrow, A. G. Jack, and J. M. Masterman, "Determination of rotor eddy current losses in permanent magnet machines," in *EMD,* 1993, pp. 299-304.

[109] K. Atallah, D. Howe, P. H. Mellor, and D. A. Stone, "Rotor loss in permanent-magnet brushless AC machines," *IEEE Trans. Ind. Appl.,* vol. 36, no. 6, pp. 1612-1618, 2000.

[110] Z. Q. Zhu, K. Ng, N. Schofield, and D. Howe, "Improved analytical modelling of rotor eddy current loss in brushless machines equipped with surface-mounted permanent magnets," *IEE Proc. Elec. Power. App.,* vol. 151, no. 6, pp. 641-650, 2004.

[111] E. Hoang, M. Gabsi, M. Lecrivain, and B. Multon, "Influence of magnetic losses on maximum power limits of synchronous permanent magnet drives in flux-weakening mode," in *IAS,* 2000, pp. 299-303 vol.1.

[112] N. Bianchi, M. D. Pre, G. Grezzani, and S. Bolognani, "Design considerations on fractional-slot fault-tolerant synchronous motors," in *IEMD,* 2005, pp. 902-909.

[113] A. M. El-Refaie, "Fractional-slot concentrated-windings synchronous permanent magnet machines: opportunities and challenges," *IEEE Trans. Ind. Elec.,* vol. 57, no. 1, pp. 107-121, 2010.

[114] J. T. Chen and Z. Q. Zhu, "Comparison of all- and alternate-poles-wound flux-switching PM machines having different stator and rotor pole numbers," *IEEE Trans. Ind. Appl.,* vol. 46, no. 4, pp. 1406-1415, 2010.

[115] B. Chao, Z. J. Liu, and T. S. Low, "Analysis of unbalanced-magnetic-pulls in hard disk drive spindle motors using a hybrid method," *IEEE Trans. Magn.,* vol. 32, no. 5, pp. 4308-4310, 1996.

[116] Z. Q. Zhu, D. Ishak, D. Howe, and J. Chen, "Unbalanced magnetic forces in permanent-magnet brushless machines with diametrically asymmetric phase windings," *IEEE Trans. Ind. Appl.,* vol. 43, no. 6, pp. 1544-1553, 2007.

[117] G. J. Li, J. Ojeda, E. Hoang, M. Lecrivain, and M. Gabsi, "Comparative studies between classical and mutually coupled switched reluctance motors using thermal-electromagnetic analysis for driving cycles," *IEEE Trans. Magn.,* vol. 47, no. 4, pp. 839-847, 2011.

[118] L. L. Wang, J. X. Shen, Y. Wang, and K. Wang, "A novel magnetic-geared outer-rotor permanent-magnet brushless motor," in *PEMD*, 2008, pp. 33-36.

[119] S. L. Ho, S. Niu, and W. N. Fu, "Transient analysis of a magnetic gear integrated brushless permanent magnet machine using Circuit-field-motion coupled time-stepping finite element method," *IEEE Trans. Magn.,* vol. 46, no. 6, pp. 2074-2077, 2010.

[120] D. J. Powell, S. D. Calverley, F. de Wildt, and K. Daffey, "Design and analysis of a pseudo direct-drive propulsion motor," in *PEMD,* 2010, pp. 1-2.

[121] H. R. Bolton and Y. Shakweh, "Performance prediction of Laws's relay actuator," *IEE Proc. Elec. Power. App.,* vol. 137, no. 1, pp. 1-13, 1990.

[122] E. Ilhan, B. L. J. Gysen, J. J. H. Paulides, and E. A. Lomonova, "Analytical hybrid model for flux switching permanent magnet machines," *IEEE Trans. Magn.,* vol. 46, no. 6, pp. 1762-1765, 2010.

[123] F. Weizhong, P. C. K. Luk, S. Jian Xin, X. Bin, and W. Yu, "Permanent-magnet flux-switching integrated starter generator with different rotor configurations for cogging torque and torque ripple mitigations," *IEEE Trans. Ind. Appl.,* vol. 47, no. 3, pp. 1247-1256, 2011.

[124] E. Sulaiman, T. Kosaka, N. Matsui, and M. Z. Ahmad, "Design improvement and performance analysis of 12-Slot-10-Pole permanent magnet flux switching machine with field excitation coils," in *PEOCO*, 2011, pp. 202-207.

[125] E. Sulaiman, T. Kosaka, and N. Matsui, "High power density design of 6-slot-8-pole hybrid excitation flux switching machine for hybrid electric vehicles," *IEEE Trans. Magn.,* vol. 47, no. 10, pp. 4453-4456, 2011.

[126] H. Wei, C. Ming, and Z. Gan, "A novel hybrid excitation flux-switching motor for hybrid vehicles," *IEEE Trans. Magn.,* vol. 45, no. 10, pp. 4728-4731, 2009.

[127] T. Raminosoa, C. Gerada, and M. Galea, "Design considerations for a fault-tolerant flux-switching permanent-magnet machine," *IEEE Trans. Ind. Elec.,* vol. 58, no. 7, pp. 2818-2825, 2011.

[128] W. Fei, P. C. K. Luk, J. Shen, and Y. Wang, "A novel outer-rotor permanent-magnet flux-switching machine for urban electric vehicle propulsion," in *PESA*, 2009, pp. 1-6.

[129] Z. Q. Zhu and X. Liu, "Individual and global optimization of switched flux permanent magnet motors," in *ICEMS*, 2011, pp. 1-6.

[130] J. T. Chen and Z. Q. Zhu, "Influence of rotor pole number on optimal parameters in flux-switching PM brushless AC machines by lumped parameter magnetic circuit model," in *IEMDC*, 2009, pp. 1216-1223.

[131] J.B. Wang and D. Howe, “Influence of soft magnetic materials on the design and performance of tubular permanent magnet machines,” *IEEE Trans. Magn.,* vol. 41, no. 10, pp. 4057-4059, 2005.